Unione europea
Fondo sociale europeo

Università degli Studi di Cagliari

DOTTORATO DI RICERCA

"Sviluppo e sperimentazione di farmaci antinfettivi"

Ciclo XXVIII

TITOLO TESI

Identificazione & Caratterizzazione di Composti Naturali e di Sintesi come Nuovi Agenti Antitumorali

Settore scientifico disciplinare di afferenza

BIO/19 – Microbiologia Generale

Presentata da: Dott.ssa Rossana Tuveri

Coordinatore Dottorato Prof.ssa Alessandra Pani

Tutor Prof.ssa Alessandra Pani

Esame finale anno accademico 2014 – 2015

Università degli Studi di Cagliari

RESEARCH DOCTORATE IN

"Research and Development of Anti-infective Drugs"

Cycle XXVIII

THESIS TITLE

Identification & Characterization of Natural and Synthetic Compounds as New Anticancer Agents

Scientific Area

BIO/19 –General Microbiology

Candidate: Dott. Rossana Tuveri

Doctorate Coordinator Prof. Alessandra Pani
Supervisor Prof. Alessandra Pani

Academic year 2014 – 2015

Acknowledgements

Rossana Tuveri gratefully acknowledges **Italian Government** for the financial support of her PhD scholarship (M.I.U.R. ex D.M.n. 198 del 23.10.2003-D.R. n. 535 del 12.02.2013).

La presente tesi è stata prodotta durante la frequenza del corso di dottorato in Sviluppo e Sperimentazione dei Farmaci anti-infettivi dell'Università degli Studi di Cagliari, a.a. 2014/2015 - XXVIII ciclo, con il supporto di una borsa di studio finanziata con le risorse del M.I.U.R. ex D.M.n. 198 del 23.10.2003- D.R. n. 535 del 12.02.2013.

I would like to thank all the people who helped me in the thesis realization:

- ✓ First of all ***Prof. Alessandra Pani***, my supervisor, for having been a precious, professional and personal guide during these three PhD years. Thanks to her strong temper and love for the research, she gave me the chance to grow up both at a professional and a personal level.

- ✓ ***Dr Catherine H. Kaschula***, my abroad supervisor at the University of Cape Town, for her precious and wise contribution in the results interpretation and in this thesis writing, but overall for having been a precious point of reference during my whole staying in Cape Town.

- ✓ ***Prof. Roger Hunter***, my abroad supervisor at Cape Town, for having given me the possibility to cooperate with a great research team.

- ✓ ***Prof. Ariel Katz*** for having me welcomed in his laboratory.

- ✓ ***Dr Georgia Schäfer*** for her assistance during the cloning and the western blot experiments.

- ✓ ***Vernita Reid***, my colleague at Cape Town, for having been my friend for the all-time and helped me in the little daily things.

- ✓ ***Elisabetta Pinna*** and ***Sarah Vascellari*** for being both my friends and colleagues, but overall for having shared with me a short period in South Africa.

- ✓ ***Giuseppina Sanna***, ***Daniela Perra***, ***Silvia Madeddu***, ***Roberta Melis***, ***Elisa Carta*** and ***Fabio Contu*** for being my friends and colleagues.

- ✓ To ***my parents*** and to all ***my family*** for supporting me and sharing with me all my professional and personal experiences.

- ✓ To all ***my friends*** for being there.

- ✓ Finally, I would like to thank ***Carlo***, not only for his huge patience and generosity, but also for supporting me and encouraging to go ahead, even in the most difficult moments of this experience and in the daily life.

Abstract

This thesis collects the work I have done during the three-year PhD Course. During my first year I have started a path that has allowed me to acquire different techniques devoted to set up and maintain primary cell cultures and cancer derived cell lines as well as to evaluate the cytotoxicity of potential novel synthetic inhibitors of human cancer cells. Part of the second and all the third year was spent at the University of Cape Town, South Africa, in the laboratory of prof. Ariel Katz under the supervision of proff. Roger Hunter and Catherine H. Kaschula investigating the anticancer activity of *Z*-ajoene, a garlic compound.

Overall, the main aim of all the my research project was to identify and characterize natural or synthetic compounds as new antineoplastic agents. The results obtained are divided according to the research topics addressed:

- ✓ *Anticancer activity of new Phenanthroline compounds (Part I);*
- ✓ *The garlic compound Z-ajoene as anticancer agents* (Part II).

Studies referring to the Part have been carried out at the University of Cagliari and were focalized on the evaluation of new Cu(II) -phenanthroline complexes as a potent antineoplastic agents against various solid and suspension tumours. The [Cu(1,10-phenanthrolin -5,6-diol)$_2$(OH2)](ClO$_4$)$_2$ complex appears to be the most potent compound against human leukemia, prostate and lung cancer cell lines. The results obtained on the biological activity of this class of compounds, providing valuable information for the design of new anticancer drugs, have been published in the Journal of Inorganic Biochemistry (2014).

As for the Part II of my research, I focused on the mechanisms underlying the anti-tumoral activity of garlic compound Z-ajoene on human triple –negative breast cancer cells. The results indicate that *Z*-ajoene localizes in the ER of MDA-MB-231 cells where it activates the unfolded protein response (UPR) and ER stress. These findings have been published in the Molecular Carcinogenesis journal (2015)

Moreover, immunofluorescence studies support the concept that the *Z*-ajoene main target is a ER-resident chaperon protein (PDI), whose functional alteration may well be the cause of the cytotoxic effect. Another molecular target of *Z*-ajoene is the cytoskeleton protein Vimentin. *Z*-ajoene interacts with Vimentin through a *S*–thiolation causing the disruption of Vimentin filaments and therefore an alteration of the cell morphology. Given that Vimentin is known to participate to the early stage of the metastatic process, I also investigated the potential effect of *Z*-ajoene at non-cytotoxic concentrations in a specific cell assay and found that it effectively inhibits cell migration, both in the absence and presence of a chemotactic agent. The metastatic inhibition induced by *Z*-ajoene seems caused by modification of several signaling pathways as expression of Axl and Src proteins, and phosphorylation of β–catenin were changed. Although following inhibition of cell migration, a reduction of Vimentin expression was to be expected, *Z*-ajoene treatment surprisingly induced an upregulation of Vimentin. We interpreted this result as a consequence of *Z*-ajoene binding to Vimentin which unable this protein to perform its physiologic functions (manuscripts in preparation).

Altogether, the data of my *in vitro* study indicate that *Z*-ajoene is a promising chemotherapeutic agent simultaneously acting on different molecular targets, also able to affect the metastatic process in cells derived from highly invasive breast tumors. Due to its potential use in the clinic, preclinical evaluation in xenograft mouse models of cancer are ongoing.

Table of contents

Part I - Anticancer activity of new Phenanthroline compounds

Chapter I - Novel copper(II) complexes as new promising antitumour agents.

The first part of my research has focused on the study of anti-tumour effects carried out by a new class of compounds, the Copper(II) complexes with 1,10-phenanthroline derivatives.

Copper is a metal ion essential for aerobic microorganisms, plants and animals. It binds molecular oxygen in oxygen-transport proteins and participates in electron transport [Terwilliger N. B., *J. Exp. Biol*. 1998]. In the human body the copper concentration level is regulated by the homeostatic system. Copper has been selected for the synthesis of new antitumour drugs since complexes containing essential metal ions, thanks to the homeostatic regulatory system, may produce less systemic toxicity than complexes with exogenous metal ions.
Copper(II) complexes with nitrogen ligands such as 1,10-phenanthroline (**phen**) show cytotoxic activity against a panel of human tumour cell lines.[T. Pivetta *et al* J. Inorg. Biochem. 2012; T. Pivetta et al.; *Talanta* 2013].
Ternary complexes of 1,10-phenanthroline-5,6-dione (**phendione**) with copper(II) show interesting cytotoxic activity against human kidney adenocarcinoma and human hepatocellular carcinoma cell lines. [3] Many other phen derivatives, alone or in complexes, have been tested for antitumour activity towards human ovarian carcinoma, melanoma and breast, colon, ovarian, renal and non-small-cell lung cancer. [S. Roy *et al.* Chem Med Chem, 2008; S. Betanzos-Lara *et al.*, J. Biol. Inorg. Chem. 2012; A. N. Wein *et al*., J. Inorg. Biochem. 2011].
On this basis, we decided to study the differences in chemical behavior and anti – proliferative activity of a new family of copper(II) complexes with **phendione** and 1,10-phenanthroline-5,6-diol (**phendiol**). Complexes with **phen** were also prepared and studied for comparison.

The results of this study had already been published in the Journal of Inorganic Biochemistry (2014) attached below.
Link at the published article: http://www.ncbi.nlm.nih.gov/pubmed/25238635.

Journal of Inorganic Biochemistry 141 (2014) 103–113

Contents lists available at ScienceDirect

Journal of Inorganic Biochemistry

journal homepage: www.elsevier.com/locate/jinorgbio

Novel copper(II) complexes as new promising antitumour agents. A crystal structure of [Cu(1,10-phenanthroline-5,6-dione)$_2$(OH$_2$)(OClO$_3$)](ClO$_4$)

Tiziana Pivetta [a,*], Federica Trudu [a], Elisa Valletta [a], Francesco Isaia [a], Carlo Castellano [b], Francesco Demartin [b], Rossana Tuveri [c], Sarah Vascellari [c], Alessandra Pani [c]

[a] Dipartimento di Scienze Chimiche e Geologiche, University of Cagliari, Cittadella Universitaria, 09042 Monserrato, CA, Italy
[b] Dipartimento di Chimica, University of Milano, Via C. Golgi, 19-20133 Milano, Italy
[c] Dipartimento di Scienze Biomediche, University of Cagliari, Cittadella Universitaria, 09042 Monserrato, CA, Italy

ARTICLE INFO

Article history:
Received 13 May 2014
Received in revised form 22 August 2014
Accepted 24 August 2014
Available online 4 September 2014

Keywords:
Copper complexes
Cytotoxicity
Solution equilibria
Crystal structure
DNA binding

ABSTRACT

The cytotoxic properties of copper(II) complexes with 1,10-phenanthroline (phen) can be modified by substitution in the phen backbone. For this purpose, Cu(II) complexes with phen, 1,10-phenanthrolin-5,6-dione (phendione) and 1,10-phenanthrolin-5,6-diol (phendiol) have been synthesised and characterised. The crystal structure of [Cu(phendione)$_2$(OH$_2$)(OClO$_3$)](ClO$_4$) is discussed. The complex formation equilibria between Cu(II) and phen or phendione were studied by potentiometric measurements at 25 and 37 °C in 0.1 M ionic strength (NaCl). The antitumour activity of the compounds has been tested *in vitro* against a panel of tumour (DU-145, HEP-G2, SK-MES-1, CCRF-CEM, CCRF-SB) and normal (CRL-7065) human cell lines. The studied compounds generally present an antiproliferative effect greater than that of cisplatin. The phen and phendione ligands present a similar antiproliferative effect against all the tested cells. Phendiol presents an antiproliferative effect 1.3 to 18 times greater than that of phen or phendione for leukemic, lung, prostatic and fibroblast cells, while it presents less activity towards hepatic cells. Complexes with two ligands are more cytotoxic towards all the tested cell lines than complexes with one ligand and are generally more cytotoxic than the ligand alone. Complexes [Cu(phendiol)$_2$(OH$_2$)](ClO$_4$)$_2$ and [Cu(phendione)$_2$(OH$_2$)(OClO$_3$)](ClO$_4$) appear to be the most active compounds for the treatment of SK-MES-1 and HEP-G2 cells, respectively, being at least 18 times more cytotoxic than cisplatin. The studied Cu(II) complexes are characterised by a strong DNA affinity and were found to interact with DNA mainly by groove binding or electrostatic interactions. The complexes appear to act on cells with a mechanism different from that of cisplatin.

1. Introduction

Copper is a metal ion essential for aerobic microorganisms, plants and animals. It binds molecular oxygen in oxygen-transport proteins and participates in electron transport [1]. In the human body the copper concentration level is regulated by the homeostatic system. Copper has been selected for the synthesis of new antitumour drugs since complexes containing essential metal ions, thanks to the homeostatic regulatory system, may produce less systemic toxicity than complexes with exogenous metal ions. Copper(II) complexes with nitrogen ligands such as 1,10-phenanthroline (phen) show cytotoxic activity against a panel of human tumour cell lines [2–4]. Also complexes of 1,10-phenanthroline-5,6-dione (phendione) with copper(II) show interesting cytotoxic activity against human kidney adenocarcinoma and human hepatocellular carcinoma cell lines [5,6]. Many other phen derivatives, alone or in complexes, have been tested for antitumour activity towards human ovarian carcinoma, melanoma and breast, colon, ovarian, renal and non-small-cell lung cancers [7–10].

Being the DNA an important target for several cytotoxic agents, the interaction of metal complexes containing phenanthroline derivatives with DNA has also been studied. In fact, DNA offers multiple binding sites and modes for covalent and non-covalent interactions. Cisplatin binds covalently DNA [11], but most of the metal complexes bind DNA by non-covalent interactions, i.e. by intercalation, groove bindings, electrostatic forces and hydrogen bonds [12,13]. Some ruthenium complexes with phenanthroline ligands cleave DNA via a proton-coupled electron transfer mechanism [14]. The DNA-interaction modes can be studied by UV–visible (UV–vis) absorption study as the intercalation is associated with hypochromism and red shifting of the DNA adduct absorption bands, while groove binding and electrostatic interactions are associated with hyperchromism [15]. The cytotoxic properties and the DNA binding of copper(II) complexes with phen may be influenced also by the substituents eventually present on the phen backbone.

In this work, a new family of copper(II) complexes with phendione and 1,10-phenanthroline-5,6-diol (phendiol) has been synthesised

* Corresponding author. Tel./fax: +39 0706754473.
E-mail address: tpivetta@unica.it (T. Pivetta).

http://dx.doi.org/10.1016/j.jinorgbio.2014.08.011
0162-0134/

and characterised by determining their chemical speciation in aqueous media, as well as their cytotoxicity and their DNA binding properties. Analogue series of complexes with phen was also prepared and studied for comparison.

2. Experimental section

2.1. Reagents

Calf thymus DNA sodium salt, chloridric acid standard solutions, copper(II) carbonate basic ($Cu_2(CO_3)(OH)_2$), copper(II) chloride, dichloromethane, dimethyl sulphoxyde (DMSO), dithiooxamide, ethanol, ethyl ether, ethylenediaminetetraacetic acid, isopropanol, nitric acid, petroleum ether, perchloric acid, 1,10-phenanthroline monohydrate, 1,4-piperazinediethanesulfonic acid (PIPES), potassium bromide, potassium hydroxide, sodium chloride, sodium hydroxide, sodium perchlorate, sodium sulphate anhydrous and sulphuric acid were purchased from Sigma-Aldrich and used without any further purification. Caution: perchlorate complexes are potentially explosive. Handle these compounds in small quantities with care.

2.2. Synthesis

2.2.1. Preparation of 1,10-phenanthroline-5,6-dione (phendione)

An ice-cold solution of concentrated HNO_3 (18 mL) and H_2SO_4 (35 mL) was added drop-wise to a mixture of phen (3.6 g, 18 mmol) and KBr (3.2 g, 27 mmol) in an ice bath (Scheme 1). The mixture was then refluxed until dark-red vapours disappeared (approx. 4 h). The light yellow solution was poured over 200 mL of ice and then neutralized by addition of a saturated solution of KOH. The presence of a white precipitate of inorganic salts was observed depending on solution concentration. The solids were filtered off and repeatedly washed with CH_2Cl_2. The desired product was extracted from the aqueous solution with fresh CH_2Cl_2. The extracted phases were combined with the portions of CH_2Cl_2 used for washing. The remaining water was removed with anhydrous Na_2SO_4. The yellow product phendione was recovered by solvent evaporation under vacuum. Yield 82%. I.R. selected bands (cm^{-1}): 2959, 2927, 2874 C–H stretching (broad, medium strong); 1688 C=O stretching (sharp, medium); 1567, 1461, 1415 C=C stretching (sharp, medium strong); and 813, 739, 623 C=C–H bending (sharp, medium). Elemental analysis: calc. C% 68.57, H% 2.88, N% 13.33, found C% 68.65, H% 2.92, and N% 13.36.

2.2.2. Preparation of 1,10-phenanthroline-5,6-diol (phendiol)

An ethanol solution (15 mL) of phendione (0.1 g, 0.48 mmol) and dithiooxamide (0.58 g, 0.48 mmol) was refluxed for 16 h. The resulting yellow solid was recovered by filtration, washed in sequence with ethanol, CH_2Cl_2 and petroleum ether and air dried. Yield 82%. I.R. selected bands (cm^{-1}): 2966, 2927, 2718, 2622 C–H stretching (broad, strong); 1575, 1497, 1426 C=C stretching (sharp, medium strong); and 806, 739, 629 C=C–H bending (sharp, medium). Elemental analysis: calc. C% 67.92, H% 3.80, N% 13.20, found C% 67.54, H% 3.84, N% 13.18.

2.2.3. Preparation of $Cu(phendione)(OH_2)_2(ClO_4)_2$ (K1)

Concentrated perchloric acid was added to an isopropanolic suspension of $Cu_2(CO_3)(OH)_2$ (0.110 g, 0.50 mmol of copper, 10 mL) warming under stirring till the complete dissolution of the salt was achieved. The light blue solution was cooled at room temperature and an isopropanolic solution of phendione (0.050 g, 0.24 mmol, 10 mL) was added drop-wise under stirring. The resulting light blue solution was left at room temperature and a light blue product was recovered after solvent evaporation. Yield 79%. I.R. selected bands (cm^{-1}): 3400 O–H stretching (broad, weak); 2955, 2927, 2853 C–H stretching (broad, weak); 1585, 1521, 1418 C=C stretching (sharp, medium strong); 1146, 1111, 1086 Cl–O stretching of coordinating perchlorate group (broad, very strong); 852, 717 C=C–H bending (sharp, medium strong), 627 C=C–H bending and OClO deforming (sharp, medium strong). Elemental analysis: calc. C% 28.33, H% 1.98, N% 5.51, found C% 29.22, H% 2.01, and N% 5.48.

2.2.4. Preparation of $[Cu(phendione)_2(OH_2)(OClO_3)](ClO_4)$ (K2)

Concentrated perchloric acid was added to an isopropanolic suspension of $Cu_2(CO_3)(OH)_2$ (0.044 g, 0.20 mmol of copper, 10 mL) warming under stirring till the complete dissolution of the salt was achieved. The light blue solution was cooled at room temperature and an isopropanolic solution of phendione (0.084 g, 0.40 mmol, 10 mL) was added drop-wise under stirring. The green precipitate of **K2** was filtered, washed with isopropanol and dried under vacuum. The solid was dissolved in ethanol and allowed to crystallise at room temperature. After four days green crystals suitable for X-ray analysis were recovered. Yield 81%. I.R. selected bands (cm^{-1}): 3450 O–H stretching (broad, weak); 2923, 2856 C–H

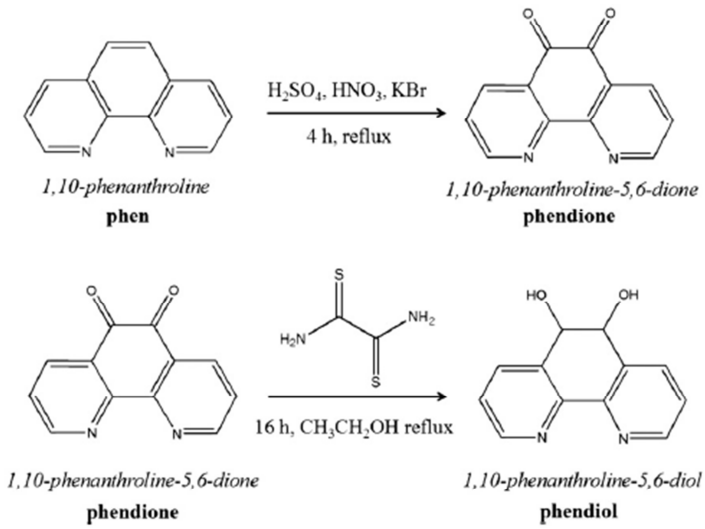

Scheme 1. Synthetic route for the preparation of 1,10-phenanthroline-5,6-dione (phendione) and 1,10-phenanthroline-5,6-diol (phendiol).

stretching (broad, weak); 1585, 1521, 1425 C=C stretching (sharp, medium); 1146, 1093 Cl–O stretching non coordinating perchlorate group (broad, very strong); 856, 725 C=C–H bending (sharp, medium strong), 625 C=C–H bending and OClO deforming (sharp, medium strong). Elemental analysis: calc. C% 41.13, H% 2.01, N% 7.99, found C% 41.44, H% 2.04, and N% 7.95.

2.2.5. Preparation of $Cu(phendiol)(OH_2)_2(ClO_4)_2$ (I1)

Concentrated perchloric acid was added to an isopropanolic suspension of $Cu_2(CO_3)(OH)_2$ (0.104 g, 0.47 mmol of copper, 10 mL) warming under stirring till the complete dissolution of the salt was achieved. The light blue solution was cooled at room temperature and an ethanolic suspension of phendiol (0.100 g, 0.47 mmol, 10 mL) was added. The dark green solution was refluxed for half an hour and cooled at room temperature. The dark green precipitate of **I1** was filtered under vacuum, washed with isopropanol and petroleum ether and air dried. Yield 46%. I.R. selected bands (cm^{-1}): 3400 O–H stretching (broad, strong); 3079, 2923, 2852 C–H stretching (broad, weak); 1086, 1070 Cl–O stretching of coordinating perchlorate group (broad, very strong); 834, 809, 718 C=C–H bending (sharp, medium strong), 626 C=C–H bending and OClO deforming (sharp, medium strong). Elemental analysis: calc. C% 28.22, H% 2.37, N% 5.49, found C% 28.78, H% 2.22, and N% 5.42.

2.2.6. Preparation of $Cu(phendiol)_2(OH_2)(ClO_4)_2$ (I2)

Concentrated perchloric acid was added to an isopropanolic suspension of $Cu_2(CO_3)(OH)_2$ (0.051 g, 0.23 mmol of copper, 10 mL) warming under stirring till the complete dissolution of the salt was achieved. The light blue solution was cooled at room temperature and an isopropanolic suspension of phendiol (0.098 g, 0.46 mmol, 10 mL) was added drop wise under stirring. The dark green product obtained was filtered under vacuum, washed with isopropanol, and air dried. Yield 75%. I.R. selected bands (cm^{-1}): 2958, 2930, 2874 C–H stretching (broad, medium); 1606, 1514, 1432 C=C stretching (medium broad, medium); 1117, 1090 Cl–O stretching non coordinating perchlorate group (broad, very strong); 820, 728 C=C–H bending (sharp, medium strong), 628 C=C–H bending and OClO deforming (sharp, medium strong). Elemental analysis: calc. C% 40.90, H% 2.57, N% 7.95, found C% 41.25, H% 2.66, and N% 7.99.

2.2.7. Preparation of $[Cu(phen)_2(OH_2)](ClO_4)_2$ (C0) and $[Cu(phen)(OH_2)_2(OClO_3)_2]$ (C10)

The synthesis of **C0** and **C10** were previously reported [2].

2.3. Determination of the crystal structure of K2

$C_{24}H_{14}Cl_2CuN_4O_{13}$, M = 700.83 g/mol, orthorhombic, $a = 14.174(3)$, $b = 16.440(3)$, $c = 22.350(5)$ Å, $U = 5208(2)$ Å^3, $T = 293$ K, space group *Pbca* (no. 61), Z = 8, μ = (Mo–Kα) 1.125 mm^{-1}. 52,523 reflections (8383 unique; $R_{int} = 0.0282$) were collected at room temperature in the range $3.64° < 2\vartheta < 63.30°$, employing a $0.30 \times 0.15 \times 0.12$ mm crystal mounted on a Bruker APEX II CCD diffractometer and using graphite-monochromatized Mo–Kα radiation ($\lambda = 0.71073$ Å). Final *R1* [*wR2*] values are 0.0584 [0.2055] on $I > 2\sigma(I)$ (all data). Datasets were corrected for Lorentz polarization effects and for absorption (SADABS, Siemens Area-Detector ABSorption correction program, Bruker AXS Inc. Madison, WI, USA 2000). The structure was solved by direct methods [16] and was completed by iterative cycles of full-matrix least squares refinement on F_o^2 and ΔF synthesis using the SHELXL-97 [17,18]. Hydrogen atoms, with the exception of those of the water molecule, were located on the ΔF maps and allowed to ride on the carbon atoms of the phendione ligand. Crystallographic data for compound **K2** (excluding structure factors) have been deposited with the Cambridge Crystallographic Data Centre as supplementary publication no. CCDC-977445. These data can be obtained free of charge via www.ccdc.cam.ac.uk/conts/retrieving.html.

2.4. Biological assays

2.4.1. Compounds

Stock solutions of test compounds were prepared in DMSO at 100 mM and stored at 4 °C in the dark. For evaluation of the cytotoxicity, stocks were serially diluted in the growth media specific for each cell line. In all experiments, the highest concentration of DMSO on cells was 0.1%, corresponding to the maximum non-toxic dose of DMSO for all cell lines.

2.4.2. Cell lines

All cell lines used in this study were purchased from the American Type Culture Collection (ATCC, USA), and were stored in aliquots in liquid nitrogen between the third to the fourth passage in culture. Cell lines derived from human lung squamous carcinoma (SK-MES-1), human prostate carcinoma (DU-145), and human hepatocellular carcinoma (Hep-G2), were used as representative cells of solid cancers. Human acute T-lymphoblastic leukaemia (CCRF-CEM) and human acute B-lymphoblastic leukaemia (CCRF-SB) cell lines were used as representative cells of hematologic tumours. A cell line established from human normal skin fibroblasts (CRL-7065) was used as a control cell line to determine the degree of selectivity of each compound towards neoplastic cells. All cell lines were cultured at 37 °C in a 5% CO_2 atmosphere in their specific media according to ATCC instructions, with 5–10% foetal bovine serum (FBS), antibiotic, and, unless otherwise indicated, sodium pyruvate. Cell cultures were maintained in exponential growth by periodically (one to two times/week) diluting high density non-adherent cells (i.e. 10^6 cell/mL), or when monolayers of adherent cells reached sub-confluency (70–90% confluence). All cell lines were replaced every three–four months by freshly thawed cells from liquid nitrogen collections. The absence of mycoplasma contamination was checked periodically by the Hoechst staining method [19].

2.4.3. Cytotoxic assays

The cytotoxic effect of test compounds was evaluated in exponentially growing cells. For adherent cells (i.e. SK-MES, DU-145, Hep-G2, CRL-7065), 100 μL of cell suspensions at a density of 5×10^4 cells/mL was seeded in each well of 96-well flat bottomed plates. Cell cultures were incubated overnight before the addition of 100 μL of growth medium (controls) or of 2× the final concentrations of test compounds (four replicates/concentration). For non-adherent cells (i.e. CCRF-CEM and CCRF-SB), 100 μL of cell suspensions at a density of 1×10^5 cells/mL was seeded in 96-well flat bottomed plates, and equal volumes of growth medium (controls) or of 2× the final concentrations of each compound (four replicates/concentration) were immediately added. Cell viability was determined after 96 h (approximately three to four cell divisions) of incubation at 37 °C, 5% CO_2, by the 3-(4,5-dimethylthiazol-2-yl)-2,5-diphenyl-tetrazolium bromide (MTT) method as previously described [20]. Cisplatin was used as reference drug [21–23]. The extent of cell viability at each drug concentration tested was expressed as percentage of untreated controls. Dose–response curves and concentrations resulting in 50% of cell viability of cells, compared to the controls, were determined for each compound by non-linear curve fitting. All data reported represent the mean values ± SD of three to four independent experiments.

2.5. DNA binding

The binding constants (K_b) between ct-DNA and the phen, phendione and Cu(II) complexes were determined at 25 °C by spectrophotometric titrations with ct-DNA, in PIPES buffer 0.01 M at pH 7.0. The UV–vis measurements were carried out on an Agilent Cary 60 spectrometer equipped with a fibre optic dip probe (1 cm path length). A stock solution of ct-DNA in 0.01 M PIPES buffer at pH 7.0 was stored at 4 °C and used within four days. The concentration of DNA per nucleotide was determined by UV absorption at 260 nm using its molar absorption

coefficient (6600 M^{-1} cm^{-1}) [24]. The purity of the DNA was checked by monitoring the ratio of the absorbance at 260 nm to that at 280 nm. A ratio higher than 1.8 indicated a DNA sufficiently protein-free [25].

Two sets of solutions were prepared: i) thirty solutions containing a fixed amount of ligand or metal complex (ranging from $\approx 1.5 \times 10^{-6}$ to $\approx 8 \times 10^{-5}$ mmol, according to compound absorptivity) and variable amounts of DNA (ranging from 4.5×10^{-5} to 2.4×10^{-4} mmol, DNA/complex molar ratio from 0 to 3); ii) twenty solutions containing a fixed amount of ligand or metal complex (ranging from $\approx 6.5 \times 10^{-6}$ to $\approx 3.6 \times 10^{-5}$ mmol, according to compound absorptivity) and variable amounts of DNA (ranging from 6.5×10^{-5} to 3.6×10^{-4} mmol, DNA/complex molar ratio from 0 to 10). All the solutions were stored in the dark at room temperature. The hydrolysis of the copper complexes as well as the interaction between DNA and ligands were slow processes. Therefore, spectra in the 200–400 nm range were recorded after equilibration was reached. This was checked spectrophotometrically, by determining the time after which further changes in UV–vis spectra were not observed (≈15 h).

The number of linearly independent absorbing species was obtained by applying the eigenvalues analysis on the absorbance data matrix [26,27]. Binding constants were obtained by using the Hyperquad 2003 program [28].

2.6. Potentiometric study

Potentiometric titrations were carried out in a thermostatted vessel with a Mettler-Toledo Seven Compact pH/Ion-meter equipped with a Mettler-Toledo InLab Micro Pro combined glass electrode with an integrated temperature probe. Potentiometric titrations were performed at 25 and 37 °C in 0.1 M ionic strength (NaCl) under N_2 atmosphere. The glass electrode was calibrated daily by titration of a known amount of HCl with carbonate-free NaOH solution prepared according to Albert [29]. Electrode standard potential (E^0), water ionic product (pK_w), electrode response and carbonate content of the titrant solution were checked with Gran's procedure [30] using the Glee program [31].

The copper(II) stock solution was prepared by dissolving the proper amount of $CuCl_2$ salt in 0.01 M HCl aqueous solution (pH ≈ 2, copper(II) concentration $\approx 5 \times 10^{-3}$ M). The metal content was determined by titration with EDTA [32]. A solution of phendione was prepared daily by dissolving the proper amount of the compound in freshly distilled water (concentration of phendione $\approx 4 \times 10^{-3}$ M). Due to its low water solubility, phen (≈0.03 g) was dissolved in 20 μL of DMSO. The resulting solution was diluted with freshly distilled water up to 20 mL. The mixing of the two solvents was favoured by gentle shaking and heating (avoiding sonication to prevent emulsion formation). For the potentiometric titration, approx. 3 mL of this stock solution was diluted up to 20 mL with aqueous solution, so that the DMSO content in the titration vessel was never higher than 0.015% (final concentration of phen $\approx 5 \times 10^{-3}$ M).

Ligand protonation constants were determined by titrating solutions containing a known amount of ligand and three (for phen) or five (for phendione) equivalents of HCl per mole of ligand. Complex formation constants between phen or phendione with Cu(II) were determined by titrating solutions with 3:1, 2:1 and 1:1 ligand:metal molar ratios. The hydrolysis of the metal ion was studied at 1.0×10^{-3} M, 5.0×10^{-4} M and 3.3×10^{-4} M concentrations. The reversibility of all the studied equilibria was checked by back-titration with standard HCl. The overall stability constants were determined with the Hyperquad2003 program [28].

2.7. Computation

The quantomechanical calculations were performed on a dual core INTEL i-7 CPU with the "SPARTAN'06" program for Windows (Wavefunction Inc); geometries were optimized using ab-initio methods with 6–31G^{++} Gaussian basis sets [33,34]; dipole moments were calculated using semi-empirical methods with AM1/SM2 basis sets [35].

3. Results and discussion

3.1. Synthesis

The ligands phendione and phendiol were synthesised (Scheme 1) by slight modifications of previously reported syntheses [36,37]. A less toxic solvent was preferred for the extraction and washing steps. Compound phendiol is slightly soluble in the most common solvents such as CH_3CN, CH_2Cl_2, DMSO, dimethylformamide, ethanol, isopropanol, petroleum ether and water. Despite the presence of two hydroxyl groups, its solubility in polar solvents is reduced due to the formation of polymers. Phendiol is water soluble at basic pH but is rapidly and irreversibly oxidised.

Complexes $Cu(phen)(OH_2)_2(ClO_4)_2$ (**K1**), $[Cu(phendione)_2(OH_2)(OClO_3)](ClO_4)$ (**K2**), $Cu(phendione)(OH_2)_2(ClO_4)_2$ (**I1**), and $Cu(phendione)_2(OH_2)(ClO_4)_2$ (**I2**) are novel. No polynuclear complexes with phendione or phendiol were obtained, not even in an excess of Cu(II) salt. All the complexes are stable in the solid state at room temperature. Suspensions of **I1** and **I2** are stable in the dark at 4 °C for one week. In compounds **K1** and **I1**, one ligand is present like in **C10**, while two ligands are present in compound **I2**, as in **C0**. The I.R. spectra of **K1** and **I1** show the signals of coordinating perchlorate groups, while the I.R. spectrum of **I2** shows the signals of uncoordinated perchlorate groups. By analogy with the reported structures of **C10** and **C0** [2], the molecular formulas $[Cu(phendione)(OH_2)_2(OClO_3)_2]$, $[Cu(phendiol)(OH_2)_2(OClO_3)_2]$ and $[Cu(phendiol)_2(OH_2)](ClO_4)_2$ for **K1**, **I1** and **I2** are proposed.

3.2. Crystal structure

The asymmetric unit of **K2** contains $Cu(phendione)_2(OH_2)(OClO_3)^+$ cations with the copper atoms in a distorted tetragonal bypiramidal coordination and an additional perchlorate anion (Fig. 1). Selected bond lengths and angles are reported in Table 1. The Cu – O_2 distance in the perchlorate coordinated at the apical position is longer than typical Cu – O bond lengths of about 1.95 Å, but lies in the 2.3–2.8 Å range observed for complexes with Jahn–Teller distortion (mean axial Cu – O bond lengths for Jahn–Teller distorted complexes are about 2.48 Å). The axially-coordinated perchlorate displays an additional intramolecular hydrogen bond with the equatorial water molecule [O4···Ow 3.076(9) Å]. The other perchlorate interacts with the water molecule only through an intramolecular hydrogen bond O8···Ow of 2.698(8) Å. No other interactions below the sum of the van der Waals radii are observed. One of the two phendione ligands occupies two equatorial positions of the octahedron with atoms N1 and N2, whereas the other one is coordinated at one equatorial position through N4 and at one apical position through N3. The copper atom is about 0.20 Å displaced from the average coordination plane defined by atoms N1, N2, N4 and Ow, towards the apical position N3. The dihedral angle between the two nitrogen ligands is 78.6°. A comparison can be done with the structure of the similar complex $[Cu(phen)_2(H_2O)](ClO_4)_2$ [2,38], where instead the coordination of the copper ion is closer to a trigonal bipyramidal geometry and no perchlorate anion interacts with the metal ion. With respect to this compound the Cu – Ow distance is definitely shorter in our case (2.026(3) Å vs. 2.245(4) Å), whereas the Cu – N distances are larger [range 2.003(2)–2.187(3) 1.993(2) Å vs. 1.980(4)–2.032(3) Å)]. A structure similar to that of **K2** was reported for $[Co(phendione)_2Cl_2]Cl$ where the central Co(III) ion is hexacoordinated with distorted octahedral geometry. The mean Co – N bond length is 1.944(3) Å which is shorter than the Cu – N bond length in **K2** [39]. Differently, in the crystal structures of $[Cu(phendione)_2(NO_3)]NO_3 \cdot CH_3CN$ or $[Cu(phendione)_2Br]Br \cdot 2CH_3CN$, the copper ion is coordinated by two phendione

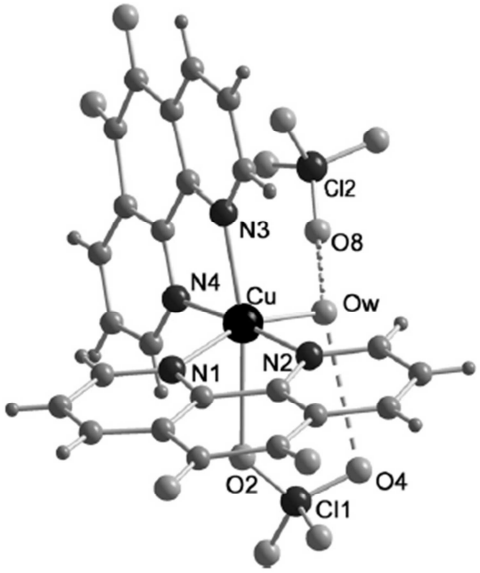

Fig. 1. Crystal structure of **K2** complex.

molecules and a nitrate or a bromide ligand in a distorted trigonal bipyramidal geometry [40]. An example of crystal structure of a metal complex with phendiol is [(di-tert-butylbipyridine)$_2$Ru(phendiol)Pt(di-tert-butylbipyridine)](PF$_6$)$_2$, where phendiol molecule acts as a linker between Ru(di-tert-butylbipyridine)$_2$- and Pt(di-tert-butylbipyridine)-units [37].

3.3. Dipole moments of ligands

The low water solubility of phendiol prevents accurate determination of its octanol/water partition coefficient. Thus, to discriminate the polarity and lipophilicity/hydrophilicity of the ligands, dipole moments in aqueous medium were calculated by quantum mechanical calculations. The calculated dipole moments for the three ligands are in the following order: phendiol (3.52 Debye) > phen (3.42 Debye) > phendione (3.11 Debye).

Table 1
Selected bond lengths (Å) and angles (deg) for **K2**. In parenthesis the standard deviation on the last significant figure is reported.

Atom1	Atom2	Length
Cu	N1	2.040 (2)
Cu	N2	2.003 (2)
Cu	N3	2.187 (3)
Cu	N4	2.019 (2)
Cu	OW	2.026 (3)
Cu	O2	2.667 (4)

Atom1	Atom2	Atom3	Angle
N1	Cu	N2	81.6 (1)
N1	Cu	N3	101.28 (9)
N1	Cu	N4	97.7 (1)
N1	Cu	OW	160.2 (1)
N1	Cu	O2	77.0 (1)
N2	Cu	N3	106.11 (9)
N2	Cu	N4	175.4 (1)
N2	Cu	OW	89.9 (1)
N2	Cu	O2	85.9 (1)
N3	Cu	N4	78.5 (1)
N3	Cu	OW	98.2 (1)
N3	Cu	O2	167.6 (1)
N4	Cu	OW	89.3 (1)
N4	Cu	O2	89.5 (1)
OW	Cu	O2	84.6 (1)

Table 2
Antiproliferative activity of the test compounds against six different cell lines. The standard deviation on the last significant figure is given in parentheses.

Compound	IC_{50}[a] (μM)					
	CRL-7065[b]	DU-145[c]	HEP-G2[d]	SK-MES-1[e]	CCRF-CEM[f]	CCRF-SB[g]
Phen	2.3 (1)	2.30 (5)	1.7 (2)	2.60 (4)	2.70 (2)	1.20 (1)
Phendione	1.90 (2)	2.16 (2)	1.60 (2)	1.90 (1)	2.90 (1)	0.95 (1)
Phendiol	1.80 (2)	0.79 (1)	2.90 (1)	0.47 (1)	0.15 (1)	0.145 (4)
C10	>5	2.6[j]	2.90 (3)	1.9[j]	3.2[j]	1.4[j]
K1	6.30 (1)	4.10 (1)	1.70 (2)	3.10 (1)	3.80 (2)	1.21 (1)
I1	3.10 (1)	4.00 (2)	3.60 (1)	2.25 (2)	0.18 (1)	0.20 (1)
C0	2.20 (3)	1.6[j]	1.05 (1)	0.93[j]	1.25[j]	0.50[j]
K2	2.47 (2)	1.16 (2)	0.67 (2)	1.20 (1)	0.80 (2)	0.42 (1)
I2	1.34 (3)	0.93 (1)	1.20 (1)	0.54 (1)	0.090 (4)	0.070 (3)
6-MP[h]	–	2.0 (1)	–	> 100	2.0 (2)	0.70 (8)
Cisplatin	–	2.0[k]	12.0[l]	20.0[m]	0.95	1.38

[a] compound concentration required to reduce the viability by 50%, as determined by the MTT method.
[b] CRL-7065 skin fibroblasts.
[c] DU-145 human prostate carcinoma.
[d] HEP-G2 human hepatocellular carcinoma.
[e] SK-MES-1 squamous cell lung carcinoma.
[f] CCRF-CEM human acute T-lymphoblastic leukaemia.
[g] CCRF-SB human acute B-lymphoblastic leukaemia.
[h] 6-MP 6-mercaptopurine.
[i] From Ref. [2].
[j] From Ref. [4].
[k] from Ref. [21].
[l] From Ref. [22].
[m] From Ref. [23]. Values represent the mean ± SD of at least three independent experiments.

3.4. Cytotoxic activities

The antiproliferative activities of the studied ligands and complexes are expressed as IC_{50}, i.e. the concentration of compound required to reduce the viability of the tested cells by 50% (Table 2).

3.4.1. Phen, phendione and phendiol ligands

The phen and phendione ligands present very similar antiproliferative effects against all the tested cells (Fig. 2). For phen the IC_{50} value ranges from 1.20 to 2.70 μM, while for phendione it ranges from 0.95 to 2.90 μM. Both compounds are more active against CCRF-SB leukemic cells. The phendiol compound presents an antiproliferative effect from 1.3 to 18 times greater than that of phen or phendione for leukemic, lung, prostatic and fibroblast cells, while it presents less activity towards hepatic cells. The cellular microenvironment appears related to the cytotoxicity shown by the ligands. In fact, their different activities on solid and/or haematological cancer cells can be explained in terms of the lipophilicity or hydrophilicity of the compound and the target cells.

The tested cells are derived from human organs characterised by different physical–chemical conditions. In prostate, blood and lungs the microenvironment is mainly hydrophilic while in liver and fibroblasts it is mainly lipophilic.[1] However, the phenotype, metabolic reactions and

[1] Prostatic cells produce a slightly acidic solution containing citric acid, spermine and spermidine, acid phosphatase, protease serum, prostate-specific antigen, calcium, zinc, sodium and dihydrotestosterone. Liver is involved with carbohydrate and lipid metabolism, cholesterol synthesis and triglyceride production. Plasma (55 % of blood fluid) contains water, dissipated proteins, glucose, mineral ions, hormones, and blood cells themselves. Lungs, involved in the CO_2/O_2 exchange, contain blood and aqueous vapour. Fibroblasts produce collagen, glycosaminoglycan, fibres and glycoproteins that are constituents of the extracellular material.

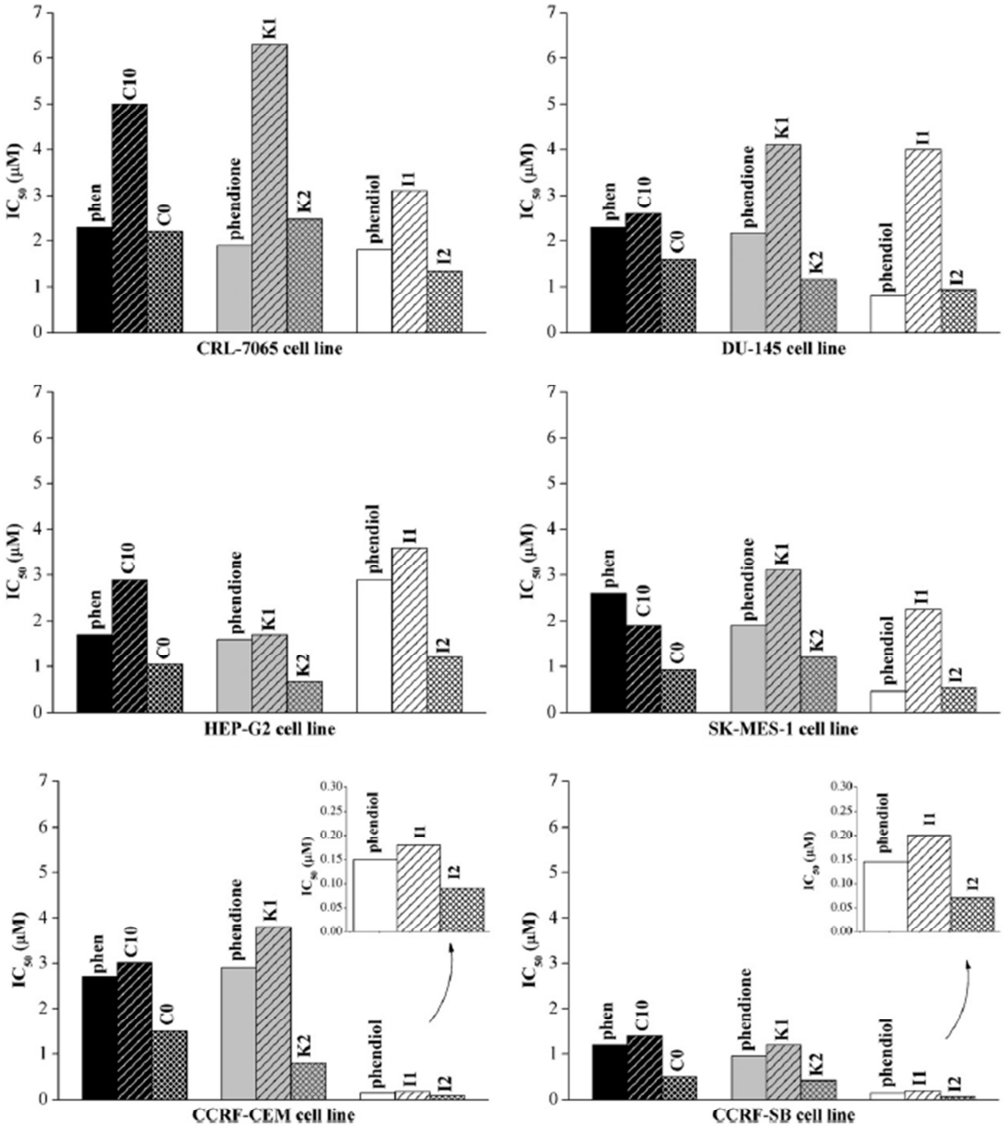

Fig. 2. Doses (IC_{50} values, μM) of the studied complexes required to reduce the viability by 50%, as determined by the MTT method. CRL-7065 skin fibroblasts; DU-145 human prostate carcinoma; HEP-G2 human hepatocellular carcinoma; SK-MES-1 squamous cell lung carcinoma; CCRF-CEM human acute T-lymphoblastic leukaemia; CCRF-SB: human acute B-lymphoblastic leukaemia.

gene expression patterns of the original organ may not be preserved in cultured cells. In our case, the experimental results, i.e. the different activities shown by the ligands, indicate that microenvironmental conditions in the cell lines reflect those of the original organ from which they were derived. This phenomenon has also been observed in other studies, for example in terms of pH and vacuolar-H-ATPase expression [41]. The less lipophilic ligand, phendiol, is preferentially active against cells in a hydrophilic environment, while the most lipophilic ligand phendione is more effective than phendiol against cells in a lipophilic one.

3.4.2. Copper(II) complexes

The cytotoxicity of the studied copper(II) complexes (Fig. 2) is mainly due to the presence of the nitrogen containing ligands, the metal ion being devoid of relevant antiproliferative activity (IC_{50} > 100 μM). Complexes with one ligand (**C10**, **K1** and **I1**) exhibit an antiproliferative activity generally lower than that of the ligand alone (phen, phendione and phendiol, respectively) on all tested cell lines. The **C10**, **K1** and **I1** compounds present the highest cytotoxic activity against CCRF-SB cells and the lowest towards CRL-7065 and DU-145 cells. Complexes with two ligands (**C0**, **K2** and **I2**) are more cytotoxic towards all the tested cell lines than the related complexes with one ligand (**C10**, **K1** and **I1**, respectively) and are generally more cytotoxic than the ligand alone (phen, phendione and phendiol, respectively). The **C0**, **K2** and **I2** compounds present the highest cytotoxic activity against CCRF-SB and the lowest towards CRL-7065 cells.

Although it is not possible to make a direct comparison between the antiproliferative activities against normal and cancerous cells that belong to different lineages, the parallel could be useful in estimating the possible selectivity of a compound, i.e. the ability of the drug to discriminate between normal and cancerous cells. The potential selectivity, calculated with respect to the normal fibroblasts, varies from 1.7 to 3.6 for **C10**, from 1.4 to 4.4 for **C0**, from 1.5 to 5.2 for **K1**, from 2.1 to 5.9 for **K2**, from 0.78 to 17.2 for **I1** and from 1.1 to 19.1 for **I2**. From all these results **I2** appears as the most active compound for the treatment of leukemic (CCRF-CEM and CCRF-SB), lung (SK-MES-1) and prostatic (DU-145) cancer cells, while **K2** is eligible for the treatment of hepatic (HEP-G2) ones.

3.5. DNA binding constants

The intrinsic binding constants of the adducts formed by ct-DNA and the studied compounds were evaluated by spectrophotometric titrations. The binding constants of phendiol were not studied because of the poor solubility of the ligand in PIPES. The UV–vis spectra of the synthesised copper(II) complexes exhibit bands at ≈800 nm (d–d transitions, $\varepsilon \approx 100\ M^{-1}\ cm^{-1}$) and at ≈270 nm (ligand-to-metal charge transfer (LMCT) transitions, $\varepsilon \approx 50{,}000\ M^{-1}\ cm^{-1}$). Due to the low absorption at 800 nm, only the changes in the LMCT bands were followed during the titrations with DNA. In the absorbance spectra of **C10**, **K1** and **C0** two peaks (at ≈ 225 and 275 nm) and a shoulder (at ≈ 295 nm) are present. In the spectrum of **K2** two pairs of overlapping peaks (at 260 and 272 nm and at 226 and 232 nm) and a shoulder (at 295 nm) are evident.

In the absorbance spectrum of **I1** a wide band is present at 267 nm and, finally, in the spectrum of **I2** two partially overlapping bands are present at 258 and 280 nm. The UV spectra of phen and phendione show peaks at 266 nm and 254 nm, respectively.

By titrating the ligands and Cu(II) compounds with DNA, the following trends were shown:

- the absorbance increases without a significant shift in the maximum wavelength for phen and phendione;
- for DNA:Cu(II) molar ratios in 0–3 range:
  - o the absorbance increases without a significant shift in the maximum wavelength for **C10**, **K1**, **K2** and **I2**;
  - o the absorbance increases with a significant shift in the maximum wavelength for **I1** (from 267 to 259 nm);
  - o the absorbance decreases without a significant shift in the maximum wavelength for **C0**;
- for Cu(II):DNA molar ratios > 3:
  - o the absorbance increases with a significant shift in the maximum wavelength for all the complexes (from ≈270 to 260 nm).

Selected spectra recorded during the titrations are reported in Supporting Information (Fig. S1).

For the studied systems, hyperchromism is evident for all the compounds except for **C0**. However, the extent of the hyperchromism/hypochromism noted and the shift towards higher wavelengths is affected by the presence of excess DNA, whose spectrum is characterised by a wide band centred at 260 nm. For this reason direct inspection of the experimental spectra to determine if hyper- or hypochromism is really present may lead to inaccurate results. Therefore, to assign the correct interaction mode, the pure spectra of the involved species were compared.

From eigenvalue analysis of spectrophotometric data, three significant eigenvalues were found. These can be interpreted as the number of linearly independent absorbing species [27]. In our case, such species are the free DNA, the free ligand or copper complex, and the related DNA adduct. The absorbance data were fitted supposing a model taking into account the 1:1 DNA:ligand or DNA:copper complex adduct, and the pure spectra of all the absorbing species were calculated (Fig. 3). The obtained absorptivity spectra show hyperchromism in all the titrations, suggesting that ligands and complexes interact with DNA principally by groove binding or electrostatic interaction. A blue shift in the absorbance maximum is revealed for **K2** (from 272 nm to 261 nm), while for the other complexes no significant shift is evident (Table 3).

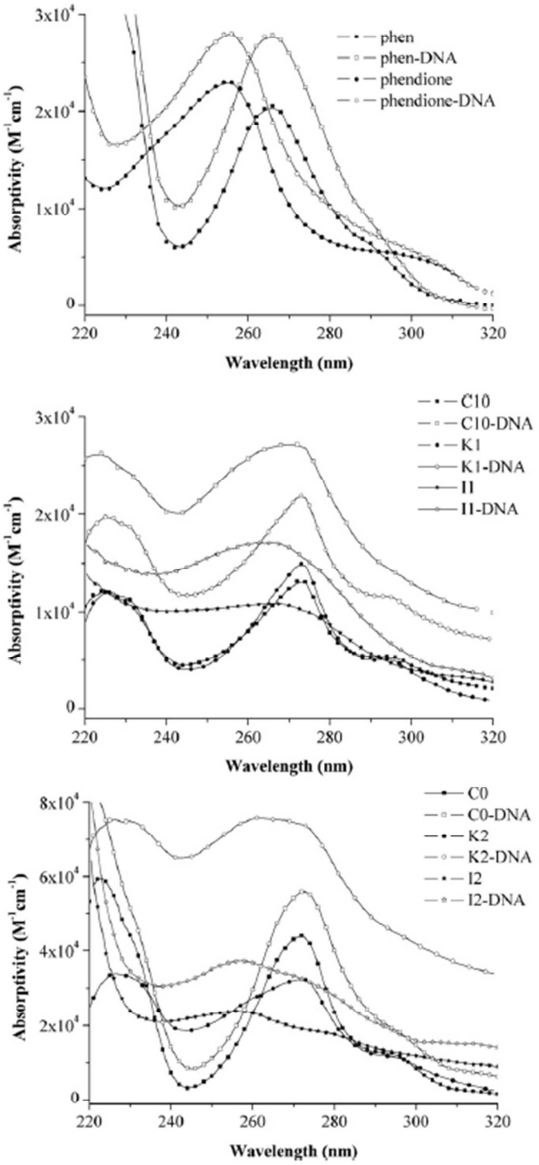

Fig. 3. Absorptivity spectra of adducts formed between DNA and the studied compounds (25 °C, 0.01 M PIPES buffer, pH = 7.0).

The extent of the hyperchromism is related to the kind of DNA interaction [42,43] and varies along the series: **K2**–DNA (135%) > **C10**–DNA (108%) > **I1**–DNA (58%) ≈ **I2**–DNA (56%) > **K1**–DNA (47%) > phen (36%) > **C0**–DNA (28%) > phendione (22%). In particular, **K2** and **C10** present the highest DNA affinity through groove binding or electrostatic interaction, while **I2**, **K1** and **I1** exhibit lower affinities. The high

Table 3
DNA binding constants and spectral data for the studied compounds (25 °C, in PIPES buffer 0.01 M, pH = 7.0).

Compound	DNA binding constants (M^{-1})	λ_{max} (nm)	ε_{max} ($M^{-1} L^{-1}$)	Ref.
Phen	–	266	20,524	This work
Phen–DNA	2.29 (1) × 10^6	266	27,861	"
Phendione	–	256	22,975	"
phendione–DNA	7.76 (1) × 10^4	256	28,019	"
C10	–	272	13,114	"
C10–DNA	1.9 (1) × 10^5	270	27,236	"
K1	–	273	14,943	"
K1–DNA	1.8 (2) × 10^5	273	21,902	"
I1	–	267	10,876	"
I1–DNA	5.5 (1) × 10^4	263	17,145	"
C0	–	273	43,916	"
C0–DNA	8.3 (1) × 10^4	273	56,432	"
K2	–	272	32,373	"
K2–DNA	7.2 (1) × 10^4	261	75,980	"
I2	–	256	23,901	"
I2–DNA	2.8 (1) × 10^4	258	37,329	"
[Cu(phen)$_2$(branched polyethyleneimine)]Cl$_2$4H$_2$O	5.95 × 10^5	–	–	[49]
Cu(phen)$_2$Cl$_2$	2.75 × 10^3	–	–	[50]
Cu$_2$(phen)$_2$Cl$_4$	4.79 × 10^4	–	–	[51]
[Cu(L-phenylalanine) (phen)(H$_2$O)](NO$_3$)	3.6 (1) × 10^5	–	–	[52]

hyperchromism shown by **C10** and **K2** suggests that these complexes do not intercalate or intercalate just partially. This is in agreement with the results reported by Chikira and co-workers [44] for **C10**. The low percentage of hyperchromism shown for phen and phendione is due to their ability to intercalate. The low hyperchromism shown by **C0** could be due to a possible partial DNA intercalation. In fact, it has been reported that bis(1,10-phenanthroline) copper(II) complexes apparently bind to DNA by intercalation but the correct binding mode is still controversial [45,46]. Furthermore, in the copper(I) complex $[Cu(phen)_2]^+$ the phen ligands are roughly perpendicular to each other, so complete intercalation of the phen ring between a set of adjacent base pairs is sterically impossible, but some type of partial intercalation involving one of the ligands can be presumed [47]. Similar considerations may also be proposed for **C0**, $[Cu(phen)_2(OH_2)]^{2+}$, where a trigonal bypiramidal coordination around Cu(II) is present. It is worthwhile remarking that the action of the $[Cu(phen)_2(OH_2)]^{2+}$ complex on DNA, besides intercalation, is due to an oxidative attack on the deoxyribose units that cleaves the DNA strand leading to cell death [48].

The magnitude of the DNA binding constants is related to the strength of the interaction, independently of the binding mode. The calculated constants (Table 3) vary along the series: **C10**–DNA ≈ **K1**–DNA > **I1**–DNA > **C0**–DNA > **K2**–DNA > **I2**–DNA. The obtained values are in agreement with binding constants reported in the literature for similar compounds [49–52].

The DNA binding constants for the studied copper(II) complexes appear directly correlated with the IC_{50} values and then inversely correlated to the cytotoxic activity. This behaviour is particularly relevant on the CCRF-CEM and CCRF-SB cell lines (Fig. 4). As can be seen, **C10** presents the highest DNA binding constant but the lowest antiproliferative activity, while **I2** presents the lowest binding constant and the highest biological activity. These results indicate that different reaction mechanisms with respect to DNA-binding are responsible for the anticancer activities of these complexes.

3.6. Potentiometric measurements

The protonation constants of phendiol and the complex formation constants of the phendiol-copper(II) system were not studied because of the poor solubility of the ligand in water or in water-DMSO solution (less than 1×10^{-5} M).

3.6.1. Protonation constants of phen and phendione

At acidic pH all the nitrogen and oxygen atoms of the ligands may hypothetically be protonated. Actually, in the 2–11 pH range only one protonation equilibrium was in evidence during the potentiometric titration. The protonation of the second nitrogen atom of phen and phendione and also that of the oxygen atoms of phendione should happen at more acidic pH, outside the working range of the glass electrode. The calculated log β and the related log K values are reported in Table 4. For both ligands the log K value decreases with temperature, and the difference is double in the case of phendione (0.31 and 0.15 log K units for phendione and phen, respectively). Besides the presence in phendione of the two oxygen atoms that exert a negative inductive effect, no significant differences between the log K values of the two ligands are evident.

3.6.2. Copper(II) hydrolysis

The formation constants of copper(II) hydrolysed species were determined by titrating several solutions containing Cu(II) at three different molar concentrations (1×10^{-3} M, 5.0×10^{-4} M and 3.3×10^{-4} M). The copper(II) concentration was varied to verify the presence of polynuclear species. All the solutions titrated with NaOH were back-titrated with HCl. The overlapping of the acidic and basic titration curves indicates the reversibility of the involved equilibria although it is slow to be reached. In fact, the time delay between additions necessary to reach equilibrium ranged from 1 to 30 min. A colloidal phase occurred after pH ≈ 6 or after pH ≈ 5 at 25 and 37 °C, respectively. At the end of the basic titrations (pH > 10) the solutions appeared slightly turbid. The potentiometric data for all the titrations carried out at the same temperature were fitted simultaneously. At the studied temperatures the formations of the $Cu(OH)_2$, $[Cu(OH)_3]^-$ and the polynuclear $[Cu_2(OH)]^{3+}$ species were evident.

The hydrolysis equilibria of copper(II) have been studied by several authors but under different experimental conditions, mainly at 25 °C and in the presence of nitrate or perchlorate ions as the background electrolyte [53–56]. The $[Cu(OH)]^+$, $[Cu_2(OH)_2]^{2+}$, $[Cu_2(OH)]^{3+}$ and $[Cu_3(OH)_4]^{2+}$ species were observed. A direct comparison between our data and those reported in the literature is problematic since most of the stability constants are expressed using different definitions and conventions. However, we observe that, after proper conversion, our values are slightly lower. These

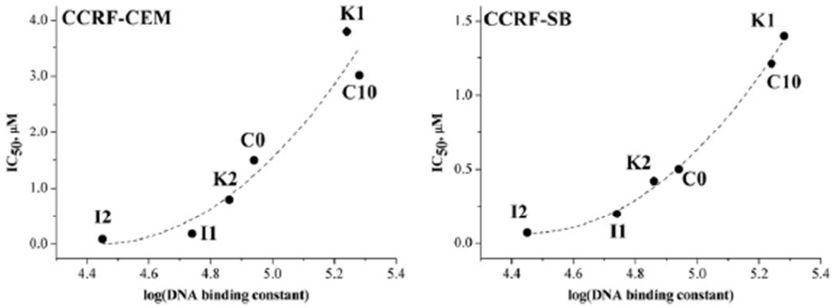

Fig. 4. Trend of IC_{50} versus logarithm of the DNA-binding constant. ($y = 4.99x^2 - 44.29x + 98.22$, $r^2 = 0.9332$ for CCRF-CEM; $y = 1.92x^2 - 17.14x + 38.28$, $r^2 = 0.9970$ for CCRF-SB; DNA binding constants were determined at 25 °C in 0.01 M PIPES buffer, pH 7.0).

differences may be due to the chosen experimental conditions. The $[Cu(OH)]^+$, $[Cu_2(OH)_2]^{2+}$ and $[Cu_3(OH)_4]^{2+}$ species were not found suitable to fit our experimental data. The calculated stability constants of hydroxo-complexes of Cu(II) are reported in Table 4.

3.6.3. Cu(II)–phen system

Complex formation equilibria between Cu(II) and the phen ligand were studied by potentiometric titrations. It was not possible to simultaneously record the UV–vis spectrum due to the absorption being too low in the visible region (d–d bands, $\varepsilon < 100\ M^{-1}\ cm^{-1}$) and too high in the UV region (charge transfer bands, $\varepsilon > 100{,}000\ M^{-1}\ cm^{-1}$). In fact, molar concentrations of complexes equal to 10^{-2} M or 10^{-5} M, not suitable for potentiometric measurements, had to be used. Some titration curves for phen:Cu(II) at molar ratios of 1:0, 3:1, 2:1 and 1:1 are reported in the Supplementary Materials (Fig. S2A and S2B). At a 3:1 ligand:metal molar ratio, variously protonated CuL_2 and CuL_3 complexes are formed. At pH < 4 the species $[CuL_3H]^{3+}$ is present. In this complex, the nitrogen atom of one ligand is still protonated and does not coordinate the metal ion. At a 2:1 phen:Cu(II) molar ratio, variously protonated CuL_2 and CuL forms are present. At a 1:1 molar ratio, CuL is the predominant species. At every molar ratio, the neutral CuL_2H_{-2} species is formed beyond pH = 10 (the term H_{-i} means that *i* water molecules coordinated to the metal ion have lost a proton). A colourless colloidal species is present after pH = 10 at a 1:1 molar ratio, probably due to the formation of the CuH_{-2} species.

The complex formation constants are reported in Table 4. In all the complexes the coordination sphere is completed by water molecules. Taking into account the solid state structures for $Cu(phen)(OH_2)_2(OClO_3)_2$ and $[Cu(phen)_2(OH_2)](ClO_4)_2$, and their visible absorption spectra [3], the hypothesised structures in solution for $[Cu(phen)_2]^{2+}$, $Cu(phen)_2H_{-2}$, and $[Cu(phen)_3H]^{3+}$ are reported in Fig. 5. The distribution curves at 25 and 37 °C are shown in Fig. S3. The complex formation constants obtained in this work are higher than those reported in the literature for this system [57–60]. However, in most of the previous studies, the constants were determined under different experimental conditions, and no protonated species were considered for fitting the experimental data.

Table 4
Overall stability constants for the studied systems, in 0.1 M ionic strength (NaCl) at 25 °C and 37 °C temperatures (the standard deviations on the last significant figure are reported in parentheses).

System	Species	Overall stability constants			
		25 °C		37 °C	
		Log β	Log K	Log β	Log K
phen	HL^+	5.08 (1)	5.08	4.93 (1)	4.93
phendione	HL^+	5.14 (1)	5.14	4.83 (1)	4.83
Cu(II)	$Cu(OH)_2$	−8.42 (1)	–	−7.08 (2)	–
	$[Cu(OH)_3]^-$	−19.07 (3)	10.65	−17.27 (3)	10.19
	$[Cu_2(OH)]^{3+}$	4.92 (3)	–	5.39 (4)	–
Cu(II)–phen	$[CuL_3H]^{3+}$	36.7 (1)	–	36.5 (1)	–
	$[CuL_3]^{2+}$	32.3 (1)	4.4	32.7 (1)	3.8
	$[CuL_2]^{2+}$	25.5 (1)	–	27.58 (4)	–
	$[CuL_2H_{-1}]^+$	17.72 (5)	7.78	19.41 (4)	8.17
	CuL_2H_{-2}	7.54 (4)	10.18	8.6 (1)	10.8
	$[CuL]^{2+}$	16.98 (2)	–	17.24 (2)	–
	$[CuLH_{-1}]^+$	10.20 (2)	6.78	10.33 (5)	6.91
	$[CuLH_{-3}]^-$	–	–	−9.3 (1)	9.8
Cu(II)–phendione	$[CuL_3H]^{3+}$	34.3 (1)	–	35.0 (1)	–
	$[CuL_3]^{2+}$	29.6 (1)	4.7	30.84 (5)	4.2
	$[CuL_2H]^{3+}$	28.0 (1)	–	30.2 (1)	–
	$[CuL_2]^{2+}$	24.0 (1)	4.0	24.34 (3)	5.9
	$[CuL_2H_{-1}]^+$	13.9 (1)	10.1	–	–
	$[CuL_2H_{-3}]^-$	–	–	−2.85 (4)	9.1
	$[CuL]^{2+}$	15.51 (2)	–	15.71 (3)	–
	$[CuLH_{-1}]^+$	8.54 (2)	6.97	8.8 (1)	6.9
	$CuLH_{-2}$	–	–	1.19 (2)	7.6
	$[CuLH_{-3}]^-$	−13.40 (1)	10.97	−8.91 (4)	10.10

3.6.4. Cu(II)–phendione system

As for the phen–Cu(II) system, complex formation equilibria between Cu(II) and the phendione ligand were studied by potentiometric titrations. Titration curves for 1:0, 3:1, 2:1 and 1:1 phendione:Cu(II) molar ratios are reported in Fig. S2C and S2D. Similarly to phen, phendione forms variously protonated CuL, CuL_2 and CuL_3 complexes with Cu(II). At a 3:1 ligand:metal molar ratio, CuL_2 and CuL_3 complexes are the predominant species. At pH < 4 the protonated species $[CuL_3H]^{3+}$ and $[CuL_2H]^{3+}$ are present. In these complexes, the nitrogen atom of one ligand is still protonated, and does not coordinate the metal ion. At a 2:1 phendione:Cu(II) molar ratio, CuL_2 and CuL are present. At a 1:1 molar ratio the predominant species is CuL. Unlike the phen–Cu(II) system, the neutral CuL_2H_{-2} species is formed only at 37 °C and 1:1 molar ratio. A colourless colloidal species is present after pH = 10 at 1:1 molar ratio, probably due to the formation of the CuH_{-2} species.

The complex formation constants are reported in Table 4. In all the complexes the coordination sphere is completed by water molecules. Taking into account the solid state structure for $[Cu(phendione)_2(OH_2)(OClO_3)](ClO_4)$ and on the basis of the visible absorption spectra, the hypothesised structures in solution for $[Cu(phendione)_2]^{2+}$ and $[Cu(phendione)_3]^{2+}$ are reported in Fig. 5. The distribution curves for the phendione–Cu(II) system at 25 and 37 °C are shown in Fig. S4.

3.6.5. Stability of the copper(II) complexes

The complex formation constants depend on ligand protonation constants and on metal hydrolysis; therefore, they cannot be directly compared to evaluate the relative complex stability. Then, in order to properly compare the stabilities of the formed complexes, the minus logarithm of the equilibrium concentration of the free metal ion ($-\log [Me_{free}] = pMe$), in a solution at specified pH, total metal and total ligand concentrations, might be calculated. In this way, a smaller free metal ion concentration, i.e. a larger pMe, indicates a more effective

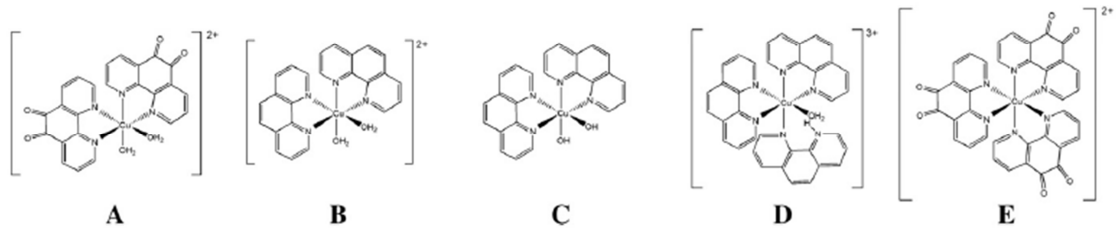

Fig. 5. Hypothesised structures for $[Cu(phendione)_2]^{2+}$ (A), $[Cu(phen)_2]^{2+}$ (B), $Cu(phen)_2H_{-2}$ (C), $[Cu(phen)_3H]^{3+}$ (D) and $[Cu(phendione)_3]^{2+}$ (E).

ligand towards that metal [61]. The pMe value depends on all the involved equilibria, and can be directly compared to state definitely which ligand forms the most stable complex under the chosen experimental conditions. The pCu(II) values for the phen–Cu(II) system are 22.8 (25 °C) and 23.7 (37 °C), while for the phendione–Cu(II) system they are 20.3 (25 °C) and 21.4 (37 °C), respectively. From these results it is evident that the formed complexes are more stable at physiological temperature and the complexes formed with phen are the most stable at both temperatures.

A direct correlation between the results obtained through potentiometric measurements and DNA binding study, could be misleading because of the different experimental conditions such as ionic strength, pH, temperature, and, in particular, concentration range. However some information could be translated. From the potentiometric study, it results that the predominant species, at pH 7.0 and 25 °C, are (L = phen or phendione): i) $[CuL_3]^{2+}$ when ligand and metal are present in 3:1 molar ratio; ii) $[CuL_2(OH_2)_2]^{2+}$ when ligand and metal are present in 2:1 molar ratio; iii) $[CuL(OH_2)(OH)]^{+}$ when ligand and metal are present 1:1 in molar ratio; and iv) L when only ligand is present. Then, dissolving **C10**, **C0**, **K1** and **K2** in PIPES buffer, the species in solution that react with DNA are supposed to be $[CuL(OH_2)(OH)]^{+}$ for **C10** and **K1**, $[CuL_2(OH_2)_2]^{2+}$ for **C0** and **K2**. Regarding **I1** and **I2**, in the absence of potentiometric data, it is possible to suppose a behaviour similar to that shown by the other complexes. Then the species in solution supposed to react with DNA, are $[CuL(OH_2)(OH)]^{+}$ for **I1** and $[CuL_2(OH_2)_2]^{2+}$ for **I2**. Among the species present in solution, only L for phen and phendione and $[Cu(phen)_2(OH_2)_2]^{2+}$ are able to partially intercalate.

4. Conclusion

Copper(II) form with 1,10-phenanthroline, 1,10-phenanthrolin-5,6-dione, and 1,10-phenanthrolin-5,6-diol, complexes with 1:1, 2:1 and 3:1 ligand:metal stoichiometry.

The studied ligands and complexes generally present a higher antiproliferative effect than that of cisplatin. Complexes with two ligands are more cytotoxic towards all the tested cell lines than the related complexes with one ligand and are generally more cytotoxic than the ligand alone. The $[Cu(1,10\text{-phenanthrolin-5,6-diol})_2(OH_2)](ClO_4)_2$ complex appears as the most active compound for the treatment of CCRF-CEM, CCRF-SB, SK-MES-1 and DU-145 human tumour cell lines. In particular this compound is very promising for the treatment of SK-MES-1, having a IC_{50} value 37 times lower than that of cisplatin. The $[Cu(1,10\text{-phenanthrolin-5,6-dione})_2(OH_2)(OClO_3)](ClO_4)$ complex is eligible for treatment of the HEP-G2 cell line, having a IC_{50} value 18 times lower than that of cisplatin. The cytotoxic activity of the ligands was found to be correlated to the cellular microenvironment. Compound 1,10-phenanthrolin-5,6-diol appears the most active ligand on cells surrounded by a hydrophilic environment.

The studied copper(II) complexes are characterised by a DNA affinity in the range 3×10^4–2×10^5 M^{-1}, and were found to interact with DNA mainly by groove binding or electrostatic interactions. The DNA complexes formed with $[Cu(1,10\text{-phenanthrolin-5,6-dione})(OH_2)_2(OClO_3)_2]$ or $[Cu(1,10\text{-phenanthroline})(OH_2)_2(OClO_3)_2]$ are characterised by greater DNA binding constants than the analogous ones formed with $[Cu(1,10\text{-phenanthrolin-5,6-dione})_2(OH_2)(OClO_3)](ClO_4)$ or $[Cu(1,10\text{-phenanthroline})_2(OH_2)(OClO_3)](ClO_4)$. The lower stability of these latter complexes may be due to the steric hindrance of two ligand molecules. It is interesting to notice that the Cu(II) complexes that present the highest DNA affinity show also the lowest cytotoxicity. The correlation found between cytotoxicity and DNA binding constants for copper complexes shows that DNA affinity cannot be considered a reliable universal indicator of the cytotoxic activity of a drug, giving only a suggestion of the involved action mechanism. Our complexes appear to act via a mechanism different from that of cisplatin. Therefore, they might be exploited for the treatment of cisplatin resistant cancer cells. Concluding, the results provide valuable information for the development of novel copper(II) complexes, as anticancer drugs with wider spectrum of action.

Acknowledgements

Federica Trudu gratefully acknowledges Sardinia Regional Government, for the financial support of her PhD scholarship (P.O.R. Sardegna F.S.E. Operational Programme of the Autonomous Region of Sardinia, European Social Fund 2007–2013 — Axis IV Human Resources, Objective l.3, Line of Activity l.3.1.)

Appendix A. Supplementary data

Supplementary data to this article can be found online at http://dx.doi.org/10.1016/j.jinorgbio.2014.08.011. These data include MOL files and InChiKeys of the most important compounds described in this article.

References

[1] N.B. Terwilliger, J. Exp. Biol. 201 (1998) 1085–1098.
[2] T. Pivetta, M.D. Cannas, F. Demartin, C. Castellano, S. Vascellari, G. Verani, F. Isaia, J. Inorg. Biochem. 105 (2011) 329–338.
[3] T. Pivetta, F. Isaia, G. Verani, C. Cannas, L. Serra, C. Castellano, F. Demartin, F. Pilla, M. Manca, A. Pani, J. Inorg. Biochem. 114 (2012) 28–37.
[4] T. Pivetta, F. Isaia, F. Trudu, A. Pani, M. Manca, D. Perra, F. Amato, J. Havel, Talanta 115 (2013) 84–93.
[5] C. Deegan, B. Coyle, M. McCann, M. Devereux, D. Egan, Chem. Biol. Interact. 164 (2006) 115–125.
[6] M. McCann, A.L.S. Santos, B.A. Da Silva, M.T.V. Romanos, A.S. Pyrrho, M. Devereux, K. Kavanagh, I. Fichtner, A. Kellett, Toxicol. Res. 1 (2012) 47–54 (Cambridge, U. K.).
[7] S. Roy, K.D. Hagen, P.U. Maheswari, M. Lutz, A.L. Spek, J. Reedijk, G.P. Van Wezel, Chem. Med. Chem. 3 (2008) 1427–1434.
[8] S. Betanzos-Lara, O. Novakova, R.J. Deeth, A.M. Pizarro, G.J. Clarkson, B. Liskova, V. Brabec, P.J. Sadler, A. Habtemariam, J. Biol. Inorg. Chem. 17 (2012) 1033–1051.
[9] A.N. Wein, A.T. Stockhausen, K.I. Hardcastle, M.R. Saadein, S.B. Peng, D. Wang, D.M. Shin, Z.G. Chen, J.F. Eichler, J. Inorg. Biochem. 105 (2011) 663–668.
[10] D.V. Luís, J. Silva, A.I. Tomaz, R.F.M. de Almeida, M. Larguinho, P.V. Baptista, L.M.D.R. S. Martins, T.F.S. Silva, P.M. Borralho, C.M.P. Rodrigues, A.S. Rodrigues, A.J.L. Pombeiro, A.R. Fernandes, J. Biol. Inorg. Chem. (2014), http://dx.doi.org/10.1007/s00775-014-1110-0.
[11] R.A. Alderden, M.D. Hall, T.W. Hambley, J. Chem. Educ. 83 (2006) 728–734.
[12] S. Kashanian, M.M. Khodaei, H. Roshanfekr, H. Peyman, Spectrochim. Acta A Mol. Biomol. Spectrosc. 114 (2013) 642–649.
[13] M. Kaplanis, G. Stamatakis, V.D. Papakonstantinou, M. Paravatou-Petsotas, C.A. Demopoulos, C.A. Mitsopoulou, J. Inorg. Biochem. 135 (2014) 1–9.

[14] S. Poteet, M. Majewski, Z.S. Breitbach, C.A. Griffith, S. Singh, D.W. Armstrong, M.O. Wolf, F.M. MacDonnell. J. Am. Chem. Soc. 135 (2013) 2419–2422.
[15] V.A. Bloomfield, D.M. Crothers, I. Tinocco Jr., Physical Chemistry of Nucleic Acids, Harper & Row, New York, 1974. 432.
[16] A. Altomare, M.C. Burla, M. Camalli, G.L. Cascarano, C. Giacovazzo, A. Guagliardi, A.G.G. Moliterni, G. Polidori, R. Spagna, J. Appl. Crystallogr. 32 (1999) 115–119.
[17] G.M. Sheldrick, Acta Crystallogr. 64A (2008) 112–122.
[18] L.J. Farrugia, J. Appl. Crystallogr. 32 (1999) 837–838.
[19] S.A. Latt, G. Stetten, L.A. Juergens, H.F. Willard, C.D. Scher, J. Histochem. Cytochem. 23 (1975) 493–505.
[20] R. Pauwels, J. Balzarini, M. Baba, R. Snoeck, D. Schols, P. Herdewijn, J. Desmyter, E. De Clercq, J. Virol. Methods 20 (1988) 309–321.
[21] S. Dhanalakshmi, P. Agarwal, L.M. Glode, R. Agarwal, Int. J. Cancer 106 (2003) 699–705.
[22] M. Okamura, K. Hashimoto, J. Shimada, H. Sakagami, Anticancer Res. 24 (2004) 655–662.
[23] P. Ceppi, M. Papotti, V. Monica, M. Lo Iacono, S. Saviozzi, M. Pautasso, S. Novello, S. Mussino, E. Bracco, M. Volante, G.V. Scagliotti, Mol. Cancer Ther. 8 (2009) 3066–3074.
[24] M.E. Reichmann, S.A. Rice, C.A. Thomas, P. Doty, J. Am. Chem. Soc. 76 (1954) 3047–3053.
[25] J. Murmur, J. Mol. Biol. 3 (1961) 208–218.
[26] M. Meloun, J. Čapek, P. Mikšík, R.G. Brereton, Anal. Chim. Acta. 423 (2000) 51–68.
[27] E.R. Malinowski, Factor Analysis in Chemistry, third ed. Wiley-Interscience, New York, 2002.
[28] P. Gans, A. Sabatini, A. Vacca, Talanta 43 (1996) 1739–1753.
[29] A. Albert, E.P. Serjant, The Determination of Ionization Constants, Chapman & Hall, London, 1984.
[30] G. Gran, Analyst 77 (1952) 661–671.
[31] P. Gans, B. O'Sullivan, Talanta 51 (2000) 33–37.
[32] J. Bassett, R.C. Denney, G.H. Jeffrey, J. Mendham, Vogel's Textbook of Quantitative Inorganic Analysis, The ELBS and Longman, London, 1989. 326.
[33] C.C.J. Roothaan, Rev. Mod. Phys. 23 (1951) 69–89.
[34] G.G. Hall, Proc. R. Soc. A 205 (1951) 541–552.
[35] J.A. Pople, D.A. Beveridge, Approximate Molecular Orbital Theory, McGraw-Hill, New York, 1970.
[36] K. Ocakoglu, C. Zafer, B. Cetinkaya, S. Icli, Dyes Pigments 75 (2007) 385–394.
[37] W. Paw, R. Eisenberg, Inorg. Chem. 36 (1997) 2287–2293.
[38] A.W. Addison, T.N. Rao, J. Reedijk, J. Van Rijn, G.C. Verschoor, J. Chem. Soc. Dalton Trans. (1984) 1349–1356.
[39] S. Ghosh, A.C. Barve, A.A. Kumbhar, A.S. Kumbhar, V.G. Puranik, P.A. Datar, U.B. Sonawane, R.R. Joshi, J. Inorg. Biochem. 100 (2006) 331–343.
[40] M.D. Stephenson, M.J. Hardie, Dalton Trans. (2006) 3407–3417.
[41] F. Luciani, M. Spada, A. De Milito, A. Molinari, I. Rivoltini, A. Montinaro, M. Marra, I. Lugini, M. Logozzi, F. Lozupone, C. Federici, E. Iessi, G. Parmiani, G. Arancia, F. Belardelli, S. Fais, JNCI J. Natl. Cancer Inst. 96 (2004) 1702–1713.
[42] M.S.S. Babu, K.H. Reddy, P.G. Krishna, Polyhedron 26 (2007) 572–580.
[43] Y. Sun, Y.J. Hou, Q.X. Zhou, W.H. Lei, J.R. Chen, X.S. Wang, B.W. Zhang, Inorg. Chem. 49 (2010) 10108–10116.
[44] M. Chikira, Y. Tomizawa, D. Fukita, T. Sugizaki, N. Sugawara, T. Yamazaki, A. Sasano, H. Shindo, M. Palaniandavar, W.E. Antholine, J. Inorg. Biochem. 89 (2002) 163–173.
[45] O. Zelenko, J. Gallagher, D.S. Sigman, Angew. Chem. Int. Ed. Engl. 36 (1997) 2776–2778.
[46] J.M. Veal, R.L. Rill, Biochemistry 30 (1991) 1132–1140.
[47] G.S. Manning, Q. Rev. Biophys. 11 (1978) 179–246.
[48] C. Marzano, M. Pellei, F. Tisato, C. Santini, Anti Cancer Agents Med. Chem. 9 (2009) 185–211.
[49] R.S. Kumar, S. Arunachalam, V.S. Periasamy, C.P. Preethy, A. Riyasdeen, M.A. Akbarsha, Eur. J. Med. Chem. 43 (2008) 2082–2091.
[50] T. Gupta, S. Dhar, M. Nethaji, A.R. Chakravarty, Dalton Trans. (2004) 1896–1900.
[51] Q.G. Zhang, F. Zhang, W.G. Wang, X.L. Wang, J. Inorg. Biochem. 100 (2006) 1344–1352.
[52] A.K. Patra, T. Bhowmick, S. Ramakumar, M. Nethaji, A.R. Chakravarty, Dalton Trans. (2008) 6966–6976.
[53] M. Whitfield, J. Chem. Eng. Data 17 (1972) 124–128.
[54] A. Vacca, A. Sabatini, L. Bologni, J. Chem. Soc. Dalton Trans. (1981) 1246–1250.
[55] S. Sjoberg, Y. Hagglund, A. Nordin, N. Ingri, Mar. Chem. 13 (1983) 35–44.
[56] J. Nordin, P. Persson, A. Nordin, S. Sjoberg, Langmuir 14 (1998) 3655–3662.
[57] T. Kohzuma, A. Odani, Y. Morita, M. Takani, O. Yamauchi, Inorg. Chem. 27 (1998) 3854–3858.
[58] G. Nakagawa, H. Wada, T. Sako, Bull. Chem. Soc. Jpn. 53 (1980) 1303–1307.
[59] M. Mohan, D. Bancroft, E. Abbott, Inorg. Chem. 18 (1979) 2468–2472.
[60] H. Irving, D. Mellor, J. Chem. Soc. (1962) 5222–5237.
[61] W.R. Harris, C.J. Carrano, S.D.R. Cooper, S.R. Sofen, A.E. Avdeef, J.V. Mc Ardle, K.N. Raymond, J. Am. Chem. Soc. 101 (1979) 6097–6104.

Conclusions

New copper(II) complexes with one or two 1,10-phenanthroline derivatives have been prepared. The studied ligands and complexes generally present a higher anti – proliferative effect than that of cisplatin. The cytotoxic activity of the ligands was found to be correlated to the cellular microenvironment. Because the microenvironment of tumour cells is important for their carcinogenesis , the study of the interactions between microenvironment and drugs gives useful information for chemotherapeutic approaches. In this light, 1,10-phenanthrolin-5,6-diol appears among the three ligands, the most active on cells surrounded by a hydrophilic environment. Cu(II) complexes with one molecule of 1,10-phenanthroline, 1,10-phenanthrolin-5,6-dione or 1,10- phenanthrolin-5,6-diol exhibited an anti – proliferative activity lower than that of the ligand alone on all the tested cell lines. Complexes with two ligands are more cytotoxic towards all the tested cell lines than the related complexes with one ligand and are generally more cytotoxic than the ligand alone.

The [Cu(1,10-phenanthrolin-5,6-diol)$_2$(OH_2)](ClO_4)$_2$ complex appears as the most active compound for the treatment of CCRF-CEM, CCRF-SB, SK-MES-1 and DU-145 human tumour cell lines. In particular this compound is very promising for the treatment of SK-MES-1, having a CC50 value 37 times lower than that of cisplatin. The [Cu(1,10-phenanthrolin-5,6-dione)$_2$(OH_2)($OClO_3$)](ClO_4) complex is eligible for treatment of the HEP-G2 cell line, having a CC50 value 18 times lower than that of cisplatin.

References

(Alphabetical order)

1. Addison A.W, Rao T.N, Reedijk J, Van Rijn J, Verschoor G.C, Chem J; Soc. Dalton Trans. (1984) 1349–1356.

2. Albert A, Serjant E.P; The Determination of Ionization Constants, Chapman & Hall, London, 1984.

3. Alderden R.A, Hall M.D, Hambley T.W, J. Chem. Educ. 83 (2006) 728–734.

4. Altomare A, Burla M.C, Camalli M, Cascarano G.L, Giacovazzo C, Guagliardi A, Moliterni A.G.G, Polidori G, Spagna R; J. Appl. Crystallogr. 32 (1999) 115–119.

5. Babu M.S.S, Reddy K.H, Krishna P.G; Polyhedron 26 (2007) 572–580.

6. Bassett J, Denney R.C, Jeffrey G.H, Mendham J; Vogel's Textbook of Quantitative Inorganic Analysis, The ELBS and Longman, London, 1989. 326.

7. Betanzos-Lara S, Novakova O, Deeth R.J, Pizarro A.M, Clarkson, G.J., Liskova B, Brabec V, Sadler P.J, Habtemariam ; J. Biol. Inorg. Chem. 17 (2012) 1033–1051.

8. Bloomfield V.A, Crothers D.M, Tinocco I. Jr; Physical Chemistry of Nucleic Acids, Harper & Row, New York, 1974. 432.

9. Ceppi P, Papotti M, Monica V, Lo Iacono M, Saviozzi S, Pautasso M, Novello S, Mussino S, Bracco E, Volante M, Scagliotti G.V; Mol. Cancer Ther. 8 (2009) 3066–3074

10. Chikira M, Tomizawa Y, Fukita D, Sugizaki T, N. Sugawara, Yamazaki T, Sasano A, Shindo H, Palaniandavar M, Antholine W.E; J. Inorg. Biochem. 89 (2002) 163–173.

11. Dhanalakshmi S, Agarwal P, Glode L.M, Agarwal R; Int. J. Cancer 106 (2003) 699–705.

12. Deegan C, Coyle B, McCann M, Devereux M, Egan D; Chem. Biol. Interact. 164 (2006) 115–125.

13. Farrugia L.J, Appl J; Crystallogr. 32 (1999) 837–838.

14. Gans P, Sabatini A, Vacca A; Talanta 43 (1996) 1739–1753.

15. Gans P, O'Sullivan B; Talanta 51 (2000) 33–37.

16. Ghosh S, Barve A.C, Kumbhar A.A, Kumbhar A.S, Puranik V.G, Datar P.A, Sonawane U.B, Joshi R.R, Inorg J; Biochem. 100 (2006) 331–343.

17. Gran G; Analyst 77 (1952) 661–671.

18. Gupta T, Dhar S, Nethaji M, Chakravarty A.R; Dalton Trans. (2004) 1896–1900.

19. Hall G.G; Proc. R. Soc. A 205 (1951) 541–552.

20. Harris W.R, Carrano C.J, Cooper S.D.R, Sofen S.R, Avdeef A.E, Mc Ardle J.V, Raymond K.N, Am J; Chem. Soc. 101 (1979) 6097–6104.

21. Irving H, Mellor D, Am J; Chem. Soc. (1962) 5222–5237.

22. Kaplanis M, Stamatakis G., Papakonstantinou V.D, Paravatou-Petsotas M, Demopoulos C.A, Mitsopoulou C.A; J. Inorg. Biochem. 135 (2014) 1–9.

23. Kashanian S, Khodaei M.M, Roshanfekr H, Peyman H; Spectrochim. Acta A Mol. Biomol. Spectrosc. 114 (2013) 642–649.

24. Kohzuma T, Odani A, Morita Y, Takani M, Yamauchi O; Inorg. Chem. 27 (1998) 3854–3858.

25. Kumar R.S, Arunachalam S, Periasamy V.S, Preethy C.P, Riyasdeen A, Akbarsha M.A; Eur. J. Med. Chem. 43 (2008) 2082–2091.

26. Latt S.A, Stetten G, Juergens L.A, Willard H.F, Scher C.D; J. Histochem. Cytochem. 23 (1975) 493–505.

27. Luciani F, Spada M, De Milito A, Molinari A, Rivoltini L, Montinaro A, Marra M, Lugini L, Logozzi M, Lozupone F, Federici C, Iessi E, Parmiani G, Arancia G, Belardelli F, Fais S; JNCI J. Natl. Cancer Inst. 96 (2004) 1702–1713.

28. Luís D.V, Silva J., Tomaz A.I, de Almeida R.F.M, Larguinho M, Baptista P.V, Martins L.M.D.R.S, Silva T.F.S, Borralho P.M, Rodrigues C.M.P, Rodrigues A.S, A.J.L.Pombeiro, A.R. Fernandes, J. Biol. Inorg. Chem. (2014)

29. Malinowski E.R; Factor Analysis in Chemistry, third ed. Wiley-Interscience, New York, 2002.

30. Manning G.S, Rev Q; Biophys. 11 (1978) 179–246.

31. Marzano C, Pellei M, Tisato F, Santini C; Anti Cancer Agents Med. Chem. 9 (2009) 185–211.

32. McCann M, Santos A.L.S, Da Silva B.A, Romanos M.T.V, Pyrrho A.S, Devereux M, Kavanagh K, Fichtner I, Kellett A; Toxicol. Res. 1 (2012) 47–54 (Cambridge, U. K.).

33. Meloun M, Čapek J, Mikšík P, Brereton R.G; Anal. Chim. Acta. 423 (2000) 51–68.

34. Mohan M, Bancroft D, Abbott E; Inorg. Chem. 18 (1979) 2468–2472.

35. Murmur J; Mol. Biol. 3 (1961) 208–218.

36. Nakagawa G, Wada H, Sako T; Bull. Chem. Soc. Jpn. 53 (1980) 1303–1307.

37. Nordin J, Persson P, Nordin A, Sjoberg S; Langmuir 14 (1998) 3655–3662.

38. Ocakoglu K, Zafer C, Cetinkaya B, Icli S; Dyes Pigments 75 (2007) 385–394.

39. Okamura M, Hashimoto K, Shimada J, Sakagami H; Anticancer Res. 24 (2004) 655–662.

40. Patra A.K, Bhowmick T, Ramakumar S, Nethaji M, Chakravarty A.R; Dalton Trans.(2008) 6966–6976.

41. Pauwels R, Balzarini J, Baba M, Snoeck R, Schols D, Herdewijn P, Desmyter J, De Clercq E, Virol J; Methods 20 (1988) 309–321.

42. Paw W, Eisenberg R; Inorg. Chem. 36 (1997) 2287–2293.

43. Pivetta T, Cannas M.D, Demartin F, Castellano C, Vascellari S, Verani G, Isaia F; J. Inorg. Biochem. 105 (2011) 329–338.

44. Pivetta T, Isaia F, Verani G, Cannas C, Serra L, Castellano C, Demartin F, Pilla F, Manca M, Pani A; J. Inorg. Biochem. 114 (2012) 28–

45. Pivetta T, F. Isaia, F. Trudu, A. Pani, Manca, D. Perra M, Amato F; J. Havel, Talanta 115 (2013) 84–93.

46. Pople J.A, Beveridge D.A; Approximate Molecular Orbital Theory, McGraw-Hill, New York, 1970.

47. Poteet S, Majewski M, Breitbach Z.S, Griffith C.A, Singh S, Armstrong D.W, Wolf M.O, MacDonnell F.M; J Am Chem Soc. 135 (2013) 2419–2422.

48. Reichmann M.E, Rice S.A, Thomas C.A, Doty P; J. Am. Chem. Soc. 76 (1954) 3047–3053.

49. Roothaan C.C.J; Rev. Mod. Phys. 23 (1951) 69–89.

50. Roy S, Hagen K.D, Maheswari P.U, Lutz M, Spek A.L, Reedijk J,. Van Wezel G.P;Chem. Med. Chem. 3 (2008) 1427–1434.

51. Sheldrick G.M; Acta Crystallogr. 64A (2008) 112–122.

52. Sjoberg S, Hagglund Y, Nordin A, Ingri N, Mar. Chem. 13 (1983) 35–44.

53. Stephenson M.D, Hardie M.J; Dalton Trans. (2006) 3407–3417.

54. Sun Y, Hou Y.J, Zhou Q.X, Lei W.H, Chen J.R, Wang X.S, Zhang B.W; Inorg. Chem.49 (2010) 10108–10116.

55. Terwilliger NB; J. Exp. Biol. 201 (1998) 1085–1098.

56. Vacca A, Sabatini A, Bologni L; J. Chem. Soc. Dalton Trans. (1981) 1246–1250.

57. Veal J.M, Rill R.L; Biochemistry 30 (1991) 1132–1140.

58. Wein A.N, Stockhausen A.T, Hardcastle K.I, Saadein M.R, Peng S.B, Wang D, Shin D.M, Chen Z.G, Eichler J.F; J. Inorg. Biochem. 105 (2011) 663–668.

59. Whitfield M; J Chem Eng. Data 17 (1972) 124–128.

60. Zelenko O, Gallagher J, Sigman D.S; Angew. Chem. Int. Ed. Engl. 36 (1997) 2776–2778.

61. Zhang Q.G, Zhang F, Wang W.G, Wang X.L; J. Inorg. Biochem. 100 (2006) 1344–1352.

Part II – The garlic compound as anticancer agents

Introduction

Garlic (*Allium sativum L.*) is a widely used medicinal plant with multiple beneficial effects against cardiovascular diseases, infections, and cancer [Wang Y *et al.* (2015) Tumour Biol. Oct.]. The sulfur –containing compounds, extracted from crushed garlic, are responsible for these beneficial health effects. These compounds include *S*-allylcysteine (SAC), *S*-allylmercaptocysteine (SAMC), diallyl sulfide (DAS), diallyl disulfide (DADS), diallyl trisulfide (DATS), diallyl tetrasulfide (DATTS), and the thiosulfinate allicin (Figure 1 below).
Allicin is an unstable compound, but by its rearrangement may give rise a more stable compounds, including ajoene (*E*- and *Z*- 4,5,9- trithiadodeca-1,6,11-triene 9-oxide).

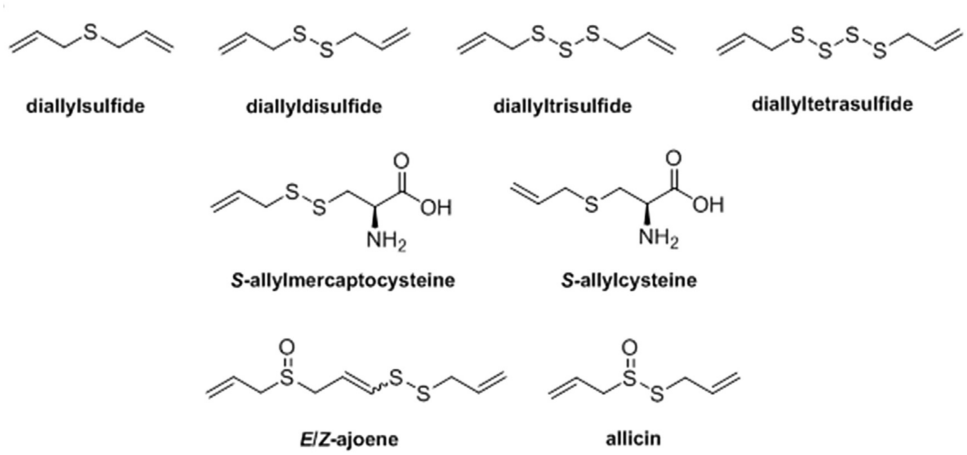

Figure 1 : **The major organosulfur compounds found in crushed garlic.**
Diallyl sulfide, diallyl disulfide, diallyl trisulfide, S-allylmercaptocysteine, S-allylcysteine *E*-ajoene, *Z*-ajoene and allicin.

These garlic organosulfur compounds are all reported to be active at inhibiting the proliferation of tumour cells [Bayan L *et al*. (2014) Avicenna J Phytomed], although our work has centred predominantly on the anti-cancer activity of Z-ajoene .

Z-ajoene (ZA) and the related garlic organosulfides all appear to induce apoptosis in cancer cells through the intrinsic pathway by activating the mitochondrial-dependent caspase cascade. In addition, Z-ajoene-induced apoptosis in these cells is reportedly accompanied by the generation of reactive oxygen species and the activation of nuclear factor kB [Dirsch, *et al.* (1998) Mol. Pharmacol]. Similar to other garlic-derived organosulfides, *Z*-ajoene is reported to arrest cells in the G2/M phase of the cell cycle [Capasso A. (2013) Molecules]. Although the downstream effects of *Z*-ajoene on cancer cells have been characterized, the specific *Z*-ajoene drug targets or early events leading to apoptosis are not known.
Ajoene has been shown to inhibit proliferation of a number of different malignant cell lines, including breast and esophageal cancers [Kaschula C.H. *et al.* (2012) Eur. J. Med. Chem].

Chapter I – Studies on the mode of action of *Z*-ajoene.

This chapter is divided into two sections: the first is entitled "*The Garlic Compound Z-ajoene Targets Protein Folding in the Endoplasmic Reticulum of Cancer Cells"* and we aimed to investigate about the mechanism by which the ajoene caused the cytotoxicity in cancer cells.
The second section is entitled "*Dansyl-ajoene (DP) colocalize with Protein Disulfide Isomerase (PDI) in the endoplasmic reticulum of human breast cancer cells"* and we aimed to identify whether the PDI is a main target for anti-cancer activity of Ajoene.

1.1 The garlic compound Z-ajoene targets protein folding in the endoplasmic reticulum of cancer cells

In this chapter, we aimed to investigate about the mechanism by which the ajoene caused the cytotoxicity in breast and esophageal cancers. For this, two fluorescently labelled ajoene analogs with dansyl- (DP) and fluorescein- (FOX) tags were synthesized.

We found that both DP and FOX inhibited the proliferation and induced apoptosis in human MDA-MB-231 breast and WHCO1 esophageal cancer cells. Both fluorescent ajoenes localized to the endoplasmic reticulum (ER) in MDA-MB-231 cells. Here, DP interacted with multiple ER resident proteins by *S*-thiolation in MDA-MB-231 cells as observed by immunoblotting under non-reducing conditions only; and a competition assay demonstrated that DP and Z-ajoene in fact share the same target. In the ER, ajoene *S*-thiolation interfered with protein folding and led to an accumulation of misfolded protein aggregates and activated the unfolded protein response (UPR). Consistent with this mechanism, increased levels of GRP78 and total ubiquitinated proteins were observed. This is the first time that ajoene has been shown to target protein folding in the ER of cancer cells.

The results of this study, that have been already published (http://onlinelibrary.wiley.com/doi/10.1002/mc.22364/full; license number 3791820755606) in Molecular Carcinogenesis in 2015 are fully described below.

The Garlic Compound Ajoene Targets Protein Folding in the Endoplasmic Reticulum of Cancer Cells

Catherine H. Kaschula,[1]* Roger Hunter,[1] Jonathan Cotton,[1] Rossana Tuveri,[2] Ellen Ngarande,[3] Kevin Dzobo,[4] Georgia Schäfer,[4,5] Vuyolwethu Siyo,[4] Dirk Lang,[6] Daniel A. Kusza,[1] Bronwen Davies,[1] Arieh A. Katz,[4,5] and M. Iqbal Parker[3,4]

[1]*Department of Chemistry, University of Cape Town, Rondebosch, Cape Town, South Africa*
[2]*Department of Biomedical Science, University of Cagliari, Monserrato (CA), Italy*
[3]*International Centre for Genetic Engineering and Biotechnology, Cape Town, South Africa*
[4]*Division of Medical Biochemistry, University of Cape Town, Cape Town, South Africa*
[5]*MRC/UCT Receptor Biology Unit, Institute of Infectious Disease and Molecular Medicine, University of Cape Town, Cape Town, South Africa*
[6]*Department of Human Biology, Division of Physiology, University of Cape Town, Cape Town, South Africa*

Ajoene is a natural allylsulfur compound found in crushed garlic that arrests growth and induces apoptosis in cancer cells. To gain mechanistic insights into the cytotoxicity of ajoene in cancer cells, two fluorescently labelled ajoene analogs with dansyl- (DP) and fluorescein- (FOX) tags were synthesized. The tagged ajoenes were found to retain their activity at inhibiting proliferation and inducing apoptosis in MDA-MB-231 human breast-cancer and WHCO1 human esophageal-cancer cells. Both tagged ajoenes localized to the endoplasmic reticulum (ER) in MDA-MB-231 cells as observed by live cell confocal laser scanning microscopy (CLSM) and confirmed by generating an MDA-MB-231 cell line expressing yellow fluorescent protein (YFP) in the ER. DP appears to *S*-thiolate multiple protein targets in MDA-MB-231 cells as observed by immunoblotting under non-reducing conditions only; and a competition assay demonstrated that DP and *Z*-ajoene in fact share the same target. Ajoene *S*-thiolation interfered with protein folding and led to an accumulation of misfolded protein aggregates and activated the unfolded protein response (UPR). Consistent with this mechanism, increased levels of GRP78 and total ubiquitinated proteins were observed; and an ER-folded protein, type-1 collagen, was tracked to the proteasome following ajoene treatment. The intracellular protein aggregates were observed by CLSM and transmission electron microscopy (TEM). This is the first time that ajoene has been shown to target protein folding in the ER of cancer cells.

Key words: ajoene; garlic; cancer prevention; endoplasmic reticulum; protein folding

INTRODUCTION

Garlic (*Allium sativum L.*) has been used in traditional medicine since ancient times as a prophylactic and therapeutic medicinal agent to treat infections, heart disease, and cancer. These beneficial health effects are ascribed to the sulfur-containing compounds found in crushed cloves, which include *S*-allylcysteine (SAC), *S*-allylmercaptocysteine (SAMC), diallyl sulfide (DAS), diallyl disulfide (DADS), diallyl trisulfide (DATS), diallyl tetrasulfide (DATTS), and the thiosulfinate allicin (see Figure 1A). Allicin is generated by the plant as a defence against pathogen invasion but is unstable, rearranging to the relatively stable ajoene (*E*- and *Z*- 4,5,9-trithiadodeca-1,6,11-triene 9-oxide) as one of the products. A common structural feature of these sulfur compounds is the presence of a sulfide or polysulfide functional group, which is proposed to be the bioactive pharmacophore [1–3]. Epidemiological evidence supports an inverse link between garlic consumption and cancer risk, particularly of the stomach and colon [4,5]. This chemopreventive activity may partially be explained by the known anti-mutagenic and immuno-modulatory effects of garlic allylsulfur compounds, as well as their ability to exert a direct anti-proliferative effect on growing tumor cells by inducing apoptosis [6–9].

Ajoene has been shown to inhibit proliferation of a number of different malignant cell lines which

Abbreviations: ER, Endoplasmic Reticulum; CLSM, Confocal Laser Scanning Microscopy; YFP, Yellow Fluorescent Protein; UPR, Unfolded Protein Response; TEM, Transmission Electron Microscopy; ROS, Reactive Oxygen Species; MAKPs, Mitogen Activated Kinases; JNK, c-Jun NH2-terminal Kinase; GR, Glutathione Reductase; TLC, Thin Layer Chromatography, m-CPBA, meta-Chloroperbenzoic acid; HPLC, High Performance Liquid Chromatography; ERAD, ER-Associated Protein Degradation.

Grant sponsor: National Research Foundation of South Africa (NRF); Grant sponsor: University of Cape Town (UCT); Grant sponsor: Cancer Society of South Africa (CANSA); Grant sponsor: International Centre for Genetic Engineering and Biotechnology (ICGEB); Grant sponsor: Cancer Research Trust

*Correspondence to: Department of Chemistry, University of Cape Town, Rondebosch, Cape Town 7701, South Africa.

Received 2 April 2015; Revised 19 June 2015; Accepted 26 June 2015

DOI 10.1002/mc.22364

Published online in Wiley Online Library (wileyonlinelibrary.com).

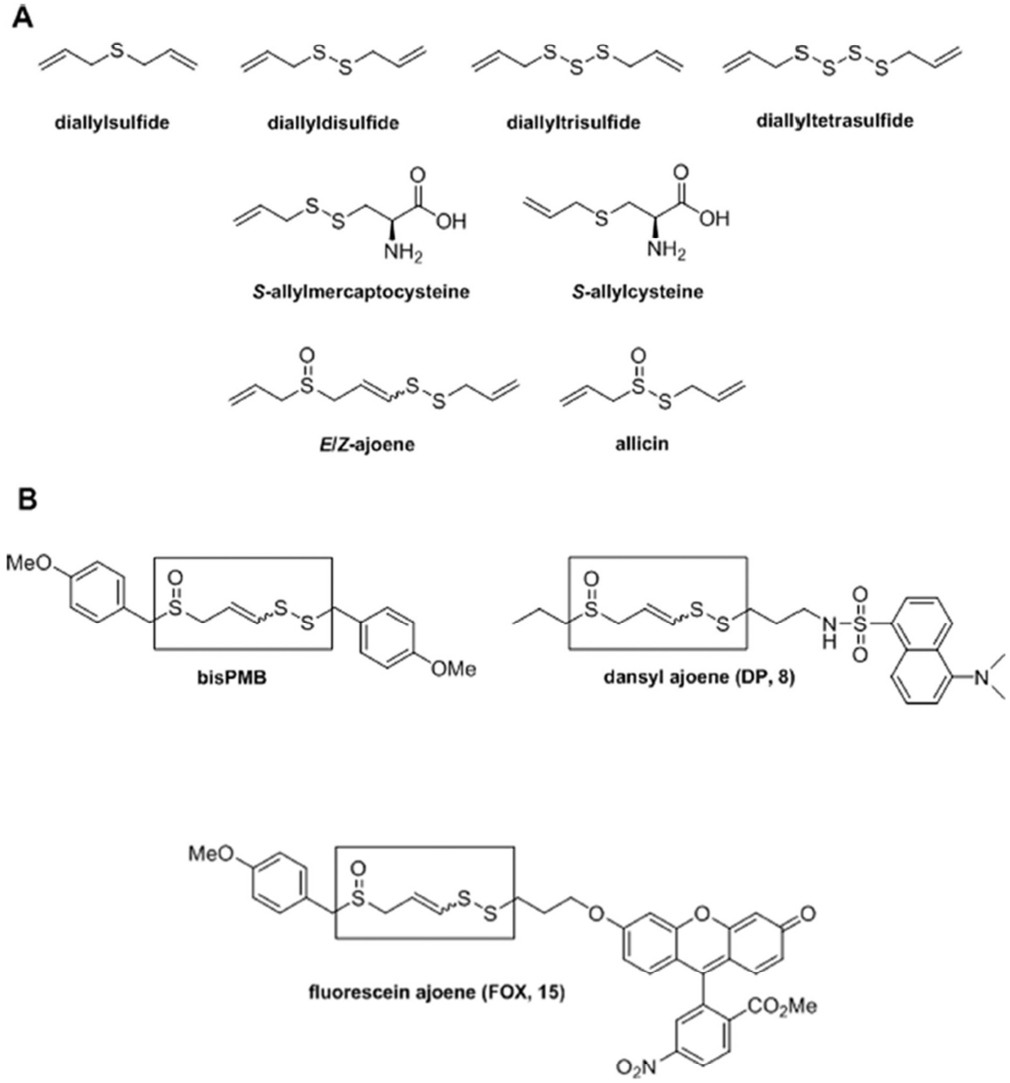

Figure 1. Chemical structures of garlic allylsulfur compounds and derivatives. (A) A collection of the major allylsulfur compounds found in crushed garlic: diallyl sulfide (DAS), diallyldisulfide (DADS), diallyltrisulfide (DATS), diallyltetrasulfide (DAS4), S-allyl mercaptocysteine (SAMC), S-allylcysteine (SAC), E/Z-ajoene, and allicin. (B) Chemical structures of synthetic ajoene analogs: bisPMB, dansyl ajoene (DP, 8), and fluorescein ajoene (FOX, 15). The sulfoxide/vinyl disulfide pharmacophore of ajoene is boxed.

include mammary, bladder, colorectal, hepatic, nasopharyngeal, gastric, esophageal, prostate, lung, pancreatic, lymphoma, leukemia, and skin with IC_{50}'s in the range 5–40 μM [2,10–12]. In vivo, ajoene has been shown to inhibit a two-stage carcinogenesis test on mouse skin [13], and to decease basal cell carcinoma size when applied topically to humans [14]. When administered by intraperitoneal injection into mice, ajoene has been shown in two reports [11,12], to cause a threefold reduction in the growth of murine tumor cells. The biological mechanism of ajoene-induced apoptosis in cancer cells appears to be complex and is not known in much detail, although the final result of apoptosis has been shown to proceed via the intrinsic pathway involving mitochondrial membrane permeabilization, cytochrome c release, and subsequent caspase activation [15,16]. Additionally, ajoene has been shown to generate reactive oxygen species (ROS) independent of mitochondrial perturbation which may also contribute to the observed cytotoxic effects [17]. Ajoene-induced cell death in human promyleoleukemic cells is reported to induce activation of the mitogen-activated kinases (MAPKs) c-Jun NH_2-terminal kinase (JNK), p38

and extracellular signal-regulated kinases (ERK) 1/2 as well as the survival kinase Akt [18].

It has long been known that garlic allylsulfur compounds can react with small molecule thiols (for example cysteine or glutathione) to form mixed disulfides [2,19–21], and that *S*-thiolation between a free cysteine thiol of a target protein and the garlic disulfide, may play a role in the cytotoxicity of ajoene in cancer cells. The specific protein target of ajoene is not known, although a few candidates have been proposed. The finding that ajoene causes complete disassembly of the microtubule network [12] has led to speculation that the microtubule network may be the ajoene target. Support for this has come from the observation that DATS oxidatively modifies β-tubulin, the major protein constituent of microtubules, at cysteine residues Cys-12β and Cys-354β although it must be cautioned that this has only been evidenced in vitro and not in cells. Ajoene has also been shown to effectively *S*-thiolate and inactivate the human glutathione reductase protein (GR) through mixed disulfide formation with Cys-58 in the active site of the enzyme, leading to speculation that GR may be the ajoene target [22]. The related garlic compound allicin has been shown to inactivate papain and alcohol dehydrogenase to form an inactive *S*-alkylated product [20]. In addition, the water soluble garlic compound 2-propenylthiosulfate (2-PTS) has been shown to inactivate sulfur transferases [21] and rhodanese [23] through *S*-thiolation.

In the current study, we have synthesized two fluorescently tagged ajoenes that were used to track the movement and localization of ajoene within the cancer cell. Our results demonstrate that ajoene *S*-thiolates multiple protein targets and interferes with protein folding in the ER of cancer cells.

MATERIALS AND METHODS

Synthesis

The detailed synthetic methods as well as characterization of intermediates and target compounds FOX and DP is located in the supplementary section.

Cell Lines and Culture Conditions

The esophageal cancer cell-line WHCO1 was derived from a biopsy of primary esophageal squamous cell carcinoma of South African origin [24]; the CT1 cells (transformed WI38 cells) were a gift from Dr Masayosi Namba (University of Tokyo, Japan); the MDA-MB-231 cells were purchased from ATCC. Cells were all incubated at 37°C under 5% CO_2 and cultured with antibiotics in DMEM (Dulbecco's Modified Eagle Medium) containing 10% FBS (Foetal Bovine Serum, Gibco, Life Technologies, South Africa).

Cellular Viability Assay

Cytotoxicity of compounds was evaluated using the standard 3-(4,5-dimethylthiazol-2-yl)-2,5-diphenyltetrazolium bromide (MTT, Sigma-Aldrich, South Africa) cellular viability assay. Briefly, MDA-MB-231 or WHCO1 cells at a density of $2.5–3.0 \times 10^3$ cells per well were seeded in 96-well plates and allowed to settle overnight. Each compound in DMSO (0.1% v/v, Sigma) was then added to the cells for the indicated incubation times. Thereafter, 10 μL of 5 mg/mL MTT was added and incubated with the cells for 4 h, followed by addition of 100 μL 10% SLS, 0.01 M HCl (Merck, Darmstadt, Germany) to solubilize the formazan crystals. The plates were read at 595 nm on a Multiscan FC plate reader (Thermo Fischer Scientific, Life Technologies, South Africa), and data was analyzed using Graphpad Prism 4 software, sigmoidal dose–response variable slope curve fitting.

Apoptosis Assay

Apoptosis was quantified using the Cell Death Detection ELISA kit (Roche, South Africa) according to the manufacturer's instruction. Briefly, MDA-MB-231 cells at a density of 6×10^3 cells per well were seeded in a 96-well plate and allowed to settle overnight. Each compound in DMSO (0.1% v/v) was then added at the indicated concentration for 24 h; thereafter, cell lysates were prepared and 20 μL transferred to a streptavidin coated plate for analysis. The absorbance at 405 and 495 nm was read using a Multiscan FC plate reader (Thermo Fischer Scientific, Life Technologies).

Stable Transfection of YFP-ER

MDA-MB-231 human breast cancer cells expressing yellow fluorescent protein (YFP) in the ER were generated by stable transfection with the plasmid pEYFP-ER. Briefly, 1×10^5 cells were seeded on a 35 mm dish and allowed to settle overnight. The cells were then transfected with 2 μg plasmid DNA (either pEYFP-ER or YFP-C1 control, Clontech, Separations, South Africa), using TransFectin Lipid Reagent (Bio-Rad) according to the manufacturer's instruction. The following day, medium containing the transfection mixture was replaced by fresh culture medium containing 400 μg/mL G418 (Invitrogen, Life Technologies, South Africa) to select for stable transfectants. Successfully transfected cells were identified by CLSM visualizing YFP localization in the ER (pEYFP-ER transfectants) or in the cytosol (control YFP-C1 transfectants), respectively.

Preparation of Fixed Slides

MDA-MB-231 or MDA-MB-231-YFP(ER) cells (1×10^5 cells per well) were seeded on sterile coverslips in six-well plates. The following day cells were treated with the respective compound in DMSO (0.1% v/v), for the indicated time. Thereafter, cells were washed with PBS, permeabilized with absolute methanol at −20°C for 5 min and fixed in 4% paraformaldehyde (Sigma-Aldrich) for 5 min. Cell sections were then washed with PBS and mounted using Mowiol 4-88 (Sigma-Aldrich). The sections were stored in the dark at 4°C until viewing.

Live Cell Imaging

Cultured MDA-MB-231 cells (3.5×10^4 cells per well) were plated on eight well chambered coverglass (Lab-Tek II, 1.5 borosilicate, Australia) in DMEM and allowed to settle overnight. Organelle labeling was performed with ER-tracker RED (1 μM), Mitotracker GREEN (250 nM) (both Invitrogen), or Nile Red (5 μM) (Sigma-Aldrich) for 30 min, followed by addition of the compounds DP or FOX at a final concentration of 25 μM in 0.1% DMSO. Cells were viewed by CLSM (Zeiss LSM510 NLO fitted with a Mai Tai DeepSee Titanium: Sapphire femtosecond laser for 2-photon excitation at 37°C under an atmosphere of 5% CO_2).

Immunoblotting

For detection of proteins from MDA-MB-231, WHCO1, or CT1 cell lysates by immunoblot, standard protocols were applied. Cells were seeded and treated as follows: (1) For the detection of dansylated proteins, 6×10^5 MDA-MB-231 cells were seeded in a 100 mm culture dish and treated with 25 μM DP in DMSO (0.1% v/v) or DMSO alone (control) for 6 or 24 h. (2) For the detection of ubiquitinated proteins, MDA-MB-232 cells were treated with 20 μM *Z*-ajoene in DMSO (0.1% v/v) for 1, 2, 3, 4, 6, and 8 h. Control cells received DMSO (0.1% v/v) alone. (3) For the detection of type-1 collagen protein, 1×10^6 CT1 fibroblast cells were seeded in 100 mm culture dishes. After adherence overnight, the culture medium was replaced with fresh medium containing 50 μg/mL ascorbic acid (Sigma-Aldrich), 50 μg/mL β-aminopropionitrile (Sigma-Aldrich), and 20 μM *Z*-ajoene or 4 μM bisPMB. Where indicated, the proteasome inhibitor MG132 (5 μM, Sigma-Aldrich) was added 30 min prior to addition of *Z*-ajoene or bisPMB. Cells were incubated with the ajoene compound for a total of 24 h.

Cells were lysed in RIPA buffer (Cell Signalling Anatech, Technology, South Africa) containing 20 mM of the reducing agent β-mercaptoethanol (Sigma-Aldrich) only where indicated. Total protein was quantified using the Pierce BCA protein assay kit (Thermo Fischer Scientific, Life Technologies). For all Western blotting, 10–20 μg of total protein was separated by SDS-PAGE and transferred to nitrocellulose membranes. Membranes were blocked for 1 h at room temperature with 5% non-fat milk in tris-buffered saline (TBS) containing Tween-20 and incubated with the primary antibodies overnight at 4°C: anti-ubiquitin (1:500, Santa Cruz, Whitehead Scientific, South Africa); anti-dansyl (1:7500, Molecular Probes, Life Technologies, South Africa); anti-pro collagen type I (1:1000, Southern Biotech); anti-β-tubulin and anti-GAPDH (1:1000) (both Santa Cruz, Whitehead Scientific). Specific proteins were detected using appropriate horseradish peroxidase-conjugated secondary antibodies and the LumiGLO chemiluminescent reagent (KPL, Biocom Biotech, South Africa). A protein ladder (Thermo Fischer Scientific, Life Technologies) was used to estimate the molecular weight of proteins.

Competition Assay

Fixed slides: MDA-MB-231 cells were seeded on glass slides in six-well plates and allowed to settle overnight. Thereafter, cells were pre-treated with *Z*-ajoene (20, 40 or 60 μM) for 2 h, followed by addition of DP (20 μM) and incubated for a further 6 h. Control cells were either untreated or treated with DP (20 μM) alone. The cells were then fixed and mounted as described above or lysate was collected for Western blotting. For fluorescence quantification, 5× *Z*-stacks were obtained per image and fluorescence per cell was quantified using Carl Zeiss blue Zen 2012 software. An average of 10 cells was quantified in triplicate slides per timepoint from which the background fluorescence in the untreated (control) cells was subtracted.

Analysis of Secreted Type-1 Collagen

Fibroblast CT1 cells were seeded at a density of 1×10^6 cells in 100 mm dishes and allowed to settle overnight. The medium was then replaced with serum-free DMEM containing 50 μg/mL ascorbic acid (Sigma-Aldrich), 50 μg/mL β-aminopropionitrile (Sigma-Aldrich), and 4 μM bisPMB. (2, 3, 4, 5-^{3}H) proline (44 Ci/mmol; AEC Amersham, South Africa) was added at a final concentration of 10 μCi/mL for 24 h. Where indicated, the inhibitor MG132 (5 μM) was added 30 min prior to addition of bisPMB. Cell monolayers and media were recovered separately and a mixture of protease inhibitors was added according to previous methods [25,26]. The media was clarified by centrifugation followed by the addition of one tenth volume of 5 M acetic acid, digestion with 100 μg/mL pepsin for 4 h at room temperature and dialysis against distilled water. Samples were then lyophilized and redissolved in lysis buffer. Aliquots of the samples were transferred to scintillation vials containing 5 mL of scintillation fluid and total radioactivity was assessed by counting separate aliquots of solubilized cells or media. A minimum of 2×10^6 dpm was loaded on 8% SDS polyacrylamide gels and run at 100 V. Gels were soaked in 1 M sodium salicylate and labelled collagen was detected by fluorography of dried gels after exposure to X-ray film at −80°C for 48 h.

Transmission Electron Microscopy

MDA-MB-231 cells were plated in 145 mm plates, allowed to settle overnight, and treated with 10 μM bisPMB in DMSO (0.1% v/v) or DMSO alone (control) for 1 or 24 h. The media was then removed and the cells washed with cold PBS, followed by addition of 2.5% glutaraldehyde in PBS for 24 h at 4°C. Fixed cells were harvested by gentle mechanical scraping and collected by centrifugation. The pellet was then re-suspended in 150 μL low gelling agarose and incubated at 4°C for 2 h to allow setting of the agarose. The jellified

pellets were dissected into pieces of approximately 1 mm^3 and 1% osmium tetroxide (Sigma-Aldrich) in PBS was added to each sample and allowed to stand for 2 h. Thereafter, the osmium tetroxide was removed and the samples washed with PBS and water. The samples were then dehydrated by subjecting to increased concentrations of ethanol (from 30–100%) for 10 min each, followed by incubations in 100% acetone for 15 min (twice). The samples were then agitated in increasing concentrations of resin in acetone: 50, 75 (1 mL for 8 h) and finally 100% (2 × 1 mL for 8 h). The samples were then transferred to molds at 60°C for overnight embedding and sectioned on a Leica Ultrasemi Microtome into 0.12 μm slices, collected on copper grids, post fixed with uranyl acetate and lead citrate and viewed by TEM (Zeiss 912 Omega EFTEM).

RESULTS

Synthesis of Fluorescently Tagged Ajoene Analogs

Two fluorescently tagged ajoene analogs were synthesized. Synthesis of the dansyl-tagged ajoene (DP) was relatively straightforward [27] and is shown in Figure 2 (Part A). Thus, using our published synthesis for ajoene analogs [2,28], 1-propylthiol was alkylated with propargyl bromide to the propargyl sulfide, which underwent a regioselective and moderately stereoselective radical addition with thiolacetic acid to furnish vinyl thioacetate (**2**) as a 3:5 *E:Z*-mixture of stereoisomers. Thereafter, low temperature base cleavage of **2** to its enethiolate isomer followed by *S*-thioalkylation with (**6**) (routinely prepared from 3-aminopropanol via a dansylation, mesylation, iodination, substitution sequence involving thiotosylate as nucleophile in the final step to give compounds **3**–**6**, respectively) furnished the coupled disulfide (**7**). This was chemoselectively mono-oxidized at the sulfide sulfur to afford the target fluorescent ajoene derivative (DP, 8) as a 3:2 *E*/*Z*-mixture of stereoisomers that proved inseparable by chromatography.

By comparison to DP, synthesis of the fluorescein derivative designated as FOX, was more complex. Initial attempts to incorporate the tag into the ajoene structure, either via the commercially available fluorescein isothiocyanate or the corresponding amine suffered difficulties involving the well-known facile opening of the lactone ring. Eventually, a way around this without compromising the spectroscopic characteristics of the tag was found by opening the lactone to its methyl ester. Hence, a total synthesis from cheap starting materials based on a well-known condensation reaction was accomplished in the following way. Thermal condensation of 4-nitrophthalic acid with resorcinol gave a mixture of regioisomeric 4- and 5-nitrofluoresceins (**9**) (lactone carbonyl-bearing carbon as C-1) that could not be separated chromatographically or by fractional crystallization. For this a literature procedure was followed [29], which involved converting the mixture to the diacetates by refluxing in acetic anhydride and then subjecting the product to a fractional crystallization. Deprotection of the individual regioisomers with sodium hydroxide, followed by exposure to acetic acid to restore the lactone ring furnished crystalline 4- and 5-isomers (**9a** and **b**) in 18 and 17% yield, respectively (Figure 2 Part B). Arbitrarily, we chose the 4-isomer (**9b**) to take through, which was esterified with refluxing methanol in sulfuric acid to afford the open-form fluorescein methyl ester (**10**) (Figure 2 Part C). Conversion of the latter into an appropriate sulfenylating agent for incorporation of the tag into the ajoene skeleton was achieved by alkylating the phenol of (**10**) with bis-electrophile (**11**) derived from mono-substitution of 1,3-dibromopropane with potassium thiotosylate. The alkylation was conducted under standard conditions of potassium carbonate in refluxing acetonitrile and furnished the *O*-alkylated product (**12**) with retention of the thiotosylate grouping, presumably as a result of a marginal hard–hard preference between the phenoxide and bromide. With (**12**) in hand we could resort to our synthesis to finish. This time, based on the finding that a *para*-methoxybenzyl end group significantly improved the bioactivity of the ajoene, vinyl disulfide (**13**), derived in a similar fashion to (**2**), was reacted under the standard conditions of KOH/MeOH at −40°C to form the enethiolate, which was then coupled with the fluorescein sulfenylating agent (**12**). This successfully furnished disulfide (**14**) in a very respectable 84% yield and as a 1:1 mixture of (*E*/*Z*)-isomers. Finally, chemoselective oxidation of the sulfide sulfur with *m*-CPBA at low temperature as before with DP afforded the target fluorescein ajoene (FOX, **15**) in 62% yield and as a 4:3 mixture of *E:Z* isomers after column chromatography, Figure 2 Part D. As with the dansyl derivative (DP), no attempt was made to separate the stereoisomers, since previous studies from our group [28] had shown that both are almost equally active against cancer cells, albeit with the *Z*-isomer generally a little more active than the *E*-isomer [2,28]. However, using the full gamut of NMR techniques, resonances for the individual isomers of (DP) and (FOX) could be identified in both ^{1}H and ^{13}C NMR spectra in which geometrical isomers could be easily distinguished by virtue of the coupling constant of the α-vinyl hydrogen of the vinyl disulfide. Additionally, dansyl ajoene (DP) as an oil, gave satisfactory high resolution mass spectral data, while the fluorescein ajoene (FOX) was a crystalline solid that could be recrystallized to return acceptable combustion analysis as well as satisfactory high resolution mass spectral and HPLC data.

The Cytotoxicity of Fluorescent Ajoenes in Cancer Cells

Fluorescent ajoenes DP and FOX were tested for their cytotoxicity in both WHCO1 human esophageal and MDA-MB-231 human breast cancer cells using the MTT cell viability assay. The parent compounds

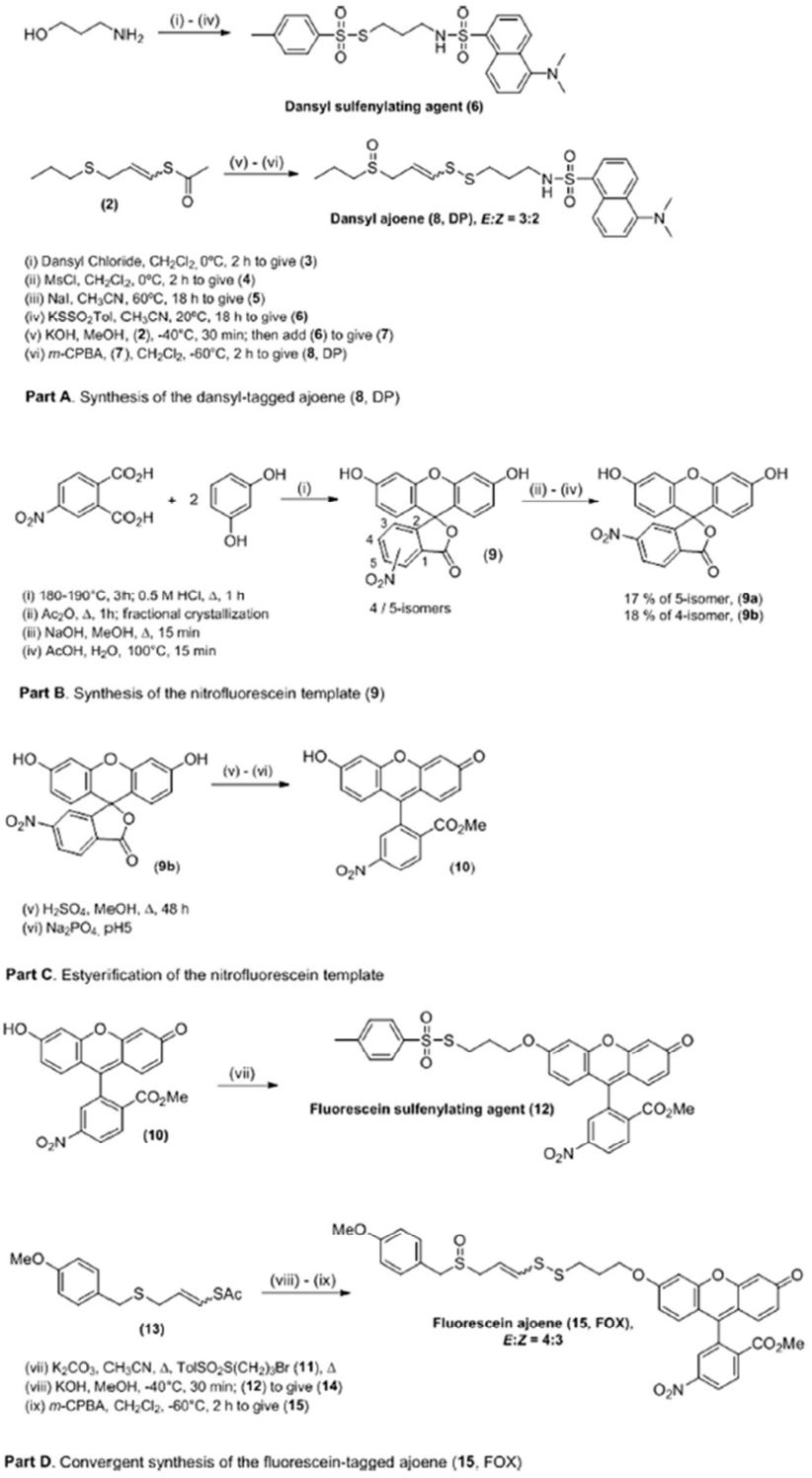

Figure 2. (A) Synthetic route to the dansyl-tagged ajoene (DP, **8**) which proceeds through generation of a dansyl sulfenylating agent (**6**); (B–D) convergent synthetic route to the fluorescein-tagged ajoene (FOX, **15**) which proceeds via the nitrofluorescein template (**9**) followed by esterification (**10**) to generate the sulfenylating agent (**12**) which is coupled to the vinyl thioacetate (**13**) to give the desired product (**15**).

A

Compound	IC_{50} ± SD (μM)	
	MDA-MB-231	WHCO1
E-ajoene	19 ± 5.5 [26]	39 ± 7.8 [26]
Z-ajoene	14 ± 2.0 [26]	25 ± 2.8 [26]
DP	21 ± 6.2	15 ± 4.2
FOX	15 ± 1.1	7.8 ± 4.6
dansyl chloride	> 200	> 200

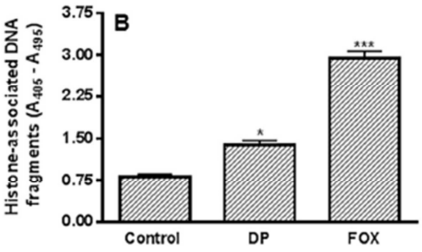

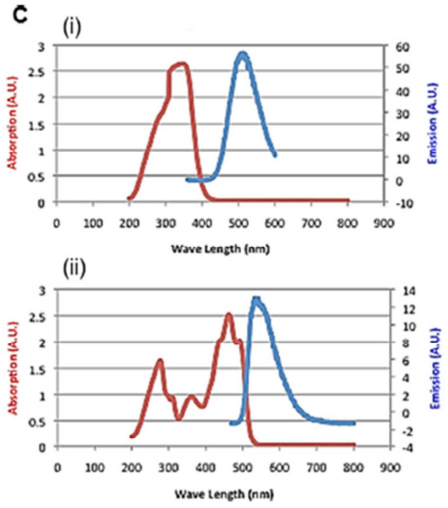

(iii)

Compound	λ_{EX} (nm)	λ_{EM} (nm)
DP	331	515
FOX	460	546
dansyl chloride	337	492
fluorescein	495	515

Figure 3. Cytotoxicity and fluorescence properties of synthetic ajoenes DP and FOX. (A) Comparison of the cytotoxicity of ajoene and fluorescent ajoenes DP and FOX in WHCO1 and MDA-MB-231 cancer cells, measured by the MTT cellular viability assay. IC_{50} values are displayed as mean ± SD of three independent determinations. (B) Fluorescent ajoenes DP and FOX (25 μM) induce apoptosis in WHCO1 cancer cells as quantitated by accumulation of histone-associated DNA fragments in the cytoplasm after 24 h treatment. Data displayed as mean ± SD ($n = 3$). *P-value < 0.05, ***P-value < 0.005. (C) Absorption and emission spectra of DP (i) and FOX (ii) together with the (iii) recorded excitation and emission maxima.

Z- and *E*-ajoene were also included in the study for comparison. The concentration of compound required to obtain 50% inhibition of cell growth (IC_{50}) was calculated and is reported in Figure 3A. Dansyl chloride itself was found to have no inhibitory effect on the viability of either cell line when tested up to 200 μM. Both DP and FOX had similar activities to *E*- and *Z*-ajoene with FOX actually displaying some enhanced activity against WHCO1 cells.

Since ajoene is known to inhibit cell proliferation by inducing apoptosis, DP and FOX were assayed for their ability to induce apoptosis in WHCO1 cells by quantifying histone-associated DNA fragments in the cytoplasm after treatment. After 24 h incubation, both DP and FOX (25 μM) were found to cause a significant increase in cytoplasmic nucleosomes implying that apoptosis had been induced by the compound (Figure 3B).

The fluorescence profile of tagged ajoene analogs DP and FOX was then investigated. DP was found to have an absorbance maximum at 331 nm, fluorescing aqua-blue with a strong emission at 515 nm (Figure 3C (i)). Compared to dansyl chloride, conjugating the dansyl group to ajoene caused a slight red shift in the dansyl emission spectrum from 492 to 515 nm. Fluorescein analog FOX, on the other hand, was found to have an absorbance maximum at 460 nm and to fluoresce green with a strong emission maxima at 546 nm (Figure 3C (ii)).

Ajoene Localizes to the Endoplasmic Reticulum in MDA-MB-231 Cells

The aim of this study was to track the movement and localization of ajoene in cancer cells. MDA-MB-231 breast-cancer cells were chosen for this experiment owing to their clearly distinguishable cytoplasmic region which enables easy intracellular viewing compared to most other cancer cells, (for example the WHCO1 cells), that have a small cytoplasmic region in comparison to a large nucleus. MDA-MB-231 breast cancer cells were cultured on borosilicate chambered coverglass and cellular organelles were fluorescently labelled with live cell dyes specific for the mitochondria or endoplasmic reticulum. The live cells were treated with DP or FOX (25 μM) and maintained in an incubation chamber on the confocal microscope stage for the duration of the experiment. Due to the excitation maximum for DP being in the UV range, cells treated with DP were excited using a Mai Tai DeepSee Titanium 2-photon laser to avoid the harmful effects of short wavelength radiation on live cells. After 2 h incubation with DP, a strong blue peri-nuclear,

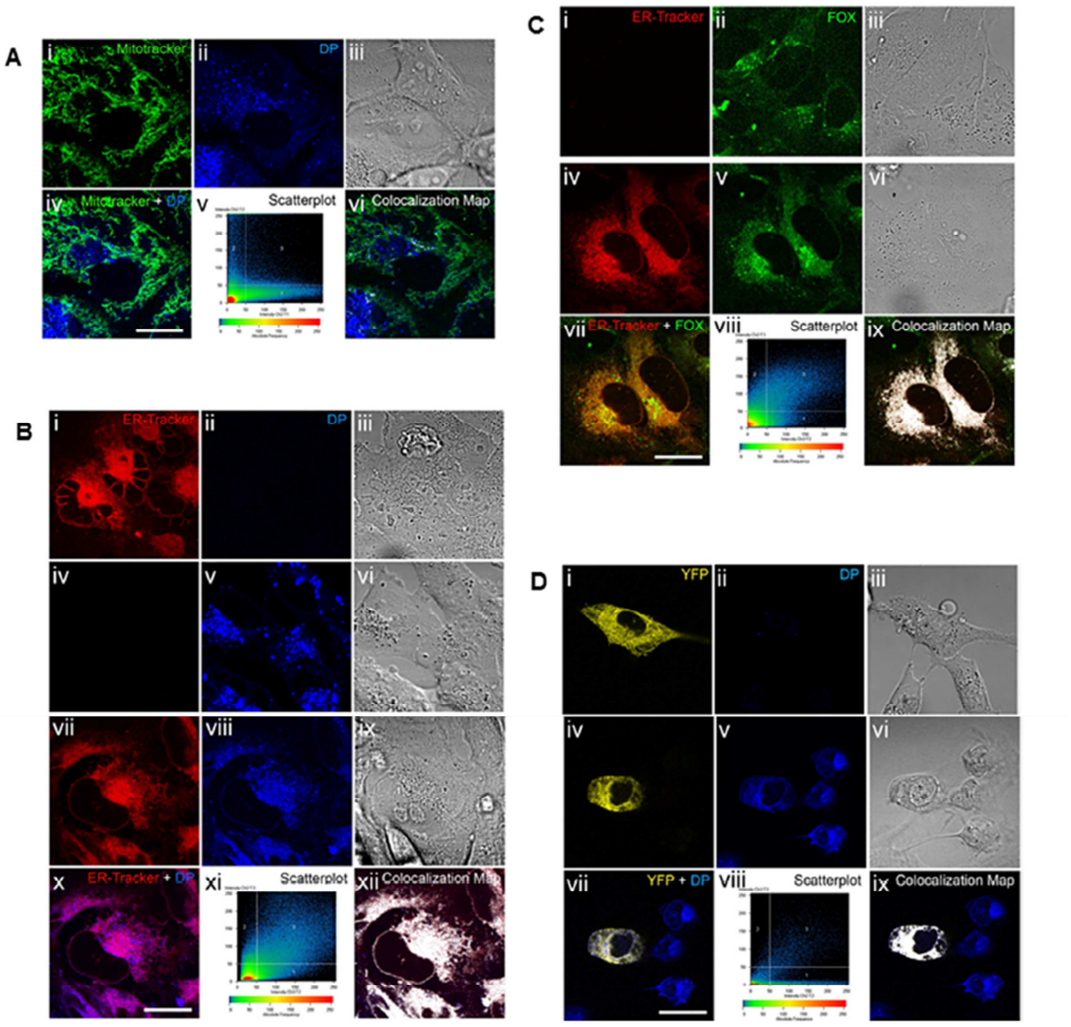

Figure 4. Fluorescent ajoenes DP and FOX localize to the endoplasmic reticulum in MDA-MB-231 breast cancer cells. Cells were pre-labelled with live cell dyes and then treated with 25 μM DP or FOX for 1–6 h. Fluorescence was viewed by CLSM housed with an incubation chamber for live cell imaging. Experiments were repeated multiple times but only representative images are displayed. (A) Live-cell imaging after 2 h treatment with DP, mitochondria stained green. (i) Green channel, (ii) blue channel, (iii) phase contrast, (iv) merged green + blue signals, (v) scatterplot, and (vi) colocalization map of green and blue signals. (B) Live cell imaging after 6 h treatment with DP, ER-stained red. Cells treated with (i, ii, iii) ER tracker alone; (iv, v, vi) DP alone; (vii, viii, ix) ER tracker + DP; (x) merged red + blue signals; (xi) scatterplot; and (xii) colocalization map of red and blue signals. (C) Live cell imaging after 4 h treatment with FOX, ER-stained red. (i, ii, iii) FOX alone; (iv, v, vi) FOX + ER-tracker red; (vii) merged red + green signals; (viii) scatterplot; and (ix) colocalization map of red and green signals. (D) Fixed slides of MDA-MD-231-YFP(ER) cells after 6 h treatment with DP. (i, ii, iii) untreated; (iv, v, vi) DP treated; (vii) merged yellow and blue signals; (viii) scatterplot; and (ix) colocalization map of yellow and blue signals.

clumped fluorescence signal was observed in the MDA-MB-231 cells (Figure 4A (ii)). This distribution was dissimilar to that of the mitochondrial labelling (Figure 4A (i)) and no colocalization was observed between the mitotracker-green and the blue fluorescence signals from DP as shown in the merged image (Figure 4A (iv)). This was further confirmed by a scatterplot, that shows the numbers and intensity distributions of pixels containing information of one or both relevant channels, and colocalization map (Figure 4A (v) and (vi), respectively). By comparison, stringent colocalization was observed between ER-tracker red and DP [27] as evidenced by the similar distribution patterns of the two fluorophores (Figure 4B (vii) and (viii)). In control experiments, it was observed that ER-tracker red does not fluoresce in the blue channel (Figure 4B (ii)) and that DP does not fluoresce in the red channel (Figure 4B (iv)). The colocalization was confirmed by overlaying the two signals to generate a pink overlay (Figure 4B (x)) and

confirmed by scatter plot and colocalization map (Figure 4B (xi) and (xii), respectively). A similar experiment was then repeated using the second fluorescent ajoene analog FOX. In this instance, FOX alone fluoresced green (Figure 4C (ii)) with no red fluorescence detected (Figure 4C (i)). In cells treated with both FOX and ER-tracker red (Figure 4C (iv) and (v)), stringent colocalization was observed between the ER-tracker and the green fluorescence from FOX to give a merged yellow signal (Figure 4C (vii)). Colocalization was confirmed by the intensity distribution of pixels for the relevant channels and the colocalization map (Figure 4C (viii) and (ix)).

To further confirm this result without the use of live cell dyes, an MDA-MB-231 cell line expressing yellow fluorescent protein (YFP) in the ER was generated by stable transfection of parental MDA-MB-231 cells with the vector pEYFP-ER. Fixed slides were prepared of DP-treated MDA-MB-231-YFP(ER) cells (6 h incubation). Not every cell expressed the YFP-ER; however, in those cells positive for YFP, fine ER organelle substructures were observed (Figure 4D (i)). In addition, no yellow fluorescence from YFP was observed in the blue channel (Figure 4D (ii)). MDA-MB-231-YFP(ER) cells treated with DP showed a similar blue distribution pattern to the yellow YFP expressing cells alone. Colocalization was confirmed between the YFP signal and the blue fluorescence from DP by scatter plot and colocalization map (Figure 4D (viii) and (ix)). Taken together, these data clearly show that both fluorescent ajoenes DP and FOX enter MDA-MB-231 breast cancer cells where they localize to the endoplasmic reticulum.

Dansyl-Ajoene *S*-Thiolates Multiple Protein Targets in MDA-MB-231 cells

Garlic sulfur-containing compounds including ajoene are hypothesized [1,30] to *S*-thiolate, a free cysteine thiol in a target protein to form an alkylated protein product (see Figure 5) which may alter the

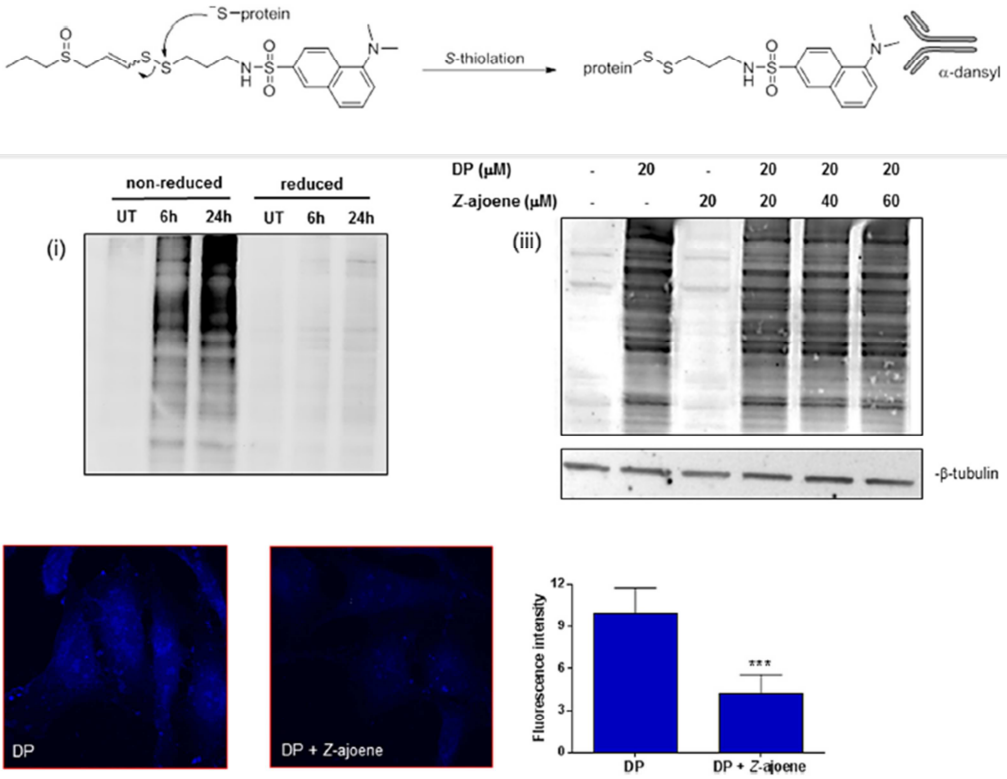

Figure 5. Ajoene *S*-thiolates multiple protein targets in MDA-MB-231 breast cancer cells. Scheme depicting proposed mechanism of protein *S*-thiolation involving transfer of the dansyl group from dansyl ajoene to the protein target during thiolysis. (i) Western blot showing multiple dansylated proteins in DP-treated MDA-MB-231 cell lysate when run under non-reducing conditions only. Cells were either untreated (UT), or treated for 6 or 24 h with 25 μM DP. Same lysate treated without (non-reducing) or with (reducing) β-mercaptoethanol. (ii) Competition assay between DP and *Z*-ajoene. MDA-MB-231 cells were pre-treated with *Z*-ajoene (20, 40, or 60 μM) for 2 h followed by addition of 20 μM DP for an additional 6 h. Cell lysate was collected, and total dansylated proteins were detected by immunoblot under non-reducing conditions. (iii) Representative images acquired by CLSM of MDA-MB-231 cells treated with 20 μM DP alone or 20 μM DP in combination with 20 μM *Z*-ajoene. Intracellular fluorescence was quantified as described in the materials and methods section. Data displayed as mean ± SD (***P-value < 0.005).

function of that protein. MDA-MB-231 tumor cells were treated with DP (25 μM) for 6 and 24 h, and the resulting protein lysate was collected under non-reducing conditions, separated by SDS-PAGE and probed with an anti-dansyl antibody (Figure 5 (i)). Multiple dansylated protein bands were observed that were absent in the untreated control (UT, 0.1% DMSO only). Reduction of the samples using β-mercaptoethanol resulted in disappearance of the anti-dansyl active protein bands. This data suggests that DP *S*-thiolates multiple protein targets in MDA-MB-231 cells, which is reversed upon reduction of the sample (cleavage of the disulfide bond).

Since we are interested in the cytotoxic effects of ajoene and not that of DP per se, we decided to perform a competition assay to ascertain whether DP and ajoene in fact compete for the same target. To this end, MDA-MB-231 cells were treated with 20 μM DP alone or with 20 μM DP in the presence of *Z*-ajoene (20, 40, or 60 μM). The cells were then either fixed and viewed by CLSM (Figure 5 (ii)) or lysed under non-reducing conditions and the dansylated proteins probed by immunoblot (Figure 5 (iii)). It is evident that the fluorescence intensity from the dansyl fluorophore is greater in those cells treated with DP alone compared to those cells treated with DP + *Z*-ajoene and quantification of the fluorescence revealed a twofold reduction in the intracellular signal. In addition, a reduction in the number of dansylated proteins was observed in cells treated with a combination of *Z*-ajoene and DP compared to those cells treated with DP alone. These data support the hypothesis that DP and Z-ajoene share the same protein targets in MDA-MB-231 cells owing to the fact that they share the same vinyl disulfide/sulfoxide pharmacophore.

Being lipophilic, ajoene may cross the membrane and enter the cytoplasm via passive diffusion [31]. The cytoplasm is a highly reducing environment not conducive to disulfide bond formation. The lumen of the ER is, however, more oxidizing, maintained to support disulfide bond formation between cysteine residues in the same protein or between adjacent proteins to ensure that proteins destined for secretion or display on the cell surface, are correctly folded [32]. Since ajoene has been shown to localize in the ER, we propose that *S*-thiolation of ER proteins by ajoene, may interfere with protein folding.

Ajoene Induces Misfolded Protein Aggregates

To test the hypothesis that ajoene interferes with protein folding, we tracked the fate of an ER-folded protein, type-1 collagen following treatment with ajoene. This protein was chosen as it had been previously studied in our laboratory with established experimental methods [33]. Type-1 collagen is a secreted protein that is post-translationally modified within the lumen of the ER where it is folded into a functional protein (triple helix) through disulfide bond formation [34,35]. The triple helix contains two pro-α1(1) and one pro-α2(1) chains that are encoded by the COL1A1 and COL1A2 genes, respectively. The newly synthesized peptides are deposited into the lumen of the ER for post-translational modification, where the pro-α chains form disulfide bridges with one another to form a triple helix. The functional protein is then secreted. We hypothesize that ajoene may interfere with the folding of type-1 collagen to generate misfolded collagen chains that should be targeted to the proteasome for degradation via ER-associated protein degradation (ERAD) [36]. As type-1 collagen is expressed in fibroblasts, we used the transformed CT-1 fibroblast cell line for this experiment. Cells were treated with a subtoxic concentration of *Z*-ajoene (20 μM) for 24 h as established by the MTT assay (Figure 6A). This experiment is an important control, as apoptosis induction would be expected to release proteases which would decrease the type-1 collagen protein concentration. Fibroblast cells were, therefore, treated with *Z*-ajoene for 24 h; and some cells were also pre-treated with the proteasome inhibitor MG132. The lysate was then collected and the type-1 collagens were detected by immunoblot (Figure 6B). It is evident that addition of sub-toxic concentrations of *Z*-ajoene results in a dramatic decrease in the level of type-1 collagen protein (lane 3) which is reversed upon addition of the proteasome inhibitor MG132 (lane 5). This data supports the hypothesis that ajoene *S*-thiolates pro-α collagen chains to prevent its folding into a functional protein. These alkylated pro-α collagen chains are targeted to the proteasome, since inhibition of the proteasome with the inhibitor MG132 was found to reverse this effect.

To confirm this result further, we performed a radiolabelling experiment to enable distinction between pre-existing collagen in the cell prior to treatment and that produced subsequent to the ajoene treatment. Therefore, fibroblast cells were treated with non-cytotoxic concentrations of the ajoene analog bisPMB (4 μM) [2,37] in conjunction with [^{3}H] proline which is incorporated into newly synthesized collagens. After 24 h, both the media and lysate fractions were collected and the media fraction was digested to degrade non-collagen proteins. After dialysis of the digested proteins, the samples were separated by SDS-PAGE, and the radiolabelled collagens were detected by fluorography on X-ray film (Figure 6C (i)). Lysate collagens were detected by immunoblot using an anti-pro collagen type-I antibody (Figure 6C (ii)). It is evident from the radiogram that [^{3}H] proline is incorporated into both the pro-α1 and pro-α2 collagen chains over a 24 h incubation period and that addition of the vehicle (0.1% DMSO) has no effect on this incorporation (lanes 1 and 2). Addition of a subtoxic concentration of bisPMB caused a dramatic decrease in the level of type-1 collagen protein (lane 3) which again was dramatically reversed upon the addition of the proteasome inhibitor MG132 (lane 5).

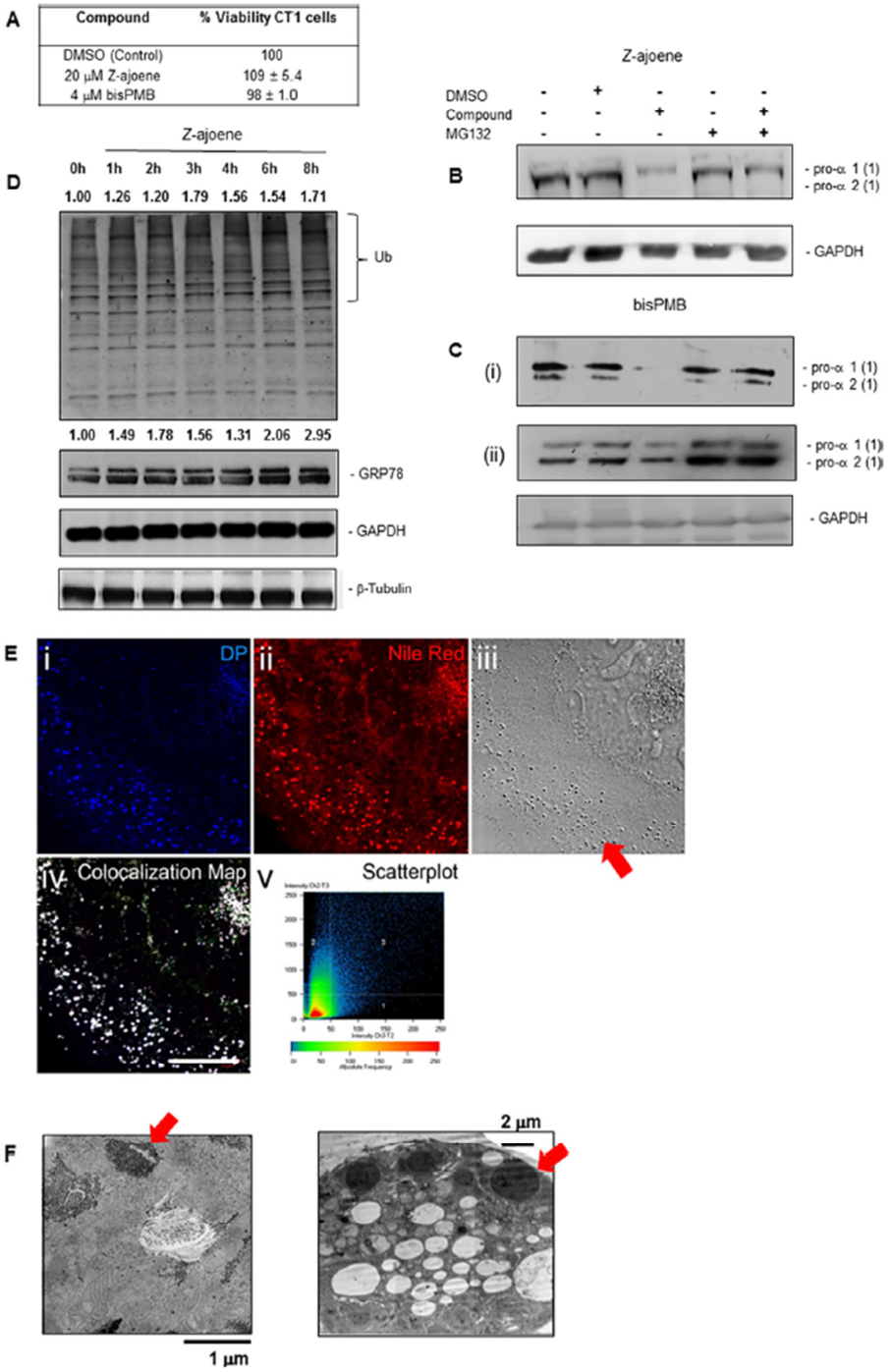

Figure 6. Ajoene induces misfolded proteins. (A) Percentage cell viability of CT-1 transformed fibroblast cells treated with 20 μM *Z*-ajoene or 4 μM bisPMB for 24 h relative to untreated cells (0.1 % DMSO alone) as determined by the MTT cell viability assay. Data displayed as mean ± SD of three independent determinations. (B) CT-1 cells treated with 20 μM *Z*-ajoene for 24 h and evaluated for pro-α1 (1) and pro-α2 (1) collagen expression in the lysate by immunoblot either in the absence or presence of the protease inhibitor MG132 (5 μM) (C) CT-1 cells treated with 4 μM bisPMB for 24 h and evaluated for pro-α1 (1) and pro-α2 (1) collagen expression in the media by radiogram (i) and in the lysate by immunoblot (ii) in the presence and absence of MG132 (5 μM). (D) MDA-MB-231 cells treated with 20 μM *Z*-ajoene display increased levels of ubiquitinated proteins and GRP78 levels which is evident from 1 h but more pronounced at 6–8 h relative to GAPDH and β-tubulin, respectively, and to untreated cells. Numbers on the top of bands represent change in protein level normalized to GAPDH or β-tubulin. All immunoblots and radiograms were performed twice but only data from one experiment are shown. (E) Live cell confocal microscopy of MDA-MB-231 cells treated with 25 μM DP for 3 h and stained with Nile Red. (i) DP, (ii) Nile Red, (iii) phase contrast, (iv) colocalization map, (v) scatterplot. Arrow indicates the possible protein aggregation inclusions which also fluoresce blue. (F) Transmission electron micrographs of MDA-MB-231 cells treated with 10 μM bisPMB for 1 (i) and 24 h (ii). Arrow indicates possible protein aggregate inclusions.

Consistent with the proteasomal degradation of misfolded proteins induced by ajoene, we observed a time-dependent increase in global levels of ubiquitinated proteins in lysate collected from MDA-MB-231 cells after treatment with non-cytotoxic concentrations of *Z*-ajoene (Figure 6D). Total levels of ubiquitinated proteins were found to increase from 1 h post-treatment.

The Ca^{2+}-dependent molecular chaperone GRP78/Bip is a central regulator of the unfolded protein response (UPR) and ER stress due to its role as gatekeeper of the ER signalling proteins PERK, Ire1, and ATF6. When misfolded proteins accumulate, GRP78 is released from the transmembrane signalling proteins resulting in activation of the Unfolded Protein Response (UPR) [38,39]. Consistent with increased levels of misfolded proteins, ajoene treatment was found to time-dependently increase levels of GRP78 protein in MDA-MB-231 cells with maximal levels at 6 and 8 h after treatment (Figure 6D).

Further evidence for misfolded proteins was obtained from confocal and transmission electron micrographs. A characteristic feature observed in MDA-MB-231 cells treated with DP and FOX is fluorescent clusters that increase in size and intensity over time. We hypothesize that these clusters are fluorescently labelled aggregates of misfolded proteins. Misfolded proteins are lipophilic due the hydrophobic regions of the protein that are normally buried within the protein core being externalized with the aqueous environment [40,41]. The lipophilic nature of the fluorescent clusters was confirmed by the addition of the hydrophobic binding dye Nile Red, which fluoresces only upon binding to hydrophobic surfaces [42]. Colocalization with the fluorescent signal from DP (Figure 6E (iv) and (v)) was observed and these possible protein aggregate inclusions are even evident in the phase contrast image (100× magnification). Similarly, electron micrographs of MDA-MB-231 cells treated with *Z*-ajoene (Figure 5F) for 1 and 24 h revealed the possible protein aggregate inclusions.

DISCUSSION

Although there have been reports on the downstream events leading to the cytotoxicity of ajoene in cancer cells, we present novel results identifying the primary ajoene target as well as the early events which may trigger cytotoxicity. This has been achieved using a novel chemical biology approach involving modified ajoene analogs which have enabled us to track the movement and localization of ajoene in cancer cells. The fluorescent groups, dansyl and fluorescein, were chosen in view of their well-known synthetic and biological chemistry as well as their emission maxima being in the visible range (~500 nm) in accordance with the requirements of CLSM. In our previous studies, we established that the ajoene terminal end groups could be substituted for alkyl, aryl, and heteroaromatic groups without loss of bioactivity, as the pharmacophore was found to reside within the sulfoxide/vinyl disulfide structural motif [2,28]. Our model reaction for ajoene thiolysis has previously identified the allyl–sulfur as the more electrophilic sulfur in a mixed disulfide reaction with a thiolate nucleophile. Therefore, it was deemed necessary to tether the fluorescent tag to this allyl–sulfur end to allow transfer of the tag to the protein during thiolysis. At the sulfoxide end, propyl was chosen for the dansyl derivative and *para*-methoxybenzyl for the fluorescein derivative, since both these groups had shown good profiles in our previous studies [28,37].

Both DP and FOX were found to be fully active at inhibiting the proliferation of both MDA-MB-231 breast and WHCO1 esophageal cancer cells when compared to *E*- and *Z*-ajoene. This is in agreement with our previous findings that the ajoene pharmacophore resides within the vinyl disulfide/sulfoxide core and not within the terminal end groups. It is interesting that such structural diversity is well tolerated in the side groups implying a common chemistry rather than a selective binding interaction between the compound and a specific protein target. Similar to ajoene [2], both compounds were found to induce apoptosis in MDA-MB-231 breast cancer cells when tested at the same concentration of 25 μM.

Conjugation of the dansyl and fluorescein tags to the ajoene core generated strongly fluorescent molecules with DP fluorescing aqua-blue at 515 nm; and FOX fluorescing green at 546 nm. The fluorescent ajoenes were added to live MDA-MB-231 cells cultured on chambered coverglass in an incubation chamber housed on the confocal stage. After 1 h incubation, a weak intracellular fluorescence signal was observed which increased in intensity over time with strong emission at 6 h. The fluorescence signal appeared clumped, was perinuclear in distribution, and localized to the endoplasmic reticulum as observed by colocalization of the DP or FOX signals with the endoplasmic reticulum labelling dye ER-tracker. As a negative control, no colocalization was observed between DP and the mitochondrial live cell dye mitotracker.

Owing to the similar distributions and striking overlap between the fluorescence signals from ER-tracker and both fluorescent ajoenes, as well as the fact that the live cell dye is itself a small molecule, we checked whether ER-tracker and DP are able to chemically react (by TLC) and, therefore, co-localise by association. Incubation of the two compounds together in ethyl acetate as a solvent revealed no chemical reaction between the two molecules implying that the colocalization is a result of accumulation of the individual molecules within a common location of the cell.

We further confirmed ER-localization of DP by generating an MDA-MB-231 cell line which expresses

yellow fluorescent protein (YFP) in the ER. Fixed slides obtained from these cells treated with DP again revealed colocalization between the YFP fluorescence and that emitted from the dansyl fluorophore. Taken together, these data clearly show that both fluorescent ajoenes DP and FOX rapidly enter MDA-MB-231 cells where they target the endoplasmic reticulum. Since the only structural similarity between both fluorescent ajoenes is the presence of the vinyl disulfide/sulfoxide core we speculate that ER-targeting may be generic for compounds with this structural motif.

An interesting morphology in DP-treated cells is clusters of fluorescently labelled particles. The fluorophore appears to be covalently attached to these particles as slide preparation involved membrane permeabilization and washing with methanol, which failed to remove the fluorescence, as would be expected if free drug were present. This observation prompted us to speculate that the dansyl fluorophore of DP may be transferred to ER-proteins via thiolysis. In agreement with this hypothesis, a multitude of proteins were found to be dansylated in MDA-MB-231 cells treated with DP as observed by immunoblot under non-reducing conditions only. Addition of the reducing agent β-mercaptoethanol to the sample caused removal of the dansyl label which supports attachment through a disulfide linkage.

To confirm that DP and ajoene share the same target, we performed a competition assay between the two compounds. When MDA-MB-231 cells treated with DP were also treated with increasing concentrations of *Z*-ajoene, the intracellular fluorescence of DP was found to be significantly reduced with a concurrent reduction in the number of dansylated proteins. These results demonstrate that both *Z*-ajoene and DP accumulate to the same ER location within MDA-MB-231 cells where they compete for thiolysis of the same protein targets.

It is interesting that all the disulfide containing proteins which are listed in the Protein Data Bank (PDB) are distributed into the extracellular environments of the ER, golgi, endosome, and plasma-membrane with only about 2% functioning in the cytoplasm or nucleus, as this environment is not supportive of the disulfide bond [43]. This is because the cytoplasm is a highly reducing environment maintained by molar amounts of GSH that exceed those of GSSG by 100-fold. GSH probably reacts with ajoene in the cytoplasm to prevent *S*-thiolation of cytoplasmic proteins. Ajoene entering the lumen of the ER will, however, encounter a more oxidative environment, which is maintained to support thiol oxidation. It is here that newly synthesized proteins destined for secretion or display on the cell surface are correctly folded via disulfide formation between cysteine residues in the same protein or between adjacent proteins [32]. It is reported that approximately 50% of the glutathione in the ER is bound to proteins via *S*-glutathionylation [44] compared to less than only 1% in other locations [45,46]. *S*-glutathionylation is reversible and important in protecting protein thiol groups from irreversible oxidation, guiding correct protein folding, stabilizing protein tertiary structure, and modulating proteins critical in redox signaling [47–51]. We, therefore, speculate that ajoene may *S*-thiolate cysteine thiols in the ER in competition with *S*-glutathionation involving GSSG. Indeed, based on the presence of a vinyl disulfide (as a better leaving group in the disulfide exchange), ajoene would be expected to be a superior thiolating agent in ajoene mediated *S*-thiolation (ajoenethiolation) compared to GSSG. Ajoene *S*-thiolation of ER proteins at elevated concentrations may interfere with protein folding by preventing the correct formation of mixed disulfides between cysteine thiols leading to an accumulation of misfolded protein aggregates. Misfolded proteins are estimated to comprise approximately 30% of newly synthesized proteins in healthy cells [52] and are removed from the cell through ERAD [36]. Elevated levels of misfolded proteins, however, trigger an evolutionary conserved response termed the unfolded protein response [39,53], which if not corrected, leads to ER stress. We observed increased levels of ubiquitinated proteins in the lysate of MDA-MB-231 cells following treatment with *Z*-ajoene which supports increased levels of misfolded proteins.

We sought further evidence that ajoene may interfere with protein folding. Type-1 collagen is a secreted protein that consists of two pro-α1(1) and two pro-α2(1) chains which are folded into a functional triple helix protein in the lumen of the ER through disulfide bond formation [34,35]. We, therefore, tracked the fate of newly synthesized type-1 collagen protein following treatment with *Z*-ajoene and the ajoene analog bisPMB, using [^{3}H]-proline incorporation. After 24 h, it was evident that both *Z*-ajoene and bisPMB caused a dramatic decrease in the levels of newly synthesized type-1 collagen both in the lysate and media which was then reversed upon inhibition of the proteasome using MG132. This result supports a mechanism whereby ajoene interferes with the folding of newly synthesized pro-α1(1) and pro-α2(1) chains into the type-1 collagen protein leading to its elimination via the proteasome.

Evidence for the existence of misfolded protein aggregates was obtained from confocal imaging and TEM. During the protein folding process, the hydrophilic regions of the protein are externalized with the aqueous environment, whereas the hydrophilic regions are internalized within the protein core [40,41]. Upon misfolding, the lipophilic protein regions are exposed, which result in clumped aggregates. The lipophilic nature of the fluorescent clusters was confirmed upon the addition of the hydrophobic binding dye Nile Red, which fluoresces only upon binding to hydrophobic surfaces [42]. These protein

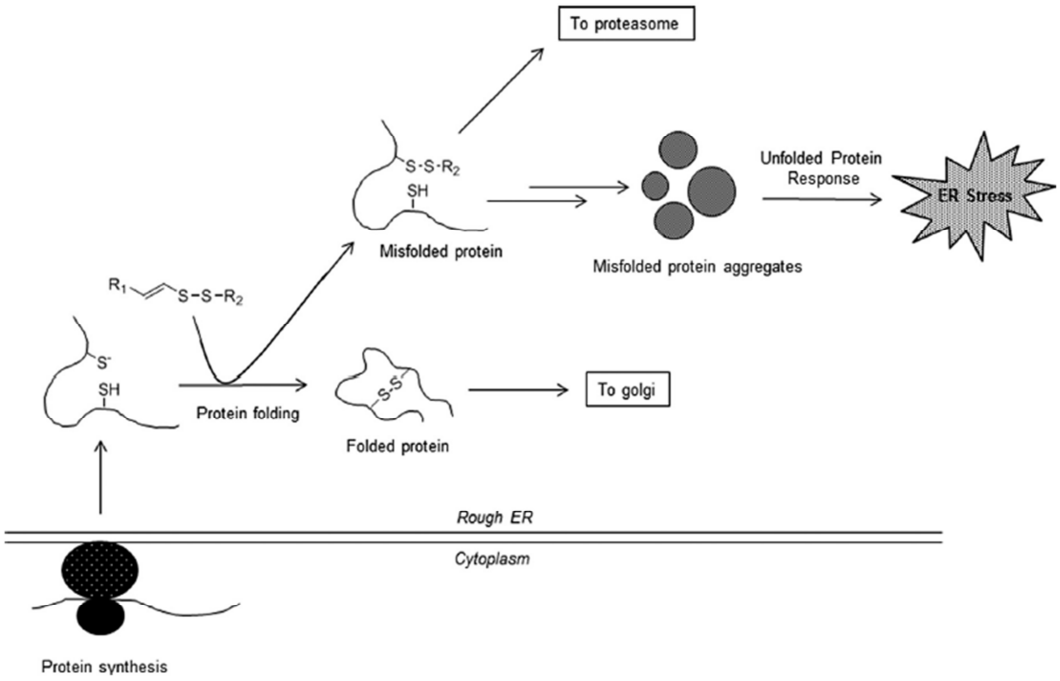

Figure 7. Hypothesis on the cytotoxic mechanism of action of ajoene in cancer cells. Ajoene exerts its cytotoxic effect in cancer cells by targeting and accumulating in the ER. Within this organelle, ajoene interferes with protein folding through *S*-thiolation of newly synthesized proteins to form a multitude of *S*-alkylated protein products (ajoenylation). This may lead to an accumulation of misfolded protein aggregates Thereby activating the Unfolded Protein Response and inducing ER Stress.

aggregate inclusions were also observed by transmission electron microscopy of MDA-MB-231 cells treated with *Z*-ajoene.

Proteins that are susceptible to *S*-glutathionylation are probably the protein targets of ajoene. In recent years, advances in proteomics have enabled the identification of proteins found to undergo *S*-glutathionylation, and although the numbers are not large in comparison to the proteome, they are clustered into seven categories [47,51,54,55] to include: (i) mitochondrial; (ii) cytosolic glycolytic proteins and those related to energy metabolism; (iii) signalling proteins-particularly kinases and phosphatases; (iv) cytoskeletal proteins; (v) protein folding and editing proteins; (iv) ion channel/calcium homeostasis proteins; and (vii) redox balance proteins. Interestingly, the proteins identified to date to be *S*-thiolated by garlic allylsulfur compounds (tubulin, glutathione reductase, and sulfurtransferases) all fall into the above categories. *S*-glutathionylation occurs spontaneously under basal conditions and is increased in cells or tissues under oxidative stress [56]. Indeed, the marginal selectivity of garlic allylsulfides reported for cancer cells over normal cells [10,37] may be due to the higher levels of oxidative stress in cancer cells over their normal counterparts which renders them more susceptible to *S*-thiolation.

We hypothesize (Figure 7) that ajoene rapidly enters the cancer cell by passive diffusion where it crosses the cytoplasm to enter the oxidative environment of the ER. Here we show for the first time that ajoene *S*-thiolates multiple proteins, possibly in competition with GSSG. If cells are treated with cytotoxic concentrations of ajoene, protein *S*-thiolation of ER proteins interferes with protein folding to give rise to misfolded protein aggregates which activates the Unfolded Protein Response and triggers ER stress.

Indeed, there is a growing body of evidence that ER stress is important in the cytotoxicity of garlic allylsulfides in cancer cells. It has long been known that garlic allylsulfides influence calcium homeostasis in cultured cancer cells [57–64], an indicator of ER stress. In addition, activation of the ER stress execution caspases-3, -4, -8, and -9 have been reported following treatment with DATS in basal cell carcinoma cells (BCC) [65] and DADS in the COLO205 human colon cancer cell line [61]. Activation of the Ca^{2+}-dependent protease calpain has been reported following treatment of both human malignant neuroblastoma [62] and glioblastoma [66] cells with DAS and DADS. In our current study, we show that *Z*-ajoene induces the time-dependent expression of the ER stress sensor protein GRP78/Bip in

MDA-MB-231 cells. This is in agreement with a recent report that the ER stress proteins, GRP78/Bip and CHOP/GADD153, are expressed in BCC cells following treatment with DATS [65]. Other ER-stress proteins include ATF4 as well as phosphorylation of eif2α in HCT116 human colon cancer cells following treatment with DATTS [57,67]. Based on our identification of the ajoene target, we propose that activation of the unfolded protein response and ER stress may be the central trigger surrounding the cytotoxicity of ajoene in cancer cells.

ACKNOWLEDGMENTS

This work was supported by grants and fellowships from the National Research Foundation of South Africa (NRF), the University of Cape Town (UCT), the Cancer Society of South Africa (CANSA), the International Centre for Genetic Engineering and Biotechnology (ICGEB), and the Cancer Research Trust.

REFERENCES

1. Münchberg U, Anwar A, Mecklenburg S, Jacob C. Polysulfides as biologically active ingredients of garlic. Org Biomol Chem 2007;5:1505–1518.
2. Kaschula CH, Hunter R, Stellenboom N, et al. Structure-activity studies into the anti-proliferation activity of ajoene derivatives in WHCO1 oesophageal cancer cells. Eur J Med Chem 2012;50:236–254.
3. Kaschula CH, Hunter R, Parker MI. Garlic-derived anti-cancer agents: Structure and biological activity of ajoene. Biofactors 2010;36:78–85.
4. Fleischauer AT, Arab L. Garlic and cancer: A critical review of the epidemiologic literature. J Nutr 2001;3S:1032S–1040S.
5. Ngo SN, Williams DB, Cobiac L, Head RJ. Does garlic reduce risk of colorectal cancer? A systematic review. J Nutr 2007;137:2264–2269.
6. Powolny AA, Singh SV. Multitargeted prevention and therapy of cancer by diallyl trisulfide and related Allium vegetable-derived organosulfur compounds. Cancer Lett 2008;269:305–314.
7. Iciek M, Kwiecien I, Wlodek L. Biological properties of garlic and garlic-derived organosulfur compounds. Environ Mol Mutagen 2009;50:247–265.
8. Schäfer G, Kaschula CH. The immunomodulation and anti-inflammatory effects of garlic organosulfur compounds in cancer chemoprevention. Anti-Cancer Agent Med Chem 2014;14:233–240.
9. Wang HC, Pao J, Lin SY, Sheen LY. Molecular mechanisms of garlic-derived allyl sulfides in the inhibition of skin cancer progression. Ann NY Acad Sci 2012;1271:44–52.
10. Scharfenberg K, Wagner R, Wagner KG. The cytotoxicity effect of ajoene, a natural product from garlic, investigated with different cell lines. Cancer Lett 1990;53:103–108.
11. Taylor P, Noriega R, Farah C, Abad M-J, Arsenak M, Apitz R. Ajoene inhibits both primary tumor growth and metastasis of B16/BL6 melanoma cells in C57BL/6 mice. Cancer Lett 2006;239:298–304.
12. Li M, Ciu J-R, Ye Y, et al. Antitumor activity of Z-ajoene, a natural compound purified from garlic: Antimitotic and microtubule-interaction properties. Carcinogenesis 2002;23:573–579.
13. Nishikawa T, Yamada N, Hattori A, Fukuda H, Fujino T. Inhibition by ajoene of skin-tumor promotion in mice. Biosci Biotechnol Biochem 2002;66:2221–2223.
14. Tilli CMLJ, Stavast-Kooy AJW, Vuerstaek JDD, et al. The garlic-derived organosulfur component ajoene decreases basal cell carcinoma tumor size by inducing apoptosis. Arch Dermatol Res 2003;295:117–123.
15. Nagaraj NS, Anilakumar KR, Singh OV. Diallyl disulfide causes caspase-dependent apoptosis in human cancer cells through a Bax-triggered mitochondrial pathway. J Nutr Biochem 2010;21:405–412.
16. Dirsch VM, Antlsperger DSM, Hentze H, Vollmar AM. Ajoene, an experimental anti-leukemic drug: Mechanism of cell death. Leukemia 2002;16:74–83.
17. Dirsch VM, Gerbes AL, Volmar AM. Ajoene, a compound of garlic, induces apoptosis in human promyleoleukemic cells, accompanied by generation of reactive oxygen species and activation of nuclear factor kB. Mol Pharmacol 1998;53:402–407.
18. Antlsperger DSM, Dirsch VM, Ferreira D, Su J-L, Kuo M-L, Vollmar AM. Ajoene-induced cell death in human promyeloleukemic cells does not require JNK but is amplified by the inhibition of ERK. Oncogene 2003;22:582–589.
19. Cavallito CJ, Buck JS, Suter CM. Allicin the antibacterial principle of Allium sativum. II. Determination of the chemical structure. J Am Chem Soc 1944;66:1952–1954.
20. Rabinkov A, Miron T, Mirelman D, et al. S-Allylmercaptoglutathione: The reaction product of allicin with glutathione possesses SH-modifying and antioxidant properties. Biochim Biophys Acta 2000;1499:144–153.
21. Nepravishta R, Sabelli R, Iorio E, Micheli L, Paci M, Melino S. Oxidative species and S-glutathionyl conjugates in the apoptosis induction by allyl thiosulfate. FEBS J 2012;279:154–167.
22. Gallwitz H, Bonse S, Martinez-Cruz A, Schlichting I, Schumacher K, Krauth-Siegel RL. Ajoene is an inhibitor and subversive substrate of human glutathione reductase and trypanosoma cruzi trypanothione reductase: Crystallographic, kinetic, and spectroscopic studies. J Med Chem 1999;42:364–372.
23. Sabelli R, Iorio E, De Martino A, et al. Rhodanese-thioredoxin system and allyl sulfur compounds. FEBS J 2008;275:3884–3899.
24. Veale RB, Thornley AL. Increased single class low-affinity EGF receptors expressed by human oesophageal squamous carcinoma cell lines. S Afr J Sci 1989;85:375–379.
25. Bodo M, Carinci P, Baroni T, et al. Collagen synthesis and cell growth in chick embryo fibroblasts: Influence of colchicine, cytochalasin B and concanavalin A. Cell Biol Int 1996;20:177–185.
26. Webster DF, Harvey W. A quantitative assay for collagen synthesis in microwell fibroblast cultures. Anal Biochem 1979;96:220–224.
27. Hunter R, Kaschula C, Stellenboom N, Cotton J, Parker MI. New excursions into the synthesis and medicinal chemistry of the disulfide bond. Phosphorus Sulfur Silicon Relat Elem 2013;188:1497–1507.
28. Hunter R, Kaschula CH, Parker MI, et al. Substituted ajoenes as novel anti-cancer agents. Bioorg Med Chem Lett 2008;18:5277–5279.
29. Sigmund H, Pfleiderer W. A new type of labelling of nucleosides and nucleotides. Helv Chim Acta 2003;86:2299–2334.
30. Pinto JT, Qiao C, Xing J, et al. Effects of garlic thioallyl derivatives on growth, glutathione concentration, and polyamine formation of human prostate carcinoma cells in culture. Am J Clin Nutr 1997;66:398–405.
31. Miron T, Rabinkov A, Mirelman D, Wilchek M, Weiner L. The mode of action of allicin: Its ready permeability through phospholipid membranes may contribute to its biological activity. Biochim Biophys Acta 2000;1463:20–30.
32. Xu C, Bailly-Maitre B, Reed JC. Endoplasmic reticulum stress: Cell life and death decisions. J Clin Invest 2005;115:2656–2664.
33. van Rooyen BA, Schafer G, Leaner VD, Parker MI. Tumour cells down-regulate CCN2 gene expression in co-cultured

fibroblasts in a Smad7- and ERK-dependent manner. Cell Commun Signal 2013;11:75.
34. Bornstein P. The biosynthesis of collagen. Annu Rev Biochem 1974;43:567–603.
35. Koivu J, Myllyla R. Interchain disulfide bond formation in types I and II procollagen. Evidence for a protein disulfide isomerase catalyzing bond formation. J Biol Chem 1987;262:6159–6164.
36. Meusser B, Hirsch C, Jarosch E, Sommer T. ERAD: The long road to destruction. Nat Cell Biol 2005;7:766–772.
37. Kaschula CH, Hunter R, Hassan HT, et al. Anti-proliferative activity of synthetic ajoene analogues on cancer cell lines. Anti-Cancer Agent Med Chem 2011;11:260–266.
38. Lee AS. The ER chaperone and signaling regulator GRP78/BiP as a monitor of endoplasmic reticulum stress. Methods 2005;35:373–381.
39. Lai E, Teodoro T, Volchuk A. Endoplasmic reticulum stress: Signaling the unfolded protein response. Physiology 2007;22: 193–201.
40. Feige MJ, Hendershot LM. Disulfide bonds in ER protein folding and homeostasis. Curr Opin Cell Biol 2011;23:167–175.
41. Kosuri P, Alegre-Cebollada J, Feng J, et al. Protein folding drives disulfide formation. Cell 2012;151:794–806.
42. Demeule B, Gurny R, Arvinte T. Detection and characterization of protein aggregates by fluorescence microscopy. Int J Pharm 2007;329:37–45.
43. Hogg PJ. Targeting allosteric disulphide bonds in cancer. Nat Rev Cancer 2013;13:425–431.
44. Bass R, Ruddock LW, Klappa P, Freedman RB. A major fraction of endoplasmic reticulum-located glutathione is present as mixed disulfides with protein. J Biol Chem 2004;279:5257–5262.
45. Chai YC, Ashraf SS, Rokutan K, Johnston RB, Jr., Thomas JA. S-thiolation of individual human neutrophil proteins including actin by stimulation of the respiratory burst: Evidence against a role for glutathione disulfide. Arch Biochem Biophys 1994;310:273–281.
46. Ravichandran V, Seres T, Moriguchi T, Thomas JA, Johnston RB, Jr. S-thiolation of glyceraldehyde-3-phosphate dehydrogenase induced by the phagocytosis-associated respiratory burst in blood monocytes. J Biol Chem 1994;269:25010–25015.
47. Townsend DM. S-glutathionylation: Indicator of cell stress and regulator of the unfolded protein response. Mol Interv 2007;7:313–324.
48. Dalle-Donne I, Colombo G, Gagliano N, et al. S-glutathiolation in life and death decisions of the cell. Free Radical Res 2011;45:3–15.
49. Biswas S, Chida AS, Rahman I. Redox modifications of protein-thiols: Emerging roles in cell signaling. Biochem Pharmacol 2006;71:551–564.
50. Hill BG, Bhatnagar A. Protein S-glutathiolation: Redox-sensitive regulation of protein function. J Mol Cell Cardiol 2012;52:559–567.
51. Cooper AJ, Pinto JT, Callery PS. Reversible and irreversible protein glutathionylation: Biological and clinical aspects. Exp Opin Drug Metab Toxicol 2011;7:891–910.
52. Schubert U, Anton LC, Gibbs J, Norbury CC, Yewdell JW, Bennink JR. Rapid degradation of a large fraction of newly synthesized proteins by proteasomes. Nature 2000;404:770–774.
53. Schroder M, Kaufman RJ. ER stress and the unfolded protein response. Mutat Res 2005;569:29–63.
54. Dalle-Donne I, Rossi R, Colombo G, Giustarini D, Milzani A. Protein S-glutathionylation: A regulatory device from bacteria to humans. Trends Biochem Sci 2009;34:85–96.
55. Klatt P, Lamas S. Regulation of protein function by S-glutathiolation in response to oxidative and nitrosative stress. Eur J Biochem 2000;267:4928–4944.
56. Giustarini D, Dalle-Donne I, Lorenzini S, et al. Protein thiolation index (PTI) as a biomarker of oxidative stress. Free Radic Biol Med 2012;53:907–915.
57. Saidu NE, Touma R, Asali IA, Jacob C, Montenarh M. Diallyl tetrasulfane activates both the eIF2alpha and Nrf2/HO-1 pathways. Biochim Biophys Acta 2013;1830:2214–2225.
58. Sakamoto K, Lawson LD, Milner JA. Allyl sulfides from garlic suppress the in vitro proliferation of human A549 lung tumor cells. Nutr Cancer 1997;29:152–156.
59. Sundaram SG, Milner JA. Diallyl disulfide inhibits the proliferation of human tumor cells in culture. Biochim Biophys Acta 1996;1315:15–20.
60. Chen W-C, Hsu S-S, Chou C-T, et al. Effect of diallyl disulfide on Ca^{2+} movement and viability in PC3 human prostate cancer cells. Toxicol in Vitro 2011;25:636–643.
61. Yang J-S, Chen G-W, Hsia T-C, et al. Diallyl disulfide induces apoptosis in human colon cancer cell line (COLO 205) through the induction of reactive oxygen species, endoplasmic reticulum stress, caspases casade and mitochondrial-dependent pathways. Food Chem Toxicol 2009;47:171–179.
62. Karmakar S, Banik NL, Patel SJ, Ray SK. Garlic compounds induced calpain and intrinsic caspase cascade for apoptosis in human malignant neuroblastoma SH-SY5Y cells. Apoptosis 2007;12:671–684.
63. Chen C-H, Su S-J, Chang K-L, Huang M-W, Kuo S-Y. The garlic ingredient diallyl sulfide induces Ca^{2+} mobilization in Madin-Darby canine kidney cells. Food Chem Toxicol 2009;47:2344–2350.
64. Park EK, Kwon KB, Park KI, Park BH, Jhee EC. Role of Ca(2+) in diallyl disulfide-induced apoptotic cell death of HCT-15 cells. Exp Mol Med 2002;34:250–257.
65. Wang HC, Hsieh SC, Yang JH, Lin SY, Sheen LY. Diallyl trisulfide induces apoptosis of human basal cell carcinoma cells via endoplasmic reticulum stress and the mitochondrial pathway. Nutr Cancer 2012;64:770–780.
66. Das A, Banik NL, Ray SK. Garlic compounds generate reactive oxygen species leading to activation of stress kinases and cysteine proteases for apoptosis in human glioblastoma T98G and U87MG cells. Cancer 2007;110:1083–1095.
67. Saidu NE, Abu Asali I, Czepukojc B, Seitz B, Jacob C, Montenarh M. Comparison between the effects of diallyl tetrasulfide on human retina pigment epithelial cells (ARPE-19) and HCT116 cells. Biochim Biophys Acta 2013;1830:5267–5276.

SUPPORTING INFORMATION

Additional supporting information may be found in the online version of this article at the publisher's web-site.

1.2 Dansyl-Ajoene (DP) co-localizes with Protein Disulfide Isomerase (PDI) in the endoplasmic reticulum of MDA-MB-231 breast cancer cells

Introduction

The background to this section is based on our previous work in which we found that ajoene *S*-thiolates many proteins in MDA-MB-231 cells [C. H. Kaschula et al. (2015) Mol Carcinog].

In this study we found that the fluorescent ajoene analogue (dansyl-ajoene, DP) localizes to the endoplasmic reticulum (ER) in MDA-MB-231 breast cancer cells through the S-thiolation of ER resident proteins. We hypothesize that the ER-resident protein, Protein Disulfide Isomerase (PDI), may be an important ajoene target protein as it is an enzyme directly involved in the formation of disulfide bonds.

PDI is a 57-kDa dithiol-disulfide oxidoreductase and molecular chaperone. It is found in the ER, nucleus, cytosol, mitochondria and cell membrane [Turano C. *et al.* (2002) J. Cell. Physiol.], and is one of the most abundant soluble proteins in the ER reaching near –millimolar concentrations and accounting for up to 0.8 % of the total cellular proteins in this organelle [Ferrari D.M. & Soling H.D. (1999) Biochem. J.].

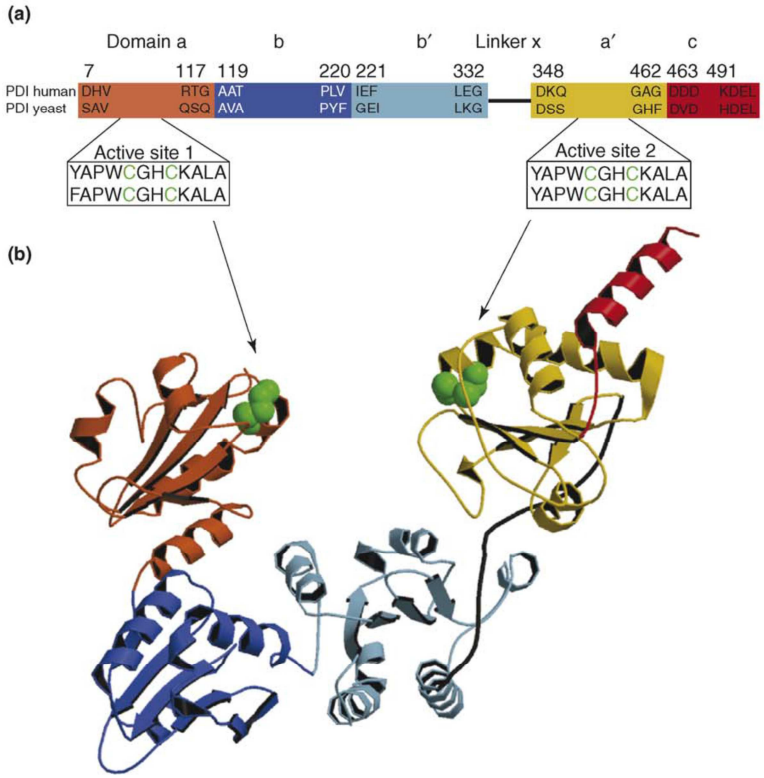

Figure 2: **Structure of PDI.** (a) On the basis of various models of human PDI [Ferrari, D. *et al.* (1999) Biochem. J.; Freedman, R. *et al.* (2002) Embo Rep.] and the crystal structure of yeast PDI (S. cerevisiae, PDB ID code 2B5E) [Tian, G. *et al.* (2006) Cell], the structure of PDI consists of five domains and one linker organized in the order *abb′xa′c*. Residues are numbered according to mature human PDI (H. sapiens, SwissProt code P07237). Domains *a* (orange) and *a′* (yellow) are homologous and contain the catalytic CxxC motif (green). Domains *b* (dark blue) and *b′* (light blue)

are not homologous but adopt a same thioredoxin folding. The flexible linker region *x* (black) is located between domains *b′* and *a′* [Ferrari, D. *et al.* (1999) Biochem. J.]. The link between domains *a* and *b* is only one residue. The C-terminal extension (red) contains a (K/H)DEL retention signal for the ER. (b) Representation of the crystal structure of yeast PDI, which highlights the active-site cysteines in green. Colors of the domains are the same as in (a). [Gruber CW *et al.* (2006) Trends Biochem Sci.].

PDI is composed of 5 domains: *a*, *a′*, *b*, *b′* and *c* and one linker domain *x* found between the *a′* and *b′* regions (Figure 2). Domains *a* and *a′* are homologous, and each contain a catalytic *Cys–X–X–Cys* sequence which is involved in their redox and isomerization activities. Domains b and b′ do not have high sequence similarity but both adopt a thioredoxin folding tertiary structure; which is responsible for substrate binding [Okumura M. *et al.* (2015) Free Radical Biology and Medicine]. Depending on the redox state of *a*, PDI is subject to conformational rearrangement between the *a* and *b* domains and can assume an open or closed structure during its catalytic reaction (Figure 3) [Yagi-Utsumi M.*et al.* (2015) Sci Rep.]

In fact, PDI is one of the most important enzymes of the ER, catalyzing disulfide bond formation (oxidase activity), rearrangement (isomerase activity) and reduction between cysteine residues in proteins and peptide substrates by mediating oxidative protein folding [B. Wilkinson & H. F. Gilbert (2004) Biochimica et Biophysica Acta (BBA)-Proteins and Proteomics,; R. Noiva & W. Lennarz, (1992) J. Biol. Chem.].

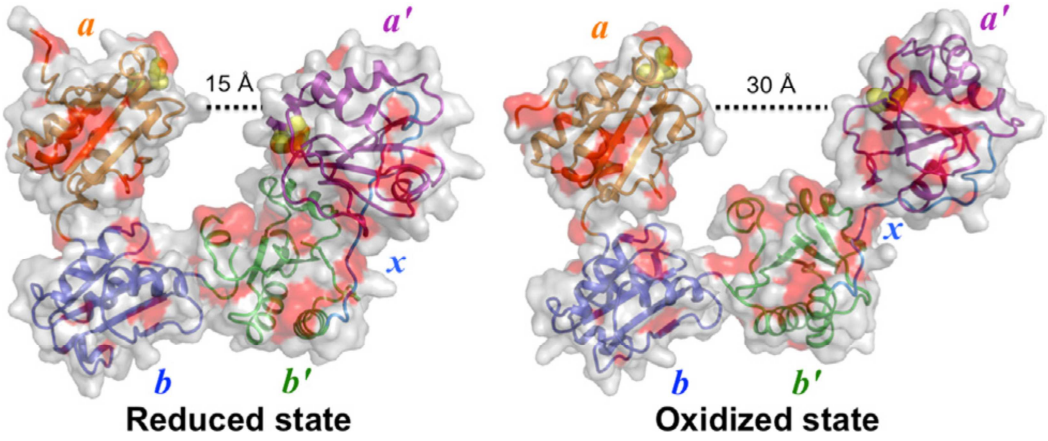

Figure 3: **Conformational structure of PDI.**
The PDI is subject to structural rearrangement depending on the reaction to be catalyzed (see above) [L. Wang *et al*. (2015) Free Radical Biology and Medicine]

Increasing evidence suggests that PDI supports the survival and progression of several cancers [Xu S. *et al.* (2014) Drug Discovery Today]. It is reported that this protein is up-regulated in many tumors, including human multiple myeloma [Claudio JO *et al.* (2002) Blood], acute lymphoblastic leukemia (B cell), neuroblastoma, lung, colon, ovarian [Shin BK *et al.* (2003) J Biol Chem] and breast cancers [Updike MS *et al.* (2007) Anticancer Res; Persson S *et al.*, (2005) Mol Phylogenet Evol.].

In this section, we aimed to verify whether PDI may be another target of the garlic compound ajoene. We therefore used fluorescence microscopy to determine

whether our fluorescent ajoene analogue DP and the protein PDI co-localize in MDA-MB-231 triple-negative breast cancer cells.

Results and Discussion

To investigate whether DP and PDI co–localize in MDA-MB-231 triple-negative breast cancer cells, immunofluorescence was performed. It was important to first select the correct concentration of DP which is not cytotoxic to MDA-MB-231 cells and is therefore not expected to affect the integrity of the cells. This was assessed by performing an MTT cell viability assay in MDA-MB-231 cells following treatment with 25 µM of DP for 6 hours as shown in Figure 4. We found that the values of cell viability of the treated samples were not different to those of the untreated control.

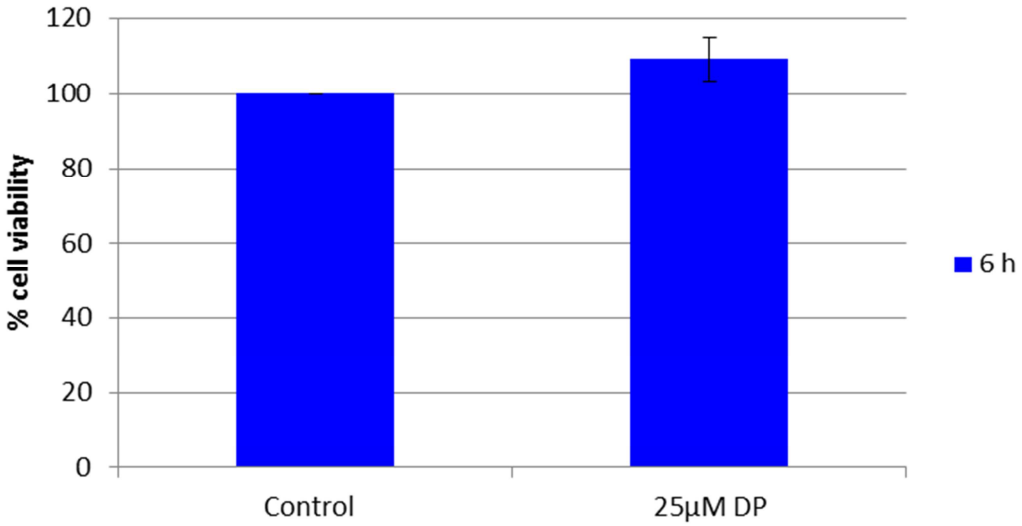

Figure 4: **Cytotoxicity of 25µM DP in MDA-MB-231 cells by MTT assay**.
Using an MTT cell viability assay, 25 µM DP was not found to be cytotoxic to MDA-MB-231 breast cancer cells after six hours of treatment. Control cells received 0.1 % DMSO (vehicle) alone. Data is expressed as a percentage of the mean ± SD of three independent experiments vs. untreated control.

For immunohistochemistry, MDA-MB-231 cells were seeded on a glass cover-slip and treated with 25 µM DP for six hours. Thereafter, the cells were fixed and stained with the primary polyclonal PDI antibody and the cy-3 fluorescently-tagged secondary antibody. Cell sections were mounted on a glass slide for viewing under a confocal microscope. Under the microscope, DP emits blue fluorescence due to its fluorescent dansyl–group; whereas the PDI protein is detected in the red channel through a specific anti-PDI antibody. The treated samples are displayed in both channels (Blue and Red) to verify a possible co-localization of DP and PDI.

We have previously found that ajoene localizes to the ER in MDA-MB-231 cells (Fig. 5-**A**). In the untreated cells (**B**), we found that PDI formed granular structures throughout the cytoplasm and concentrated at the level of the ER.
In the DP-treated cells, we observed that the PDI signal, which is stained red (**C**), and DP, which fluoresces blue (**E**), co-localize strongly (**F**, pink stain) with each other in the cytoplasm of the MDA-MB-231 cells. The phase contrast images of the cells are also shown (**D**) as well as the co-localization map where strong co-localization is displayed This data suggests that most of the DP and PDI co-localize within the MDA-MB-231 cells.

The co-localization signal is displayed graphically by scatterplot. In this graph, the blue intensity is shown on the x-axis and the red intensity is shown on the y-axis. Four quadrants are designated with *Black Zeiss Software*, obtained through the exclusion of regions in which the intensity of the signal is low. Quadrants 1 represent pixels with high blue intensity and low red intensity and Quadrant 2 display pixels with high red intensity and low blue intensity. Quadrant 3 identified the pixels with high intensity for both channels and (blue and red), therefore in this region is observed the co-localization.

Analyzing this scatterplot, we found that the DP signal is located in both quadrants 1 and 3, suggesting that DP strongly co-localizes with PDI but that there are also regions in the cell in which PDI is not present. This result implies that DP may target PDI but that it may also have other protein targets within the MDA-MB-231 cells. Interestingly, no red signal was detected in quadrant 2, suggesting that all of the PDI detected co-localized with DP (quadrant 3).

The *Black Zeiss Software* provides several parameters including the *Overlap Coefficient* which indicates the degree of co-localization between the two channels, quantified according to the formula below (Figure 5 (i)):

$$Overlap\ Coefficient = \frac{\sum(Ch1_i)(Ch2_i)}{\sqrt{\sum(Ch1_i)^2(Ch2_i)^2}}$$

The numerator measures pixels with significant intensity signals from both channels (red and blue) and is proportional to co-localized pixels; whereas the denominator quantifies all pixels with significant intensity values, regardless of co-localization. The values for the *Overlap Coefficient* range from 0 to 1, where 1 represents perfectly co-localized pixels.
Analyzing the data of 5 different images, we found that the average *Overlap Coefficient* between DP and PDI is 0.4925 ± 0.09. Considering that DP acts on many other targets, this value of the overlap coefficient indicates an excellent level of co-localization between DP and PDI.

Through co-localization examination, we can confirm that PDI is one of the main targets of dansyl–ajoene and that DP appears to saturate all the intracellular PDI (Figure 5, see quadrant 2 of scatterplot).

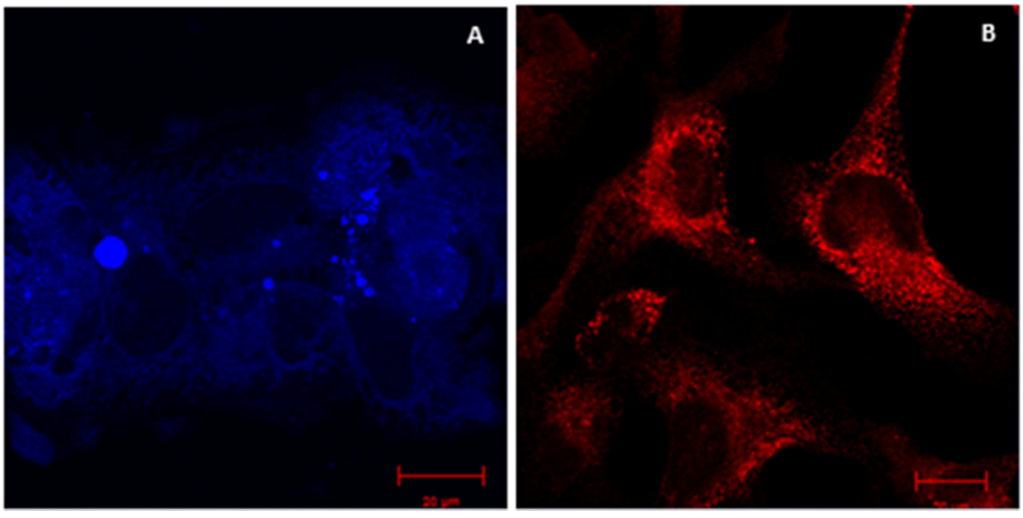

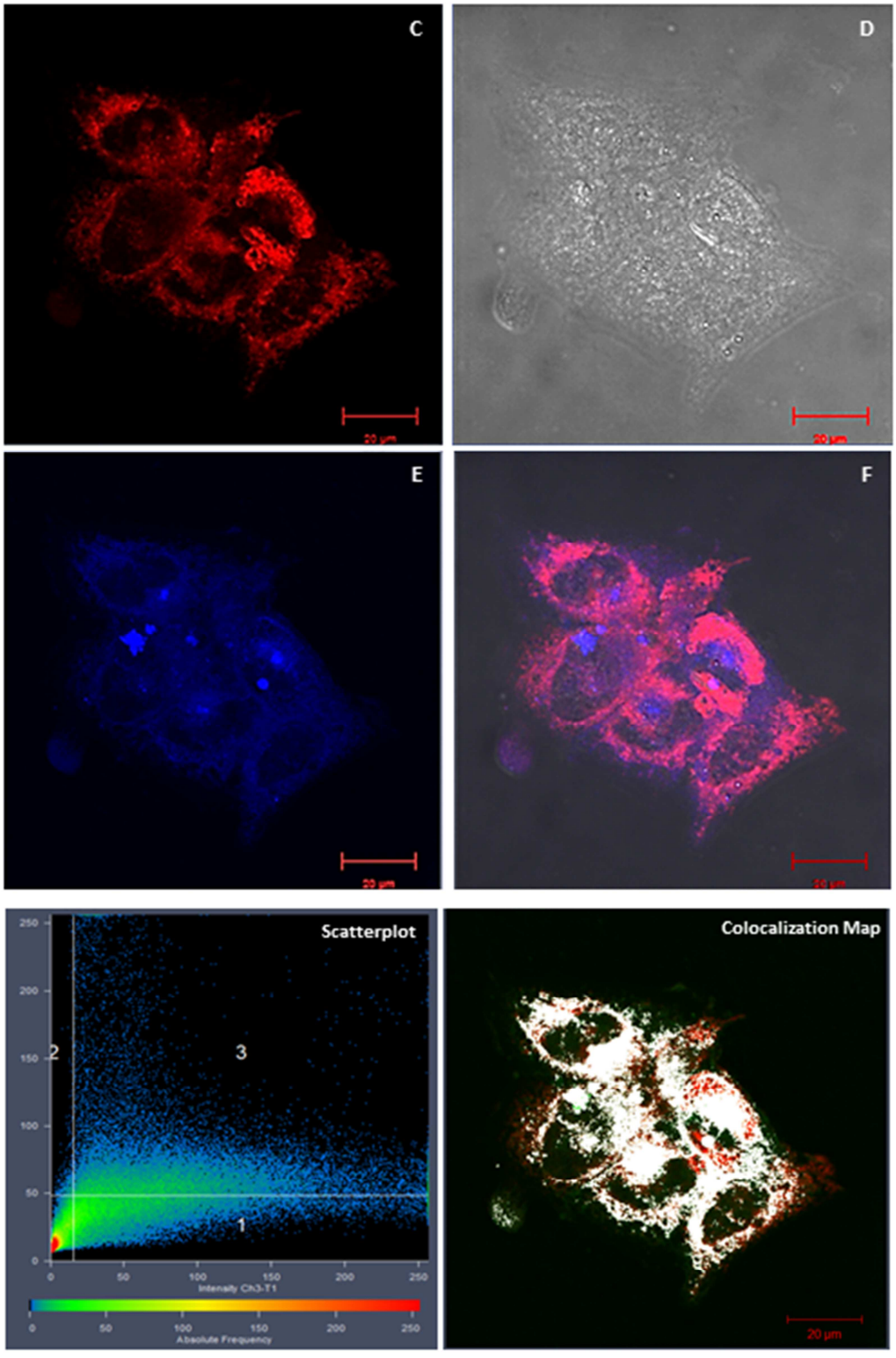

Scatter Region	Number Pixels	Area [µm x µm]	Relative Area [%]	Mean Intensity Ch3-T1	Mean Intensity Ch2-T2	Standard Deviation Ch3-T1	Standard Deviation Ch2-T2	Colocalization Coefficient Ch3-T1	Colocalization Coefficient Ch2-T2	Weighted Coloc. Coefficient Ch3-T1	Weighted Coloc. Coefficient Ch2-T2	Overlap Coefficient	Correlation R	Correlation R x R
1	36767	1987.74	24.2	54.5	35.4	40.9	8.9							
2	520	28.11	0.3	11.1	63.1	2.8	29.2							
3	30044	1624.27	19.8	80.9	66.5	48.1	25.3	0.450	0.983	0.548	0.984	0.43	-0.07	0.01

Figure 5: **Co-localization between PDI and DP in MDA-MB-231 breast cancer cells.**

To determine whether Protein Disulfide Isomerase and ajoene co-localize in cancer cells, MDA-MB-231 cells were treated with the fluorescent dansyl-ajoene (DP), and

blue fluorescence was detected (**A**). All samples were also treated with the primary PDI antibody coupled to secondary Cy-3-antibody which fluoresces red. In the untreated control (**B**), PDI was found to localize to the ER. The image of DP–treated cells shows that PDI **(C)** and DP (**E**) co-localize (**F**) in MDA-MB-231 cells. The phase contrast image is shown (**D**) and signal co-localization is displayed with both the co-localization map (white signal) but also graphically by the scatterplot.

(i) Table of parameters provided by the *Black Zeiss Software* relative to this image, including the *Overlap Coefficient* which indicates the degree of co-localization between DP and PDI protein.

Conclusions

We have previously found that ajoene targets and localizes in the ER of MDA-MB-231 cells, where it *S*–thiolates many proteins. This was found to activate the unfolded protein response (UPR) and ER stress which may be the modalities with which ajoene induces cytotoxicity in cancer cells. Based on our immunofluorescence findings, we propose that PDI may be one of the major protein targets of ajoene in the ER and that inhibition of PDI enzyme activity will inhibit the proper folding of proteins in the ER which may lead to activation of the unfolded protein response and ER stress by ajoene may cause the observed cytotoxic effects (Manuscript in preparation).

Chapter II – Vimentin as a target of Z-ajoene

Introduction

Vimentin, a 57 kDa cytoplasmic protein, is ubiquitously expressed in normal mesenchymal cells, and is a major constituent of the type III intermediate filament (IF) proteins, which forms a part of the cytoskeleton. [A. Satelli & S. Li (2011) Cell Mol Life Sci].

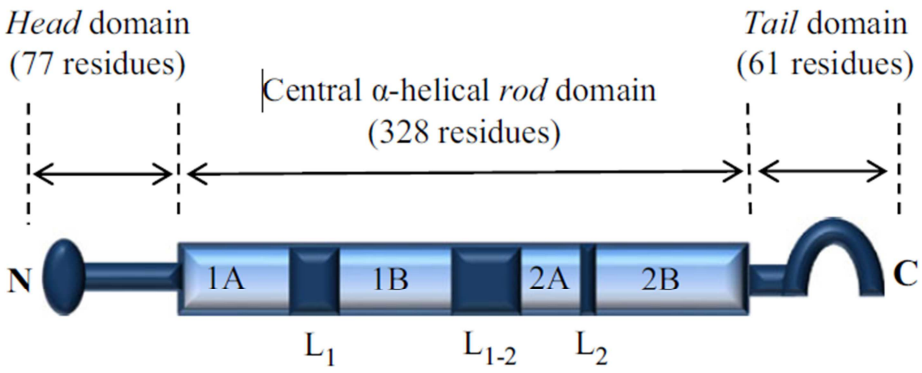

Figure 6: **Molecular structure of Vimentin.**
The structure of Vimentin consists of a central rod domain, an N-terminal "head" domain, and a C-terminal "tail" domain. The head and tail domains consist of 77 and 61 residues, respectively. The central rod domain (328 residues) contains an α-helical region. These domains are separated by 3 linker regions referred to as L1, L12 and L2. [Dave JM and Bayless KJ. (2014) Microcirculation].

Different cytoplasmic proteins play a role in the transformation of a normal cell to an invasive tumor cell and among these, Vimentin is particularly important [Calaf G.M. *et al*. (2014) Oncology Letters].

In recent years, Vimentin has been found to be a marker for epithelial-mesenchymal transition (EMT), a process in which epithelial cells lose characteristics that enable differentiation, including cell–cell adhesion, apical–basal polarity, and acquire a mesenchymal phenotype, characterized by motility, invasiveness and apoptotic resistance [A. Satelli & S. Li, (2011) Cell Mol Life Sci; Ye-Seul Kim *et al* (2014) Experimental & Molecular Medicine].

Moreover, Vimentin is frequently over-expressed in neoplastic cells with metastatic properties, including *breast cancer*, prostate cancer, gastrointestinal tumors, CNS tumors, malignant melanoma, lung cancer and other types of tumors.

In this chapter we aimed to firstly clone, express and purify recombinant Vimentin protein from E. coli in order to achieve the second aim which involved Investigating into the Role of Vimentin in the Anti-Cancer Activity of the Garlic Compound Ajoene.

2.1 Expression and purification of recombinant His-tagged Vimentin protein from E. Coli

In this section, we aimed to clone Vimentin into a cloning/expression vector so as to have available large amounts of purified protein for further experiments.

The South African team had already isolated Vimentin cDNA from MDA-MB-231 breast cancer cells. Therefore the appropriate primers had already been identified for insertion of Vimentin into the cloning vector.

Briefly, in order to start the experimental procedure, the Vimentin gene was amplified from cDNA (obtained from mRNA conversion) by PCR using specific Vimentin primers. The Vimentin fragment was then purified before it could be ligated into the Topo maintenance vector. During the transformation into Top10 competent cells, the Topo vector with the ligated Vimentin gene entered the cells and only the cells that have incorporated the vector (which contained an ampicillin resistance gene) were able to grow in the presence of ampicillin and their insert would be cloned. Subsequently, the colonies that had taken up the Topo vector with the ligated Vimentin gene were screened, and colony PCR was carried out. Then, the plasmids were extracted and all clones with the correct sequence of Vimentin gene were identified by sequencing.

Lastly, to express the final Vimentin protein, its coding sequence had to be transferred from the Topo maintenance vector into the pET-22b (+) cloning/expression vector. Both the Topo vector (which contained vimentin fragment) that the pET-22b (+) vector were subjected to a digestion analysis with *Bam HI* and *Sal I* RE, which allowed removal of the Vimentin sequence from the Topo vector followed by insertion directly into the pET vector with ligation.
During the transformation into BL 21 star DE3 competent cells, only the cells that had incorporated the pET-22b (+) vector with the ligated Vimentin gene were able to grow, then the colonies were screened, and colony PCR was carried out. Finally, the plasmids were extracted and all clones with the correct Vimentin sequence were identified by sequencing.

Finally the clone with the correct Vimentin sequence grown so that Vimentin protein could be extracted and then purified by Nickel column. This purified protein would be used to study the interactions between Vimentin and Z-ajoene by proteomics, western blot and in vitro binding assays.

Results and Discussion

2.1.1 Vimentin gene was isolated from cDNA.

The two most important factors during primer design were to achieve a good complementarity sequence with the Vimentin coding sequence as well as finding matching melting temperatures (i.e. annealing temperatures) for both primers.
The Forward and Reverse primers were designed with the help of the Vimentin coding sequence taken from NCBI and was found to be NM_003380.3. The coding

sequence (see Figure 7) was then used to design the forward and reverse primers, which would allow a Vimentin PCR product of 1.4 kb to be isolated, with the help of the program DNA Man.

```
 361 ggagccagtc cgcgccaccg ccgccgccca ggccatcgcc accctccgca gccatgtcca
 421 ccaggtccgt gtcctcgtcc tcctaccgca ggatgttcgg cggcccgggc accgcgagcc
 481 ggccgagctc cagccggagc tacgtgacta cgtccacccg cacctacagc ctgggcagcg
 541 cgctgcgccc cagcaccagc cgcagcctct acgcctcgtc cccgggcggc gtgtatgcca
 601 cgcgctcctc tgccgtgcgc ctgcggagca gcgtgcccgg ggtgcggctc ctgcaggact
 661 cggtggactt ctcgctggcc gacgccatca acaccgagtt caagaacacc cgcaccaacg
 721 agaaggtgga gctgcaggag ctgaatgacc gcttcgccaa ctacatcgac aaggtgcgct
 781 tcctggagca gcagaataag atcctgctgg ccgagctcga gcagctcaag ggccaaggca
 841 agtcgcgcct gggggacctc tacgaggagg agatgcggga gctgcgccgg caggtggacc
 901 agctaaccaa cgacaaagcc cgcgtcgagg tggagcgcga caacctggcc gaggacatca
 961 tgcgcctccg ggagaaattg caggaggaga tgcttcagag agaggaagcc gaaaacaccc
1021 tgcaatcttt cagacaggat gttgacaatg cgtctctggc acgtcttgac cttgaacgca
1081 aagtggaatc tttgcaagaa gagattgcct ttttgaagaa actccacgaa gaggaaatcc
1141 aggagctgca ggctcagatt caggaacagc atgtccaaat cgatgtggat gtttccaagc
1201 ctgacctcac ggctgccctg cgtgacgtac gtcagcaata tgaaagtgtg gctgccaaga
1261 acctgcagga ggcagaagaa tggtacaaat ccaagtttgc tgacctctct gaggctgcca
1321 accggaacaa tgacgccctg cgccaggcaa agcaggagtc cactgagtac cggagacagg
1381 tgcagtccct cacctgtgaa gtggatgccc ttaaaggaac caatgagtcc ctggaacgcc
1441 agatgcgtga aatggaagag aactttgccg ttgaagctgc taactaccaa gacactattg
1501 gccgcctgca ggatgagatt cagaatatga aggaggaaat ggctcgtcac cttcgtgaat
1561 accaagacct gctcaatgtt aagatggccc ttgacattga gattgccacc tacaggaagc
1621 tgctggaagg cgaggagagc aggatttctc tgcctcttcc aaacttttcc tccctgaacc
1681 tgagggaaac taatctggat tcactccctc tggttgatac ccactcaaaa aggacacttc
1741 tgattaagac ggttgaaact agagatggac aggttatcaa cgaaacttct cagcatcacg
1801 atgaccttga ataaaaattg cacacactca gtgcagcaat atattaccag caagaataaa
```

Figure 7: **The coding sequence of human Vimentin gene (highlighted in gray) from NCBI website.**

The primer sequences were the following: **5'-GGA TCC CAT GTC CAC CAG GTC CGT GTC-3'** and **5'-GTC GAC TTC AAG GTC ATC GTG ATG CTG-3'** for forward and reverse primers respectively, and both had a length of 27 base pairs (bp). Their melting temperatures were 65.7 °C for the forward primer and 61.2 °C for the reverse primer, which were somewhat high but still good considering that the difference between them was not more than 5°C (SA biosciences). Before the start of the PCR reaction, both forward and reverse primers were each diluted to 10 µM (see materials and methods section).

Moreover, the forward primer sequence contained the *Bam HI* enzyme restriction (RE) site (in red), while the reverse primer contained the *Sal I* RE site (in blue). These two sites were very important because the Vimentin fragment was localized between these RE sites when cloned into the Topo vector.

Briefly, master mix for two PCR tubes was made by adding 10 µM of each primer, nucleotides, Taq polymerase, buffer with magnesium (Mg) and nuclease free water; so that each PCR tube could hold a total volume of 50 µL. Then, the Vimentin cDNA was added to one PCR tube; while the negative control was prepared without cDNA to verify the absence of contaminants which could be present in the reaction mixture. All tubes were left in the thermal cycler machine for about two hours to

allow the reactions to take place. The thermal cycler machine was set for the first time to 30 cycles and then increased to 40 cycles to obtain a more abundant PCR product and according to the Promega protocol for Taq® PCR Systems core. Then the PCR tubes were taken out and were stored at 4°C.

The PCR product was mixed with blue loading dye to allow the tracking of the DNA during gel electrophoresis. This was carried out according to standard procedures with 1% agarose gel after PCR, in order to see if the Vimentin gene had been successfully amplified from the cDNA. The Gene Ruler 1 kb DNA ladder was used as a marker as an indication of band size. The Vimentin cDNA reaction and the negative control were loaded, and electrophoresis was run. When completed, the gel was exposed to UV–light and the DNA bands detected due to the presence of ethidium bromide, which binds to DNA and emits fluorescence. In the visualization of the gel by the trans-illuminator, we detected only one band in the sample with the cDNA (see Figure 8). Moreover, this band was 1.4 kb in size, meaning that the Vimentin gene had been isolated successfully.

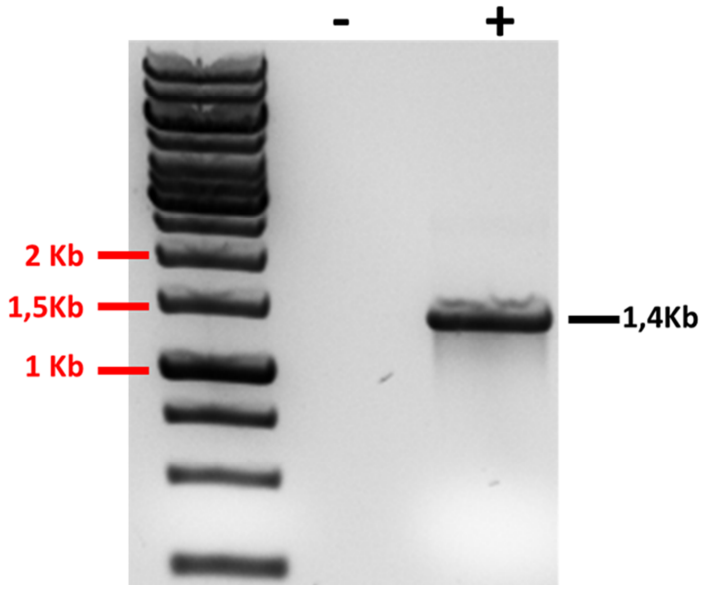

Figure 8: **Vimentin PCR product.**

Results from the gel electrophoresis with only one band showing the successfully amplified Vimentin gene of size 1.4 kb.

With the successful isolation of Vimentin, the PCR product was purified according to the Promega protocol (*Wizard® SV Gel and PCR Clean-up System kit*), in order to exclusively leave the pure Vimentin gene and remove all the PCR reaction components, as Taq polymerase. Before storing at -20 ° C, the purified PCR product was labeled Vimentin, and the DNA content was quantified by the Nanodrop spectrophotometer (see Table 1). A good result was obtained, in fact, the absorbance ratio at 260 and 280 nm should be between 1.8 and 2, indicating that the Vimentin purification has been successful.

	Conc.(ng/ µl)	260/280
Vimentin	36.5	1.91

Table 1: Quantification of the purified Vimentin gene by the Nanodrop spectrophotometer.

2.1.2 Vimentin was inserted into the Topo vector and transformed into BL 21 star DE3 competent cells.

In order to later be able to clone the purified Vimentin gene into the pET-22b (+) expression vector its sequence had to be ligated into the Topo cloning vector (TOPO® TA Cloning Kit for Sequencing, Invitrogen).

The Topo vector is a plasmid linearized to roughly 4 kb in size, to which has been covalently bound a topoisomerase (enzyme responsible for the supercoiling of DNA), which is characterized by the presence of single 3' thymidine (T) overhangs, which allows for the insertion of PCR to ligate efficiently with the vector. Furthermore, the vector also contains the genes for resistance to antibiotics Ampicillin (Amp) and Kanamycin, which makes it insensitive to action of these drugs.

Because the concentration of our purified Vimentin is not very high, we decided to use the maximum concentration to be sure to insert Vimentin in Topo vector according to the Life technologies protocol for *TOPO® TA Cloning Kit for Sequencing*. Briefly, we mixed purified Vimentin with salt solution and Topo vector. The reaction was incubated at room temperature for 30 minutes and then stored at -20 °C until we were ready to proceed with the butanol purification to remove all components of the reaction through a precipitation. Therefore butanol was added to the Topo vector reaction, and after centrifugation the supernatant was removed and the pellet resuspended in nuclease free water.

Finally, the transformation into competent cells was performed by adding the purified Topo vector to a vial of TOP10 cells. Using the heat-shock, the entrance of the plasmid was carried out. Later, the TOP10 cells were incubated for one hour with S.O.C. medium (a nutrient-rich bacterial growth medium) to stimulate bacterial growth, and a small amount of this was spread in a selective Luria – Bertani (LB) agar –plate, containing Amp, and incubated overnight. The negative control was performed to verify that there were no other bacterial contaminations.

The following day, we found that only two colonies had grown in the Topo sample, named Vim–Topo 1 and Vim–Topo 2 clones respectively, and nothing in the negative control. In fact only the bacteria, where the Topo vector was present, acquired resistance to this antibiotic, as they were able to grow on the Amp–LB agar –plate.

2.1.3 Colony screening and isolation of each Vim–Topo clone

A small amount of each colony was taken with a tip, and first, it was added to a new PCR tube for carrying out colony PCR screening; and then added in a falcon tube with LB medium broth, which contained Amp, to allow only the growth of the selected clone.

The colony PCR screening is a technique that is used to identify the clones which have the gene of interest cloned in the Topo vector, in our case the Vimentin gene. Briefly, the PCR reaction was carried out in the presence of the primers for Vimentin, Taq polymerase, nucleotides, and buffer. The PCR reaction was run for 40 cycles under the same conditions as described in the materials and methods section. The products of this reaction were separated by agarose–gel electrophoresis and assessed on the trans–illuminator.

The colony screening showed that only in the Vim –Topo 1 clone band was present whereas the Vim–Topo 2 clone was absent (Figure 9). Moreover, the Vim–Topo 1 clone band was a 1.4 kb in size, which suggested that the Vimentin gene was inserted correctly.

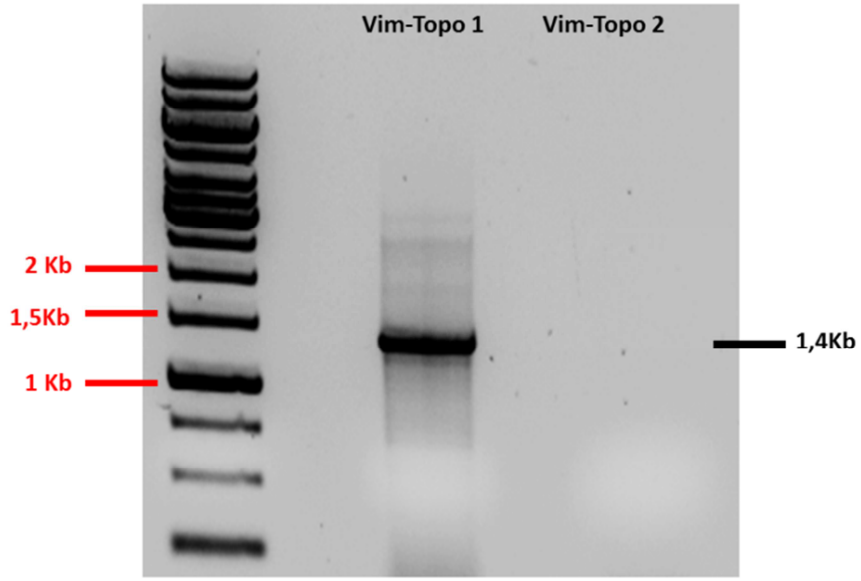

Figure 9: **Colony screening of Vim-Topo clones.**
Visualization by gel electrophoresis of both Vim–Topo clones following the PCR reaction.

For the growth of the selected clone, as described above, each Vim-Topo clone was grown in the presence of LB broth medium which contains Amp for one night. The LB medium is a clear broth, but could become more turbid depending on the bacterial charge (amount of bacteria grown in it).

In contrast with the colony screening, both selective cultures showed abundant bacterial growth, indicating the presence of the vector in both clones. Considering these conflicting data and the possibility of drawing erroneous conclusions, we decided to analyze both clones.

Thus, DNA from each culture was purified according to the protocol of the *Wizard plus SV minipreps DNA purification system kit* and the DNA was resuspended in nuclease free water and quantified by the Nanodrop spectrophotometer (see Table 2).

	Conc. (ng/µl)	260/280
Vim –Topo 1	43,5	1,86
Vim –Topo 2	60,4	1,85

Table 2: Quantification of purified DNA of each Vim–Topo clone by the Nanodrop spectrophotometer.

A good result was obtained from both clones where an absorbance ratio at 260 and 280 nm was found to be 1.8, indicating that the purification has been successful. Moreover, in both clones we had good DNA content, especially for the Vim-Topo 2 clone.

Considering these conflicting data, we drew two hypotheses. The first hypothesis would be that there was a mistake in the preparation of colony screening, where probably an insufficient amount of bacteria was added and then the PCR reaction did not take place.

Another hypothesis could be that the bacteria of the Vim-Topo 2 clone was transformed by the empty Topo vector. With these results we were not able to rule out either of the two hypotheses, so we had decided to use both clones for the following investigations.

2.1.4 Sequencing of Vimentin from both Topo clones.

Before the RE digestion, both Vim–Topo clones were sent off to *Central DNA Sequencing Facility* laboratory of University of Stellenbosch for sequencing electrophoresis analysis. This technique allows verification that the sequence obtained agrees with the Vimentin gene sequence from the NCBI website, which was later confirmed.

The sequencing was divided in three different phases: a PCR reaction, a separation by capillary electrophoresis and finally an optical detection (see material and methods section).
The sequencing was performed with the Topo primers. An additional verification step was performed for the other two primers named sequence 1 and 2 respectively. The primer sequence 1 was the following: **5'-ACC AAC GAC AAA GCC CGC GT-3'**, and the primer sequence 2 was **5'-TCC CTC ACC TGT GAA GTG GA-3'** respectively, and both had a length of 20 base pairs (bp). Their melting temperatures were 55.8 °C for the sequence 1 primer and 53.7 °C for the sequence 2 primer, were good because they were not high and the difference between them was not more than 5°C (SA biosciences).

The Vimentin gene sequencing of the Vim–Topo 1 clone, detected with the M13 reverse primer (see Topo vector map in materials and methods section), is shown in figure 10 and 11.

With this primer, we were not able to verify the sequence of the entire Vimentin gene but only the initial portion.

(a)

1 80

GAAATCATTTTTTATTTATTTTTTTTTTATAMSGGACTTTTTYCTGCRGGTTTAAAMGAATTCKCCCTTGGATYCY**ATG**T

Start codon

CCATTTTTGTACTTG**TCCTCGTCCTCCTACCGCAGGATGTTYGGCGGTTCKGGTACCGTKAGCCGGCCGAGCTCCAKCCG**

Start vimentin sequence

GAGCTACGTGACTACGTCCACCCGCWCCTACWGCCTGGGCAGCGCGCTGCGCCCCAGCWCCAKCCGCWGCCTCTACGCCT

CGTCCCCGGKCGGCGTGTATGCCACGCGCTCCTCTGCCKTGCGCCTGCYGAGCAGCGTGCCCGGGGTGCGGCTCCTGCWG

GACTCKGWGGACTTCTCGCTGGCCGACKCCWTCAACACCGAGTTCAAKAACACCCGCACCAACKAGAAGGTGGAGCTGCA

GGAGYTGAATGACCGCTTCKCCAACTACATCSACWAGGTGCGCTTCCTGGAGCAGCAGAATAAGATCCTGCTGGCCGATC

TCGTGTAKCTCWAGGGCCAAGGCAAGTCGCGCCTGGGGGACCTCTACTAGGATGATATGCKGTATCTTCKCCGGCAGGTG

GACCAGCTAACCAACGACGAAGCCCGCGTCGAGGTGGAGCGCGACAACCTGGCCKAGGACATCATGCGCCTCCGGGAGAA

Sequence 1

ATTGCAGGASGASATGCTTCAKAGAKAGKAAGCCGAAAACACYCTGCWATCTTTCWGACAGGATGTTGACAATGCTTCTC

TGGTCATGTCTTGAYCTTGAWCGCAWAKTGTAATCTYTT

(b)

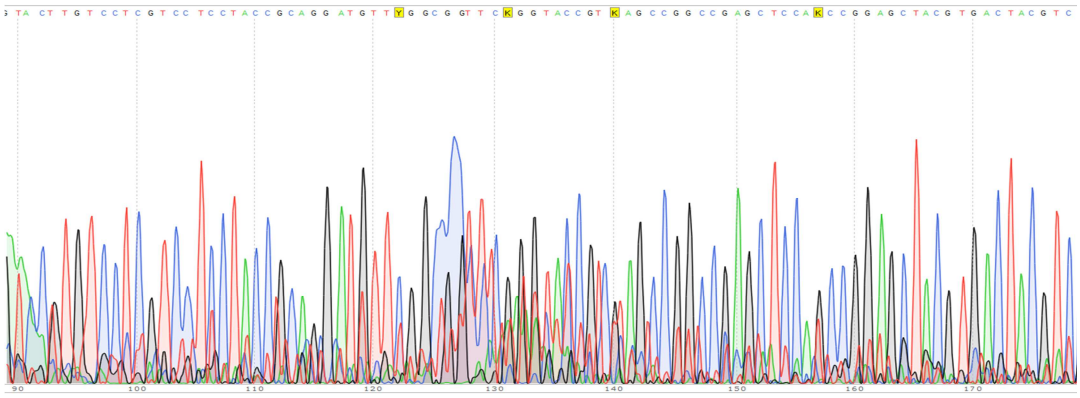

Figure10**: The raw DNA sequence in Vim-Topo 1 clone obtained with M13 reverse primer**.
Using the M13 reverse primer, DNA sequencing of the Vim-Topo 1 clone showed this sequence.

a) The correct sequence of Vimentin is highlighted in gray and bold, in yellow is highlighted the ATG start codon, while green is the region recognized by the primer sequence 1. In red is indicated unrecognized nucleotides by the software, and these have been corrected manually through use of the chromatogram.
b) It is shown a representative portion of the chromatogram obtained with the M13 reverse primer.

Furthermore, as shown by the figure 10, the software was not able to correctly recognize all nucleotides, especially where an overlap of signals of different nucleotides occurred. So, it was necessary to check the chromatogram manually and then the sequence was corrected through use of the chromatogram (figure 11).

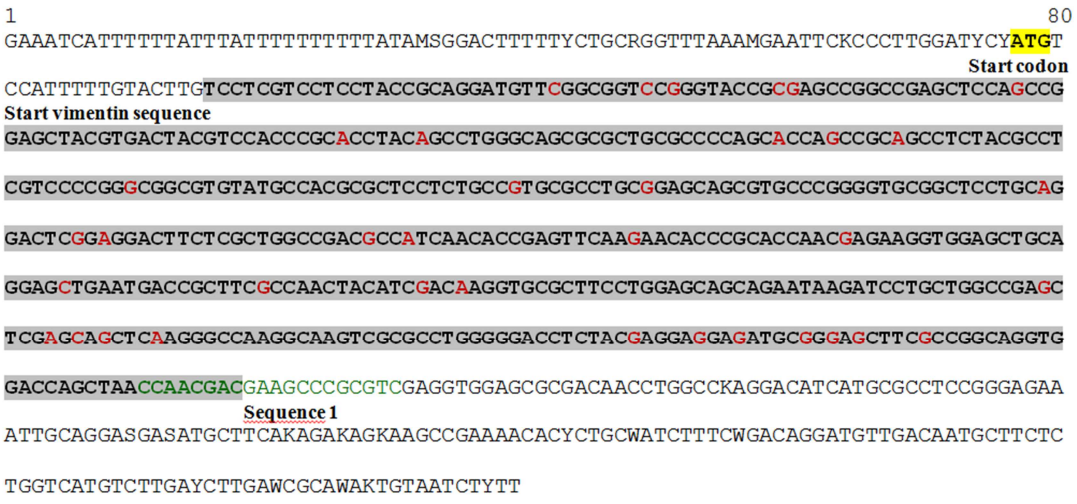

Figure 11: **The sequencing of Vimentin gene in Vim-Topo 1 clone obtained with M13 reverse primer after checking of the chromatogram.** In red, the nucleotides were manually corrected based on the color display of the individual peaks in the chromatogram.

Despite the manual correction of the sequence detected with the M13 reverse primer, the Vimentin sequence, inserted in Vim–Topo 1 clone, appeared with different mutations and in particular in the region recognized by the sequence 1 primer (figure 11). Furthermore the inability to verify this sequence in other chromatograms, allowed us to conclude that the Vim–Topo 1 clone had inserted the Vimentin fragment but its sequence was incorrect probably due to erroneous amplification during the PCR reaction.

Therefore, we started to analyze the sequencing data of the Vim–Topo 2 clone. The sequencing obtained with the M13 reverse primer produced a long gene sequence shown in figure 12, and the quality of this sequencing was high, in fact only two bases were not recognized by the software and the manual adjustment has been performed (figure 12 –c) following the display of the chromatogram.

(a)

1 80

TWMMRMMKKYYYYYKKWWWTWMCCCTCWCTWAAGGGACTAGTCYTGCAGGTTTAAACGAATTCGCCCTTGGATCCCATGT

Start codon

CCMCCAGGTCCGTGTCCTCGTCCTCCTACCGCAGGATGTTCGGCGGCCCGGGCACCGCGAGCCGGCCGAGCTCCAGCCGG

Vimentin sequence

AGCTACGTGACTACGTCCACCCGCACCTACAGCCTGGGCAGCGCGCTGCGCCCCAGCACCAGCCGCAGCCTCTACGCCTC

GTCCCCGGGCGGCGTGTATGCCACGCGCTCCTCTGCCGTGCGCCTGCGGAGCAGCGTGCCCGGGGTGCGGCTCCTGCAGG

ACTCGGTGGACTTCTCGCTGGCCGACGCCATCAACACCGAGTTCAAGAACACCCGCACCAACGAGAAGGTGGAGCTGCAG

GAGCTGAATGACCGCTTCGCCAACTACATCGACAAGGTGCGCTTCCTGGAGCAGCAGAATAAGATCCTGCTGGCCGAGCT

CGAGCAGCTCAAGGGCCAAGGCAAGTCGCGCCTGGGGGACCTCTACGAGGAGGAGATGCGGGAGCTGCGCCGGCAGGTGG

ACCAGCTAACCAACGACAAAGCCCGCGTCGAGGTGGAGCGCGACAACCTGGCCGAGGACATCATGCGCCTCCGGGAGAAA

Sequence 1

TTGCAGGAGGAGATGCTTCAGAGAGAGGAAGCCGAAAACACCCTGCAATCTTTCAGACAGGATGTTGACAATGCGTYTCT

GGCACGTCTTGACCTTGAACGCAAAGTGGAATCTTTTGCAAGAAGAGATTGYCTTTTTTGAAGAAACTCCACKAAGAGGA

AATCCAGGAGCTGCAGGYTCAGATTCAGGAACAGCATGTCCAAATCGATGTGGGATGTTTCCAAGYCCTGACCTTCACGG

CTGCCCTGCGTGACGTWCKTCAGCWAWTATGAAAGTGTGGCTGCCAAGAACCTTGCARGAAGGCARAAGAWTGGTWCAAA

WTCCAAGTTTGCTGACCTCTYTGAKGCTGYCWAACCGKATCAWTGACKCCTTGCGCAAGGCAAAKCAGGAGTCCACTKAR

TTACCGGARAAYAGKTGCAKTYCCTTCAYCTKKKGAAGTGATGSTCCTTTWAAGGGAACCAMTGAAGYTCCTGGGAAWCK

CTRGATGYGTGWAAATGTAAGAGAACCTTKGCCGTTGAAGCCTGCCTWAMYTACTAGACACTATATGACCGCTCTKCAAG

GAATGGAATTCCKAATTGAGGTRAGGAAAATGTCTCTGSTACTCTTCCGKTAAMTACT

(b)

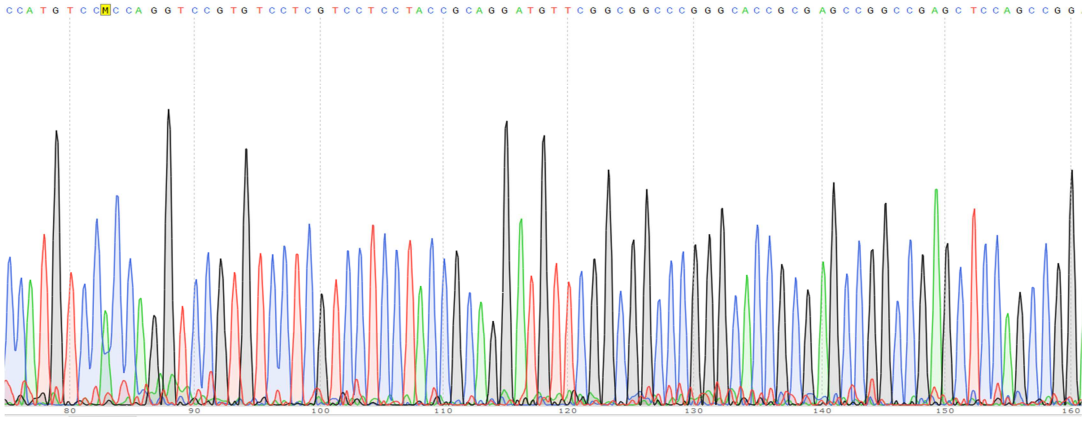

(c)

Figure 12: **Sequencing of the Vimentin gene in the Vim-Topo 2 clone obtained with M13 reverse primer**.
Using the M13 reverse primer, DNA sequencing of the Vim-Topo 2 clone showed this sequence.

a) The correct sequence of Vimentin is highlighted in gray and bold, in yellow is highlighted the ATG start codon, while green is the region recognized by the primer sequence 1. In red is indicated unrecognized nucleotides, and these have been corrected manually through use of the chromatogram.
b) A representative portion of the chromatogram obtained with the M13 reverse primer.
c) In red, the nucleotides were manually corrected based on the color display of the individual peaks in the chromatogram.

Considering the good sequencing of the Vim–Topo 2 clone with the M13 reverse primer, we proceeded with the analysis of the fragment obtained with sequence 1 primer.

The sequencing with sequence 1 primer was obtained with excellent quality. The long portion of the Vimentin gene was correct even after the recognition site of sequence 2. The manual correction was carried out on only a few bases located within the correct Vimentin sequence (figure 13).

(a)

(b)

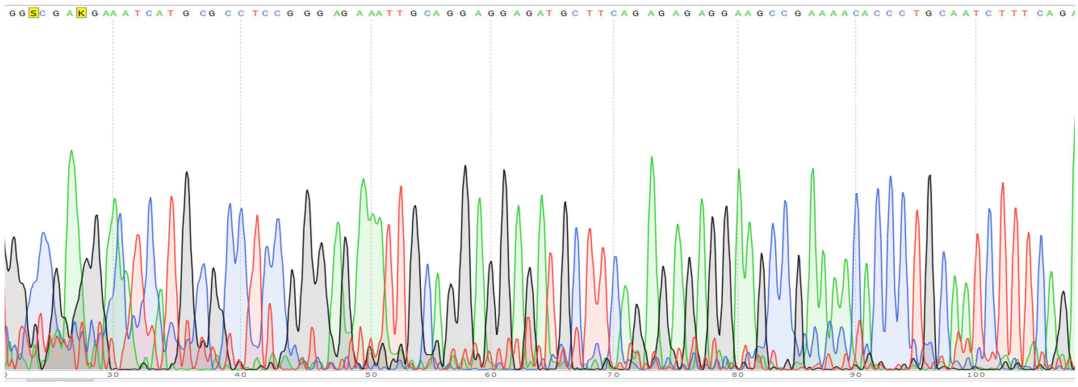

(c)

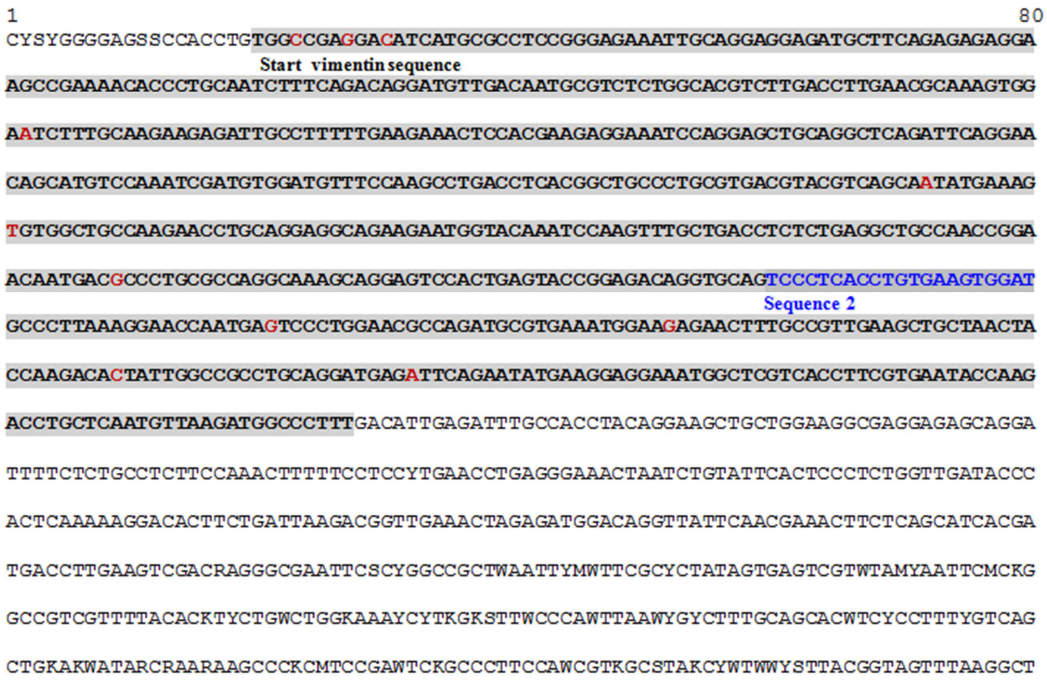

Figure 13: **The sequencing of Vimentin gene in Vim-Topo 2 clone obtained with sequence 1 primer**.
Using the sequence 1 primer, DNA sequencing of the Vim-Topo 2 clone showed this sequence.

a) The correct sequence of the Vimentin gene is highlighted in gray and bold, while blue is the region recognized by the primer sequence 2. In red is indicated unrecognized nucleotides, and these have been corrected manually through use of the chromatogram.
b) A representative portion of the chromatogram is obtained with the sequence 1 primer.
c) In red, the nucleotides were manually corrected based on the color display of the individual peaks in the chromatogram.

Considering these promising data, we finally analyzed the sequencing of the terminal portion of the Vimentin gene obtained starting from the sequence 2 primer. This sequencing was excellent because it was not necessary to manually make any correction (figure 14).

(a)

1 80

TWWTWKTTTTTYCKTAWWAAATGKAKTYCCYTG**GAACGCCAGATGCGTGAAATGGAAGAGAACTTTGCCGTTGAAGCTGC**

Start vimentin sequence

TAACTACCAAGACACTATTGGCCGCCTGCAGGATGAGATTCAGAATATGAAGGAGGAAATGGCTCGTCACCTTCGTGAAT

ACCAAGACCTGCTCAATGTTAAGATGGCCCTTGACATTGAGATTGCCACCTACAGGAAGCTGCTGGAAGGCGAGGAGAGC

AGGATTTCTCTGCCTCTTCCAAACTTTCCTCCCTGAACCTGAGGGAAACTAATCTGGATTCACTCCCTCTGGTTGATAC

CCACTCAAAAAGGACACTTCTGATTAAGACGGTTGAAACTAGAGATGGACAGGTTATCAACGAAACTTCTCAGCATCACG

ATGACCTTGAAGTCGACAAGGGCGAATTCGCGGCCGCTAAATTCAATTCGCCCTATAGTGAGTCGTATTACAATTCACTG

End vimentin sequence

GCCGTCGTTTTACAACGTCGTGACTGGGAAAACCCTGGCGTTACCCAACTTAATCGCCTTGCAGCACATCCCCCTTTCGC

CAGCTGGCGTAATAGCGAAGAGGCCCGCACCGATCGCCCTTCCCAACAGTTGCGCAGCCTATACGTACGGCAGTTTAAGG

TTTACACCTATAAAAGAGAGAGCCGTTATCGTCTGTTTGTGGATGTACAGAGTGATATTATTGACACGCCGGGGCGACGG

ATGGTGATCCCCCTGGCCAGTGCACGTCTGCTGTCAGATAAAGTCTCCCGTGAACTTTACCCGGTGGTGCWTATCGGGGA

TGAAAGCTGGCGCATGATGACCACCGATATGGCCAGTGTGCCGGTCTCCGTTATCGGGAAGAAGTGGCTGATCTCAGCCW

CCGCGAAATGACATCAAAACKCATTAACCTGATGTTCTGGGGAATATAATGTCAGCATGAGATTATCAWAAGATCTTCAC

YTAGATCTTTTCACKWGAAAGCCAGTCCSMRAAACGTGCTGACYCCGAATGAATKTYAGYTWYTGGCTATTCTGAMCAGG

CAAWACGYAAGCGCAAAGRAAKCWWGTACTGMATGGCTAMCTGCATAGCTAGAYTGCGTTWTGAMWGCAGCTAACGGATT

GCAGCTGGGYCCCTCGGTAGTTGAGCCTTGCAAGTAAMYGGATGCTCTGCTCAGGAYTGAGTGCAAGGATMAGCTGTAAY

CGAGAMCWG

(b)

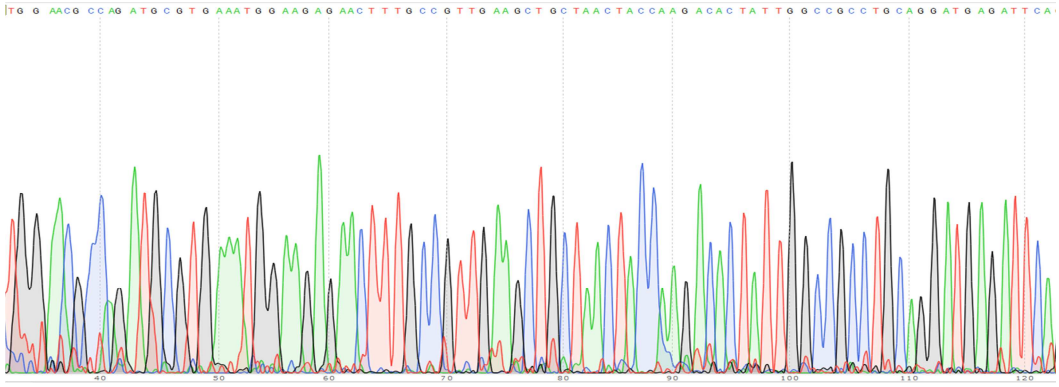

Figure 14: **The sequencing of Vimentin gene in Vim-Topo 2 clone obtained with sequence 2 primer**.
Using the sequence 2 primer, DNA sequencing of the Vim-Topo 2 clone showed this sequence.
a) The correct sequence of the Vimentin gene is highlighted in gray and bold.
b) A representative portion of the chromatogram is obtained with the sequence 2 primer.

Contrary to Vim-Topo 1 clone, the sequencing data revealed that the Vimentin sequence of the Vim-Topo 2 clone was correct. Therefore we cconcluded that the insertion of Vimentin gene in Topo vector had taken place successfully in the Vim-Topo 2 clone, that it was therefore selected for the following assays.

2.1.5 Restriction enzyme site digestion analysis

Waiting for the results of sequencing, a RE site digestion analysis was performed in both Vim-Topo clones. Thus, the purified DNA of each selective culture was subjected to digestion with appropriate restriction enzymes (RE). The REs are enzymes produced by bacterial cells, which may be considered as molecular "clippers", because they allow the cutting of double strand DNA in fragments. The cut takes place in correspondence with short specific base sequences (4-8 bases), at restriction sites.

During the previous amplification of the Vimentin gene, the used primers contained one recognition site for the *Bam HI* and *Sal I* REs respectively, and the Vimentin fragment has been inserted between these two sites.

To liberate only the Vimentin gene from the Topo vector, a double digestion with *Sal I* and *Bam HI* enzymes was performed.

Thus, we prepared a reaction mixture with both *Bam HI* and *Sal I* enzymes, and the purified DNA from each clone was added. The reaction was then incubated at 37° C and a double digestion was made. The products of double digestion were separated by agarose –gel electrophoresis and assessed on the trans–illuminator.

As shown in figure 15, we found that two bands were present as a result of double digestion with *Bam HI* and *Sal I* enzymes in both the Vim–Topo clones. The larger band was detected at 4 kb being the DNA of Topo vector. The smallest band of size 1.4 kb, is the same size of Vimentin gene. Therefore, we assume that the double digestion had liberated the Vimentin gene from the Topo vector successfully in both Vim-Topo clones.

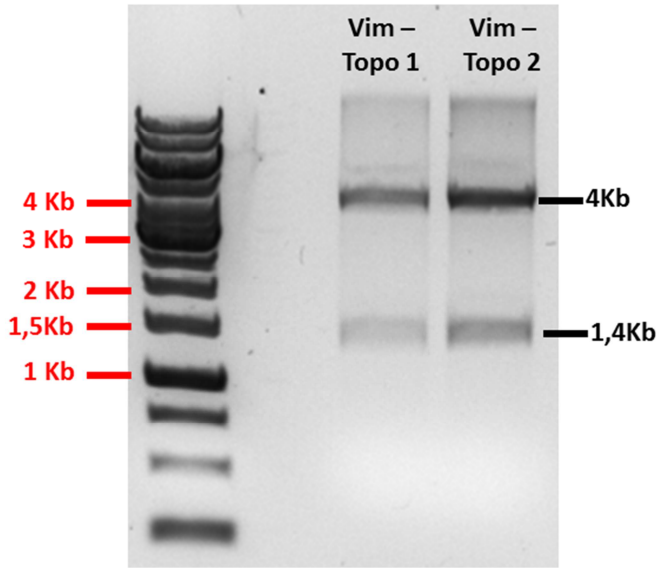

Figure 15: **Double digestion with Sal I and Bam HI enzymes of Vim-Topo vector clones.**

Gel electrophoresis of Vim-Topo clones following the double digestion with *Bam HI* and *Sal I*.

After the sequencing data had shown that the Vim-Topo 2 clone had successfully inserted the correct Vimentin sequence, a new double digestion was performed by increasing the concentration of the sample. Electrophoresis gel was run and the band corresponding to the 1.4 kb band was cut out and purified according to the Promega protocol of *Wizard® SV Gel and PCR Clean-up System kit*. The DNA names Vimentin 2, was resuspended, and quantified using the NanoDrop spectrophotometer (see Table 3).

	Conc. (ng/µl)	**260/280**
Vimentin 2	15,4	2,02

Table 3: Quantification of the purified Vimentin 2 obtained following double digestion with Bam HI and Sal I restriction enzymes, using the Nanodrop spectrophotometer.

We found that the concentration of Vimentin 2 was not particularly high, with the 260/280 ratio being at the maximum limit. This DNA content reduction was caused by the various steps that were necessary to purify the Vimentin gene.

This phase is particularly important because purified Vimentin gene can be thus inserted into a new cloning/expression vector, said pET22b+ vector, which it is able to synthesize the Vimentin protein.

2.1.6 Preparation of the pET22b+ cloning / expression vector

The pET System is one of the best systems so far developed for the cloning and expression of recombinant proteins, such as Vimentin, in the E.coli strain BL 21 star DE3.

We had chosen the pET-22b(+) cloning/expression vector as it is a stable vector, making it good for cloning and expression purposes of the Vimentin protein, moreover the presence of a His Tag, means it is possible to purify the Vimentin protein expressed by the vector via a Nickel column. This vector also had the Ap gene, which is responsible for resistance to Amp antibiotic. Finally, all target genes were cloned into pET plasmids under control of strong bacteriophage T7 transcription; and the expression was induced by providing a source of T7 RNA polymerase in the host cell.

Before insertion of the Vimentin gene, the pET-22b(+) vector must be prepared to accept it. Firstly, the stock of the pET-22b(+) vector (Novagen) was diluted 1:10 and 1:100 in nuclease-free water to ensure isolation of colonies. Each dilution of pET-22b(+) vector was transformed into BL 21 star DE3 competent cells by heat-shock, and then incubated with S.O.C. medium to stimulate bacterial growth. A small amount of this bacterial suspension was spread in a selective Luria–Bertani (LB) agar–plate, containing Amp, and incubated overnight. The negative control was performed to verify that there was no other bacterial contamination.

The following day, we found that the negative control had not grown, confirming the absence of contaminants; instead, in both pET–plates there were numerous colonies present, showing that the transformation had occurred successfully with both dilutions.

Three colonies of the 1: 100 pET–plate were therefore identified and selected. A small number were taken with a tip, then tempered and incubated overnight in LB medium broth, which contains Amp, to allow only the growth of the selected clone. The LB medium is a clear broth, but could become more turbid depending on the bacterial charge.

All selective cultures showed abundant bacterial growth, indicating the presence of the vector in all the clones and thus we proceeded with the DNA purification of each culture according to the protocol of the Wizard plus SV minipreps DNA purification system kit. The DNA was then resuspended and quantified by the Nanodrop spectrophotometer (see Table 4 below).

We found that the DNA concentrations of pET–1, –2 and –3 clones were 33.9, 22 and 34 ng/µl, respectively. These DNA concentrations were not very however purification of clones 1 and 2 was successful, in fact, the absorbance values of 260/280 ratio were around 1.8. Instead, the purification of pET–3 was not successful as indicated by the absorbance value of 260/280 ratio that was over 2.

	Conc. (ng/µl)	**260/280**
pET– 1	33,9	1,87
pET– 2	22	1,89
pET– 3	34	2,17

Table 4: Quantification of the purified DNA of each pET –clone by the Nanodrop spectrophotometer.

Since the concentration of pET–1 clone was higher than the of pET–2 clone, we decided to only use this clone for subsequent assays.

Analyzing the map of the pET-22b(+) vector, we identified each restriction site for the *Bam HI* and *Sal I* enzymes respectively, which were the same REs used in the previous cloning in Topo vector.

Thus, we prepared a reaction mixture using both *Bam HI* and *Sal I* enzymes, *Bam HI* buffer and the purified DNA of each clone was added. Digestion was carried out and then gel electrophoresis was run and assessed on the trans–illuminator.

As shown in figure 16, in the gel was present only one well-defined band at 5.5 kb in size, confirming that the double digestion was carried out successfully.

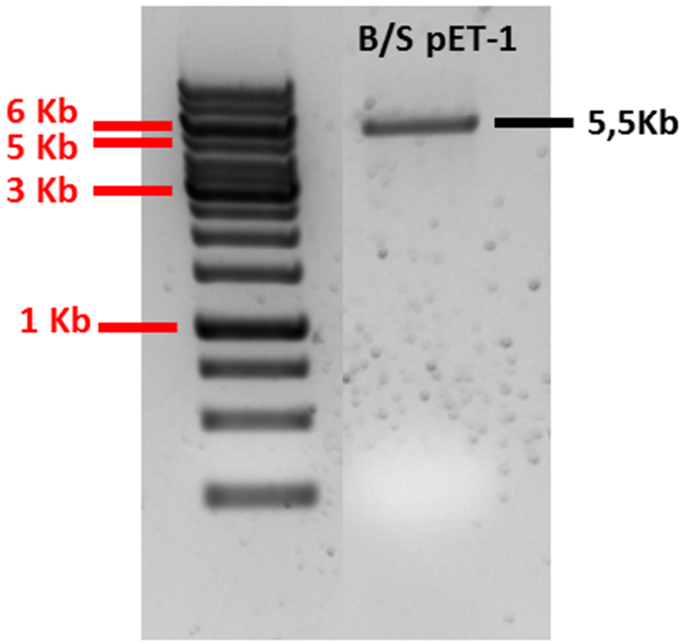

Figure 16: **Double digestion of pET 1 clone by *Bam HI* and *Sal I* REs .**

Gel electrophoresis of pET-1 clone following the double digestion with *Bam HI* and *Sal I*.

Given that the enzymes had acted correctly, a new double digestion was performed by increasing the concentration of the sample. The electrophoresis gel was run and the 5.5 kb band (pET vector size) was cut out and purified according to the Promega protocol of Wizard® SV Gel and PCR Clean-up System kit. The DNA was resuspended, named B/S–pET–1, and finally quantified using the NanoDrop spectrophotometer (see Table 5).

	Conc. (ng/µl)	**260/280**
B/S-pET-1	21,6	2,01

Table 5: Quantification of the purified DNA of pET –1 clone after double digestion with Bam HI and Sal I REs using the Nanodrop spectrophotometer.

We found that the concentration of pET-1 was 21.6 ng/µl, which is not particularly high, and the 260/280 ratio is the maximum limit for considering its purification as positive.

Thus, we proceeded with the removal of phosphate groups from the 5'- and 3'-ends of the pET vector DNA to prevent its self–ligation before the insertion of the Vimentin fragment. Briefly, purified DNA of B/S–pET–1 clone was mixed with Shrimp alkaline phosphate enzyme and its specific buffer, then incubated at 37° C to allow removal of phosphate groups. After one hour, the enzyme was inactivated by incubating at 65° C and the reaction was then purified according to the Promega protocol of Wizard® SV Gel and PCR Clean-up System kit. The DNA was resuspended, named SAP–pET–1, and finally quantified using the NanoDrop spectrophotometer (see Table 6).

	Conc. (ng/µl)	260/280
SAP-pET-1	16,7	2,03

Table 6: DNA quantification of SAP-pET –1 clone after phosphate elimination using the Nanodrop spectrophotometer.

We found that the concentration of SAP–pET–1 was quite low amounting to 16.7 ng/µl, and the 260/280 ratio is the maximum limit for considering its purification as positive. This reduction of DNA content was caused by the various steps that were necessary to the preparation of pET vector prior to allowing insertion of the Vimentin fragment.

2.1.7 Ligation of Vimentin gene in pET22b+ vector and Transformation in BL 21 star DE3 competent cells

After the SAP –pET–1 vector and Vimentin 2 insert were prepared for ligation, and their concentrations were determined, we prepared a reaction mixture in which the molar ratio of vector / insert was a 1/3. In this reaction, we added the T4 ligase enzyme and its respective buffer. The negative control was prepared without the Vimentin 2 insert. Both samples were incubated overnight at 16° C to allow for ligation between the pET vector and Vimentin.
Before the transformation into competent cells, both ligation samples were purified by butanol precipitation, in order to remove all of the reaction components. Once the supernatant was removed and the DNA was resuspended in nuclease –free water.

Finally, the transformation into competent cells was performed by adding in each vial of BL 21 star DE3 cells the purified ligation reaction or the negative control. Using the heat-shock, the entrance of the plasmid was carried out. Later, the BL 21 star DE3 cells were incubated for one hour with S.O.C. medium to stimulate bacterial growth, and a small amount of this was spread in a selective LB agar–plate, containing Amp, and incubated overnight.
The following day, we found that uncountable colonies had grown in the ligation sample, and nothing in the negative control. These data had shown that the ligation process was successful. Thus, in the ligation plate, eight well–isolated colonies were selected for subsequent analysis and named Vim-pET clones.

2.1.8 Colony screening and isolation of each Vim –pET clone

The procedure is the same for the Vim–Topo vector clones (see above). Thus for colony PCR screening and culture isolations, eight Vim –pET clones were selected. The PCR reaction was run and its products were separated by agarose–gel electrophoresis and assessed on the trans–illuminator.
The colony PCR screening showed that a band at 1.4 kb (Vimentin size) was present in all the clones indicating that the ligation was successful (figure 17).

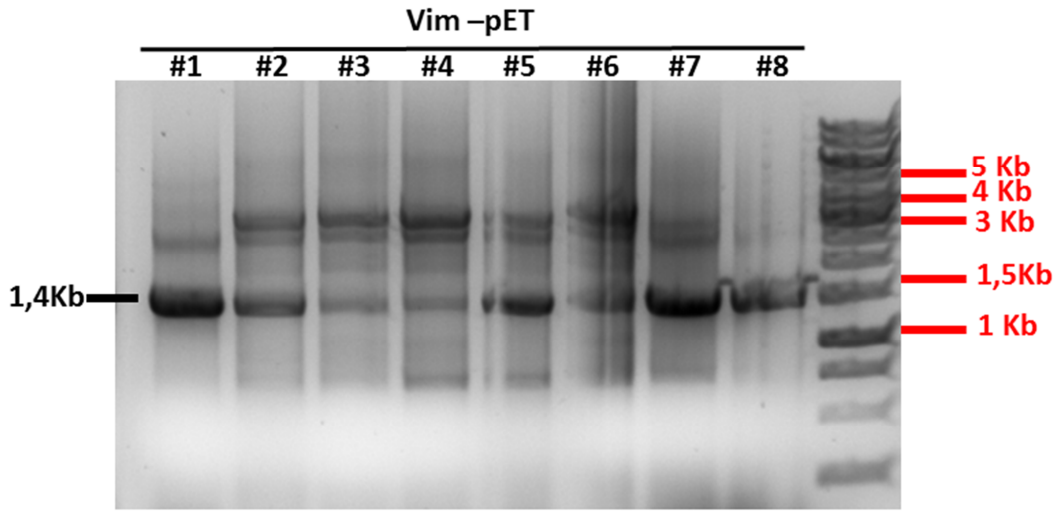

Figure 17: **Colony screening of Vim-pET clones.**
Visualization of the gel electrophoresis of both Vim–pET clones following the PCR reaction.

For the growth of the selected clone, as described above, each Vim-pET clone was grown overnight in Amp –LB broth medium. The following day, all selective cultures showed an abundant bacterial growth, indicating the presence of the vector in all the clones.

Thus, the DNA of each culture was purified according to the protocol of the *Wizard plus SV minipreps DNA purification system kit* and its DNA was resuspended in nuclease free water and quantified by the Nanodrop spectrophotometer (see Table 7).

	Conc. (ng/µl)	**260/280**
Vim –pET 1	62,3	1,56
Vim –pET 2	63,2	1,60
Vim –pET 3	53,6	1,54
Vim –pET 4	46,9	1,60
Vim –pET 5	50,1	1,64
Vim –pET 6	61,6	1,62
Vim –pET 7	50,5	1,64
Vim –pET 8	49,2	1,54

Table 7: Quantification of the purified DNA of each Vim –pET clone by the Nanodrop spectrophotometer.

A good result was obtained from purification of the isolated culture although the absorbance ratio at 260 and 280 nm was slightly below the value of 1.8, indicating that the purification was not perfect but still good. Moreover, in all the Vim-pET clones we had a good DNA content, and it was very similar in all the samples.

2.1.9 Restriction enzyme site digestion analysis

To liberate only the Vimentin gene from the pET vector, a double digestion with *Sal I* and *Bam HI* enzymes was performed. Thus, we prepared a reaction mixture with both *Bam HI* and *Sal I* enzymes, and the purified DNA from each clone was added. The reaction was then incubated at 37° C and double digestion was made. The products of double digestion were separated by agarose–gel electrophoresis and assessed on the trans–illuminator.

As shown in figure 18, we found that two bands were present as a result of double digestion with *Bam HI* and *Sal I* enzymes in all Vim–pET clones, except for the Vim-pET-4 clone. The larger band was detected at 5.5 kb, in the DNA of pET vector. The smallest band was a size of 1.4 kb, which was the Vimentin fragment.

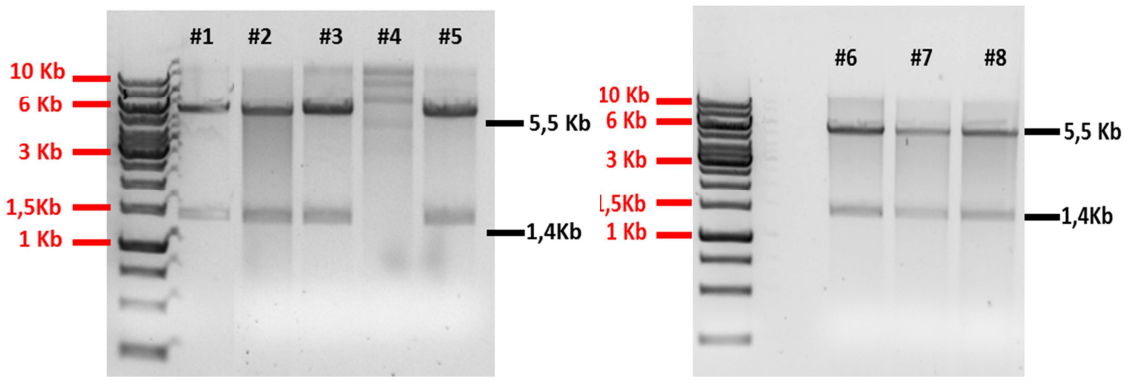

Figure 18: **Double digestion of Vim-pET clones by Bam HI and Sal I.**
Gel electrophoresis of Vim –pET clones following the double digestion with *Bam HI* and *Sal I*.

It appears that the double digestion had liberated the Vimentin gene from the pET vector successfully in all Vim –pET clones, except to Vim –pET-4 clone.

2.1.10 Sequencing of Vimentin from two pET clones

Except for the Vim –pET-4 clone, all the other clones had inserted the Vimentin fragment in the pET vector. Moreover, considering the data of DNA quantification from isolated culture, the first two clones had the highest concentration (i.e. Vim –pET-1 and Vim –pET-2 clones) so they were selected for sequencing at the Central DNA Sequencing Facility in the laboratory of University of Stellenbosch.
The procedure was the same as used for the Topo vector (see above), but this sequencing was performed with the pET-22b(+) primers, being T7 promoter and T7 terminator.

Analyzing the sequencing data of Vim–pET-1 clone, we found that the Vimentin sequence had inserted in this clone with many mutations, probably due to erroneous amplification during the PCR reaction. The inability to verify this sequence in other chromatograms, allowed us to conclude that the Vimentin sequence of Vim –pET-1 clone was incorrect and it was deleted.

The Vim–pET-2 clone data are shown below. We found that the T7 promoter was not able to sequence the entire Vimentin fragment, but only its initial portion. Furthermore, the sequencing quality provided by the software was high, and with only a few bases to check again manually. After these corrections, the Vimentin

sequence was correct for an extended part after the recognition site of the sequence 1 primer (figure 19).

(a)

(b)

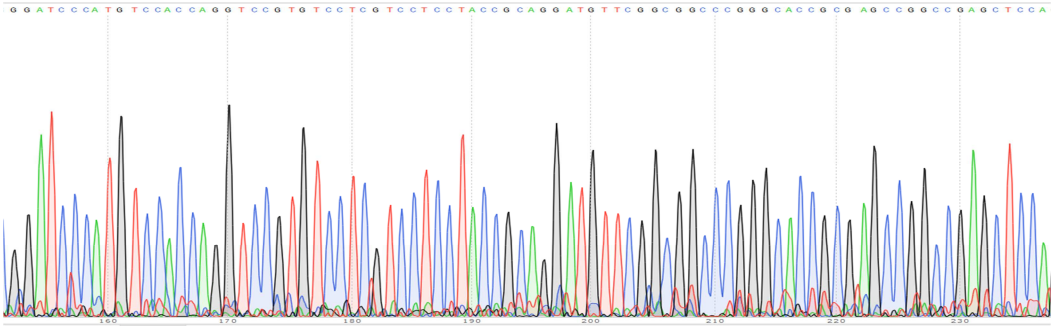

(c)

Figure 19: **The sequencing of Vimentin gene in Vim- pET 2 clone obtained with T7 Promoter**.

Using the T7 promoter primer, DNA sequencing of the Vim-pET 2 clone was shown.

a) The correct sequence of Vimentin is highlighted in gray and bold, in yellow is highlighted the ATG start codon, while green is the region recognized by the primer sequence 1. In red is indicated unrecognized nucleotides, and these have been corrected manually through use of the chromatogram.

b) A representative portion of the chromatogram obtained with the T7 promoter primer.

c) In red, the nucleotides were manually corrected based on the color display of the individual peaks in the chromatogram.

Considering that the correct sequence of Vimentin in the Vim –pET-2 clone obtained with the T7 promoter, we proceeded with the data analysis of the sequencing with sequence 1 primer.

Also, the sequencing with sequence 1 primer was obtained with excellent quality. The long portion of the Vimentin gene was perfectly correct even after the recognition site of sequence 2. The manual correction was carried out on only a few bases located within the correct Vimentin sequence (figure 20).

(a)

(b)

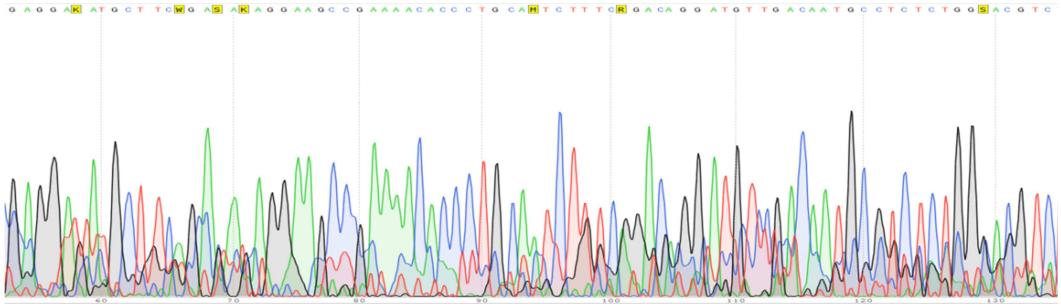

(c)

Figure 20: **Sequencing of the Vimentin gene in the Vim–pET 2 clone obtained with sequence 1 primer**.

Using the sequence 1 primer, DNA sequencing of the Vim- pET 2 clone was shown.

a) The correct sequence of Vimentin gene is highlighted in gray and bold, while blue is the region recognized by the primer sequence 2. In red is indicated unrecognized nucleotides correctly by the software, and these have been corrected manually through use of the chromatogram.
b) A representative portion of the chromatogram obtained with the sequence 1 primer.
c) In red, the nucleotides were manually corrected based on the color display of the individual peaks in the chromatogram.

Considering these promising data, we finally analyzed the sequencing of the terminal portion of the Vimentin gene obtained starting from the sequence of primer 2 (figure 21). In this case, the provided data by the software had been very good, and a manual corrections were made on only a few bases (figure 21-c).

(a)

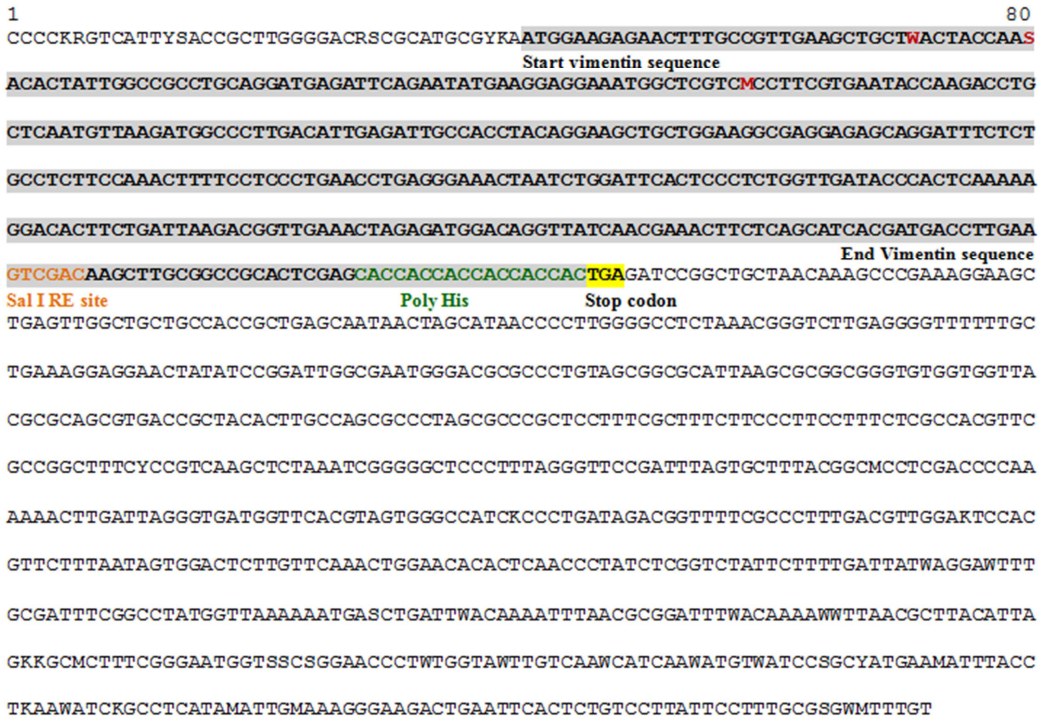

(b)

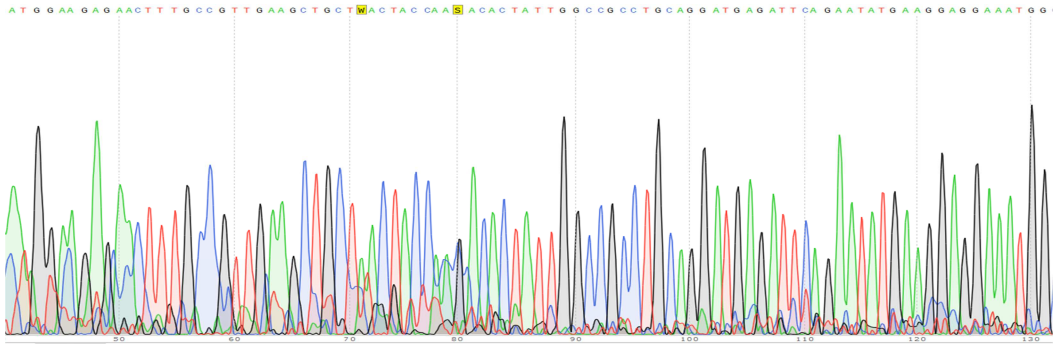

(c)

1 80

CCCCKRGTCATTYSACCGCTTGGGGACRSCGCATGCGYKA**ATGGAAGAGAACTTTGCCGTTGAAGCTGCTAACTACCAAG**

Start vimentin sequence

ACACTATTGGCCGCCTGCAGGATGAGATTCAGAATATGAAGGAGGAAATGGCTCGTCACCTTCGTGAATACCAAGACCTG

CTCAATGTTAAGATGGCCCTTGACATTGAGATTGCCACCTACAGGAAGCTGCTGGAAGGCGAGGAGAGCAGGATTTCTCT

GCCTCTTCCAAACTTTTCCTCCCTGAACCTGAGGGAAACTAATCTGGATTCACTCCCTCTGGTTGATACCCACTCAAAAA

GGACACTTCTGATTAAGACGGTTGAAACTAGAGATGGACAGGTTATCAACGAAACTTCTCAGCATCACGATGACCTTGAA

End Vimentin sequence

GTCGAC**AAGCTTGCGGCCGCACTCGAG**CACCACCACCACCACCAC**TGA**GATCCGGCTGCTAACAAAGCCCGAAAGGAAGC

Sal I RE site Poly His Stop codon

TGAGTTGGCTGCTGCCACCGCTGAGCAATAACTAGCATAACCCCTTGGGGCCTCTAAACGGGTCTTGAGGGGTTTTTTGC

TGAAAGGAGGAACTATATCCGGATTGGCGAATGGGACGCGCCCTGTAGCGGCGCATTAAGCGCGGCGGGTGTGGTGGTTA

CGCGCAGCGTGACCGCTACACTTGCCAGCGCCCTAGCGCCCGCTCCTTTCGCTTTCTTCCCTTCCTTTCTCGCCACGTTC

GCCGGCTTTCYCCGTCAAGCTCTAAATCGGGGGCTCCCTTTAGGGTTCCGATTTAGTGCTTTACGGCMCCTCGACCCCAA

AAAACTTGATTAGGGTGATGGTTCACGTAGTGGGCCATCKCCCTGATAGACGGTTTTCGCCCTTTGACGTTGGAKTCCAC

GTTCTTTAATAGTGGACTCTTGTTCAAACTGGAACACACTCAACCCTATCTCGGTCTATTCTTTTGATTATWAGGAWTTT

GCGATTTCGGCCTATGGTTAAAAAATGASCTGATTWACAAAATTTAACGCGGATTTWACAAAAWWTTAACGCTTACATTA

GKKGCMCTTTCGGGAATGGTSSCSGGAACCCTWTGGTAWTTGTCAAWCATCAAWATGTWATCCSGCYATGAAMATTTACC

TKAAWATCKGCCTCATAMATTGMAAAGGGAAGACTGAATTCACTCTGTCCTTATTCCTTTGCGSGWMTTTGT

Figure 21: **Sequencing of the Vimentin gene in the Vim–pET 2 clone obtained with sequence 2 primer**.

Using the sequence 2 primer, DNA sequencing of the Vim-pET 2 clone is shown.

a) The correct sequence of Vimentin gene is highlighted in gray and bold.
b) A representative portion of the chromatogram obtained with the sequence 2 primer.
c) In red, the nucleotides are manually corrected based on the color display of the individual peaks in the chromatogram.

Contrary to Vim–pET-1 clone, analyzing all the sequencing data of Vim –pET-2 clone we found that the sequence of Vimentin was inserted successfully.
Confirming that all the cloning process were carried out correctly, after the end of the Vimentin sequence was present at the recognition site for *Sal I* RE.
Moreover, after analysis (see figure 21), we found that about twenty bases from the *Sal I* RE site, were also present in a region coding for a tail of poly-histidine (poly-His) immediately followed by a stop codon. This poly-His tail is essential during the step of protein purification.

Thus, the purified Vimentin protein could be used to evaluate the effect of Z-ajoene on this protein by *in vitro* assays, such as proteomics, western blot and *in vitro* binding assays. Unfortunately due to technical problems in the purification lab, it was not possible to purify the Vimentin protein from the Vim–pET 2 clone. However, this phase of the process will be performed in the future (Manuscript in preaparation).

2.2 Z-ajoene influences the intracellular organization of Vimentin protein on MDA-MB-231 cancer cells

The background of this section is based on our previous work where we found that ajoene *S*-thiolates numerous protein targets in MDA-MB-231 cells [C. H. Kaschula, *et al.* (2015) Mol Carcinog.]. By 2D electrophoresis the ajoene-targeted and labelled proteins were separated and one of these proteins was identified by proteomics to be Vimentin.

In this section, we aimed to confirm Vimentin is indeed a target of the garlic compound ajoene. We therefore aimed to confirm *S*-thiolation of Vimentin by ajoene and to identify whether the ajoene-Vimentin interaction is important in the anti –cancer activity of ajoene in the triple-negative breast cancer cell line MDA-MB-231.

Results and Discussion

2.2.1 Dansyl-Ajoene (DP) and *Z*-Ajoene (ZA) *S*-Thiolate Vimentin at Cys328

As described in our article we found that the ajoene *S*-thiolates numerous proteins in MDA-MB-231 cells through mixed disulfide formation between ajoene and a cysteine residue of a protein [C. H. Kaschula, *et al.* (2015) Mol Carcinog.]. Subsequent to the paper, we found that one of these labeled proteins was separated from the MDA-MB-231 cell lysate by 2D-gel electrophoresis and identified by proteomics to be Vimentin.

As mentioned above the first step of the project was therefore to clone and express recombinant Vimentin, useful to validate that Vimentin is an *S*-thiolation target of ajoene. We performed this assay using a synthetic ajoene analogue called DP, in which one of the allyl groups is substituted for a dansyl group. This ajoene analogue was found to be fully active compared to ajoene at inhibiting proliferation and inducing apoptosis in MDA-MB-231 cells.

The dansyl group of DP was chosen as in addition to being fluorescent which makes it useful for fluorescence studies, there is also a commercially available anti-dansyl antibody against it which allows its detection for immunoblotting investigations.

As described in our previous article, we had demonstrated that DP and ajoene share the same targets, and thus DP can be a useful tool for understanding the mechanistic aspects of ajoene.

Since we were unsuccessful in expressing and purifying recombinant Vimentin, we purchased some protein from a company to use for *in vitro* experiments, i.e. proteomics and alkylation assay.

We therefore treated purified recombinant Vimentin (1 µM) with 25 µM DP in the absence of reducing agents. We observed the formation of a covalent bond only in the treated sample by western blot which was evidenced by the transfer of the dansyl label from ajoene to Vimentin during thiolysis. Furthermore, by subjecting all the samples to the reducing agent DTT, the DP label was cleaved off the protein (Figure 22) thereby confirming that DP binds Vimentin via a disulfide linkage.

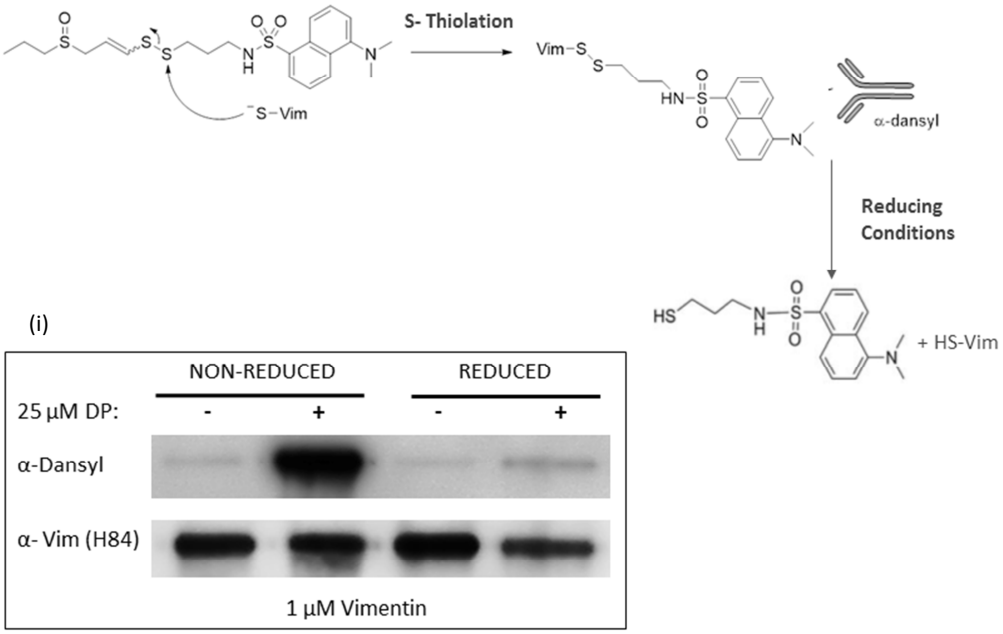

Figure 22: **Dansyl –ajoene *S*-thiolates recombinant Vimentin protein**

Scheme depicting proposed mechanism of Vimentin *S*-thiolation involving transfer of the dansyl group from DP to Vimentin.

(i) Western blot showing dansylated Vimentin in DP-treated samples when run under non-reducing conditions only. Purified Vimentin (1 µM) samples were either untreated or treated with 25 µM DP. Same samples treated without (non-reducing) or with (reducing) 100 mM dithiothreitol (DTT).

We were therefore confident that Vimentin is indeed one of the ajoene targets in MDA-MB-231 cells and that it is targeting Vimentin through *S*-thiolation of a cysteine residue. When considering the Vimentin amino acid sequence, it is immediately evident that there is only a single cysteine amino acid in the Vimentin sequence at position 328 (see Fig 23 below). It is therefore highly possible that Cys 328 is the target site of ajoene in Vimentin.

1 mstrsvssss yrrmfggpgt asrpsssrsy vttstrtysl gsalrpstsr slyasspggv
61 yatrssavrl rssvpgvrll qdsvdfslad aintefkntr tnekvelqel ndrfanyidk
121 vrfleqqnki llaeleqlkg qgksrlgdly eeemrelrrq vdqltndkar veverdnlae
181 dimrlreklq eemlqreeae ntlqsfrqdv dnaslarldl erkveslqee iaflkklhee
241 eiqelqaqiq eqhvqidvdv skpdltaalr dvrqqyesva aknlqeaeew ykskfadlse
301 aanrnndalr qakqesteyr r**qvqsltcev dalk**gtnesl erqmremeen faveaanyqd
361 tigrlqdeiq nmkeemarhl reyqdllnvk maldieiaty rkllegeesr islplpnfss
421 lnlretnlds lplvdthskr tlliktvetr dgqvinetsq hhddle

Fragment of interest containing **Cys328**: **qvqsltcevdalk**

Figure 23: **Amino acid sequence of Human Vimentin.**

In bold is highlighted the fragment of interest, which is one of those generated by trypsin digest (see the text below). This fragment contains the **Cysteine 328** (in red), which is the amino acid which is proposed to be involved in *S*-thiolation with ajoene.

We therefore prepared three Vimentin samples by incubating purified recombinant Vimentin protein without (control) or with 100 µM (a) ZA or (b) DP and sent these samples for proteomics analysis at the Centre for proteomics and Genomics research (CPGR), Cape Town, South Africa.

The proteomic analysis is a sensitive analytical technique which allows identification of protein peptides by mass analysed by mass spectrometry. This technique therefore can give information about whether the protein has been covalently modified [J. Rappsilber *et al.* (2003) *Anal. Chem*]. Briefly, the pure protein is first subjected to enzymatic digestion by the trypsin. This protease cleaves the protein at the level of the C-terminal after either lysine or arginine [J. V. Olsen *et al.*, (2004) Mol. Cell. Proteomics]. Therefore a protein fragment mixture is formed, and the peptides are then separated by liquid chromatography coupled to mass spectrometry analysis that enables fragment identification against a known data base of the expected fragments for that protein (See figure 24 below). If the fragment is not detected than it may be modified and therefore a different mass to that of the native protein in the database.

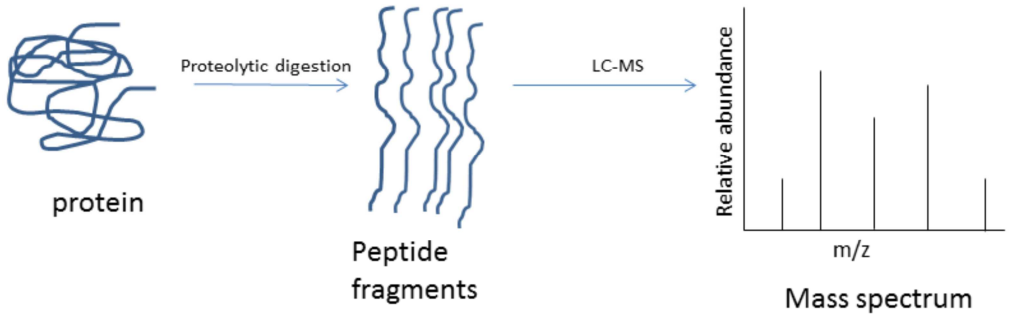

Figure 24: **Proteomic analysis of a protein**

The experimental procedure of proteomic analysis of a protein. First, the protein is subjected to proteolytic digestion by trypsin to generate peptide fragments. These fragments are then separated by liquid chromatography that it is coupled to mass spectrometry analysis which enables a identification of the protein based on expected mass of fragments within a known database for the protein.

According to *Expasy peptide software*, the predicted mass to charge ratio (*m/z*) of the Vimentin fragment **QVQSLTCEVDALK** could be a number of options depending on the charge of the peptids (Figure 25 (i)):

[M] = 1432.7232

$[M+H]^{+}$ = 1433.7304

$[M+2H]^{2+}$ = **717.3688.**

By experimental analysis we found the mass of the untreated fragment to be **717.3689**, meaning that the peptide was identified and that the parent ion carries a 2+ charge ($[M + 2H]^{2+}$) (Figure 25(ii)).

The fragment masses of the treated samples were found to be different in the *Z*-ajoene and DP-treated samples being 72.00337 and 322.08096 respectively.

So, if we apply this formula:

Modified fragment: (Compound MW + Fragment MW+ 2xHydrogens).

The predicted mass of the modified fragment by *Z*-ajoene is (72.00337 +1432.7233 + 2x1.0078)/2 = **753.3711**, whereas for DP–fragment is (322.08096 + 1432.7233 + 2x1.0078)/2 = **878.4099** (Figure 25 (i)):

By proteomic analysis, we found that the fragment masses of *Z*A-treated and DP-treated samples are **753.3708** and **878.4096**, respectively (Figure 5(ii)).

These masses are identical to the predicted masses (Figure 5(iii)). These data are a very excellent result, because this confirms our hypothesis that both Z-ajoene and its analogue DP covalently modify Vimentin through *S*-thiolation at **Cysteine 328** of Vimentin (Figure 5(iii)). These data have validated and confirmed our finding that DP *S*-thiolates a Vimentin target protein in MDA-MB-231 breast cancer cells. Vimentin is therefore an intracellular drug target of ajoene in MDA-MB-231 cells.

(i) Vimentin fragment **qvqsltcevdalk**:$[M+2H]^+$ = 717.3688

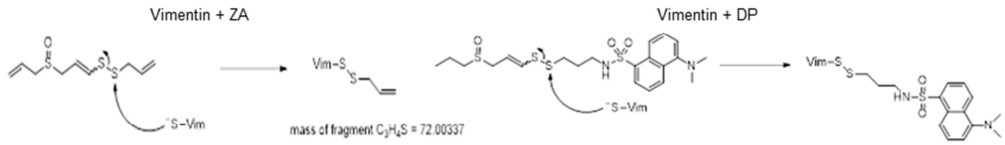

(ii)

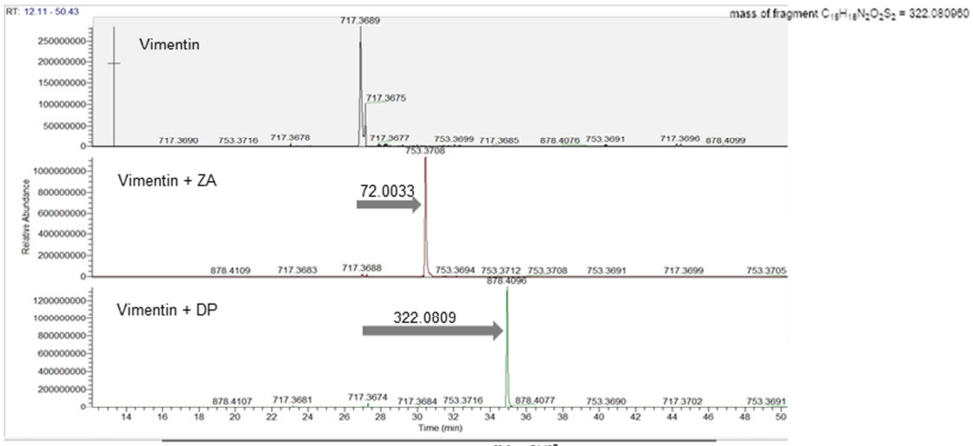

(iii)

Sample	$[M + 2H]^{2+}$	
	Predicted *m/z*	Found *m/z*
Vimentin (untreated)	717.3688	717.3689
Vimentin + ZA	753.3711	753.3708
Vimentin + DP	878.4099	878.4096

Figure 25**: Z-Ajoene and DP *S* –thiolates Vimentin through Cysteine 328.**

(i) Using Expasy peptide software we predicted the masses of the Vimentin fragment in untreated, ZA and DP –treated samples.

(ii) Proteomics showing *S*-thiolated Vimentin in all samples treated with ajoenes. Vimentin samples (10 µg) untreated and treated with DP or ZA (both 100 µM) were sent to CPGR Laboratory for peptide analysis. In accordance with the differences of their mass, the chromatograms had showed different retention times for the three samples.

(iii) Table showing predicted vs experimental masses, confirming that both DP and ZA that bind covalently to Cysteine 328.

2.2.2 Ajoene disrupts the structure of Vimentin filaments in MDA-MB-231 breast cancer cells.

We next sought to establish whether covalent modification of the Vimentin protein at Cys-328 with ajoene may cause a structural modification to the protein.
Thus, to evaluate the potential effects of ajoene on the Vimentin structure, the triple negative breast cancer cell line, MDA-MB-231, was treated with *Z*-ajoene and the fluorescent ajoene analogue DP, and fluorescence was detected by immunofluorescence using antibodies for Vimentin.

When selecting the correct concentration of *Z*-ajoene and DP for this experiment, we aimed to find a non-cytotoxic concentration in which the cellular integrity was not compromised. We therefore first performed an MTT cell viability assay prior to performing immunofluorescence staining of the Vimentin protein in MDA-MB-231 cells. We found that 25 µM of *Z*-Ajoene or DP is not cytotoxic to MDA-MB-231 cells after 6 hours of treatment, as shown in Figure 26, where the values of cell viability of the treated samples are not different to those of the untreated control. Cell viability was measured by the MTT cell viability assay.

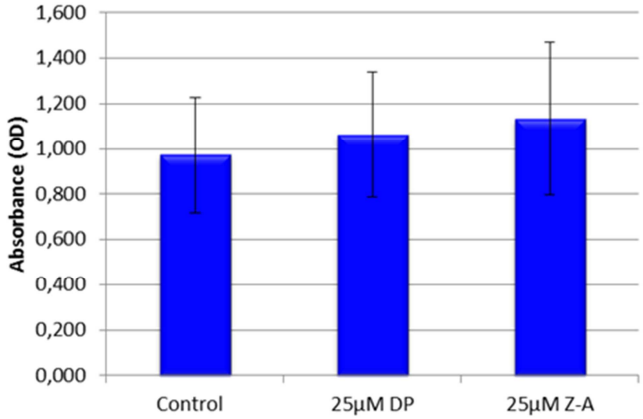

Figure 26: **Cytotoxicity of 25 µM DP or 25 µM *Z*-Ajoene in MDA-MB-231 breast cancer cells by the MTT assay**.
Using an MTT cell viability assay, 25 µM DP or *Z*-Ajoene was found not to be cytotoxic to MDA-MB-231 breast cancer cells after six hours of treatment.

Vimentin forms structural filaments mainly in the cytoplasm but there is also a small amount anchored within the membranes as well as in the ER and in the mitochondria [Katsumoto T. *et al.* (1990). Biol Cell].
The intracellular organization of Vimentin can be evaluated by immunofluorescence assays, where the Vimentin is detected through the use of specific antibodies against it. We have two commercially available vimentin antibodies in our laboratory being a polyclonal antibody H84 and a monoclonal antibody V9.
The H84 antibody is a rabbit polyclonal IgG subclass, that can recognize multiple epitopes corresponding to amino acids 1–84 mapping at the N–terminus of Vimentin protein which is a region of Vimentin embedded in the membrane [Georgatos S. D., *et al*. (1985) Journal of Cell Biology] and is therefore better used for detection of membrane Vimentin.

The V9 antibody is a mouse monoclonal IgG1 subtype that recognizes the epitope corresponding to the C-terminal domain of Vimentin protein, and is therefore sensitive to the detection of cytoplasmic Vimentin. The stains therefore resemble more filaments which are located in the cytoplasm.

For Vimentin immunofluorescence, MDA-MB-231 cells were seeded on a glass cover-slip and treated with 25 µM DP or *Z*-ajoene in 0.1% DMSO for six hours. Control cells were treated with 0.1% DMSO alone. Thereafter, the cells were fixed and stained with one of the primary Vimentin antibodies (V9 or H84) followed by treatment with a secondary antibody coupled to a red fluorescent Cy3 fluorophore. Cell sections were mounted on a glass slide for viewing under the confocal microscope.

DP emits blue/green due to the presence of its fluorescent dansyl–group; whereas the Vimentin protein emits red due to the Cy3 fluorescent secondary antibody. The treated samples are displayed in separate channels (Blue/Green and Red) and in an overlaying channel to verify any possible co–localization of DP and Vimentin. We have previously found that ajoene localizes to the ER in MDA-MB-231 cells. The vast majority of Vimentin in the cell is cytoplasmic with some membrane and its small amount is located into the ER.

In untreated cells, detection by a the primary polyclonal Vimentin antibody (H84) revealed the filamentous structures of Vimentin which is probably cytoplasmic and membranous comprising long and branched filaments of the cytoskeleton. The Vimentin is also localized in the plasma membrane(see Fig 27-B below), but it not detected when Vimentin is localized in ER, probably the epitope is different and H84 antibody cannot recognized it.

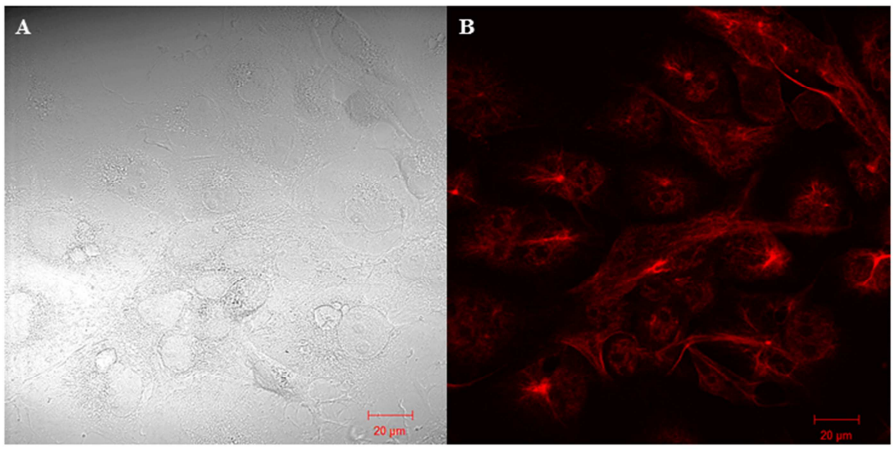

Figure 27: **The intracellular organization of Vimentin detected by the H84 polyclonal antibody.** In order to view the intracellular organization of Vimentin, Vimentin in MDA-MB-231 was detected with a H84 anti-vimentin antibody and stained with a red with Cy3. In (**B**), Vimentin protein was found to form long and branched cytoplasmic filaments, and it is also localized in plasma membrane. (**A**)The phase contrast image is shown.

In DP- and *Z*-ajoene- treated cells, we observed that the intracellular organization of Vimentin was not so well defined and that the signal was less intense. Vimentin was found to be mainly localized in the plasma membrane with the structures appearing more dispersed, with significant reduction in integrity of the filamentous structures (Fig 28-A and C). Moreover, in DP-treated cells, H84 –antibody detection did not revealed co–localization between DP and Vimentin (Fig. 28- C) although this was not unexpected as we had previously determined that DP localizes to the ER and a vast majority of Vimentin is in the cytoplasm.

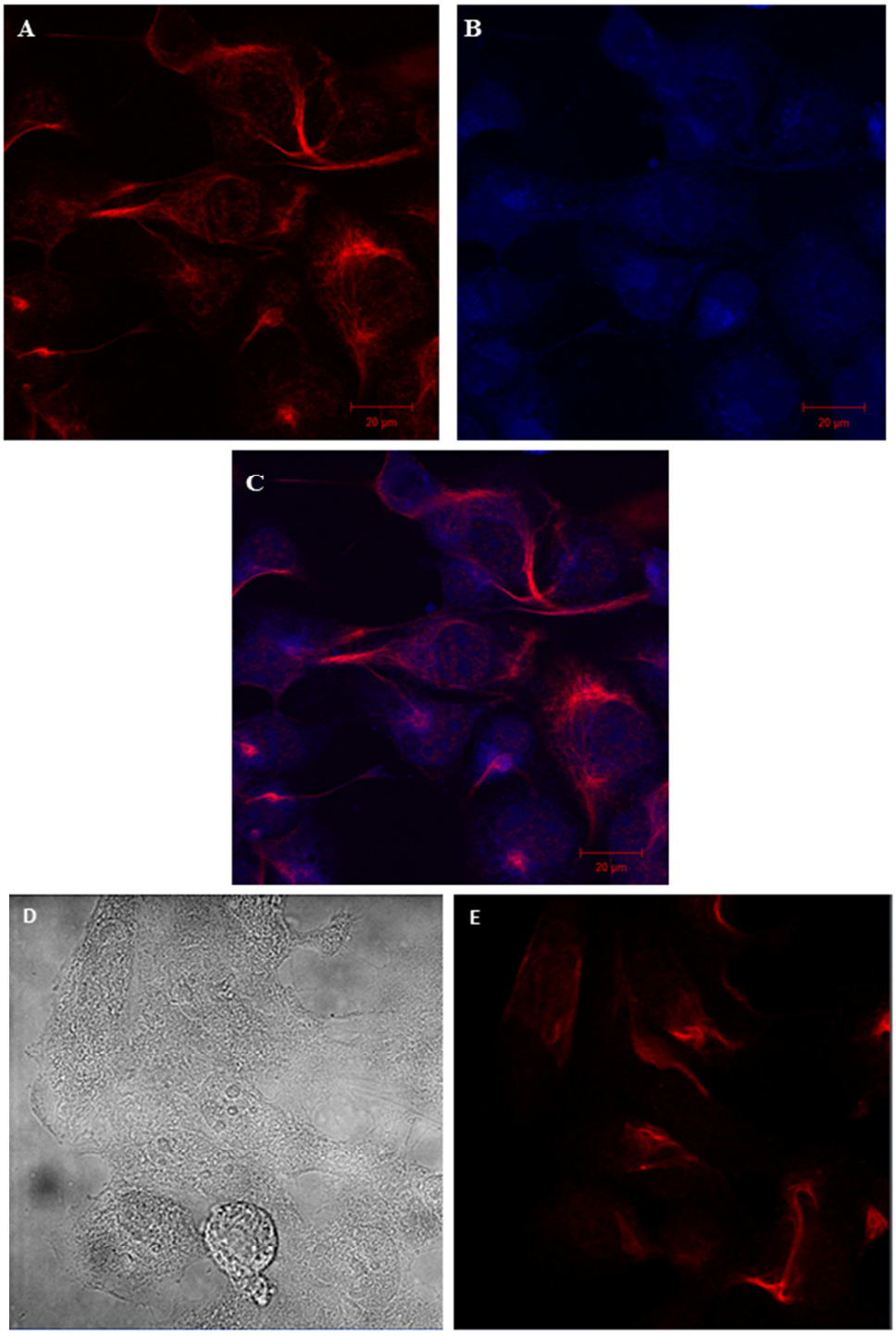

Figure 28: **Effect of DP and Z-Ajoene on Vimentin protein detected by H84 primary polyclonal vimentin antibody in MDA-MB-231 breast cancer cells.**

To determine whether Vimentin and Ajoene co-localize in cancer cells, MDA-MB-231 cells were treated with the fluorescent ajoene analogue (DP). Vimentin filaments were detected with the H84 anti–vimentin antibody and stained red with Cy3. The image of DP–treated cells shows that Vimentin (red channel, **A**) and DP (blue channel, **B**) didn't co-localize (both red and blue channels, **C)** . The image of ZA –treated cells shows that the Vimentin filament is located mainly at the plasma membrane and dispersed in cytoplasm (in red, **E**). (D) The phase contrast to ZA-treated cells is shown. Moreover, both DP and *Z*-ajoene caused structural changes in the Vimentin filaments (**C** and **E**).

To confirm these data, we also analyzed the Vimentin intracellular organization using a primary monoclonal Vimentin antibody V9.
In the untreated control, V9–appeared to detect Vimentin localized to the nuclear membrane but mostly the Intermediate Filaments of cytoskeleton (Fig 29-B). Furthermore, it would seem that the Vimentin localized in the ER is not detected even by V9 antibody, probably the epitope is different and not recognized by this antibody; or the ER –bound Vimentin signal is so weak that it is hidden by their abundant cytoplasmic filaments. What we know is that we have failed to see clearly Vimentin localized in the ER.

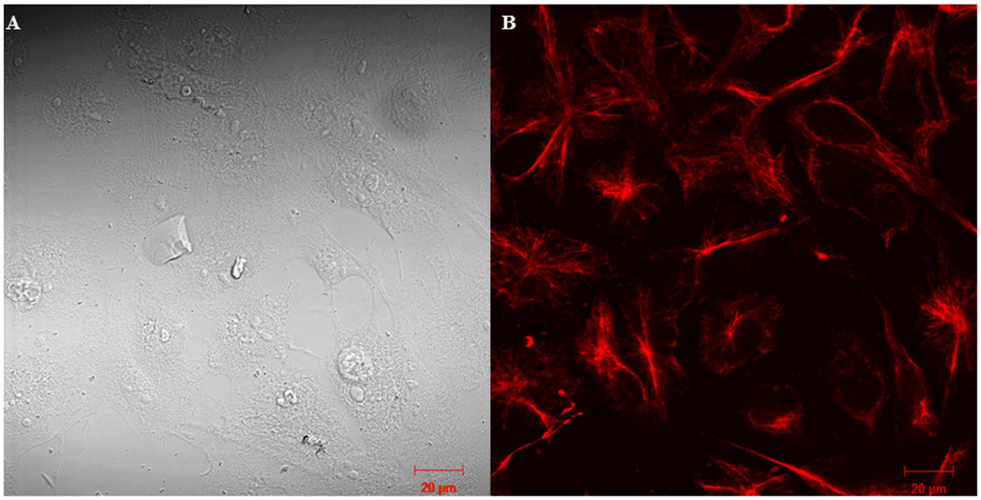

Figure 29: **The intracellular organization of Vimentin detected by the V9 monoclonal antibody.**

To display intracellular organization of Vimentin, untreated MDA-MB-231 cells were subjected to immunofluorescence, where the Vimentin filaments were labelled with the V9 anti–vimentin antibody and labelled red with Cy3. **(B)** Vimentin appeared filamentous and localized in long and branched cytoplasmic filaments and in the nuclear membrane . (**A**) The phase contrast image is shown.

In both DP- and ZA-treated samples, we observed that the intensity of the Vimentin fluorescent signal was reduced, the structures appeared more dispersed, and there was a significant reduction in integrity of the filamentous structures in the cytoplasm (Fig 30-C and -E).

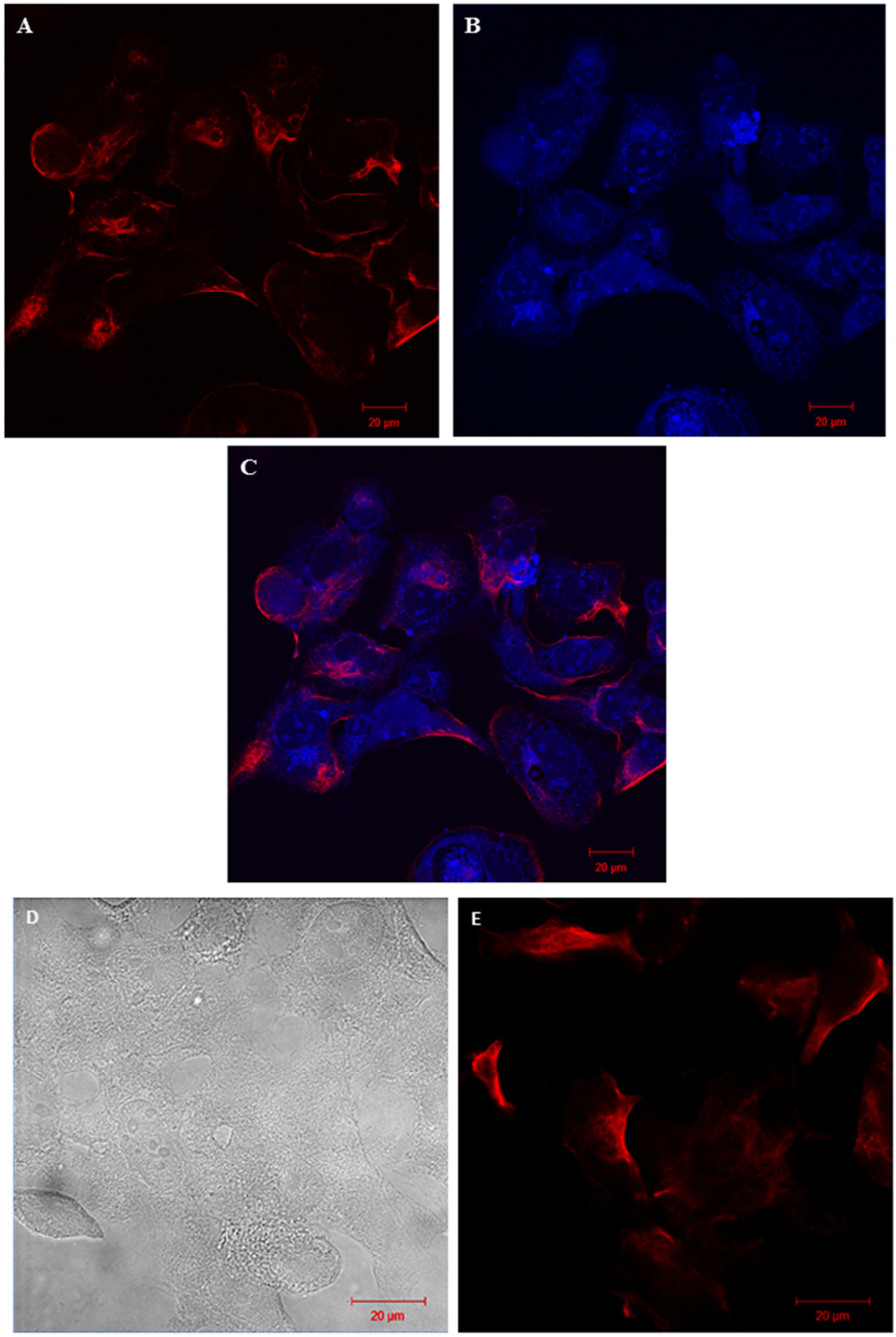

Figure 30: **Effect of Ajoene on Vimentin protein detected by V9 primary monoclonal in MDA-MB-231 breast cancer cells.**

To determine whether Vimentin and Ajoene co-localize in cancer cells, MDA-MB-231 cells were treated with the fluorescent ajoene analogue (DP), and blue fluorescence was detected using immunofluorescence, instead *Z*-ajoene (**D** and **E**) does not emit fluorescence. All samples are also treated with primary vimentin antibody (V9, monoclonal) and the Cy-3 fluorescently-tagged secondary antibody that emitted red fluorescence. The image of DP –treated cells shows that Vimentin (in red, **A**) and DP (in blue, **B**) didn't co-localize (both red and blue channels, **C)**. The image of *Z*A –treated cells shows that a intracellular organization of Vimentin (in red, **E**) was changed and

mainly located at the plasma membrane. (**D**) The phase contrast to *Z*A-treated cells is shown. Moreover, both DP and *Z*-ajoene caused structural changes in the Vimentin filaments (**C** and **E**).

In accordance with disruption of Vimentin structures, we also observed a change in cell morphology where the cells assumed a more rounded shape compared to the physiological dendritic shape, in the presence of ajoene (Figure 31).

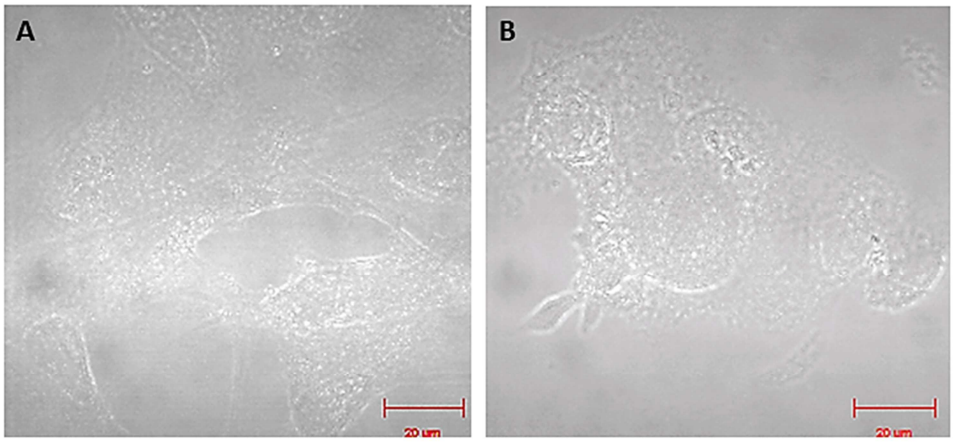

Figure 31: **Change in morphology induced by Ajoene in MDA-MB-231 cells.**
By the confocal microscope, the cell morphology was observed in untreated (**A**) and ajoene-treated (**B**) MDA-MB-231 cells. As shown here, the MDA-MB-231 cells physiologically had a dendritic morphology (**A**), when these cells were treated with 25 µm ajoene assumed a rounded shape (**B**).

In fact, Vimentin plays a major role in the maintenance of strong and stable cell morphology by participating in the formation of intermediate filaments [A. Satelli & S. Li, (2011) Cell Mol Life Sci.], consequently we propose that the disruption of the Vimentin filaments may lead to an alteration of the cytoskeleton and a change in cell morphology.

It is not too surprising that there is not co–localization between DP and Vimentin as we had previously found that DP localizes to the ER and Vimentin is broadly expressed in the cytoplasm where it is a structural protein of intermediate filaments, however it is also found embedded in all membranes and anchored in mitochondria and ER [Katsumoto T. *et al* (1990) *Biol Cell*].
There is only probably a small amount of DP interacting with Vim compared to the overwhelming localization of DP in the ER where it *S*-thiolates the vast majority of its protein targets. It is probably only a small amount of ER –anchored Vimentin which is interacting with DP and *Z*-ajoene and this is sufficient to cause the structural changes that we observe.

Conclusions

We have found that *Z*-ajoene and its analogue DP interact with Vimentin in MDA-MB-231 breast cancer cells. In fact, in MDA-MB-231 cell lysates treated with ajoene were extracted and the dansyl –labeled Vimentin protein was detected. Given that the vast majority of DP or *Z*-ajoene accumulates in the ER, a site where only a small amount of ER –bound Vimentin is present, it is not surprising that drug/protein co-localization experiments gave negative results. However, as it has been indicated by *in vitro* experiments (i.e. proteomics and alkylation assays), *Z*-ajoene/Vimentin interactions do readily occur via a direct binding of *Z*-ajoene with the cysteine 328 of Vimentin. Thus, although only a small amount of the cellular Vimentin is involved in the reaction, it seems sufficient to cause the disruption of Vimentin filaments leading to an alteration of the cytoskeleton and a change in the cell morphology in MDA-MB-231 breast cancer cells.

In conclusion, these data sustain that the cytoskeleton protein Vimentin is unquestionably one of Ajoene targets and indicate that its binding to the protein may play a role in the anti-cancer activity of *Z*-ajoene in MDA-MB-231 human triple-negative breast cancer cells. (Manuscript in preparation)

Chapter III –Studies on the anti-metastatic activity of Z-ajoene

Introduction

Metastasis is the most common cause of death among women with breast cancer. Triple-negative breast cancers (TNBC) comprise approximately 15 % of breast cancers [De Santis C. *et al.*, (2011) Curr. Oncol.].

TNBC is characterized by the absence of the estrogen receptor (ER), progesterone receptor (PR) and lack of overexpression of the human epidermal growth factor receptor 2 (HER2). This breast cancer subtype is responsible for high mortality due to the highly invasiveness and migratory capacity of this cancer. Moreover, there are limited clinical targeted therapies to TNBCs and these cancers frequently develop chemotherapy resistance. Therefore new and effective chemotherapies are needed for this cancer subtype [Wolfe A. R. *et al.,* (2015) Breast Cancer Res Treat].

The breast metastatic phenotype is characterized by elevated expression of mesenchymal markers such as Vimentin and N-cadherin, and decreased expression of epithelial markers such as E-Cadherin (figure 32) [Satelli & Li (2011) Cell Mol Life Sci; C. Foroni *et al.* (2012) Cancer Treatment Reviews]. More specifically, it is reported that the Vimentin protein is over-expressed in metastatic cancers, including that of the breast, and that Vimentin overexpression correlates with an invasive phenotype [Satelli & Li (2011) Cell Mol Life Sci].

This invasive phenotype may in part be directly or indirectly regulated by Vimentin through epithelial-mesenchymal transition (EMT) (Figure 32 and 33). EMT is a cellular reprogramming process in which epithelial cells acquire both invasive and the migratory capacity, that are typical of mesenchymal cells.[Wei J. *et al,* (2008) Anticancer Research].
Vimentin may also act by breaching the basement membrane, and by facilitating dissociation of cells from the original tumor with the invasion into new tissue (See figure 32 and 33).

It is well established that Vimentin knockdown in cancer cell lines inhibits the metastatic phenotype [Vuoriluoto K, *et al.* (2011) Oncogene; D.C.Y. Phua *et al.* (2009) Molecular Biology of the Cell] making Vimentin an attractive therapeutic target. Furthermore, studies have shown that transgenic mice lacking functional Vimentin develop normally suggesting that Vimentin inhibitors may exhibit limited toxicity [Colucci-Guyon *et al* (1994) Cell].

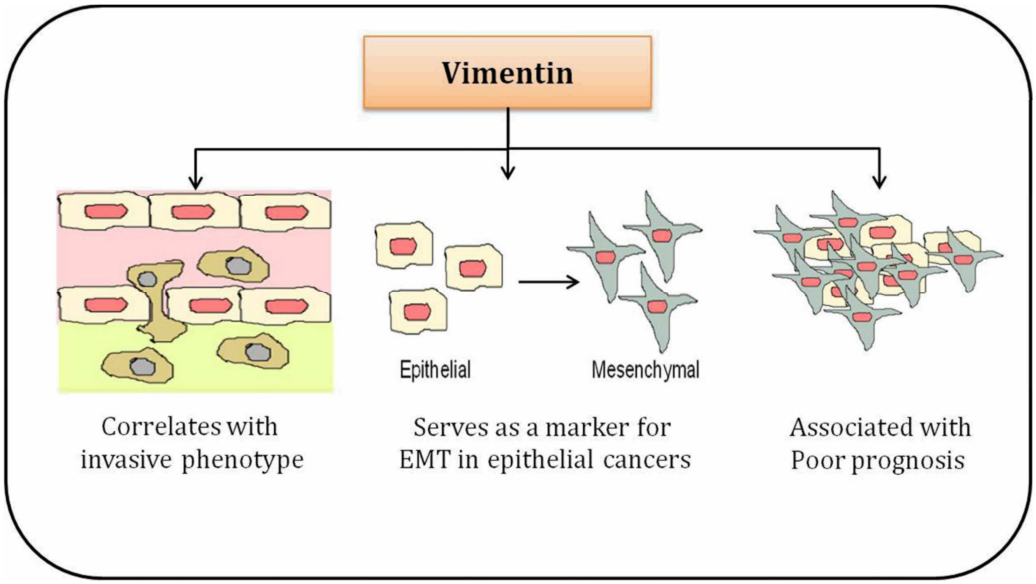

Figure 32: **Vimentin's role in the metastatic process.** [Satelli & Li (2011) Cell Mol Life Sci]

On a signaling level, Vimentin is proposed to play a role in metastasis though a number of pathways. The PI3K/AKT signaling pathway had been shown to be up-regulated in many tumors. In this pathway, AKT1 kinase phosphorylates Vimentin at serine 39, thereby inhibiting caspase-induced proteolysis of Vimentin [M. E. Kidd *et al.* (2014) American Journal of Respiratory Cell and Molecular Biology].

Phosphorylated Vimentin may up-regulate various events involved in EMT. For example, phosphorylated Vimentin has been shown to interact with the 14-3-3 proteins. 14-3-3 proteins are a family of highly conserved proteins which play crucial roles in regulating multiple cellular processes, including cell cycle regulation, DNA repair, apoptosis, cell adhesion, and motility [Liu T-A *et al.* (2013) PLOS ONE]. The interaction of Vimentin with 14-3-3 proteins serve as a cofactor for the inactivation of Raf kinase [G. Tzivion *et al.* (1998) Nature] thus preventing the assembly of the Raf/14-3-3 complex (figure 33, on the left) [G. Tzivion, *et al.* (2000) Journal Biological Chemistry]. This leads to activation of the MEK/ERK signaling pathway and the transcription and expression of genes that involve in the regulation of EMT process (figure 33, on the left).

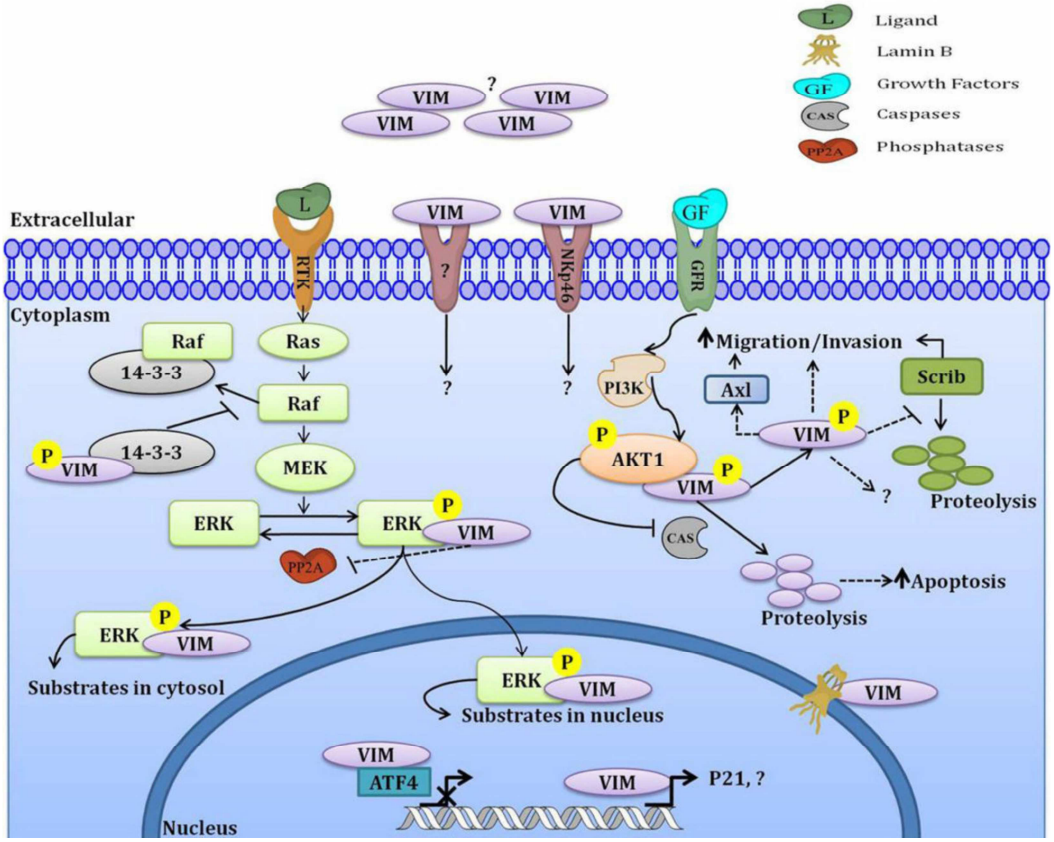

Figure 33: **Role of Vimentin in cell signaling.**

First, AKT1 acts by phosphorylating Vimentin and is thus able to up-regulate several signaling pathways. Then, phosphorylated Vimentin can induce AXL expression to stimulate cell migration (on the right) or bind to 14-3-3 and to prevent the inactivation of Raf kinase and the up-regulation of the MEK / ERK signaling pathways (on the left) [Satelli & Li (2011) Cell Mol Life Sci].

Phosphorylated Vimentin may also promote the EMT modification by regulating Axl expression. It has been demonstrated that Axl expression correlates with motility and invasiveness in breast cancer cells [Zhang YX *et al.* (2008) Cancer research ; X. Wu *et al.* (2014) Oncotarget].

Axl is a TAM receptor which belongs to the subfamily of receptor tyrosine kinases (RTKs) that include Tyro3 and Mer [Y Li et al. (2009) Oncogene]. This receptor is composed of two immunoglobin-like domains and dual fibronectin type III repeats in the extracellular region and a cytoplasmic kinase domain [Y Li *et al.* (2009) Oncogene].

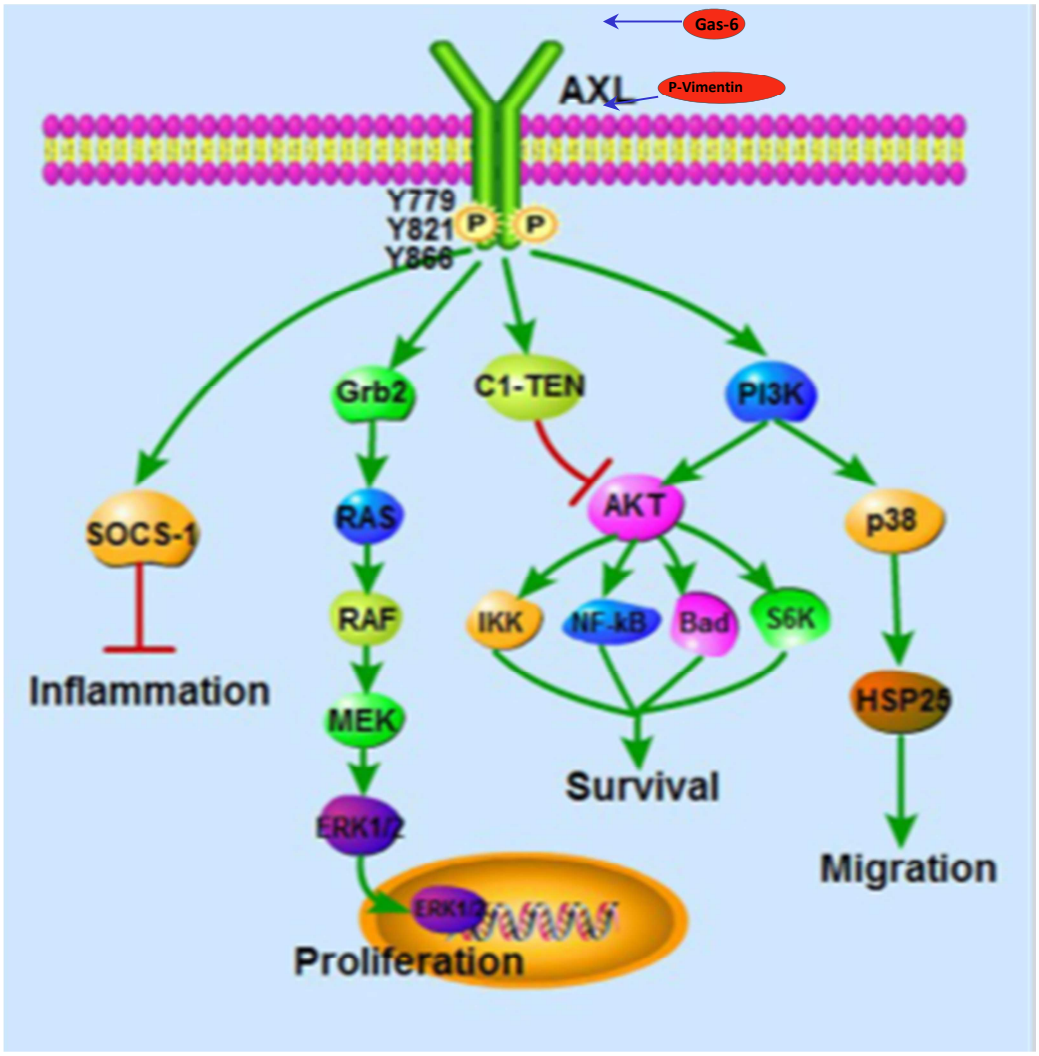

Figure 34: **Axl signaling pathways**.
Axl plays important signaling roles in cell proliferation, survival, migration, and inflammation This figure is adapted from Wu X. *et al*. [Wu X. *et al*. (2014) Oncotarget].

Axl can be activated through a number of different mechanisms, but ligand-dependent dimerization (principally driven by Gas-6) is crucial in the activation of the PI3K/AKT pathway, which is one of the most important signaling pathways involved in the migration of breast cancer (Figure 34) [X. Wu *et al.* (2014) Oncotarget]. In invasive mesenchymal breast cancer cells, Vimentin is reported to play a key role by acting as Axl inducer, which then operates through Slug- and Ras- pathways to cause an increase in cell motility in breast cancer [Vuoriluoto K *et al.* (2011) Oncogene].
Axl activation induces the mesenchymal phenotype by acting simultaneously on multiple signaling pathways according to the type of signal received.

Another possible pathway through which Vimentin may facilitate migration is through the protein kinase Src. Src is another cellular factor that plays a crucial role during tumor development and progression. Src was the first proto-oncogene discovered (normal gene that encodes a protein usually involved in regulation of cell growth or proliferation and that can be mutated in a oncogene by altering its expression) and is a protein kinase involved in numerous cellular signal

transduction pathways (Figure 35). Overexpression and aberrant activation of Src family kinases have been identified in various human tumours, including the breast cancer [Irby RB & Yeatman TJ (2000) Oncogene ; Coluccia AM *et al.* (2006) Cancer Res].

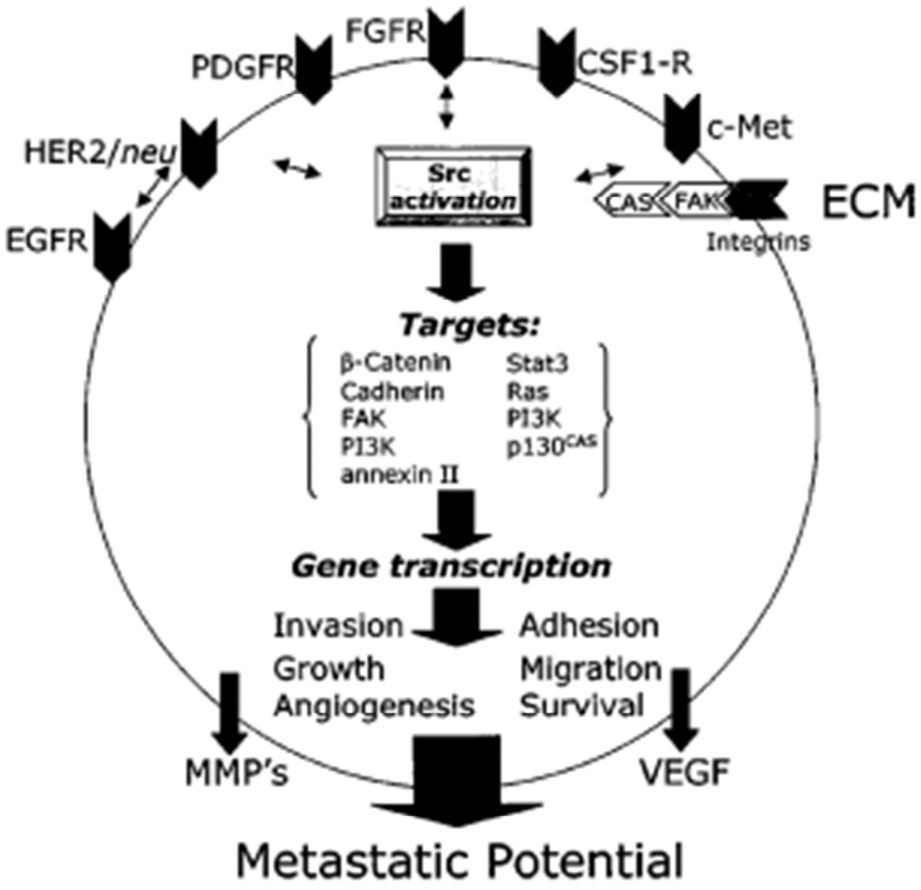

Figure 35: **Src activation promotes cell migration**.
Src activation plays a central role in activating multiple signaling pathways in the induction of metastatic cancer cells [R. B Irby & T. J Yeatman, (2000) Oncogene]

Wei *et a*l have demonstrated that Vimentin and Src kinase are physically linked in human prostate cancer cells, and that this interaction influences the E-cadherin / β-catenin complex which is involved in the formation of cell-cell adherent junctions (Figure 36) [Wei J. *et al*, (2008) Anticancer Research]. Activated Src acts through the phosphorylation of β-catenin at the tyrosine residue 654. This event causes a 6 fold reduction in the affinity of β-catenin to E-cadherin [Roura S. *et al.* (1999) J Biol Chem]. The partial or complete dysfunction of the E-cadherin/β-catenin complex causes decreased stability of cell-cell adherent junctions, the loss of epithelial polarization and the nuclear translocation of β-catenin [Thakur R & Mishra DP (2013) J Cell Mol Med].

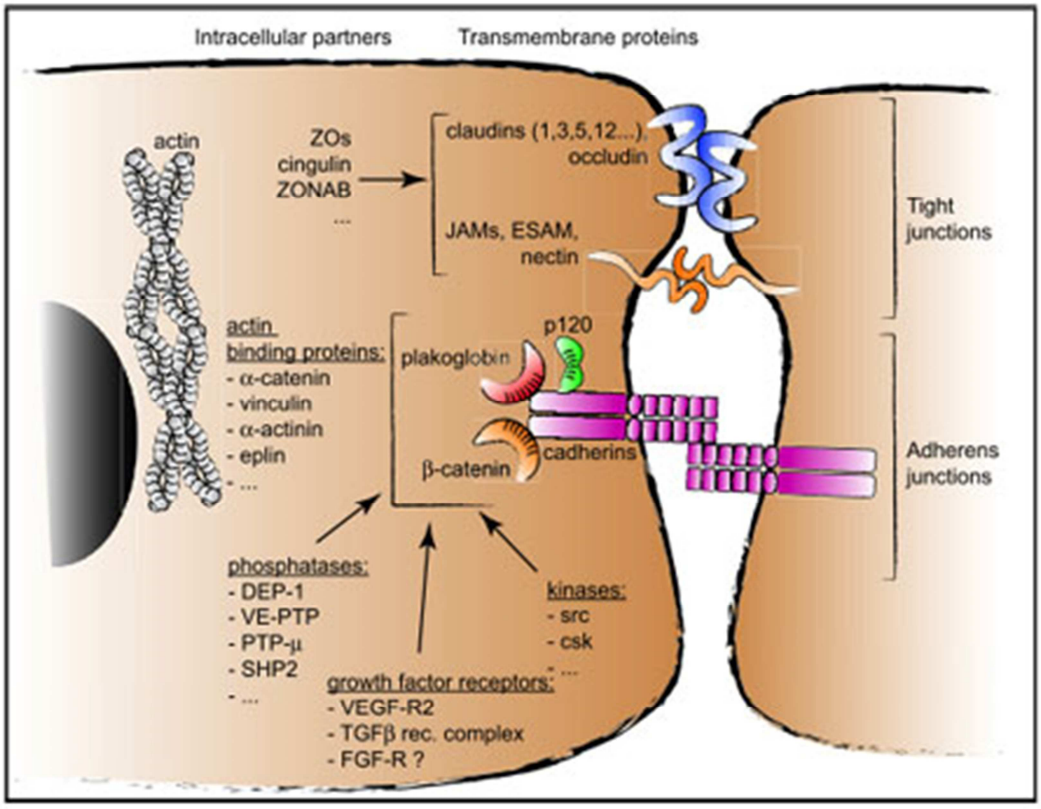

Figure 36: **Schematic representation of the intracellular interactions involved in the formation of cell-cell adherent junctions** [E. Dejana *et al.* (2009) Developmental Cell]

Upon dissociation of β-catenin from E-cadherin, free β-catenin can act as a key signal transducer in the Wnt signaling pathway, which is involved in polarized cell migration and cell-cell adhesion [Nelson & Nusse, (2004) Science].

In the absence of Wnt signaling, cytoplasmic β-catenin is normally recruited by the multiprotein complex, which consists of Axin, APC (product of the tumour suppressor gene adenomatous polyposis coli) and glycogen synthase kinase-3β (GSK-3β). This complex facilitates GSK-3β to induce the hyper-phosphorylation of β-catenin which promotes its ubiquitination and subsequent its degradation via the ubiquitin-proteasome pathway [JC Howard, *et al.* (2003) BMC Musculoskeletal Disorders].

However, in the presence of the Wnt signal, GSK-3β activity is inhibited, leading to the accumulation of β-catenin in the nucleus where it interacts with the Lef/Tcf (lymphoid enhancer factor /T-cell factor) family of transcription factors to activate he β-catenin-mediated gene transcription [Nelson & Nusse, (2004) Science; J. Qi, et al.; (2006) Molecular Biology of the Cell].

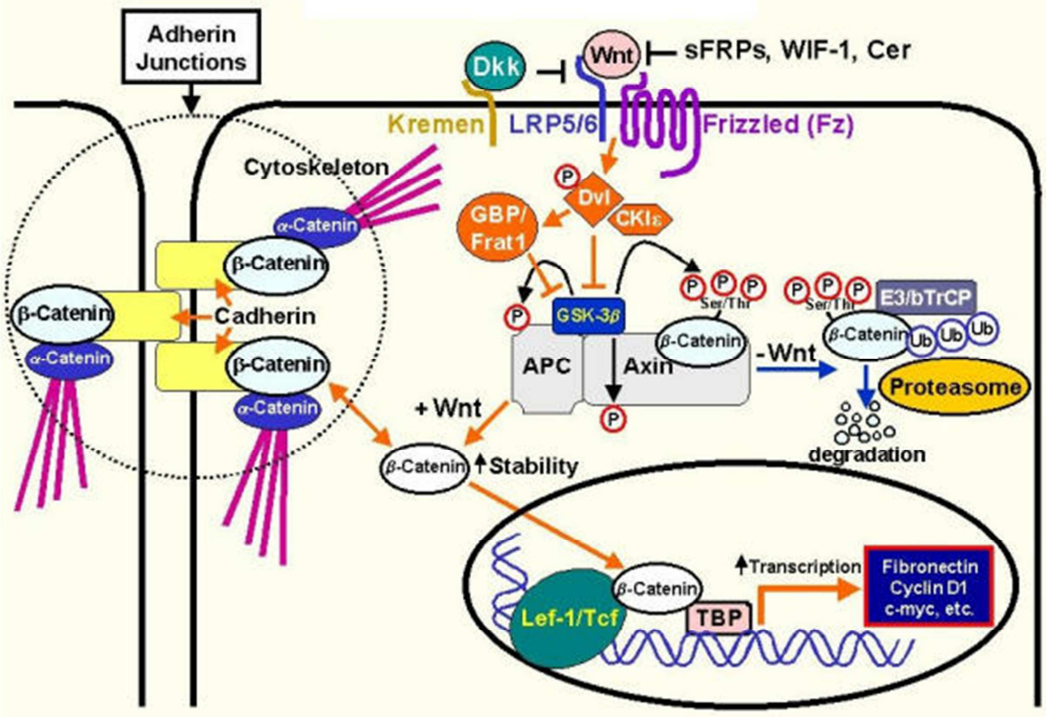

Figure 37: **Canonical Wnt/β-catenin pathway.**
β-catenin is a component of cell-cell adherent junctions with E-Cadherin, and a key signaling factor in the Wnt pathway. [J. Qi *et al.* (2006) Molecular Biology of the Cell]

There are literature reports that several organosulfur compounds extracted from garlic, are effective at inhibiting metastases. These include Diallyl disulfide (DADS) [Xiao *et al.*, (2014) Plos one; Huang *et al*, (2015) Mol Nutr Food Res], *S*-allylmercaptocysteine (SAMC) [Howard *et al*, (2007) Clin Cancer Res] Diallyl trisulfide (DATS) and ajoene [J. Huang *et al.* (2015) Mol. Nutr. Food Res].

Interestingly, Huang et al. are the first and the only ones reporting that DADS causes a dose-dependent decrease in Vimentin protein levels in human triple-negative breast cancer [Huang *et al*, (2015) Mol Nutr Food Res].

Both DADS [Xiao *et al*, (2014) Plos one] and DATS [K-C Lai *et al.* (2015) J. Cell. Mol. Med] were found to decrease Src expression in human triple-negative breast cancer and in human colon cancer, respectively.

The β -catenin pathway was down –regulated by DADS in a dose– and time–dependent manner, increasing E–cadherin expression and decreasing levels of free β–catenin [Huang *et al*, (2015) Mol Nutr Food Res]. In agreement with these findings, SAMS was found to suppress the metastatic phenotype via the up –regulation of E–cadherin, increasing the cell-cell adherent junctions [Howard *et al*, (2007) Clin Cancer Res].

Ajoene inhibit both primary tumor growth and metastasis of B16/BL6 melanoma cells in C57BL/6 mice [Taylor P. *et al.* (2006) Cancer Letters], but there are no studies that identify the signaling pathways involved in this inhibition.

Therefore, there are no studies linking the antimetastatic potential of garlic compounds to Vimentin, although some of the downstream signaling pathways of Vimentin have been identified (i.e. Axl, Src, β-Catenin / E-cadherin complex). Thus, seen the involvement of Vimentin in the regulation of these proteins, it is very likely that Vimentin has been strongly implicated in metastasis. Since we found that ajoene targets Vimentin and causes structural changes to the filaments, we decided to test whether ajoene itself can inhibit the migratory capacity in invasive breast cancer cells, and which signaling pathways are involved.

Results and Discussion

3.1 *Z*-Ajoene inhibits cell migration in the MDA-MB-231 invasive breast cancer cell line

Since elevated concentrations of *Z*-ajoene induce apoptosis in cancer cells, it was important for us to find a lower non-cytotoxic concentration for studies on the anti – metastatic activity of *Z*-ajoene in MDA-MB-231 cells. In previous experiments, we found that at the 6 h timepoint, 25µM *Z*-ajoene was not cytotoxic to MDA-MB-231 cells, , but we had the need to treat the cells for 24 h, which represent the timepoint for the wound healing assay. We therefore performed an MTT cell viability assay prior to testing for anti-metastatic activity by the wound healing assay. We tested the cell viability of MDA-MB-231 cells following treatment with three different concentrations of *Z*-ajoene, namely 5, 10 and 20 µM of *Z*-ajoene for 24 hours. We found that *Z*-ajoene at 5 µM and 10 µM was not cytotoxic to MDA-MB-231 cells (Figure 38), in which the percentage of cell viability compared to the negative control (untreated with 1% FBS) was found to be 108 and 98 % respectively; while 20 µM *Z*-ajoene for 24h displayed a small cytotoxic effect (83 %), although this was not significant.

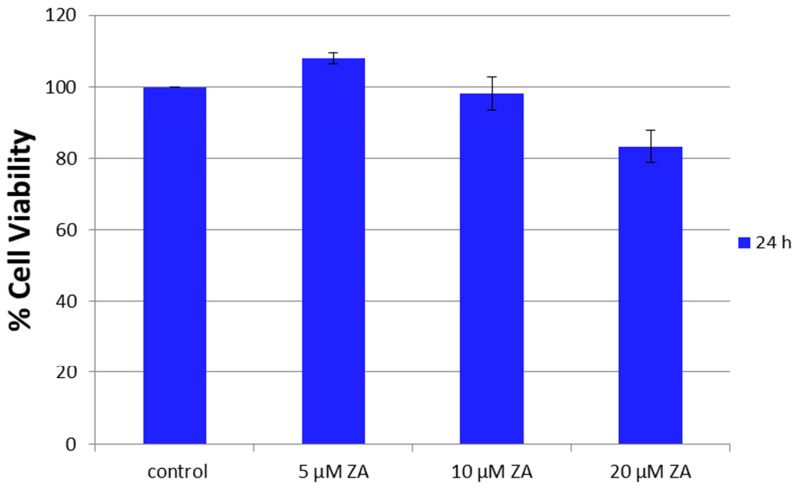

Figure 38: **Cytotoxicity of *Z*-Ajoene in MDA-MB-231 breast cancer cells after 24h treatment**
MDA-MB-231 cells were exposed to different concentrations of *Z*-ajoene (in medium with 1% FBS) for 24 h under the same experimental conditions as that of the wound healing assay, and cell viability was evaluated by the MTT assay. Control cells received 1% FBS and 0.1 % DMSO alone.

Data is presented as a percentage of the mean ± SD of three independent experiments vs. untreated control (1% FBS).

We then assessed the effect of *Z*-ajoene (5, 10 and 20 µM) on cell migration in MDA-MB-231 cells (Figure 39). Due to the highly invasive nature of breast cancers, we investigated the effect of *Z*-ajoene on the motility of MDA-MB-231 cells *in vitro* using a wound healing assay.

Briefly, MDA-MB-231 cells were seeded in a six-well plate and allowed to attach overnight. The following day a wound was introduced in the presence of different concentrations of *Z*-ajoene (5, 10 and 20 µM) in 1% FBS. We also prepared two different untreated controls: one containing only 1% FBS (negative control) to detect the physiological wound closure in the absence of chemotactic agents; and the other containing 10% FBS (positive control) to stimulate complete closure of the wound in the presence of a chemoattractant. It was also important to track the same wound region as a function of time. To allow easy detection of these zones, lines perpendicular to the wound were marked on the bottom of each well. Each of these zones were then photographed at timepoints 0 and 24 h, and free area was quantified by ImageJ software at both time points. The area quantification of each zone was processed by applying the following formula:

$$\%\ Area\ Reduction = \frac{t_{24}\ Area}{t_0\ \ Area} * 100$$

where a higher value indicates lower migration ability.

To greater emphasize the migratory ability, data is also represented in terms of a migration distance ratio using the following formula:

$$Migration\ Distance\ Ratio = 100 - \%\ Area\ Reduction$$

where a higher value indicates a greater migration ability.

After 24 hours, we found that the wound was completely closed in the positive control, while the negative control (no chemotactic agent added) only migrated by 65 %. Cells treated with *Z*-ajoene + 1 % FBS showed reduced migration in a dose-dependent manner. *Z*-ajoene (5 µM) treatment caused reduced migration by 51 % in MDA-MB-231 cells when compared to the complete wound closure (positive control) (Figure 39), but we do not believe that this concentration was particularly effective, although the data are significant (** p value < 0.01), because it was near to the physiological closure of the negative control (65 % respect to the complete wound closure). However, 10 µM and 20 µM *Z*-ajoene caused a greater inhibition, in which the wounds only healed 30 % and 22 % respectively, when compared to the positive control (Figure 39) and the data are convincingly significant (*** p value < 0.001) versus negative control (1% FBS).

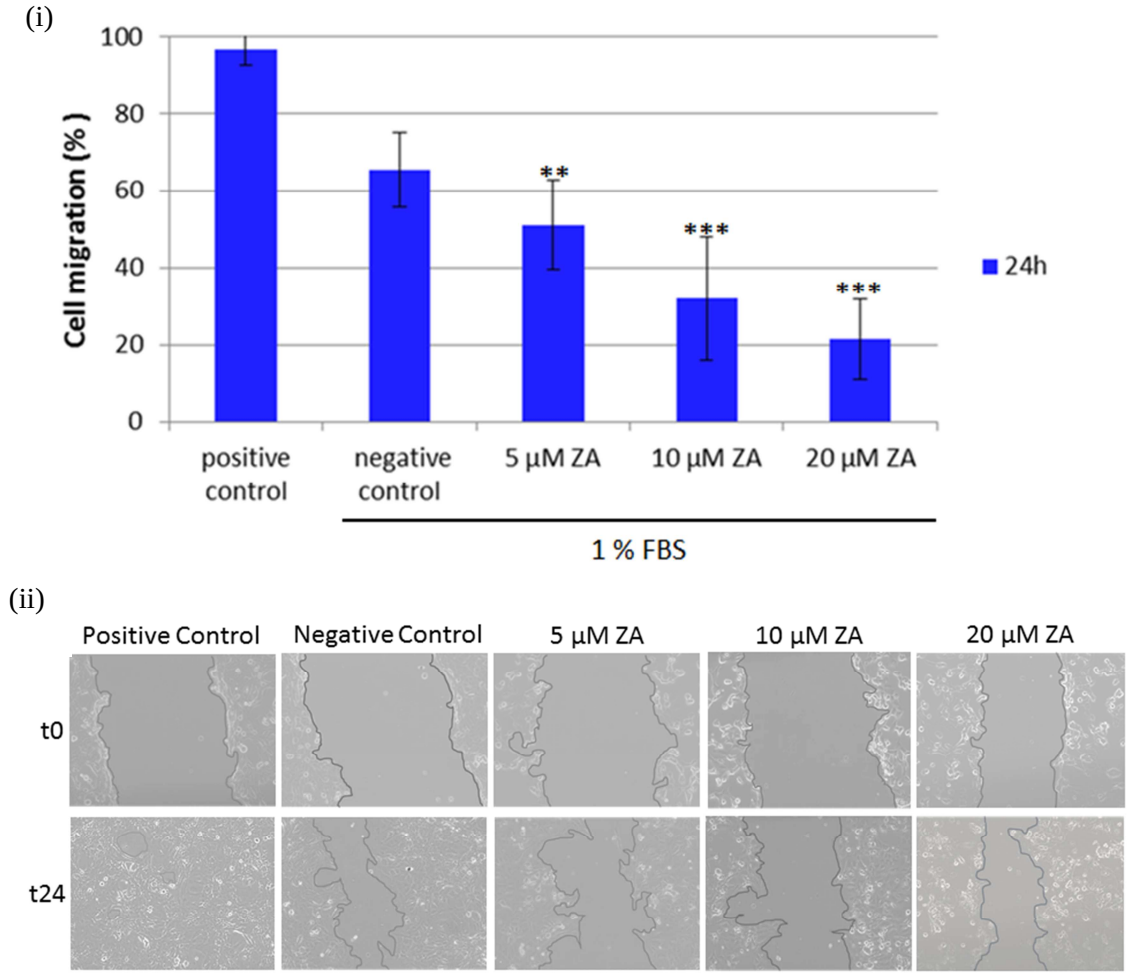

Figure 39: **Dose–dependent effect of Z-Ajoene on migration in the MDA-MB-231 human triple negative breast cancer cell line.**

A wound is introduced into a 90% confluent monolayer of MDA-MB-231 cells followed by addition of different concentrations of Z-ajoene (5, 10 and 20 µM) in 0.1% DMSO and 1% FBS. The negative (1% FBS) and positive (10% FBS) controls were performed. After 24 hours, the wounded areas is photographed by phase-contrast microscopy using an inverted microscope (Olympus CKH41) (ii) in three different regions to assess wound closure and quantified by ImageJ software (i). Data represents triplicate determinations of a single experiment which was repeated in duplicate. ** $p < 0.01$ and *** $p < 0.001$ vs. untreated *Z*-Ajoene (negative control, 1% FBS).

Z-ajoene appears to be inhibiting migration in a dose-dependent manner however we preferred to use a concentration of 10 µM *Z*-ajoene as this was convincingly shown to not cause any cytotoxicity.

We therefore performed a wound healing assay in which the control produced marked cell migration, characterized by a physiological closure of 45% compared to the 10% FBS sample, in which the wound area was completely closed after 24 h (Figure 40). Wounds exposed to 10 µM *Z*-Ajoene in medium with 1% FBS showed significant delays in healing (Figure 40 (ii)). Specifically, as indicated by the quantitative analyses (Figure 40 (i)), exposure to 10 µM *Z*-Ajoene for 24 h inhibits cell migration by 67% compared to the untreated control (negative) and the data are highly significant (***$p < 0.001$).

(i)

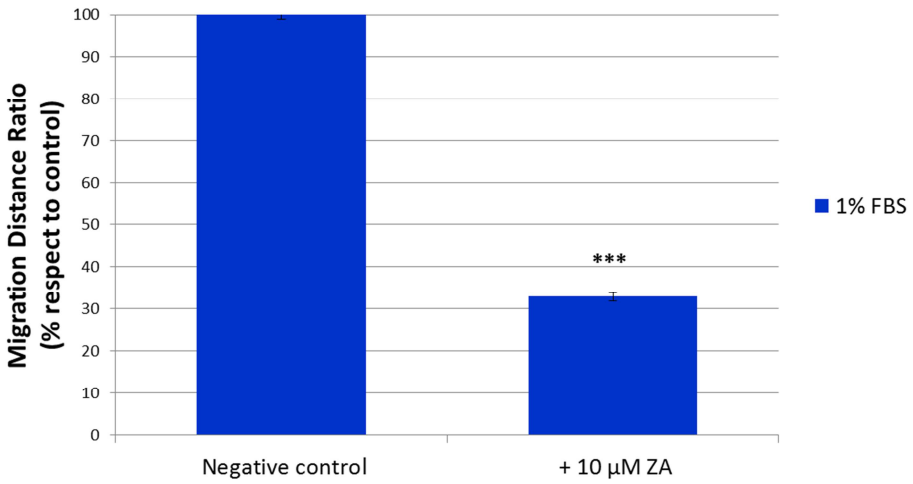

(ii)

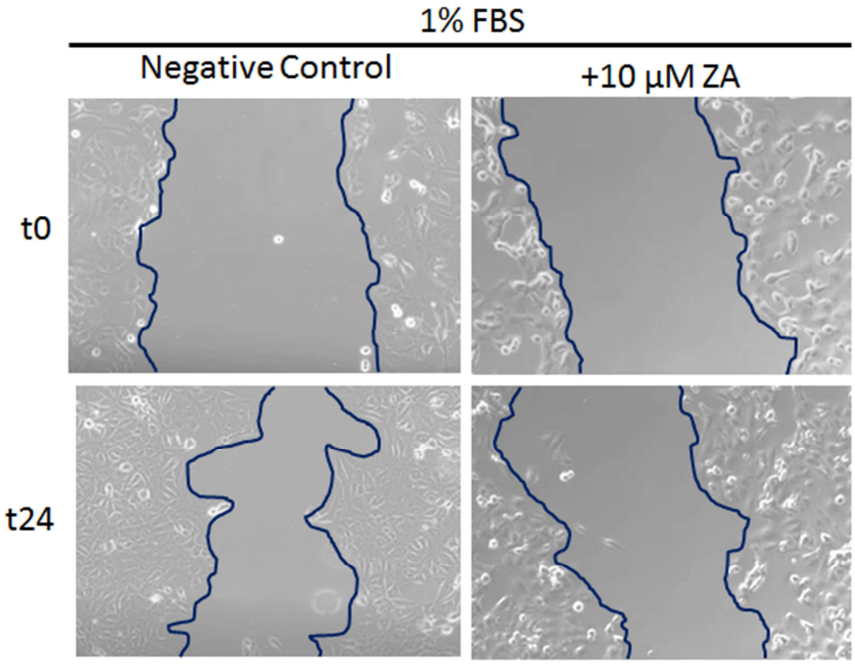

Figure 40: **Effect of *Z*-Ajoene on migration of human breast cancer cells in the presence of 1 % FBS.**

For the wound healing assay, MDA-MB-231 cells were seeded and allowed to attach overnight. A vertical wound was created into a 90% confluent monolayer. The cells were exposed to 10 µM *Z*-Ajoene for 24 h with 1% FBS. After 24 hours, the wounded areas were recorded by phase-contrast microscopy using an inverted microscope (Olympus CKH41) and were photographed (ii) in six different regions to assess wound closure and quantified by ImageJ software (i). Quantitative assessment of wound reduction is expressed as the percentages of mean ± SD of three independent experiments. ***$p < 0.001$ vs. untreated *Z*-Ajoene (control, 1% FBS). Assays were carried out in triplicate but the one displayed above is that of a single experiment (Figure 39).

We then investigated whether 10 µM *Z*-ajoene caused an inhibitory effect in the presence of a chemotactic agent that stimulates both proliferation and migration (Figure 41). Thus, MDA-MB-231 cells were treated with 10 µM *Z*-ajoene in the presence of 10% FBS for 24 h. We found that wounds exposed to 10 µM *Z*-ajoene showed reduced healing in breast cancer cells. Quantitative analysis showed that *Z*-Ajoene inhibits cell migration by 40% compared to the untreated control (positive) and that the data are highly significant (*** p<0.001).

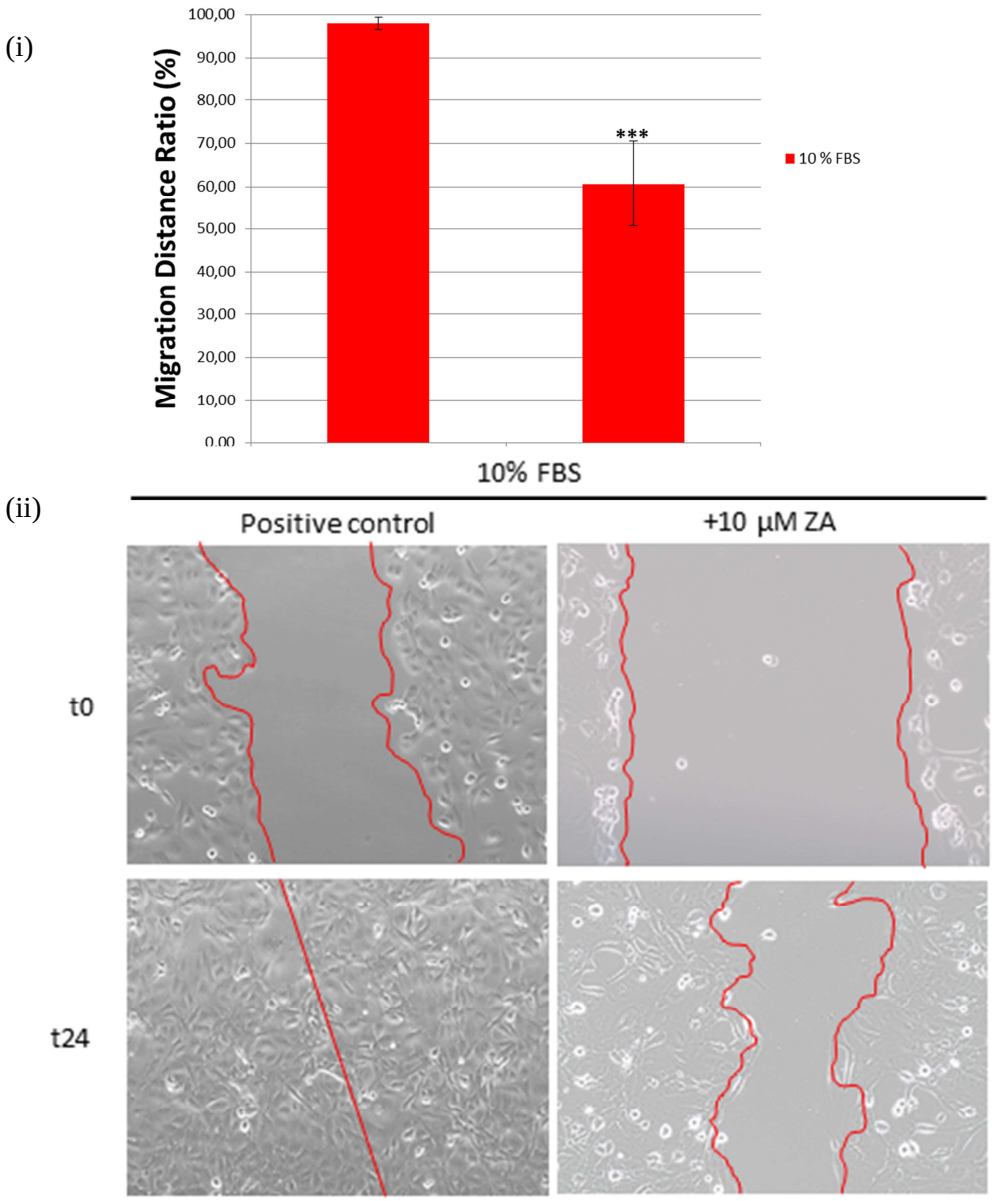

Figure 41: **Effect of Z-Ajoene on migration of human breast cancer cells in the presence of 10% FBS.**

The wound healing assay was performed as described before. MDA-MB-231 cells were exposed to 10 µM *Z*-Ajoene for 24 h, but in the presence of the chemoattractant (10 % FBS). The wounded areas were quantified by phase-contrast microscopy using an inverted microscope (Olympus CKH41) and (ii) were photographed in six different regions at designated times to assess wound closure and quantified by ImageJ software (i). Quantitative assessment of wound reduction is displayed as the percentages of mean ± SD of two independent experiments. ***p < 0.001 vs. untreated *Z*-Ajoene (positive control, 10 % FBS). Assays were carried out in duplicate but the one displayed above is that of a single experiment (Fig. 39).

These results have shown that at non-cytotoxic concentrations, *Z*-Ajoene effectively inhibits the migration of the highly invasive breast cell line MDA-MB-231 both in the presence and absence of a chemotactic agents, but the best effect induced by 10µM *Z*-ajoene is the one we observed in the absence of chemoattractant agent, where there is an inhibition of the cell migration equal to 70%.

Although 10 µM *Z*-ajoene is not cytotoxic in MDA-MB-231 after 24 hours, we found that the *Z*-ajoene –treated cells were beginning to assume a bit rounded morphology. This cell morphological change, as we have demonstrated before, is caused by the disruption of the Vimentin filaments and the consequent rearrangement of the cytoskeleton. Thus, we supposed that Vimentin protein play a key role in the cell migration of MDA-MB-231 breast cancer cells.

3.2 *Z*-ajoene stimulates Vimentin expression in MDA-MB-231 breast cancer cells

It is reported that Vimentin plays an important role in metastasis, and that its overexpression is involved in the increased motility and invasiveness in breast cancer. [Korsching E, *et al.* J Pathol. (2005); A. Satelli & S. Li (2011) Cell Mol Life Sci].

We have shown that *Z*-ajoene interacts directly with Vimentin by forming a mixed disulfide with Cys328 and that *Z*-ajoene causes disorganization of the Vimentin filaments in MDA-MB-231 breast cancer cells. We therefore hypothesize that binding of *Z*-ajoene to Vimentin may cause a structural change in the protein which may affect the ability of these cells to migrate. In order to test this hypothesis, we investigated the effect of *Z*-Ajoene on Vimentin and some of its downstream targets involved in metastasis.

We therefore silenced the expression of Vimentin protein in MDA-MB-231 cells to see whether removal of the protein has a similar effect to treating with *Z*-ajoene. MDA-MB-231 cells were therefore plated and allowed to attach overnight. The following day, cells were transiently transfected with two different concentrations (50 or 100 nM) of Vimentin SiRNA. After 6 h, media containing the transfection mixture was replaced with fresh culture media and the cells were incubated for 24, 48 or 72 h. Cells were then lysed and the lysate subjected to Western blot analysis.

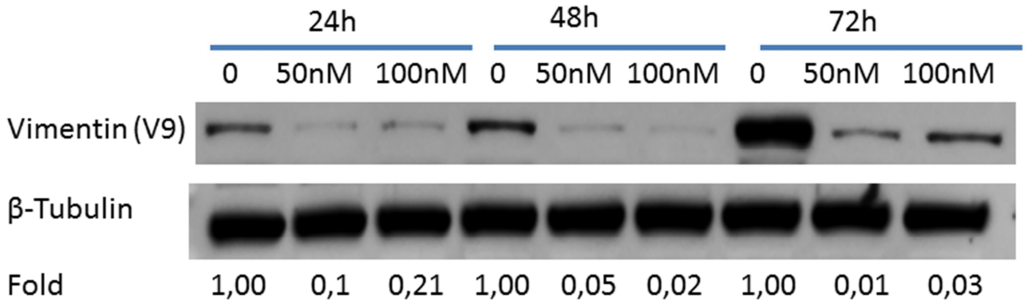

Figure 42: **Silencing of Vimentin in MDA-MB-231 cells.**
Cells were incubated for 6 hours with 50 or 100 nM SiRNA diluted in Lipofectamine® RNAi MAX Reagent. Thereafter, the media was replaced and the cells were incubated for 24, 48 and 72h. Cells were then lysed and subjected to Western blot analysis using the antibodies indicated. β-Tubulin was used as an internal loading control. The data are presented as the fold change compared to the untreated group.

As shown in Figure 42, the Vimentin expression is inhibited after 24 hours of treatment at both the 50 and 100 nM concentrations of SiRNA with little inhibition exhibited at 72 hours. Maximal inhibition was obtained at 48 h using 100 nM SiRNA and therefore these conditions were selected for future experiments involving Vimentin knockdown.

Next, we investigated the effect of *Z*-ajoene on Vimentin expression in the triple-negative breast cancer cell line MDA-MB-231. Briefly, MDA-MB-231 cells were seeded and allowed to attach overnight. The following day, cells were incubated with 10 µM *Z*-ajoene for time points up to 24 h. After treatment, cells were lysed and subjected to Western blot analysis for detection of the Vimentin protein.
We found that *Z*-ajoene induced an up-regulation of Vimentin in a time-dependent manner. In fact, Vimentin expression was found to increase in *Z*-Ajoene-treated cells between 6 and 24 h with the maximal effect at 24 h, in which the levels were found to increase three fold relative to the untreated control (Figure 43).

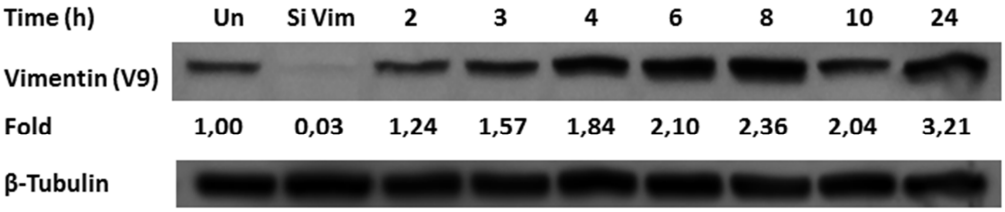

Figure 43: **Effect of *Z*-Ajoene on Vimentin expression on MDA-MB-231 cells**.
MDA-MB-231 cells were incubated with 10 µM *Z*-Ajoene up to 24 h. After treatment, cells were lysed and subjected to Western blot analysis using the antibodies indicated. Silenced Vimentin (SiVim; 100 nM SiRNA after 48h) was used as a knock-down Vimentin. β-Tubulin was used as an internal loading control. The blots shown are representative of two independent experiments. The data are presented as the fold change compared to the untreated group.

We previously found that ajoene compounds affect the ability of the Vimentin protein to perform its proper function. It may be possible therefore that the cell may compensate for this deficiency by synthesizing more protein.

3.3 *Z*-ajoene reduces the expression of Axl in MDA-MB-231 cells

It is well established that Axl expression is correlated with the motility and invasiveness of breast cancer cells [X. Wu *et al.* (2014) Oncotarget.; Zhang YX *et al.* (2008) Cancer research]. In a study by K. Vuoriluoto *et al*, it was found that the Vimentin plays a key role in cell migration induced by AXL, acting as its enhancer. [Vuoriluoto K *et al*. (2011) Oncogene.; V. A. Korshunov *(*2012) Clin Sci; A. Satelli & S. Li (2011) Cell Mol Life Sci].
We hypothesize that *Z*-ajoene may covalently bind to Vimentin and therefore affect its ability to properly function in the metastasis process which may be through Axl.

We decided to use a concentration of 10 µM *Z*-Ajoene which we had previously shown to be non-toxic to MDA-MB-231 cells up to 24 h.
We found by Western blot analysis that in the MDA-MB-231 cell line, Axl expression was downregulated by 10 µM *Z*-ajoene at 10 and 24 h by 2 and 4 fold respectively (Figure 44), and this result was observed in duplicate experiments .

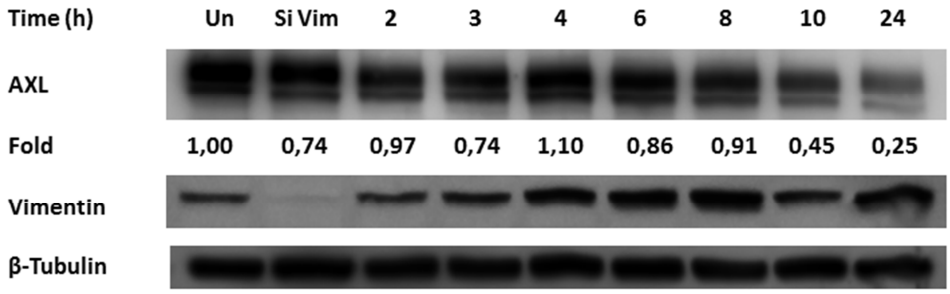

Figure 44: **Effect of *Z*-ajoene on Axl expression in MDA-MB-231 cells**.
MDA-MB-231 cells were incubated with 10 µM *Z*-ajoene for time points up to 24 h. After treatment, cells were lysed and subjected to Western blot analysis using the antibodies indicated. SiVim (100 nM SiRNA after 48h) was used as a knock-down the Vimentin protein. β-Tubulin was used as an internal loading control. The blots shown are representative of two independent experiments. The data are presented as the fold change compared to the untreated group.

It is reported that Axl is activated by phosphatidylinositol 3-kinase [Hafizi S. & Dahlbäck B. (2006) FEBS Journal], and that Vimentin participates in this process by upregulating Axl [Korshunov V. A. (2012) Clin Sci]. Contrary to the report by Vuoriluoto *et al* [*Oncogene 2011*], we found that the Vimentin depletion did not significantly affect the expression of Axl in Vimentin-silenced MDA-MB-231 cells (Figure 44). Vuoriluoto *et al* used the same cell line and found that Axl expression was inhibited by 56 % in MDA-MB-231 cells lacking the Vimentin protein. However in our study at 48h post transfection we did not see any change in the Axl levels although it was not specified in the article the timepoint the authors used. We did not look at other timepoints to rule out the lack of an effect in our experiment.
Importantly we found that *Z*-ajoene reduces the expression of Axl. This link between a garlic compound and Axl expression has not been observed before and is a novel result which may play an important role in metastasis inhibition in breast cancer cells. But the mechanism by which ajoene induces down–expression of Axl is not yet clear and will be the subject of future investigations, we supposed that the down-expression of Axl may affect the PI3K pathway, wich is involve in the EMT process.

3.4 *Z*-ajoene reduces the expression of Src in MDA-MB-231 cells

Src is a signal–transducing protein kinase that plays an important role in the control of cell growth and differentiation. The alteration of expression and aberrant activation of kinases such as Src is involved in tumor progression [Irby RB & Yeatman TJ (2000) Oncogene; Coluccia AM. *et al.* (2006) Cancer Res; Wei *et al*; (2008) Anticancer Research]
Damiano *et al.* reported that Src regulates the motility in breast and colon cancer cells by affecting the Ras/ERK signaling pathway [Damiano L *et al*. (2010) Oncogene]. In another paper, Wei *et al* demonstrated that Vimentin stimulates tumor cell invasiveness by regulating the E-cadherin/β-catenin complex via Src in prostate cancer cells [Wei *et al*; (2008) Anticancer Research]. There therefore appears to be a link between Vimentin and Src in the progression of metastasis. We performed Western blot analyses to determine whether a non-cytotoxic concentration of *Z*-ajoene (10 µM) affects the expression of Src in MDA-MB-231 cells. This analysis revealed that in the MDA-MB-231 cell line, *Z*-ajoene induced

down-regulation of Src protein in a time –dependent manner. In fact, cells treated with *Z*-ajoene showed a reduction in Src expression from 6 - 24 h with the maximal effect at 24 h (Figure 45).

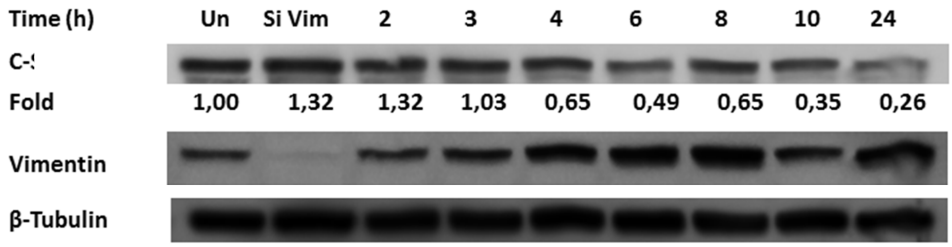

Figure 45: **Effect of *Z*-ajoene on Src expression in MDA-MB-231 cells.**
MDA-MB-231 cells were incubated with 10 µM *Z*-ajoene for various time points up to 24 h. After treatment, cells were lysed and subjected to Western blot analysis using the antibodies indicated. SiVim (100 nM SiRNA after 48 h) was used as a knock-down the Vimentin protein. β-Tubulin was used as an internal loading control. The blots shown are representative of two independent experiments. The data are presented as the fold change versus the ZA untreated group.

Interestingly, and contrary to literature reports [Wei *et al* (2008) Anticancer Research], we found that silencing of Vimentin protein did not affect the expression of Src in MDA-MB-231 breast cancer cells. Instead, Wei *et al*. found that the silencing of Vimentin protein caused a reduction of Src expression in the antisense-Vimentin transfected prostate cancer cells 1E8-H. The origin of these conflicting data could be caused by the diversity of cell lines, in our case of a breast cancer cell line while they were using prostate cancer cells. Moreover, the silencing procedure was also different, because while they used an antisense–oligonucleotides transfection, in our experiment we used SiRNA transfection in the MDA-MB-231 breast cancer cell line which did not show any reduction in Src expression following 48h.
We did find however that *Z*-ajoene, like other garlic compounds (DADS & DATS), reduces the expression of Src, which may play a role in its anti-metastatic activity in MDA-MB-231 breast cancer cells. As mentioned before, Src acts by activating β-catenin and PI3K pathways. Thus, down-expression of Src probably inhibits both β-catenin and PI3K pathways, blocking the Epitelial-Mesenchymal transition process signals and at last the metastasis in MDA-MB-231 breast cancer cells.

3.5 *Z*-Ajoene may influence the β-Catenin / E-Cadherin pathway in MDA-MB-231 cells.

Alteration of the β-catenin signaling pathway is involved in the development and progression of various cancers including that of the breast [Huang. *et al.* (2015) Mol. Nutr. Food]. Huang *et al* reported that DADS inhibits activation of the β-catenin pathway, in both MDA-MB-231 and BT-549 cell lines, in both a dose- and time-dependent manner [Huang. *et al.* (2015) Mol. Nutr. Food].
Thus, we analyzed lysates of MDA-MB-231 cells by western blot to evaluate whether *Z*-ajoene affects the β-catenin/ E-Cadherin complex.
As shown in the figure 46, *Z*-Ajoene was not found to significantly influence the levels of β-Catenin/E-Cadherin complex during the first 10 hours of treatment, the initial phase of the metastatic process. Between 10 – 24 h a small reduction in

phospho-β-catenin expression was found with expression levels around 30-40% of the control. Contrary to the literature [Wei *et al.* (2008) Anticancer Research], in the Vimentin knock-down sample, levels of phospho-β-Catenin similar to untreated control were observed.

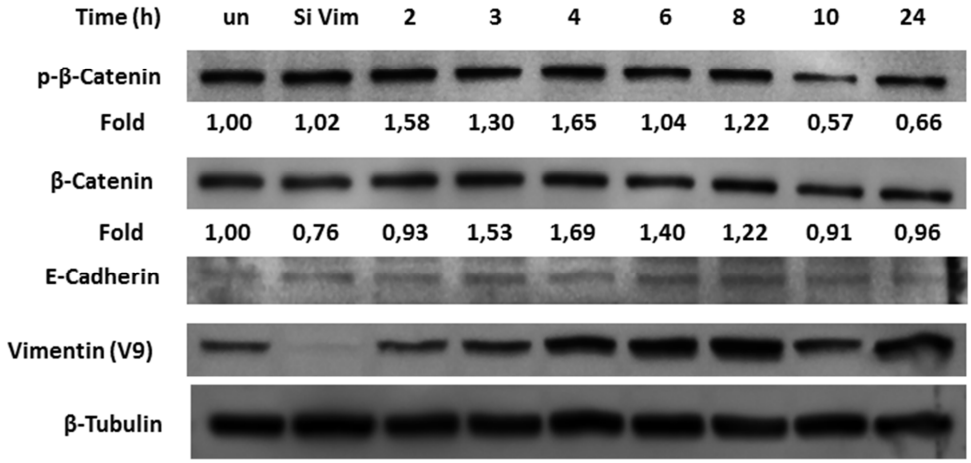

Figure 46: **Effect of *Z*-ajoene on the β-Catenin/E-Cadherin signaling pathway**.
MDA-MB-231 cells were incubated with *Z*-ajoene for time points up to 24 h. After treatment, cells were lysed and subjected to Western blot analysis using the antibodies indicated. β-Tubulin was used as an internal loading control. SiVim (100 nM SiRNA after 48 h) was used as to knock-down the Vimentin protein. The blots shown are representative of two independent experiments. The data are presented as the fold change versus untreated group.

Wei *et al* used 1E8-H prostate cancer cells, whose Vimentin was silenced by antisense –oligonucleotides transfection. Similar to our results for the Src protein, it may be a combination of both the cell line and the silencing procedure which could give rise to the conflicting results. However in our experiment, the total lack of Vimentin, obtained after 48 h the SiRNA transfection, did not affect the phospho-β-catenin levels.
We did find however that *Z*-ajoene, like garlic DADS compound, modestly affected the phospho-β-catenin levels which may play a role in its anti-metastatic activity, probably blocking the Wnt pathway involves in the polarized cell migration in MDA-MB-231 breast cancer cells.

Conclusions

The inhibition of cell migration in vitro stands as indication of anti-metastatic effect in vivo. At non-cytotoxic concentrations (10 µM), in triple-negative MDA-MB-231 breast cancer cells, *Z*-ajoene was able to exert a strong inhibition of the cell migration, both in the absence (70% inhibition) and in the presence of a chemotactic agent (40% inhibition). So far, our investigations on the molecular mechanism(s) of this promising effect of *Z*-ajoene, showed that the compound markedly affect the expression levels of Axl and Src proteins (i.e. 75% reduction), and less the phosphorylation of the β–catenin protein (i.e. 40% reduction), suggesting that *Z*-ajoene may affect the regulation of several signaling pathways that are known to imply a key role for Vimentin. Interestingly, *Z*-ajoene caused a three-fold increase in the expression of Vimentin in MDA cells. This apparently contradictory result may be explained by *Z*-ajoene inhibition of the Vimentin

function in the filament-assembly process, which in turn may up-regulate its expression.

Although other authors in knockout-vimentin cells showed that Vimentin determines a down-regulation of Axl, Src and the β-catenin/E-cadherin complex, in MDA-MB-231 breast cancer cells we did not confirm these changes. Besides of the different cell lines used, reasons of this discrepancy may be also explained by the different methods of transfection used.

Whether the *in vitro* effect of *Z*-ajoene on the expression of Axl, Src and the β-catenin/E-cadherin complex is mediated by Vimentin or not, our findings represent the first report on the activity of Ajoenes on the expression of a protein, Axl, responsible for activation of the PI3K pathway implied in the epithelial-mesenchymal transition process.

Materials and methods (alphabetical order)

Alkylation assay

Purified recombinant Vimentin protein (1 µM, Prepotech, USA) treated with or without Dansyl-Z-ajoene (25 µM) for 2 minutes at room temperature. All samples boiled at 95 °C for 5 minutes with or without reducing agent (100 mM dithiothreitol). The reaction was detected by immunoblot using anti-vimentin (H84, 1:1000, Santa Cruz, Whitehead Scientific, South Africa) anti-dansyl (1:7500, Molecular Probes, Life Technologies, South Africa) antibodies, standard protocols were applied.

Cell culture

The MDA-MB-231 cells were purchased from ATCC. Cells were incubated at 37°C under 5% CO_2 and cultured with antibiotics in D-MEM (Dulbecco's Modified Eagle Medium) containing 10% FBS (Foetal Bovine Serum, Gibco, Life Technologies, South Africa).

Cell viability assay

Cytotoxicity of compounds was evaluated using the standard 3-(4,5-dimethylthiazol-2-yl)-2,5-diphenyltetrazolium bromide (MTT, Sigma-Aldrich, South Africa) cellular viability assay. Briefly, MDA-MB-231 cells at a density of 1.2 or 3.0 x 10^5 cells per well were seeded in 6-well plates for immunohistochemistry or wound healing assay respectively. Following overnight adhesion, for immunohistochemistry cells were incubated with media alone or media supplemented with 25µM *Z*-ajoene or Dansyl-ajoene in DMSO (0.1% v/v, Sigma) at 37°C for 6 h. On the other hand, for wound healing assay, cells were treated with 10 µM *Z*-ajoene in DMSO (0.1% v/v, Sigma) at 37°C for 24 h. Thereafter, 200 µL/well of 5 mg/mL MTT was added and incubated with the cells for 4 h, followed by addition of 2 mL/well 10% SLS, 0.01M HCl (Merck, Darmstadt, Germany) to solubilize the formazan crystals. The plates were read at 595nm using a Multiscan FC plate reader (Thermo Fischer Scientific, Life Technologies, South Africa). The cytotoxicity observed in ZA-treated cells was expressed as a percentage of the absorbance measured respect to untreated cells.

Cloning

All the cloning steps were included in a logical order.

1. *PCR*

   In order to design the primers for the PCR, the access number of Vimentin in Homo Sapiens was looked up on the NCBI website and was found to be NM_003380.3. The coding sequence was then used to design the forward and reverse primers, which would have to allow a Vimentin PCR product of 1.4 kb to be isolated, with the help of the program DNA Man.

   There are some important points to take into account during the primer design, such as the melting temperature for both primers and the complementarity with

the DNA template. It is important that the melting temperature of primers (the temperature at which a primer would anneal to the complementary cDNA sequence) did not differ by more than 5° C. The PCR should also be set to the lowest annealing temperature. Otherwise, if it is set to a temperature higher than that, the primer with the lower melting temperature would be no longer able to bind to its complementary cDNA sequence, instead of the primer with the higher melting temperature, as would in any case in able to bind to a lower temperature.

The sequence of forward primer was 5'-GGA TCC CAT GTC CAC CAG GTC CGT GTC-3', and that of reverse primer was 5'-GTC GAC TTC AAG GTC ATC GTG ATG CTG-3'. Both the forward and reverse primers were diluted at the concentration of 10 μM before the start of the PCR reaction. However, some calculations had to be carried out first in order to be able to do so,

$$\text{M: } \frac{\text{Conc. n}}{\text{MW}}$$

MW: 330 g mol^{-1} nt^{-1} x NT
$Conc.^{n}$: 37 μg ml^{-1} x OD

Where MW, $Conc.^{n}$ and M where given on each bottle of the forward or reverse primer.

For the forward primer: (14-2471 code)
NT: 27
OD: 550.6

$$\text{Molarity: } \frac{\text{OD x Conc.n x Unit of Coversion}}{\text{NT x MW}} = \frac{550.6 \text{ x } 37 \text{ x } 1000}{27 \text{ x } 330} = 2286.44 \text{ μM}$$

In order to obtain the final concentration of the forward primer equal to 10 μM, the initial concentration of the forward primer (2286.44 μM) was diluted 1:228. So, 1 μl of this stock was added to 227 μl of nuclease –free water.

For the reverse primer (14-2471 code):
NT: 27
OD: 745.1

$$\text{Molarity: } \frac{\text{OD x Conc.n x Unit of Coversion}}{\text{NT x MW}} = \frac{745.1 \text{ x } 37 \text{ x } 1000}{27 \text{ x } 330} = 3094.13 \text{ μM}$$

In order to obtain the final concentration of the reverse primer equal to 10 μM, the initial concentration of the forward primer (3094.13 μM) was diluted 1:309. So, 1 μl of this stock was added to 308 μl of nuclease –free water.

Thereafter, PCR was done in order to isolate the gene of interest, i.e. the coding sequence for Vimentin from the cDNA, and two reactions were carried out following the Life technologies protocol for TOPO® TA Cloning Kit for Sequencing. Each PCR tube contained the mixture shown in Table 8 and a total volume should be of 50 μl. One of these reactions contained the Vimentin cDNA, while the other one was used as a negative control and contained nuclease –free water.

Concentration of stocks	Negative control (µL)	Vimentin cDNA (µL)
10ng/µl Vimentin cDNA	-	1
10 nM dNTPs	1	1
10 µM F primer	1	1
10 µM R primer	1	1
Taq Pol	1	1
10 x taq pol buffer	5	5
Nuclease-free water	41	40
Total volume	**50**	**50**

Table 8: Components of the PCR reactions, where the cDNA would be substituted by nuclease free water for the negative control.

The Taq polymerase is a thermostable DNA polymerase which binds to the 3' end of each primer, in order to build a new DNA strand from the cDNA template by addition of dNTPs. During the course of the PCR this new DNA strand, i.e. the Vimentin cDNA, would get amplified.
The PCR mixtures were left in the thermocycler machine for about two hours to allow the reaction to take place. The thermal cycler machine was set initially to 30 cycles and then increased to 40 cycles to obtain a more abundant PCR product and according to the Life technologies protocol for *TOPO® TA Cloning Kit for Sequencing*:

Initial temperature for denaturation of the DNA: 94° C for 5 minutes
Temperature for denaturation of the DNA: 94° C for 1 minutes
Temperature for the annealing of the primers: 50° C for 1 minute
Temperature for the elongation of the primers: 72° C for 2 minutes
} for each cycle
Final temperature for the complete elongation of the primers: 72° C for 7 minutes

Then the PCR tubes were taken out and their products were mixed together with 10 µl of blue loading dye (Fermentas), which would allow the tracking of the DNA during the subsequent agarose –gel electrophoresis. All the samples were finally stored at 4°C until required.

2. *Gel electrophoresis*

The gel electrophoresis was carried out according to standard procedures with 1% agarose gel after the PCR, in order to see if the Vimentin gene had been successfully amplified from the cDNA.
To start with, 1 grams of agarose were weighted and added into a beaker with 100 ml of 1x TAE buffer. The beaker with its contents was heated up in the microwave oven until the agarose was dissolved and the solution looked transparent. It was important to avoid the contents from boiling in the microwave oven, as some water could then evaporate and the concentration of agarose would then become more than 1%.
The solution was allowed to cool down, then 10 µl of a 10mg/ml ethidium bromide solution was added to it under the fume hood, as ethidium bromide is carcinogenic. Ethidium bromide was added as it is a fluorescent dye that intercalates with the DNA. When the gel was exposed to UV-light, the ethidium

bromide emitted fluorescence and the DNA could be detected. The gel was afterwards poured onto a gel chamber and was then left for about 20 minutes to solidify.

Once the gel was solid, the Gene Ruler 1 kb DNA ladder (Fermentas) was used and loaded onto the first lane. Then 10 µl of the negative control with blue loading dye (Fermentas) was loaded onto the second lane, followed by the Vimentin cDNA sample, which contained also the blue loading dye.

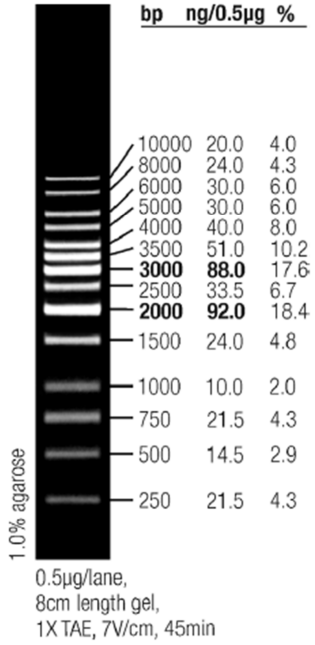

Figure 47: **Gene Ruler 1 kb DNA ladder.**
The size of each band was shown.

To verify that the PCR reaction was successful, gel electrophoresis was performed with a small amount of each sample. For this, 10 µl of Vimentin cDNA sample were loaded in the gel. The gel electrophoresis was run for about one hour at 60 Volt, then the gel was assessed on the trans –illuminator and finally photographed.

If the PCR reaction was successful, a new gel electrophoresis was performed by loading the remaining sample to isolate the PCR product, and the gel portion corresponding to it was cut out. This fragment was then subjected to purification by the Wizard® SV Gel and PCR Clean-Up System kit (see the section below).

3. *Purification of PCR products*

Once the gel electrophoresis had been carried out, the gel slices containing the amplified vimentin cDNA fragment were dissolved and then purified. The entire process of purification was further divided into three steps according to the Promega protocol for Wizard® SV Gel and PCR Clean-Up System, namely binding, washing and elution of the gene DNA.

Firstly, the gel slice was dissolved in the presence of guanidine isothiocyanate, contained in the Membrane Binding Solution, and per 10 mg of agarose gel slice was added a ratio of 10 µl of solution. This mixture was incubated at 65°C for 10 minutes or until the gel slice was completely dissolved. For the binging step, the dissolved gel mixture was transferred to the SV minicolumn assembly into the collection tube and incubated for 1 minute at room temperature. The mixture was

then centrifuged at 13,000 rpm for 1 minute, followed by the removal of the flow – through and the SV minicolumn was reinserted into the collection tube.
During the washing step, 700 µl of membrane wash solution (containing ethanol) was added to the SV minicolumn to remove all excess components of the reaction but the DNA bound to the membrane. The SV minicolumn assembly was centrifuged at 13,000 rpm for 1 minute and the flow through was again removed. This same procedure was repeated one more time, but with 500 µl of membrane wash solution and 5 minutes of centrifugation at 13,000 rpm. To finish off the washing of the gene DNA, only the SV Minicolumn was again centrifuged for about 1 minute to allow evaporation of any residual ethanol.
Finally in the elution step, the SV minicolumn was transferred into a new sterile 1.5 ml eppendorf tube, and incubated at room temperature for 1 minute after the addition of 50 µl of nuclease –free water. The minicolumns were then centrifuged at 13,000 rpm for 1 minute, and the quantification of the purified Vimentin gene was carried out using the Nanodrop spectrophotometer. Lastly, the purified Vimentin gene was stored at –20° C.

4. *Ligation of Vimentin in Topo vector*

The Vimentin ligation in Topo vector was performed according to the Life technologies protocol for TOPO® TA Cloning Kit for Sequencing. The cloning strategy of this kit was highly efficient and very fast, as it allowed direct insertion of the Taq polymerase-PCR products into a plasmid vector. No ligase, post-PCR procedures, PCR primers or specific sequences were required.
The PCR ™ 4-TOPO® vector was a linear plasmid with single 3' thymidine (T) overhangs; it also was an "activated" vector being covalently bound to a Topoisomerase. As showed in the vector map (Figure 48), the vector also contained the genes for resistance to the antibiotics Ampicillin (Amp) and Kanamycin.

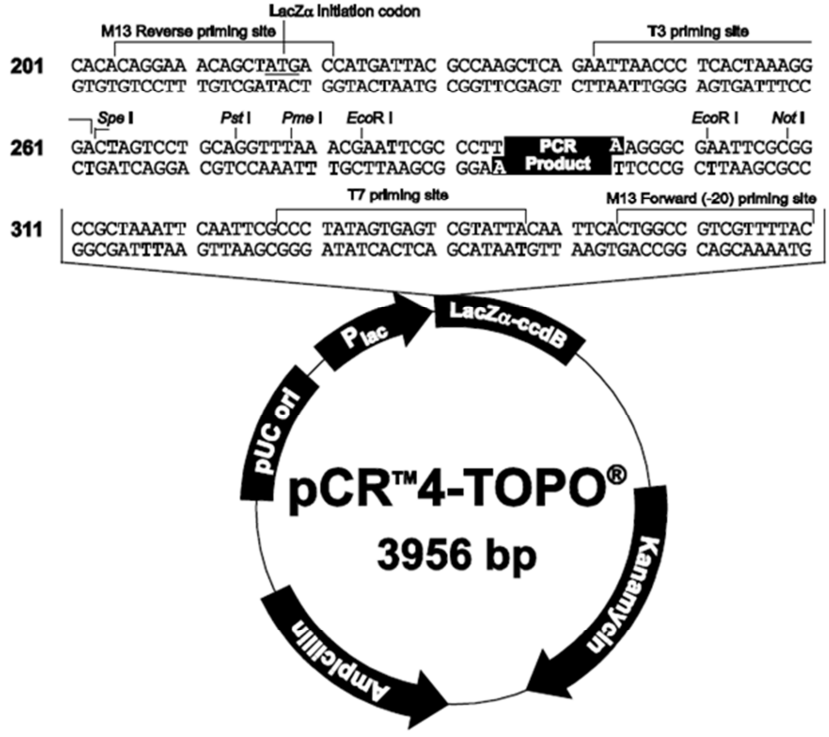

Figure 48: **Map and sequence for the Topo vector** (Invitrogen).

During the PCR reaction, the Taq polymerase adds a single deoxyadenosine (A) to the 3' ends of PCR products, due to its non –template –dependent terminal

transferase activity. As mentioned above, the linearized vector has single residues overhanging 3' deoxythymidine (T) and this has allowed the PCR inserts to ligate efficiently with the vector.

For the ligation reaction, 4 µl of purified Vimentin (obtained with PCR reaction) were mixed with 1 µl of salt solution and 1 µl of Topo vector. This mixture was incubated at room temperature for 30 minutes. Finally, this reaction was purified with butanol and then transformed into Top 10 competent cells.

5. *pET-22b(+) vector system*

The pET System is one of the best systems so far developed for the cloning and expression of recombinant proteins, such as Vimentin, in the E. coli strain BL 21 star DE3.

The pET-22b(+) cloning/expression vector (Novagen) was chosen for the cloning and expression of the Vimentin protein for a number of reasons. The pET-22b(+) vector is a stable plasmid of about 5.5 kb in size. This vector has the following characteristics: a high expression promoter, i.e. the T7 promoter that allowed to obtain high expression levels, and the Ap gene, that is responsible for resistance to Amp antibiotic. It has also an His Tag, which is very important for purification of the Vimentin protein via Nickel column.

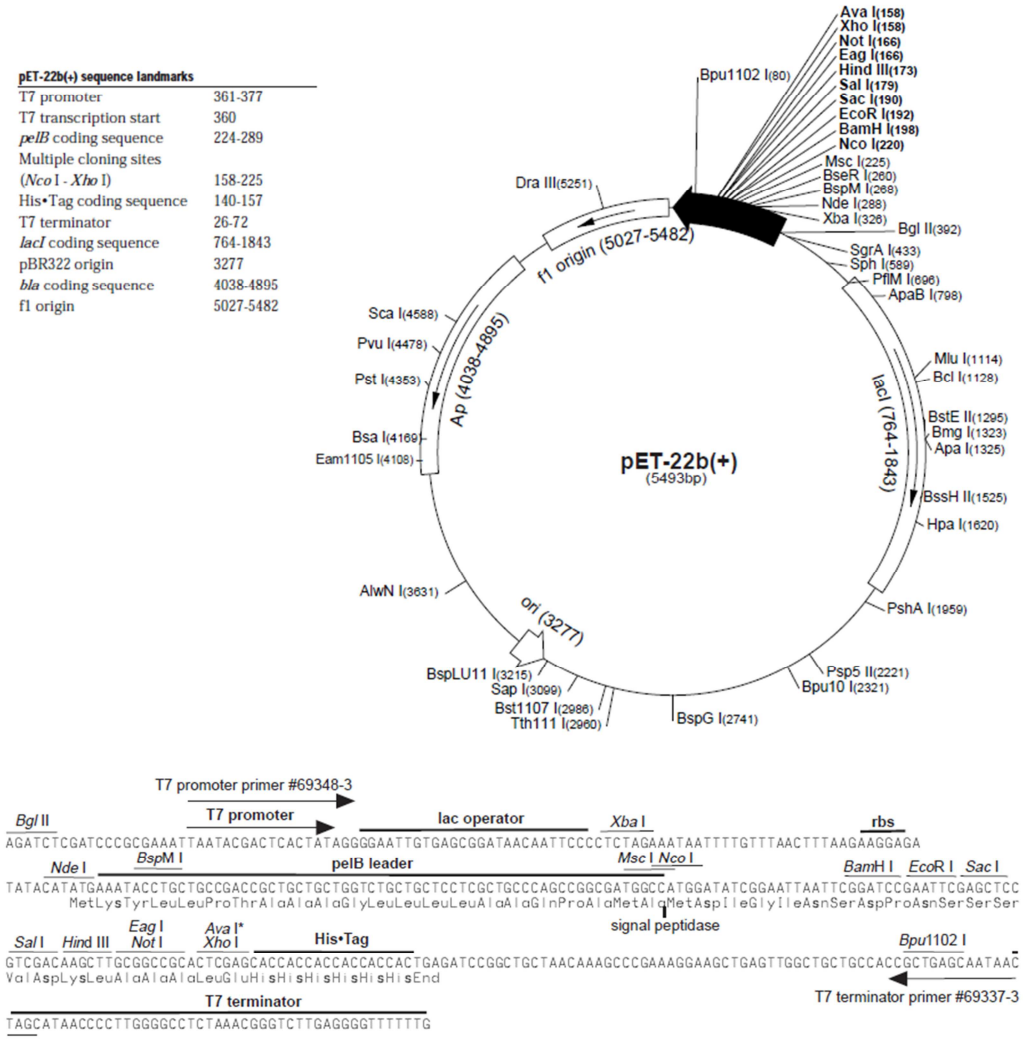

Figure 49: **Map and sequence for the pET-22b(+) cloning/expression vector** (Novagen).

Initially, 2 µl of the pET pET-22b(+)vector stock was transformed into competent cells and then the vector was prepared for the Vimentin ligation (see below REdigestion and SAP treatment).

6. *DNA precipitation with Butanol*

The Vimentin ligation reaction with Topo (6µl) or pET vector (10 µl) was purified through the precipitation with butanol to remove all the components that could interfere during the transformation of E. coli competent cells. Reaction was filled up to 50 µl with water, then 450ul butanol was added. This mixture was centrifuged 13000 rpm at 4° C for 10 minutes. The supernatant was removed and any residual butanol was evaporated. Finally, the pellet was resuspended in nuclease –free water equal to 2 µl for Topo vector or 5 µl of pET vector, respectively.

7. *Transformation into competent cells (E. Coli)*

The transformation into competent cells was carried out in order to clone the Vimentin gene. The procedure was the same for both vectors according to the Invitrogen protocol, except that different types of competent cells were used.

The TOP10 chemically competent E. coli (Invitrogen) was chosen for the Topo vector transformation, because these cells were able to obtain a stable replication of high-copy number plasmids. Moreover, they were provided at a transformation efficiency of 1 x 10^9 cfu/µg supercoiled DNA and were ideal for high-efficiency cloning and plasmid propagation.

Instead, the BL21 Star™(DE3) chemically competent cells (Invitrogen) were designed for applications that require T7 promoter-based expression systems, i.e. the pET-22b(+) vector, and high-level expression of non-toxic recombinant proteins. These cells were provided at a transformation efficiency of 1 x 10^8 cfu/µg plasmid DNA.

Into a vial of competent cells, 2 µl of ligation reaction (after butanol precipitation) were added and incubated on ice for 30 minutes. The cells were then heat-shocked for 30 seconds at 42°C without shaking and incubated again on ice for 10 minutes. Later, 700 µl of S.O.C. medium were added into each vial of competent cells and incubated for one hour with shaking. The bacterial suspension was centrifuged at 3000 rpm for 2 minutes, and 650 µl of supernatant were removed. Finally, 50 µl of each suspension was spread onto a selective Luria –Bertani (LB) agar-plate, containing Amp, and all the plates where afterwards put into an incubator at 37 °C overnight so that the colonies could grow. The negative control was performed to verify that there were no other bacterial contaminations. The following day, the plates were observed and the isolated colonies were selected.

8. *Plasmid extraction of selected clones*

After the transformation into competent cell, selected isolated colonies were added in 3 ml of LB broth medium containing Amp, and incubated overnight at 37° C. The following day, 1 ml of each bacterial suspension was mixed with glycerol (final concentration 20-30%) and stored at -80° C to keep frozen stocks. The remaining 2ml of the bacterial suspension were used for plasmid extraction according to the Promega protocol for *Wizard plus SV minipreps DNA purification system kit*. The Plasmid extraction was divided into four main steps, namely production of cleared lysate as well as binding, washing and elution of the vector DNA.

Firstly, the 1.8 ml of bacterial suspension were centrifuged at 13,000 rpm for 2 minutes and LB medium was removed. The pellet was then resuspended with 250

µl of cell resuspension solution in an eppendorf tube, followed by the addition of another 250 µl of cell lysis solution, used to degrade the cells completely. To degrade the remaining proteins, 10 µl of alkaline protease solution was added and the mixture was incubated for about 5 minutes at room temperature. After this time, 350 µl of neutralization solution were added and centrifuged at 13,000 rpm for 10 minutes, and thus all the reactions (lysis or alkaline protease) were stopped.
In order to start the binding step of the extraction, a spin column was inserted into the collection tube and the lysate was transferred into the spin column. The assembly was then centrifuged at 13,000 rpm for 1 minute. The flow –through was removed and then the spin column was reinserted into the collection tube.
During the washing step, 750 µl of wash solution (containing ethanol) was added. The assembly was centrifuged at 13,000 rpm for 1 minute and the flow –through was removed again. This same procedure was repeated one more time, but with 250 µl of wash solution and 2 minutes of centrifugation at 13,000 rpm.
Lastly, in order to elute the plasmid DNA, the spin column was transferred to a 1,5 ml new sterile eppendorf tube. 50 µl of nuclease-free water was added, followed by centrifugation at 13,000 rpm for 1 minutes and removal of the spin column. The DNA was quantified by the Nanodrop 2000 spectrophotometer and then stored in a fridge at –20 °C before further use.

9. *Restriction enzyme site digestion analysis*

Restriction enzyme site digestion analysis was performed to identify suitable sites that could be used for cloning purposes, i.e. to move the coding sequence of Vimentin from the Topo maintenance vector into the pET-22b(+) cloning/expression vector.
In order to do this, two common restriction enzyme sites (i.e. *Bam HI* and *Sal I* REs) had to be found on both the Vimentin coding sequence, Topo Vector sequence and the pET-22b(+) vector sequence.

The restriction site digestion analysis for the Vimentin coding sequencehad identified a list of appropriate RE sites, whose enzymes could not cut the Vimentin gene (Figure 50).

```
Non Cut Enzymes
AatII Acc65I AccIII AclI AflII AgeI
AhaIII Alw44I ApaBI ApaI ApaLI AscI
Asp718I AsuII AvrII BalI BamHI BbeI
BbvII BclI BglI BglII Bpu1102I Bsc91I
BsiI BsmI Bsp1407I BspHI BspMII BstD102I
BstEII BstXI Csp45I CspI DraI DraIII
DrdI Eco31I Eco47III Eco72I EcoRI EcoRV
EheI EspI FseI HindIII HpaI I-PpoI
KpnI MfeI Mlu113I MluI MscI MstI
NarI NcoI NdeI NheI NotI NruI
NsiI PacI PflMI PinAI PmaCI PmeI
PvuI PvuII RleAI SacII SalI SapI
ScaI SfiI SgrAI SnaBI SpeI SphI
SpoI SspI SstII StuI SwaI VspI
XbaI XmnI XorII
```

Figure 50: **RE sites in pET-22b(+) vector.**
List of RE sites indicating which REs that would not cut the Vimentin gene, with two possible RE sites, which were also found in the RE list of the pET-22b(+) vector, highlighted in red.

The recognition sequences of these enzymes are shown in the figure 51 below:

```
Bam HI:
5' - G^G A T C C - 3'
3' - C C T A G^G - 5'

Sal I:
5' - G^T C G A C - 3'
3' - C A G C T^G - 5'
```

Figure 51: **The sequence of restriction enzyme site for *Bam HI* and *Sal I* enzymes.** This ^ was indicated of the enzyme cleavage site.

Therefore, a set of primers had to be designed which also contained the *Bam HI* and *Sal I* RE sequences. The chosen REs would then also be used to cut the pET-22b(+) vector open so that the isolated Vimentin sequence could fit in it and ligate to it, in order to later clone and express the final Vimentin protein (figure 52).

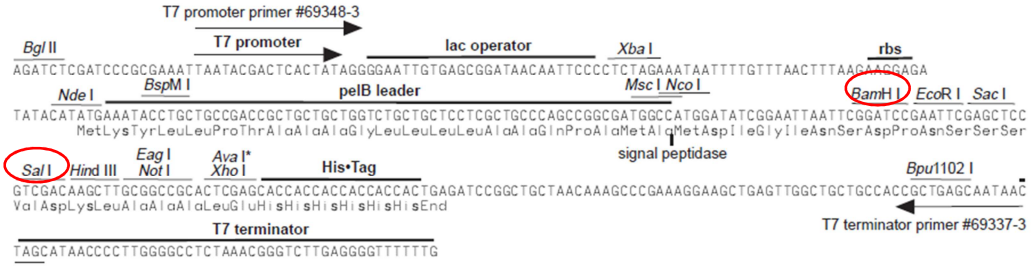

Figure 52: **Sequence and multiple cloning site for the pET-22b(+) cloning/expression vector.** Tree possible RE sites, which are also found in the Vimentin coding sequence, circled in red.

Before the Vimentin ligation, if a double digestion with *Bam HI* and *Sal I* was performed on the pET-22b(+) vector, the portion of its genome located between these enzymes was removed.

For a double site digestion analysis(with *Bam HI* and *Sal I* REs), we had prepared 10 µl of a mixture that contained 5 µl of purifiedDNA plasmid, 1 µl of *Bam HI* RE, 2 µl of *Sal I* RE, 2 µl of *Bam HI Lsp* buffer and nuclease –free water. The procedure is the same as used for the *Eco RI* digestion.
Instead, to isolate and purify the RE digested DNA, a large double digestion with *Bam HI* and *Sal I* REs was carried out by increasing the concentration of the sample and all the reagents. Therefore, 20 µl of purified DNA plasmid, 1,5 µl of *Bam HI* RE, 3 µl of *Sal I* RE and 3 µl of *Bam HI* Lsp buffer were incubated at 37° C for 2 hours and the digestion was made. The products of digestion were separated by agarose –gel electrophoresis and the specific DNA band was cut and this gel slice was processed with Wizard® SV Gel and PCR Clean-Up System (Promega).

10. SAP Treatment of Restriction Digested DNA

Shrimp alkaline phosphate (SAP) was used to remove 5'- and 3'-phosphate groups from DNA.We used this enzyme to prevent self-ligation of restriction digested pET vector DNA before the insertion of Vimentin fragment.
In order to reach the final volume of 20 µl, a mixture was made with 12 µl restriction digested pET vector DNA, 2 µl SAP enzyme and 2 µl 10x SAP buffer and nuclease –free water. This reaction was then incubated at 37° C for 1 hour to

allow the removal of phosphate groups. After this time, the enzyme was inactivated by incubating at 65° C.

The SAP reaction was then purified according to the Promega protocol of Wizard® SV Gel and PCR Clean-up System kit, resuspended in nuclease –free water, then quantified using the NanoDrop spectrophotometer and finally it was stored at -20°C before further use.

11. ***Ligation of Vimentin in*** pET -22b(+) ***vector***

For the Vimentin / pET -22b(+) vector ligation, the optimal molar ratio between them was a 1/3. Therefore, two ligation reactions were carried out. One was a standard reaction which contained 6 µl of Vimentin fragment (i.e. purified Vimentin 2 was previously extracted by Topo vector), 2 µl of the SAP digested pET vector (about 30 ng), 1 µl the T4 Ligase enzyme (which catalyzes the bind between insert and vector) and 1 µl of the T4 Ligase buffer (necessary to activate the reaction and maintain a stable pH). And another one was a negative control, which contained all the reaction components except the Vimentin insert. Both the ligation reactions were incubated overnight at 16° C, butanol-precipitated and then were transformed into BL 21 (DE3) competent cell.

12. Sequencing electrophoresis analysis

The sequencing electrophoresis analysis is a technique that allows to verify if the fragment sequence (i.e. the Vimentin gene) inserted into the vector is correct. This technique was composed of three different phases: an initial PCR reaction, a separation by capillary electrophoresis and finally an optical detection.

This analysis was not possible to carry out in our laboratory. Thus, 10 µl of each sample, and 20 µl of each primer were sent off to the *Central DNA Sequencing Facility* laboratory of the University of Stellenbosch where the sequencing electrophoresis analysis was performed.

The sequencing was performed with the vector primers, i.e. M13 reverse and M13 forward primers for Topo vector samples or T7 promoter and T7 terminator primers for pET-22b(+) vector samples, respectively.

In addition, to be sure to verify with success the entire sequence of Vimentin, two internal primers were identified with the NCBI website, named sequence 1 and 2 respectively, and their aliquots (20 µl) sent out.

Therefore, the PCR cycle of sequencing required a DNA template, primers, but also, a thermal stable DNA polymerase, nucleotides (dNTPs), dideoxynucleotides (ddNTPs), and buffer. These components were combined in a reaction that has been subjected to cycles of annealing, extension and denaturation in a thermocycler. During this phase, the DNA polymerase had created and amplified extension products on the DNA template. The extension of these products was terminated when DNA polymerase had inserted one of the four dideoxynucleotides, each of which was bound to a specific fluorophore dye.

Subsequently, using a capillary electrophoresis, the extension products of the PCR cycle of sequencing were separated depending to their size, and then were exposed to a laser beam, which had stimulated the dideoxynucleotides dyes to emit fluorescence. Because each dye emits light at a different wavelength when excited by the laser, all four colors, and therefore all four bases, can be detected and distinguished by an optical detection [by DNA Sequencing by Capillary Electrophoresis, Applied Biosystems Chemistry Guide, Second Edition].

Finally, the instrument is connected to a Software that converted the fluorescence signal to digital data, then records the data in a *.ab1 file. The digital data were shown in a chromatogram, constituted by a series of peaks of four different colors, each corresponding to one dideoxynucleotide. In addition to the chromatogram, the software has also supplied the nucleotide sequence, which could then be analyzed with the help of the program DNA Man.

Immunoblotting

For detection of proteins from MDA-MB-231 cell lysates by immunoblot, standard protocols were applied. Cells were seeded in 6-well plates at 2.0×10^5 cells per well and incubated overnight in a humidified atmosphere of 5% CO_2 at 37°C. After adherence overnight, the culture medium was replaced with fresh medium and the cells were treated with 10 µM Z-Z-ajoene in DMSO (0.1% v/v). Control cells received DMSO (0.1% v/v) alone. Cells were incubated with *Z*-Z-ajoene for a total of 24 h. Cells were lysed in Lysis buffer 5X (Promega) Total protein was quantified using the Pierce BCA protein assay kit (Thermo Fischer Scientific, Life Technologies). For all Western blotting, 10 µg of total protein was separated by SDS-PAGE and transferred to nitrocellulose membranes. Membranes were blocked for 1 h at room temperature using 5% non-fat milk in PBS containing Tween-20 and incubated with the primary antibodies overnight at 4°C: anti-AXL, anti- β-catenin, anti- phospho-β-catenin (Ser 33), anti- E-cadherin, anti- vimentin (V9 and H84) (1:1000) (all Santa Cruz, Whitehead Scientific, South Africa); anti-Src (1:1000; Cell Signaling Technology); anti-β-tubulin and anti-GAPDH (1:1000) (both Santa Cruz, Whitehead Scientific). Specific proteins were detected using appropriate horseradish peroxidase-conjugated secondary antibodies and the LumiGLO chemiluminescent reagent (KPL, Biocom Biotech, South Africa). A protein ladder (ThermoFischer Scientific, Life Technologies) was used to estimate the molecular weight of proteins.

Immunohistochemistry

MDA-MB-231 cells were seeded on sterile coverslips in six-well plates (1.2×10^5 cells per well) and cultured in D-MEM (Dulbecco's Modified Eagle Medium) containing 10 % FBS. The following day, cells were treated with 25 µM DP (in DMSO 0.1 % v/v), for 6 hours. Thereafter, cells were washed with PBS, permeabilized with absolute methanol at -20°C for 5 min and fixed in 4% paraformaldehyde (Sigma-Aldrich) for 5 min at room temperature. Cell sections were then washed with PBS, incubated in blocking solution (1% bovine serum albumin (BSA) in PBS) for 1 hour at room temperature, and finally incubated with the primary antibodies (anti-vimentin: V9 and H84; anti -PDI) diluted in blocking solution (1:100) overnight at 4°C in the dark. The following day, cell sections were washed with PBS and incubated with the Cy–3 fluorescently –tagged secondary antibodies (anti-mouse for V9 and PDI; anti-rabbit for H84, diluted in blocking solution (1:500) for 90 minutes at room temperature in the dark. Then, cell sections were washed with PBS and mounted using Mowiol 4-88 (Sigma-Aldrich). The sections were stored in the dark at 4°C until viewing with confocal microscope (Carl Zeiss).

Proteomics

To perform the analysis of proteomics, purified recombinant Vimentin protein (10µg, Prepotech, USA) treated with or without garlic compounds (100 µM DP or ZA) for 30 minutes at 37°C. All samples were stored at -80°C until a following peptide analysis by the Centre for proteomics and Genomics research (CPGR), Cape Town, South Africa. The proteomic analysis is a sensitive analytical technique which allows proteins to be analysed by mass spectrometry. Briefly, the protein is first subjected to enzymatic digestion by the trypsin. This protease cleaves the protein at the level of the C-terminal after the amino acid lysine and arginine; except in the case where these residues are followed by a proline. In this way, protein fragment mixture is formed, and then peptides are separated by liquid chromatography that it is coupled to mass spectrometry analysis that enables a identification of each fragment.

SiRNA transfection

MDA-MB-231 cells were seeded on a 6-well plates at 1.0×10^5 cells per well and cultured in DMEM (Dulbecco's Modified Eagle Medium) containing 10 % FBS and allowed to settle overnight. The cells were then transfected with 50 or 100 nM Vimentin SiRNA (25µM Stock), using Lipofectamide RNAi MAX Reagent (Invitrogen) according to the manufacturer's instruction. After 6 h, medium containing the transfection mixture was replaced by fresh culture medium containing 10 % FBS and the cells were incubated in a humidified atmosphere of 5 % CO_2 at 37°C for 24, 48 and 72 h. Cells were lysed in Lysis buffer 5X (Promega). Total protein was quantified using the Pierce BCA protein assay kit (Thermo Fischer Scientific, Life Technologies). Lysates were stored at -20°C until required.

Wound healing assay

MDA-MB-231 cells were seeded in 6-well plates at 3.0×10^5 cells per well and cultured in DMEM (Dulbecco's Modified Eagle Medium) containing 10 % FBS to 90 % confluence. The cell monolayer was carefully wounded using a yellow pipette tip, and cellular debris were removed by washing twice with PBS and finally with DMEM. The wounded monolayer was incubated with or without ZA (10 µM) for 24 h in DMEM containing 1 % (control) and 10 % FBS (positive control, chemoattractant). Cell migration into the wound area was monitored and photographed immediately after wound formation and then after 24 h, using a phase contrast inverted microscope (Olympus CKH41). The degree of wound closure was then quantitatively evaluated by *ImageJ software* and four fields per well were documented. Each experiment was performed in triplicate.

References

(Alphabetical order)

1. Antlsperger DSM, Dirsch VM, Ferreira D, Su J-L, Kuo M-L, Vollmar AM; Ajoene-induced cell death in human promyeloleukemiccells does not require JNK but is amplified by the inhibition of ERK. *Oncogene 2003;22:582–589.*
2. Bayan L, Koulivand PH, Gorji A; Garlic: a review of potential therapeutic effects. *Avicenna J Phytomed. 2014, 4 (1):1-14*
3. Bass R, Ruddock LW, Klappa P, Freedman RBM; A major fraction of endoplasmic reticulum-located glutathione is present as mixed disulfides with protein. *J Biol Chem 2004;279:5257–5262*.
4. Biswas S, Chida AS, Rahman I; Redox modifications of protein-thiols: Emerging roles in cell signaling. *Biochem Pharmacol 2006;71:551–564*.
5. Bodo M, Carinci P, Baroni T; Collagen synthesis and cell growth in chick embryo fibroblasts: Influence of colchicine, cytochalasin B and concanavalin A. *Cell Biol Int 1996;20:177 185.*
6. Bornstein P; The biosynthesis of collagen. *Annu Rev Biochem 1974;43:567–603*.
7. Calaf G. M, Balajee A.S, Montalvo-Villagra M. T, Leon M., Navarrete D. M, Alvarez R. G., Roy D., Narayan G., Abarca-Quinoes J.; *Oncology Letters 2014, 7:721-727, DOI: 10.3892/ol.2014.1781*
8. Capasso A; Antioxidant action and therapeutic efficacy of Allium sativum L. *Molecules 2013, 18: 690-700*
9. Cavallito CJ, Buck JS, Suter CM; Allicin the antibacterial principle of Allium sativum. II. Determination of the chemical structure. *J Am Chem Soc 1944;66:1952–1954.*
10. Chai YC, Ashraf SS, Rokutan K, Johnston RB, Jr., Thomas JA; S-thiolation of individual human neutrophil proteins including actin by stimulation of the respiratory burst: Evidence against a role for glutathione disulfide. *Arch Biochem Biophys 1994;310:273–281*.
11. Chen C-H, Su S-J, Chang K-L, Huang M-W, Kuo S-Y; The garlic ingredient diallyl sulfide induces Ca2þ mobilization in Madin Darby canine kidney cells. *Food Chem Toxicol 2009;47:2344-2350*.
12. Chen W-C, Hsu S-S, Chou C-T; Effect of diallyl disulfide on Ca2þ movement and viability in PC3 human prostate cancer cells. *Toxicol in Vitro 2011;25:636–643*.
13. Claudio JO, Masih-Khan E, Tang H, Goncalves J, Voralia M, Li ZH, Nadeem V, Cukerman E, Francisco-Pabalan O, Liew CC, Woodgett JR, Stewart AK; A molecular compendium of genes expressed in multiple myeloma. *Blood 2002, 100: 2175-2186*.
14. Coluccia AM, Benati D, Dekhil H, De Filippo A, Lan C, Gambacorti-Passerini C.; SKI-606 decreases growth and motility of colorectal cancer cells by preventing pp60(c-Src)-dependent tyrosine phosphorylation of beta-catenin and its nuclear signaling. *Cancer Res 2006,66(4): 2279-2286.*
15. Colucci-Guyon E., Portier MM, Dunia I, Paulin D, Pournin S, Babinet C.; Mice lacking vimentin develop and reproduce without an obvious phenotype. *Cell 1994,79, 679*.

16. Cooper AJ, Pinto JT, Callery PS; Reversible and irreversible protein glutathionylation: Biological and clinical aspects. *Exp Opin Drug Metab Toxicol 2011;7:891–910*.
17. Dalle-Donne I, Colombo G, Gagliano N; S-glutathiolation in life and death decisions of the cell. *Free Radical Res 2011;45:3–15*.
18. Dalle-Donne I, Rossi R, Colombo G; Protein S-glutathionylation: A regulatory device from bacteria to humans Giustarini D, Milzani A.. *Trends Biochem Sci 2009;34:85–96*.
19. Damiano L, Di Stefano P, Camacho Leal MP, Barba M, Mainiero F, Cabodi S, Tordella L, Sapino A, Castellano I, Canel M, Frame M, Turco E, Defilippi P.; p140Cap dual regulation of E-cadherin/EGFR cross-talk and Ras signalling in tumour cell scatter and proliferation. *Oncogene 2010, 29: 3677–3690*.
20. Das A, Banik NL, Ray SK; Garlic compounds generate reactive oxygen species leading to activation of stress kinases and cysteine proteases for apoptosis in human glioblastoma T98G and U87MG cells. *Cancer 2007;110:1083–1095*.
21. Dave JM, Bayless KJ; Vimentin as an integral regulator of cell adhesion and endothelial sprouting. *Microcirculation 2014; 21: 333–344*.
22. Dejana E, Tournier-Lasserve E, Weinstein B.M; The Control of Vascular Integrity by Endothelial Cell Junctions: Molecular Basis and Pathological Implications; *Developmental Cell 2009; 16*.
23. Demeule B, Gurny R, Arvinte T; Detection and characterization of protein aggregates by fluorescence microscopy. Int *J Pharm 2007;329:37–45*.
24. DeSantis C, Ma J, Bryan L, Jemal A; Breast cancer statistics, 2013. *CA Cancer J. Clin. 2014;64:52-62*.
25. Dirsch VM, Gerbes AL, Volmar AM; Ajoene, a compound of garlic, induces apoptosis in human promyleoleukemic cells, accompanied by generation of reactive oxygen species and activation of nuclear factor kB. *Mol Pharmacol 1998;53:402–407*.
26. Dirsch VM, Antlsperger DSM, Hentze H, Vollmar AM; Ajoene, an experimental anti-leukemic drug: Mechanism of cell death. *Leukemia 2002;16:74–83*.
27. Feige MJ, Hendershot LM; Disulfide bonds in ER protein folding and homeostasis. *Curr Opin Cell Biol 2011;23:167–175*
28. Ferrari, D.M. and Soling, H.D; The protein disulphide-isomerase family: unravelling a string of folds. *Biochem. J* 1999,. *339 (Pt 1): 1–10*.
29. Fleischauer AT, Arab L; Garlic and cancer: A critical review of the epidemiologic literature. *J Nutr 2001;3S:1032S–1040S*.
30. Foroni Chiara, Broggini Massimo, Generali Daniele, Damia Giovanna; Epithelial–mesenchymal transition and breast cancer: Role, molecular mechanisms and clinical impact; *Cancer Treatment Reviews 2012; 38:689–697; doi:10.1016/j.ctrv.2011.11.001*.
31. Freedman R.; Protein disulfide isomerases exploit synergy between catalytic and specific binding domains. *EMBO Rep. 2002, 136–140*
32. Gallwitz H, Bonse S, Martinez-Cruz A, Schlichting I, Schumacher K, Krauth-Siegel RL; Ajoene is an inhibitor and subversive substrate of human glutathione reductase and Trypanosoma cruzi trypanothione reductase: crystallographic, kinetic, and spectroscopic studies. *J Med Chem 1999;42:364–372*.

33. Giustarini D, Dalle-Donne I, Lorenzini S; Protein thiolation index (PTI) as a biomarker of oxidative stress. Free Radic *Biol Med 2012;53:907–915*.
34. Gruber CW, Cemazar M, Heras B, Martin JL, Craik DJ; Protein disulfide isomerase: the structure of oxidative folding; *Trends Biochem Sci. 2006 Aug;31(8):455-64. Epub 2006 Jul 11*.
35. Hafizi S., Dahlbäck B.; Gas6 and protein S. Vitamin K-dependent ligands for the Axl receptor tyrosine kinase subfamily. *FEBS Journal 2006, 273 (23): 5231–5244*.
36. Hill BG, Bhatnagar A; Protein S-glutathiolation: Redox sensitive regulation of protein function. *J Mol Cell Cardiol 2012;52:559–567*.
37. Hogg PJ; Targeting allosteric disulphide bonds in cancer. *Nat Rev Cancer 2013;13:425–431*.
38. Howard EW, Ling MT, Chua CW, Cheung HW, Wang X, Wong YC. Garlic-derived S-allylmercaptocysteine is a novel in vivo antimetastatic agent for androgen-independent prostate cancer. *Clin Cancer Res, 2007, 13, 1847*.
39. Howard J.C, Varallo V. M, Ross D. C, Roth J. H, Faber K. J, Alman B., Gan B. S.; Elevated levels of β-catenin and fibronectin in three-dimensional collagen cultures of Dupuytren's disease cells are regulated by tension in vitro*; BMC Musculoskeletal Disorders 2003, 4:16-28*.
40. Huang J, Yang B, Xiang T, Peng W, Qiu Z, Wan J, Zhang L, Li H, Li H, Ren G; Diallyl disulfide inhibits growth and metastatic potential of human triple-negative breast cancer cells through inactivation of the β-catenin signaling pathway, *Mol. Nutr. Food Res. 2015, 59, 1063–1075 DOI 10.1002/mnfr.201400668*.
41. Hunter R, Kaschula CH, Parker MI, Substituted ajoenes as novel anti-cancer agents. *Bioorg Med Chem Lett 2008;18:5277–527*.
42. Hunter R, Kaschula C, Stellenboom N, Cotton J, Parker MI; New excursions into the synthesis and medicinal chemistry of the disulfide bond. *Phosphorus Sulfur Silicon Relat Elem 2013;188:1497–1507*.
43. Iciek M, Kwiecien I, Wlodek L; Biological properties of garlic and garlic-derived organosulfur compounds. *Environ Mol. Mutagen 2009;50:247–265*.
44. Irby RB, Yeatman TJ; Role of Src expression and activation in human cancer. *Oncogene 2000, 19(49): 5636-5642*.
45. Karmakar S, Banik NL, Patel SJ, Ray SK; Garlic compounds induced calpain and intrinsic caspase cascade for apoptosis in human malignant neuroblastoma SH-SY5Y cells. *Apoptosis 2007;12:671–684*.
46. Kaschula CH, Hunter R, Parker MI; Garlic-derived anti-cancer agents: Structure and biological activity of ajoene. *Biofactors 2010;36:78–85*.
47. Kaschula CH, Hunter R, Hassan HT; Anti-proliferative activity of synthetic ajoene analogues on cancer cell lines. *Anti-Cancer Agent Med Chem 2011;11:260–266*.
48. Kaschula, CH, Hunter R, Stellenboom N, Caira MR, Winks S, Oqunleye T, Richards P, Cotton J, Zilbeyaz K, Wang Y, Siyo V, Ngarande E, Parker M I; Structure-Activity Studies on the Anti-Proliferation Activity of Z-ajoene Analogues in WHCO1 Oesophageal Cancer Cells., *Eur. J. Med. Chem. 2012, 50: 236-254.*
49. Kaschula CH, Hunter R, Cotton J, Tuveri R, Ngarande E, Dzobo K, Schäfer G, Siyo V, Lang D, Kusza D.A, Davies B, Katz A.A, Parker M.I; The Garlic Compound Ajoene Targets Protein Folding in the Endoplasmic Reticulum of Cancer Cells, *Mol Carcinog. 2015 Jul 24. doi: 10.1002/mc.22364.*

50. Katsumoto T., Mitsushima A., Kurimura T; (1990). "The role of the vimentin intermediate filaments in rat 3Y1 cells elucidated by immunoelectron microscopy and computer-graphic reconstruction". *Biol Cell* 68 (2): 139–46. doi:10.1016/0248-4900(90)90299-I. PMID 2192768.
51. Kidd M.E, Shumaker D.K, Ridge K.M.; The Role of Vimentin Intermediate Filaments in the Progression of Lung Cancer; American Journal of Respiratory. *Cell and Molecular Biology January 2014, Volume 50 Number 1*.
52. Kim YS, Yi BR, Kim NH, Choi KC; Role of the epithelial–mesenchymal transition and its effects on embryonic stem cells, *Experimental & Molecular Medicine (2014) 46, e108; doi:10.1038/emm.2014.44*
53. Klatt P, Lamas S; Regulation of protein function by Sglutathiolation in response to oxidative and nitrosative stress. Eur *J Biochem 2000;267:4928–4944*.
54. Koivu J, Myllyla R; Interchain disulfide bond formation in types I and II procollagen. Evidence for a protein disulfide isomerase catalyzing bond formation. *J Biol Chem 1987;262:6159–6164*.
55. Korsching E, Packeisen J, Liedtke C, Hungermann D, Wülfing P, van Diest PJ, Brandt B, Boecker W, Buerger H.;The origin of vimentin expression in invasive breast cancer: epithelial-mesenchymal transition, myoepithelial histogenesis or histogenesis from progenitor cells with bilinear differentiation potential? *J Pathol. 2005; 206:451–7. [PubMed:15906273*.
56. Korshunov V. A; Axl-dependent signaling: A clinical update. *Clin Sci (Lond). 2012 April ; 122(8): 361–368. doi:10.1042/CS20110411*.
57. Kosuri P, Alegre-Cebollada J, Feng J; Protein folding drives disulfide formation. *Cell 2012;151:794–806*.
58. Lai E, Teodoro T, Volchuk A; Endoplasmic reticulum stress: Signaling the unfolded protein response. *Physiology 2007;22:193–201*.
59. Lai K-C, Hsu S-C, Yang J-S, Yu C-C, Lein J-C, Chung J-G; Diallyl trisulfide inhibits migration, invasion and angiogenesis of human colon cancer HT-29 cells and umbilical vein endothelial cells, and suppresses murine xenograft tumour growth; *J. Cell. Mol. Med. 2015, Vol 19, No 2, pp. 474-484*.
60. Lee AS; The ER chaperone and signaling regulator GRP78/BiP as a monitor of endoplasmic reticulum stress. *Method 2005;35:373–381*.
61. Li M, Ciu J-R, Ye Y; Antitumor activity of Z-ajoene, a natural compound purified from garlic: Antimitotic and microtubule- interaction properties. *Carcinogenesis 2002;23:573–579.*
62. Li Y, Ye X, Tan C, Hongo J-A, Zha J, Liu J, Kallop D, Ludlam MJC, Pei L; Axl as a potential therapeutic target in cancer: role of Axl in tumor growth, metastasis and angiogenesis, *Oncogene 200,) 28: 3442–3455*.
63. Liu TA, Jan YJ, Ko BS, Liang SM, Chen SC, Wang J, Hsu C, Wu YM, Liou JY; 14-3-3ε Overexpression Contributes to Epithelial Mesenchymal Transition of Hepatocellular Carcinoma; *PLOS ONE March 2013 Volume 8 Issue 3 e57968*.
64. Meusser B, Hirsch C, Jarosch E, Sommer T; ERAD: The long road to destruction. *Nat Cell Biol 2005;7:766–772.*
65. Miron T, Rabinkov A, Mirelman D, Wilchek M, Weiner L; The mode of action of allicin: Its ready permeability through phospholipid membranes may contribute to its biological activity. *Biochim Biophys Acta 2000;1463:20–30*.

66. Münchberg U, Anwar A, Mecklenburg S, Jacob C; Polysulfides as biologically active ingredients of garlic. *Org Biomol Chem 2007;5:1505–1518.*
67. Nagaraj NS, Anilakumar KR, Singh OV; Diallyl disulfide causes caspase-dependent apoptosis in human cancer cells through a Bax triggered mitochondrial pathway. *J Nutr Biochem 2010;21:405 412*.
68. Nelson WJ and Nusse R; Convergence of Wnt, β-Catenin, and Cadherin Pathways *Science 2004, 303(5663): 1483–1487. doi:10.1126/science.1094291*
69. Nepravishta R, Sabelli R, Iorio E, Micheli L, Paci M, Melino S; Oxidative species and S-glutathionyl conjugates in the apoptosis induction by allyl thiosulfate. *FEBS J 2012;279:154–167*.
70. Ngo SN, Williams DB, Cobiac L, Head RJ; Does garlic reduce risk of colorectal cancer? A systematic review. *J Nutr 2007;137:2264–2269*.
71. Nishikawa T, Yamada N, Hattori A, Fukuda H, Fujino T; Inhibition by ajoene of skin-tumor promotion in mice. *Biosci Biotechnol Biochem 2002;66:2221–222*.
72. Noiva R, Lennarz W; Protein disulfide isomerase. A multifunctional protein resident in the lumen of the endoplasmic reticulum. *J. Biol. Chem., 1992, **267**, 3553-3556*.
73. Okumura M, Kadokura H, Inaba K.; Structures and functions of protein disulfide isomerase family members involved in proteostasis in the endoplasmic reticulum, Free *Radical Biology and Medicine 2015 Jun; 83:314-22. doi: 10.1016/j.freeradbiomed.2015.02.010*.
74. Olsen J. V, Ong S. E, Mann M; Trypsin cleaves exclusively C –terminal to arginine and lysine residues; *Mol. Cell. Proteomics, 2004, **3**, 608-614*.
75. Park EK, Kwon KB, Park KI, Park BH, Jhee EC; Role of Ca(2+) in diallyl disulfide-induced apoptotic cell death of HCT-15 cells. *Exp Mol Med 2002;34:250–257*.
76. Persson S, Rosenquist M, Knoblach B, Khosravi-Far R, Sommarin M, Michalak M; Diversity of the protein disulfide isomerase family: identification of breast tumor induced Hag2 and Hag3 as novel members of the protein family, *Mol Phylogenet Evol. 2005 Sep;36(3):734-40*.
77. Phua D.C.Y,. Humbert P.O, Hunziker W; Vimentin Regulates Scribble Activity by Protecting It from Proteasomal Degradation; *Molecular Biology of the Cell 2009, Vol. 20, 2841–2855*.
78. Pinto JT, Qiao C, Xing J; Effects of garlic thioallyl derivatives on growth, glutathione concentration, and polyamine formation of human prostate carcinoma cells in culture. *Am J Clin Nutr 1997;66:398–405*.
79. Powolny AA, Singh SV; Multitargeted prevention and therapy of cancer by diallyl trisulfide and related Allium vegetable derived organo sulfur compounds. *Cancer Lett 2008;269:305–314*.
80. Qi J, Wang J, Romanyuk O, Siu CH.; Involvement of Src Family Kinases in N-Cadherin Phosphorylation and β-Catenin Dissociation during Transendothelial Migration of Melanoma Cells; *Molecular Biology of the Cell 2006, Vol. 17, 1261–1272.*
81. Rabinkov A, Miron T, Mirelman D; S-Allylmercaptoglutathione: The reaction product of allicin with glutathione possesses SH-modifying and antioxidant properties. *Biochim Biophys Acta 2000;1499:144–153*.

82. Rappsilber J, Ishihama Y, Mann M; Stop and go extraction tips for matrix-assisted laser desorption/ionization, nanoelectrospray, and LC/MS sample pretreatment in proteomics. *Anal. Chem.,* 2003, *75:663-670*.
83. Ravichandran V, Seres T, Moriguchi T, Thomas JA, Johnston RB, Jr; S-thiolation of glyceraldehyde-3-phosphate dehydrogenase induced by the phagocytosis-associated respiratory burst in blood monocytes. *J Biol Chem 1994;269:25010–25015*.
84. Sabelli R, Iorio E, De Martino A; Rhodanese-thioredoxin system and allyl sulfur compounds. *FEBS J 2008;275:3884–3899*.
85. Reddy K. B; Triple-negative breast cancers: an updated review on treatment options. *Curr. Oncol. 2011, 18, e173–e179*
86. Roura S, Miravet S, Piedra J, Garcia de Herreros A, Dunach M; Regulation of E-cadherin/Catenin association by tyrosine phosphorylation. *J Biol Chem 1999, 274(51): 36734-36740*.
87. Saidu NE, Abu Asali I, Czepukojc B, Seitz B, Jacob C, Montenarh M.; Comparison between the effects of diallyl tetrasulfide on human retina pigment epithelial cells (ARPE-19) and HCT116 cells. *Biochim Biophys Acta 2013;1830:5267–5276*.
88. Saidu NE, Touma R, Asali IA, Jacob C, Montenarh M; Diallyl tetrasulfane activates both the eIF2alpha and Nrf2/HO-1 pathways. *Biochim Biophys Acta 2013;1830:2214–2225*.
89. Sakamoto K, Lawson LD, Milner JA; Allyl sulfides from garlic suppress the in vitro proliferation of human A549 lung tumor cells. *Nutr Cancer 1997;29:152–156*.
90. Satelli A. Li S; Vimentin as a potential molecular target in cancer therapy Or Vimentin, an overview and its potential as a molecular target for cancer therapy; *Cell Mol Life Sci. 2011; 68(18): 3033–3046. doi:10.1007/s00018-011-0735-1*.
91. Scharfenberg K, Wagner R, Wagner KG; The cytotoxicity effect of ajoene, a natural product from garlic, investigated with different cell lines. *Cancer Lett 1990;53:103–108*.
92. Schäfer G, Kaschula CH; The immunomodulation and anti-inflammatory of garlic organo sulfur compounds in cancer chemoprevention. *Anti-Cancer Agent Med Chem;14:233–240*.
93. Schroder M, Kaufman RJ; ER stress and the unfolded protein response. *Mutat Res 2005;569:29–63*.
94. Schubert U, Anton LC, Gibbs J, Norbury CC, Yewdell JW, Bennink JR; Rapid degradation of a large fraction of newly synthesized proteins by proteasomes. *Nature 2000;404:770–774*.
95. Shin BK, Wang H, Yim AM, Le Naour F, Brichory F, Jang JH, Zhao R, Puravs E, Tra J, Michael CW, Misek DE, Hanash SM; Global profiling of the cell surface proteome of cancer cells uncovers an abundance of proteins with chaperone function. *J Biol Chem 2003, 278: 7607-761*.
96. Sigmund H, Pfleiderer W; A new type of labelling of nucleosides and nucleotides. *Helv Chim Acta 2003;86:2299–2334*.
97. Sundaram SG, Milner JA; Diallyl disulfide inhibits the proliferation of human tumor cells in culture. *Biochim Biophys Acta 1996;1315:15–20*.
98. Taylor P, Noriega R, Farah C, Abad M-J, Arsenak M, Apitz R; Ajoene inhibits both primary tumor growth and metastasis of B16/BL6 melanoma cells in C57BL/6 mice. *Cancer Lett 2006;239:298–304*.

99. Thakur R, Mishra DP; Pharmacological modulation of beta-catenin and its applications in cancer therapy. *J Cell Mol Med 2013,17(4):449–456*.
100. Tian G.; The crystal structure of yeast protein disulfide isomerase suggests cooperativity between its active sites. *Cell 2006 124, 61–73*
101. Tilli CM, Stavast-Kooy AJ, Vuerstaek JD, Thissen MR, Krekels GA, Ramaekers FC, Neumann HA; The garlic derived organo sulfur component ajoene decreases basal cell carcinoma tumor size by inducing apoptosis. *Arch Dermatol Res 2003;295:117–123*.
102. Townsend DM; S-glutathionylation: Indicator of cell stress and regulator of the unfolded protein response. *Mol Interv 2007;7:313–324*.
103. Turano C, Coppari S, Altieri F, Ferraro A; Proteins of the PDI family: unpredicted non-ER locations and functions. *J. Cell. Physiol. 2002, 193:154–163.*
104. Tzivion G, Luo Z, Avruch J.; A dimeric 14-3-3 protein is an essential cofactor for Raf kinase activity; *Nature 1998, 394:88-92 doi:10.1038/27938*.
105. Tzivion G, Luo Z, Avruch J; Calyculin A-induced Vimentin Phosphorylation Sequesters 14-3-3 and Displaces Other 14-3-3 Partners in Vivo*; The Journal of Biological Chemistry 2000, 275(38): 29772–29778.*
106. Updike MS, Sawdy JC, Wang LS, Liu S, Huang YW, Ye W, Farrar WB, Lin YC, Wick M; Primary cultured human breast epithelial cells up-regulate protein disulfide isomerase in response to zeranol. *Anticancer Res. 2007; 27(1A):407-10*.
107. van Rooyen BA, Schafer G, Leaner VD, Parker MI; Tumour cells down-regulate CCN2 gene expression in co-cultured fibroblasts in a Smad7- and ERK-dependent manner. *Cell Commun Signal 2013;11:75*.
108. Veale RB, Thornley AL; Increased single class low-affinity EGF receptors expressed by human oesophageal squamous carcinoma cell lines. *S Afr J Sci 1989; 85:375–379*.
109. Vuoriluoto K, Haugen H, Kiviluoto S, Mpindi JP, Nevo J, Gjerdrum C, Tiron C, Lorens JB, Ivaska J; Vimentin regulates EMT induction by Slug and oncogenic H-Ras and migration by governing Axl expression in breast cancer. *Oncogene. 2011; 30:1436–1448*.
110. Wang HC, Hsieh SC, Yang JH, Lin SY, Sheen LY; Diallyl trisulfide induces apoptosis of human basal cell carcinoma cells via endoplasmic reticulum stress and the mitochondrial pathway. *Nutr Cancer 2012;64:770–780*.
111. Wang HC, Pao J, Lin SY, Sheen LY; Molecular mechanisms of garlic-derived allyl sulfides in the inhibition of skin cancer progression. *Ann NY Acad Sci 2012;1271:44–52*.
112. Wang L, Wang X, Wang C-C; Protein disulfide–isomerase , a folding catalyst and a redox-regulated chaperone; *Free Radical Biology and Medicine 83(2015)305–313*
113. Wang Y, Sun Z, Chen S, Jiao Y, Bai C; ROS-mediated activation of JNK/p38 contributes partially to the pro-apoptotic effect of ajoene on cells of lung adenocarcinoma. *Tumour Biol. 2015 Oct. DOI 10.1007/s13277-015-4181-9*.
114. Webster DF, Harvey W; A quantitative assay for collagen synthesis in microwell fibroblast cultures. *Anal Biochem 1979;96:220–224*.
115. Wei J1, Xu G, Wu M, Zhang Y, Li Q, Liu P, Zhu T, Song A, Zhao L, Han Z, Chen G, Wang S, Meng L, Zhou J, Lu Y, Wang S, Ma D.; Overexpression of Vimentin Contributes to Prostate Cancer Invasion and Metastasis via Src Regulation; *Anticancer Res 2008, 28: 327-334.*

116. Wilkinson B and H, Gilbert F; Protein disulfide isomerase, *Biochimica et Biophysica Acta (BBA)-Proteins and Proteomics2004, 1699: 35-44*.
117. Wolfe AR, Debeb BG, Lacerda L, Larson R, Bambhroliya A, Huang X, Bertucci F, Finetti P, Birnbaum D, Van Laere S, Diagaradjan P, Ruffell B, Trenton NJ, Chu K, Hittelman W, Diehl M, Levental I, Ueno NT, Woodward WA; Simvastatin prevents triple-negative breast cancer metastasis in pre-clinical models through regulation of FOXO3a, *Breast Cancer Res Treat 2015, 154:495–508 DOI 10.1007/s10549-015-3645-3*.
118. Wu X, Liu X, Koul S, Lee CY, Zhang Z, Halmos B; AXL kinase as a novel target for cancer therapy, *Oncotarget 2014 Oct 30;5(20):9546-63*.
119. Xiao X, Chen B, Liu X, Liu P, Zheng G, Ye F, Tang H, Xie X., Diallyl Disulfide Suppresses SRC/Ras/ERK Signaling-Mediated Proliferation and Metastasis in Human Breast Cancer by Up-Regulating miR-34a; *Plos one 2014, 9 (11): 1-7*.
120. Xu C, Bailly-Maitre B, Reed JC; Endoplasmic reticulum stress: Cell life and death decisions. *J Clin Invest 2005;115:2656–2664*.
121. Xu S, Sankar S, Neamati N; Protein disulfide isomerase: a promising target for cancer therapy; *Drug Discovery Today 2014, 19(3):222-240; dx.doi.org/ 10.1016/j.drudis.2013.10.017*
122. Yagi-Utsumi M, Satoh T, Kato K; Structural basis of redox –dependent substrate binding of protein disulfide isomerase; *Sci Rep. 2015 9(5):13909. doi: 10.1038/srep13909*.
123. Yang J-S, Chen G-W, Hsia T-C; Diallyl disulfide induces apoptosis in human colon cancer cell line (COLO 205) through the induction of reactive oxygen species, endoplasmic reticulum stress, caspases casade and mitochondrial-dependent pathways. *Food Chem Toxicol 2009;47:171–179*.
124. Zhang YX, Knyazev PG, Cheburkin YV, Sharma K, Knyazev YP, Orfi L, Szabadkai I, Daub H, Keri G, Ullrich A; AXL is a potential target for therapeutic intervention in breast cancer progression. *Cancer research. 2008; 68:1905–1915*.